BIOINSPIRED METAL-BASED OXIDANTS: SELECTIVITY IN CATALYTIC HYDROXYLATION OF ALIPHATIC C-H BONDS AND INSIGHT INTO THE REACTIVITY OF OXOIRON SPECIES

Valeria Dantignana

Universitat
de Girona

Doctoral Thesis

Bioinspired metal-based oxidants: selectivity in catalytic hydroxylation of aliphatic C-H bonds and insight into the reactivity of oxoiron species

Valeria Dantignana

2020

Doctoral programme in Chemistry

Supervised by: Dr. Miquel Costas Salgueiro, Dr. Anna Company Casadevall

Tutor: Dr. Miquel Costas Salgueiro

Presented in partial fulfilment of the requirements for a doctoral degree from the University of Girona

Universitat
de Girona

Dr. Miquel Costas Salgueiro and Dr. Anna Company Casadevall of Universitat de Girona,

WE DECLARE:

That the thesis entitled "Bioinspired metal-based oxidants: selectivity in catalytic hydroxylation of aliphatic C-H bonds and insight into the reactivity of oxoiron species", presented by Valeria Dantignana to obtain a doctoral degree, has been completed under our supervision and meets the requirements to opt for an International Doctorate.

For all intents and purposes, we hereby sign this document.

Dr. Miquel Costas Salgueiro   Dr. Anna Company Casadevall

Girona, 29 September 2020

FULL LIST OF PUBLICATIONS

This thesis is based on a compendium of the following publications:

CHAPTER III

"Chemoselective aliphatic C–H bond oxidation enabled by polarity reversal".

V. Dantignana,[‡] M. Milan,[‡] O. Cussó, A. Company,* M. Bietti,* M. Costas.*

ACS Cent. Sci., **2017**, *3*, 12, 1350-1358 (impact factor: 11.228; Chemistry (miscellaneous), Q1).

CHAPTER IV

"Spectroscopic and reactivity comparisons between nonheme oxoiron(IV) and oxoiron(V) species bearing the same ancillary ligand".

V. Dantignana, J. Serrano-Plana, A. Draksharapu, C. Magallón, S. Banerjee, R. Fan, I. Gamba, Y. Guo, L. Que Jr.,* M. Costas,* A. Company.*

J. Am. Chem. Soc. **2019**, *141*, 38, 15078-15091 (impact factor: 14.612; Chemistry (miscellaneous), Q_1).

CHAPTER V

"Ligand effects on the reactivity of oxoiron(IV) species supported by electronically tuned azamacrocycles".

V. Dantignana, J. Serrano-Plana, Á. Martínez Camarena, E. García-España, A. Company,* M. Costas.*

Manuscript in preparation.

Publications not included in this thesis:

"Acid-triggered O−O bond heterolysis of a nonheme Fe^{III}(OOH) species for the stereospecific hydroxylation of strong C−H bonds".
J. Serrano-Plana, F. Acuña-Parés, V. Dantignana, W. N. Oloo, E. Castillo, A. Draksharapu, C. J. Whiteoak, V. Martin-Diaconescu, M. G. Basallote,* J. M. Luis,* L. Que, Jr.,* M. Costas,* A. Company.* *Chem. Eur. J.*, **2018**, *24*, 20, 5331-5340.

"Catalytic oxidation of primary C-H bonds in alkanes with bioinspired catalysts".
V. Dantignana, A. Company,* M. Costas.* *Chimia*, **2020**, *74*, 6, 470-477.

LIST OF ABBREVIATIONS

2-eha	2-ethylhexanoic acid
acac	acetylacetonate
AcOEt	ethyl acetate
AcOH	acetic acid
AcOOH	peracetic acid
A/K	alcohol/ketone
BDE	bond dissociation energy
Bn	benzyl
Bu_4NIO_4	tetrabutylammonium(meta)periodate
$C^\bullet$	carbon center radical
calcd	calculated
cat	catalyst
CI	chemical ionization
Cpd-I	compound I
CSI	criospray ionization
$CumO^\bullet$	cumoxyl radical
CV	cyclic voltammetry
CYP450	Cytochrome P450
DFT	density functional theory
dMM	dimethylmethoxy
$E_{1/2}$	half-wave potential
$E_{p,c}$	cathodic peak potential
EA	elemental analysis
ee	enantiomeric excess
EI	electron ionization
EPR	electron paramagnetic resonance

equiv	equivalent
ESI	electrospray ionization
EWG	electron withdrawing group
EXAFS	extended X-ray absorption fine structure
exp	experimental
Fc	ferrocene
FID	Fourier transform infrared
FT-IR	flame ionization detector
GC	gas chromatography
h	hour
H$^\bullet$	hydrogen atom
H$_{ax}$	axial hydrogen
H$_{eq}$	equatorial hydrogen
HAT	hydrogen atom transfer
HBA	hydrogen bond acceptor
HBD	hydrogen bond donor
HFIP	1,1,1,3,3,3-hexafluoroisopropanol
HR	high resolution
iPr	isopropyl
IRPD	infrared photodissociation
k_2	second order kinetic rate constant
k_2'	normalized second order rate constant
k_{obs}	observed kinetic constant
KG	ketoglutarate
KIE	kinetic isotope effect
log	logarithm
MB	Mössbauer
m-CPBA	$meta$-chloroperoxybenzoic acid

Me	methyl
Me_2N	dimethylamino
min	minute
MS	mass spectrometry
m/z	mass/charge
NMR	nuclear magnetic resonance
OAc	acetoxy
OAT	oxygen atom transfer
OMe	methoxy
OTf	trifluoromethanesulfonate
Ph	phenyl
PhIO	iodosylbenzene
Piv	pivaloyl
pK_a	acid dissociation constant
ppm	parts per million
Py	pyridine
r	distance
R•	alkyl radical
RC	retention of configuration
RT	room temperature
S	total spin angular momentum
SCE	saturated calomel electrode
SW	spectral width
t	time
T	temperature
$t_{1/2}$	half-life time
TauD-J	intermediate J of taurine dioxygenases
^tBu	*tert*-butyl

TFE	2,2,2-trifluoroethanol
TfOH	triflic acid
TIPS	tris(isopropyl)silyl
TON	turnover number
UV-vis	ultraviolet-visible
vs	versus
XAS	X-ray absorption spectroscopy
δ	chemical shift
ΔE_Q	quadrupole splitting
ΔH^0	reaction enthalphy
$\Delta H^{\neq}$	activation enthalpy
$\Delta S^{\neq}$	activation entrophy
ε	extinction molar coefficient
λ	wavelenght
μ_B	Bohr magneton
μ_{eff}	effective magnetic moment
ρ	slope
σ_p	Hammett parameter

AGRADECIMIENTOS

Llegada al final de este camino, me gustaría agradecer a las personas que han contribuido a enriquecer esta experiencia.

En primer lugar quiero agradecer a mis directores de tesis, Miquel y Anna, por haberme acogido en el grupo y por todas sus enseñanzas. Os agradezco la paciencia, la confianza y el apoyo que nunca me habéis hecho faltar a lo largo de estos años.

También quiero agradecer a Xavi, siempre dispuesto a ayudar, y a Raquel, por su dedicación.

Además quiero agradecer a todos los compañeros del QBIS, que han compartido conmigo el día a día en el laboratorio, entre otras cosas, dando vida a muchos buenos recuerdos. A los miembros del NoNoMeCat, que han compartido conmigo cada meeting del network. A los miembros de los grupos del Prof. Albrecht, del Prof. Gebbink y del Dr. Scarborough, que me han hecho sentir bienvenida durante mis estancias. Stefano, per avermi incoraggiato agli albori.

Especialmente quiero agradecer a los amigos que han entrado en mi vida en estos años, gli amici che ne sono parte da tempo y a Diego. Habéis vivido conmigo una multitud de experiencias y emociones, añadiendo felicidad en este camino.

Infine voglio ringraziare la mia famiglia. In particolare questa tesi la dedico ai miei genitori, che giorno dopo giorno mi sostengono con amore e sono per me un punto di riferimento. A mio fratello, sempre pronto a farmi vedere le cose in una nuova luce. Ai miei nonni, che ne sarebbero stai orgogliosi.

ACKNOWLEDGEMENTS

GRAPHICAL ABSTRACT

SITE AND PRODUCT SELECTIVE C-H OXIDATION DIRECTED BY SOLVENT HYDROGEN BONDING

strong HBD solvents

CH₃CN

selective oxidation

overoxidation

remote C-H oxidation

X = OH, OR, NH₂, NHCOR

α-C-H oxidation

$BDE\ (Fe^{IV}O\text{-}H) - BDE\ (Fe^{III}O\text{-}H) \approx 20\ kcal\cdot mol^{-1}$

$Fe^{V}=O$

$Fe^{IV}=O$

$\log\ (k_2')$

BDE C-H (kcal mol⁻¹)

Chapter V. Ligand effects on the reactivity of oxoiron(IV) species supported by electronically tuned azamacrocycles (p. 83)

TABLE OF CONTENTS

LIST OF FIGURES

LIST OF TABLES

LIST OF SCHEMES

SUMMARY

Oxidations are an important type of reactions for biology and chemical synthesis, but current transformations are far from satisfactory in terms of substrate scope, selectivity and environmental impact. For the development of novel methods, oxidation reactions taking place in nature constitute an inspiration motif. Coordination complexes that reproduce basic aspects of the reactivity and selectivity of iron-dependent oxygenases may be used as oxidation catalysts. They can be considered bioinspired catalysts, operate under mild reaction conditions and employ waste-free hydrogen peroxide as oxidant. Particularly, bioinspired complexes bearing tetradentate ligands have been successfully applied in catalytic oxidation reactions, although improvement of their selectivity and activity continue to be open tasks requiring novel findings. At the same time, high-valent oxometal compounds have been extensively investigated, since they have been recognized as active species in biological and synthetic oxidation catalysts.

In this context, the objectives of this thesis were two. In first place, to investigate novel aspects to govern the selectivity of bioinspired complexes in the hydroxylation of unactivated C-H bonds. In second place, to gain understanding of factors governing the oxidative ability of high-valent oxoiron species. In Chapter III, a protocol that allows to achieve outstanding chemoselectivity and remote regioselectivity in catalytic C-H bond hydroxylation reaction was developed. In the followed strategy, fluorinated alcohols were used as reaction media, since they play a key role on the selectivity outcome due to their ability of establishing hydrogen bonding with polar groups. Employing these solvents, the relative reactivity of unactivated C-H bonds and C-H bonds in α to a polar group is reverted. Thus, chemoselective oxidation of alkanes could be achieved thanks to the minimization of overoxidation processes. Furthermore, taking advantage of the α C-H bond's deactivation, regioselectivity could be moved from proximal to remote positions in the oxidation of alcohols, ethers, amides and amines. In Chapter IV, an oxoiron(IV) and an oxoiron(V) species bearing the same supporting ligand were compared. The importance of such comparison lies in the opportunity of analyzing the impact of the different oxidation state of the metal center on the properties of the related metal based oxidants. Remarkably, the oxoiron(V) species was shown to be extremely more reactive than its oxoiron(IV) counterpart in HAT reaction and, moreover, exhibited a higher electrophilic character. Additionally, upon HAT from the substrate to the oxidant, the hydroxyl rebound step occurred rapidly exclusively when the oxoiron(V) compound was used as oxidant. Consequently, only with the latter stereospecific hydroxylations were feasible. Instead, the oxoiron(IV) species reacted with C-H bonds generating long-lived alkyl radicals. Lastly, in Chapter V, the reactivity of oxoiron(IV) species was further explored, making use of a series of complexes bearing a tetradentate ligand where the electronic properties were systematically modified by introducing different substituents in a pyridine donor. Modulation of the electron donating abilities of the ligand translated into modest effects in HAT and OAT reactions of the corresponding oxoiron(IV)

complexes. Most interestingly, two geometrical isomers were identified for each oxoiron(IV) complex, differing in the relative position of the oxo with respect to a pyridine or an aliphatic amine donor. It was demonstrated that this aspect affects the reactivity of the oxoiron(IV) species in HAT and OAT reactions.

RESUM

Les oxidacions són un tipus de reaccions importants en la biologia i en la síntesi química, malgrat que les transformacions actuals estan lluny de ser satisfactòries pel que fa al rang de substrats, selectivitat i impacte ambiental. Per al desenvolupament de nous mètodes, les reaccions d'oxidació que tenen lloc a la natura són una font d'inspiració. Els complexes de coordinació que reprodueixen els aspectes bàsics de la reactivitat i selectivitat de les oxigenases ferro-dependents poden utilitzar-se com a catalitzadors de reaccions d'oxidació. Poden considerar-se catalitzadors bioinspirats, actuen en condicions suaus de reacció i utilitzen el "waste-free" peròxid d'hidrògen com a oxidant. En particular, els complexes bioinspirats suportats per lligands tetradentats s'han aplicat de manera exitosa en reaccions d'oxidació catalítiques, tot i que la millora de la seva selectivitat i activitat requereixen nous avenços en aquest camp. Al mateix temps, s'han investigat de manera extensiva els compostos oxometàlics en alts estats d'oxidació, ja que han estat identificats com a espècies actives en catalitzadors d'oxidació biològics i sintètics. En aquest context, els objectius d'aquesta tesi són dos. En primer lloc, investigar aspectes innovadors per governar la selectivitat dels complexes bioinspirats en la hidroxilació d'enllaços C-H no activats. En segon lloc, entendre millor els factors que governen la capacitat oxidativa de les espècies oxoferro d'alta valència. En el Capítol III, s'ha desenvolupat un protocol que permet l'assoliment d'una quimioselectivitat remarcable i una regioselectivitat cap a posicions remotes en reaccions catalítiques d'hidroxilació d'enllaços C-H. En l'estratègia seguida, es van utilitzar alcohols fluorats com a medi de reacció, ja que juguen un paper crucial en la selectivitat degut a la seva capacitat d'establir ponts d'hidrogen amb grups polars. Utilitzant aquests solvents, s'aconsegueix revertir la reactivitat relativa d'enllaços C-H no activats i enllaços C-H en α d'un grup polar. Així doncs, es pot aconseguir l'oxidació quimioselectiva d'alcans gràcies a la minimització de processos de sobreoxidació. A més, aprofitant la desactivació d'enllaços α C-H, la regioselectivitat es pot desplaçar de posicions proximals a posicions allunyades en l'oxidació d'alcohols, èters, amides i amines. En el Capítol IV, s'han comparat espècies oxoferro(IV) i oxoferro(V) suportades pel mateix lligand. La importància d'aquesta comparació rau en l'oportunitat d'analitzar l'impacte del diferent estat d'oxidació del centre metàl·lic en les propietats dels oxidants metàl·lics relacionats. Notablement, l'espècie oxoferro(V) va resultar ser extremadament més reactiva que el seu equivalent oxoferro(IV) en reaccions d'HAT i, a més a més, exhibeix un caràcter més electrofílic. Addicionalment, després de l'HAT del substrat a l'oxidant, el pas de rebot del grup hidroxil ocorre de manera ràpida només en utilitzar el compost oxoferro(V) com a oxidant. En conseqüència, només amb aquest últim es poden obtenir reaccions d'hidroxilació estereoespecífiques. En canvi, l'espècie oxoferro(IV) reacciona amb enllaços C-H generant radicals alquílics de vida llarga. Finalment, en el Capítol V, es va estudiar la reactivitat d'espècies oxoferro(IV) utilitzant una sèrie de complexes suportats per un lligand tetradentat en que les propietats electròniques es van modificar de manera sistemàtica, introduint diferents substituents en

una piridina. La modulació de les capacitats electrodonadores del lligand es van traduir en efectes modestos en les reaccions de HAT i OAT dels corresponents complexes oxoferro(IV). De manera interessant, per cada complex oxoferro(IV) es van identificar dos isòmers geomètrics, diferenciats per la posició relativa de l'oxo respecte a la piridina o a una amina alifàtica. Es va demostrar que aquest aspecte afecta la reactivitat de les espècies oxoferro(IV) en reaccions de HAT i OAT.

RESUMEN

Las oxidaciones son un tipo de reacciones importantes para la biología y la síntesis química, pero las transformaciones actuales distan de ser satisfactorias en términos de rango de sustratos, selectividad e impacto ambiental. Para el desarrollo de nuevas metodologías, las reacciones de oxidación que tienen lugar en la naturaleza constituyen una fuente de inspiración. Los complejos de coordinación que reproducen los aspectos básicos de la reactividad y selectividad de las oxigenasas basadas en hierro pueden usarse como catalizadores de reacciones de oxidación. Pueden considerarse catalizadores bioinspirados, actúan en condiciones de reacción suaves y emplean "waste-free" peróxido de hidrógeno como oxidante. En particular, los complejos bioinspirados soportados por ligandos tetradentados se han aplicado con éxito en reacciones de oxidación catalíticas, aunque la mejora de su selectividad y actividad siguen siendo cuestiones abiertas que requieren descubrimientos novedosos. Al mismo tiempo, se han investigado extensamente los compuestos oxometálicos en alto estado de oxidación, ya que han sido identificados como especies activas tanto en catalizadores de oxidación biológicos como sintéticos.

En este contexto, los objetivos de esta tesis son dos. En primer lugar, investigar aspectos innovadores para gobernar la selectividad de los complejos bioinspirados en la hidroxilación de enlaces C-H no activados. En segundo lugar, comprender mejor los factores que rigen la capacidad oxidativa de las especies oxohierro de alta valencia. En el Capítulo III, se ha desarrollado un protocolo que permite lograr una quimioselectividad remarcable y una regioselectividad remota en reacciones catalíticas de hidroxilación de enlaces C-H. En la estrategia seguida, se utilizaron alcoholes fluorados como medio de reacción, ya que desempeñan un papel fundamental en la selectividad debido a su capacidad de establecer puentes de hidrógeno con grupos polares. Utilizando estos disolventes, se consigue revertir la reactividad relativa de enlaces C-H no activados y enlaces C-H en α a un grupo polar. Así pues, se puede conseguir la oxidación quimioselectiva de los alcanos gracias a la minimización de los procesos de sobreoxidación. Además, aprovechando la desactivación de los enlaces C-H en α, la regioselectividad puede desplazarse de posiciones próximas a posiciones remotas en la oxidación de alcoholes, éteres, amidas y aminas. En el Capítulo IV, se han comparado especies oxohierro(IV) y oxohierro(V) soportadas por el mismo ligando. La importancia de esta comparación reside en la oportunidad de analizar el impacto del diferente estado de oxidación del centro metálico en las propiedades de los oxidantes metálicos correspondientes. Notablemente, la especie oxohierro(V) resultó extremadamente más reactiva que su homóloga oxohierro(IV) en reacción de HAT y, además, exhibe un mayor carácter electrofílico. Adicionalmente, después del HAT del sustrato al oxidante, el paso de rebote del grupo hidroxilo ocurre rápidamente sólo cuando se utiliza el compuesto de oxohierro(V) como oxidante. Por consiguiente, sólo con este último se pueden conseguir hidroxilaciones estereoespecíficas. En cambio, la especie de oxohierro(IV) reacciona con enlaces C-H generando radicales alquílicos de

vida larga. Por último, en el Capítulo V, se estudió la reactividad de las especies oxohierro(IV) utilizando una serie de complejos soportados por un ligando tetradentado en el cual las propiedades electrónicas se modificaron sistemáticamente, mediante la introducción de diferentes sustituyentes en una piridina. La modulación de las propiedades electrodonadoras del ligando se tradujeron en efectos modestos en las reacciones de HAT y OAT de los correspondientes complejos de oxohierro(IV). De manera interesante, por cada complejo de oxohierro(IV) se identificaron dos isómeros geométricos, que difieren en la posición relativa del ligando oxo con respecto a la piridina o una amina alifática. Se demostró que este aspecto afecta a la reactividad de las especies oxohierro(IV) en las reacciones HAT y OAT.

Chapter I

General introduction

I.1 ALKANE C-H BOND OXIDATION

The development of synthetic strategies for direct functionalization of C-H bonds constitute a longstanding goal.[1-3] Particularly, alkane C-H bond oxidation represents a fundamental transformation in organic chemistry, as it allows the conversion of abundant hydrocarbons into valuable compounds, such as alcohols and ketones.[4] Nonetheless, the inert character of aliphatic C-H bonds often required the use of undesirable strong oxidants and harsh reaction conditions.

The main drawback to move forward in the field is related to selectivity issues. Considering the higher reactivity of oxygenated products with respect to the starting materials, avoiding overoxidation is particularly challenging. Moreover, the large number of C-H bonds within a molecule makes also site selectivity a very difficult problem. Certainly, in order to apply C-H bond oxidation in synthetically useful processes, efficiency and selectivity limitations must be addressed. In this context, nature is a helpful source of inspiration, as these hurdles are overcome by enzymes.[5, 6] Thus, in an attempt to reproduce the reactivity of metalloenzymes, several synthetic bioinspired complexes have been prepared and widely investigated as catalysts in oxygenation reactions.[7, 8] Additionally, efforts have been devoted towards the understanding of the reaction mechanisms, as this knowledge can help to get insight into the aspects regulating the reactivity of such model compounds.[9-11]

I.2 SELECTIVITY IN HYDROGEN ATOM TRANSFER PROCESSES

Hydrogen atom transfer (HAT), being a crucial step in a large array of C-H bond functionalizations, is an especially interesting reaction that has been extensively studied in the last century.[12-15]

This process involves the abstraction of a hydrogen atom (H$^\bullet$) by a radical or a radical-like species. Usually nitrogen and oxygen centered radicals, or less commonly carbon ones, account for the former,[16] while dioxiranes,[17, 18] oxaziridines[19, 20] or hypervalent iodine species[21, 22] are representative examples of the latter.

In biological systems, such heme and non-heme oxygenases, alkane hydroxylation is initiated as well through a HAT.[5, 6] In these cases, the proton and the electron are not transferred to the same atom. Instead, the proton moves to the oxo ligand while the electron is accepted by the metal center, which formally decreases its oxidation state, or by the porphyrin cation radical. As shown on the top of Scheme I.1, in the hydroxylation carried out by heme cytochrome P450 enzymes (CYP450) a formal oxoiron(V) species, namely the oxoiron(IV) porphyrin cation radical compound I (Cpd-I), abstract an H$^\bullet$ from the substrate. Thus, a short lived alkyl radical and a hydroxoiron(IV) intermediate are formed. The alkyl radical rapidly recombines with the hydroxyl moiety of the hydroxoiron(IV) intermediate, prior to diffuse from the active site, giving the oxidation product. As a consequence, oxidation occurs with high level of stereoretention. In the case of non-heme iron oxygenases, such as α-ketoglutarate (α-KG) dependent enzymes (Scheme I.1, bottom), a similar mechanism is

involved in the hydroxylation of C-H bonds but the initial electron acceptor is different. First, an HAT process occurs through the transfer of the proton to the oxo moiety of the oxoiron(IV) species and of the electron to the iron center. Then, the hydroxoiron(III) intermediate undergoes hydroxyl rebound to the short-lived newly formed alkyl radical, affording the final hydroxylated product.
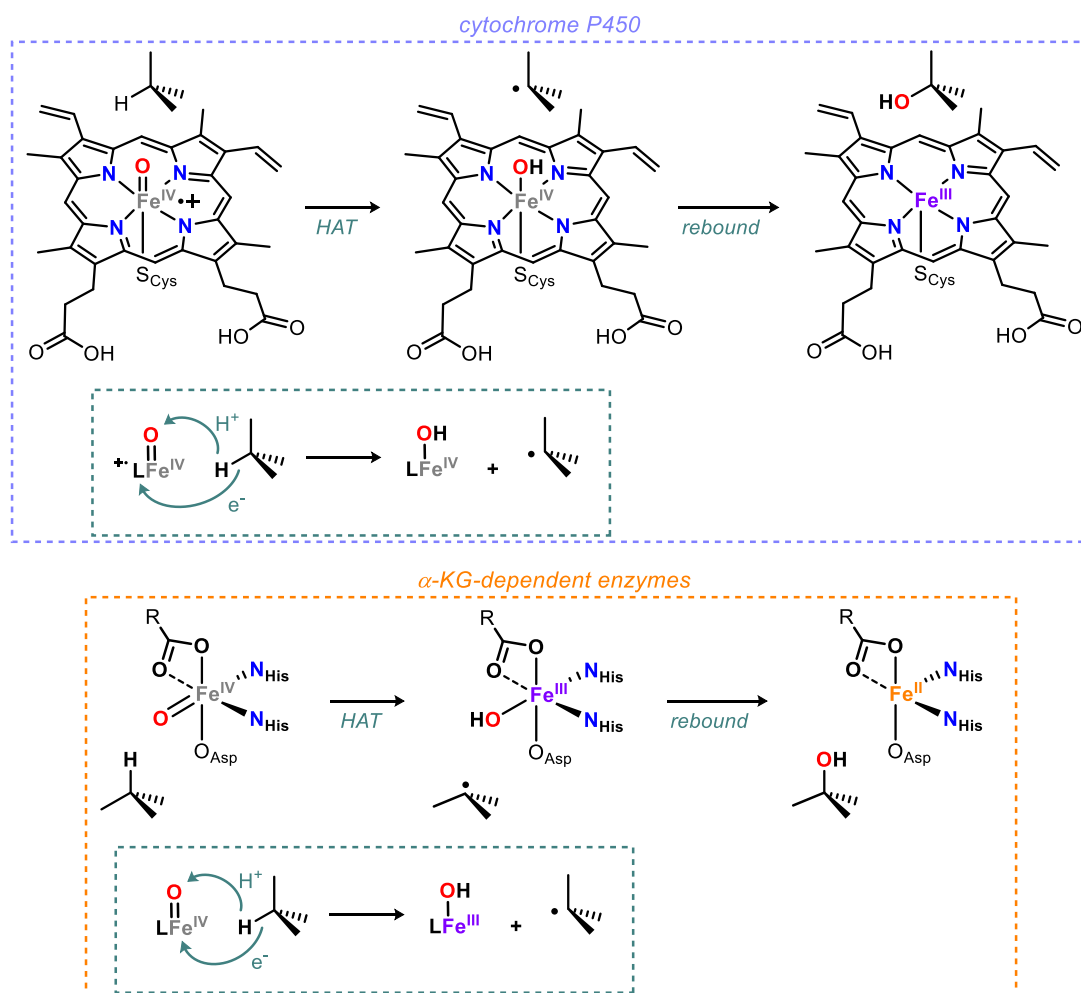
Scheme I.1. Schematic representation of hydroxylation reaction mediated by CYP450 (top)[5] and α-KG-dependent enzymes (bottom).[6]

In analogy to enzymes, the hydroxylation of C-H bonds catalyzed by bioinspired iron and manganese complexes takes place through an initial HAT, from the substrate to a high-valent oxometal species, followed by a rapid hydroxyl rebound (Scheme I.2).[8, 9, 11] In order to get a stereospecific transformation, the latter has to be fast enough to avoid the diffusion of the radical from the cage.
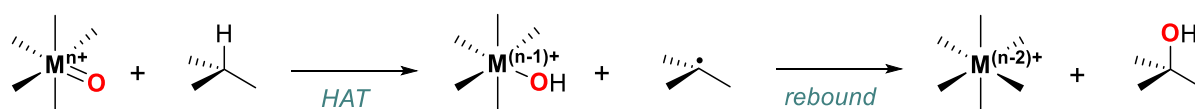
Scheme I.2. Hydroxylation reaction mediated by oxometal species of bioinspired complexes.

I.2.1 Relative reactivity of C-H bonds

In the above mentioned transformations selectivity represents a crucial issue, especially for the oxidation of aliphatic C-H bonds. Organic molecules often contain multiple and non-equivalent aliphatic C-H bonds, a feature that makes site-selectivity a major challenge. Thus, to govern the relative reactivity of C-H bonds against HAT agents and to devise mechanisms that enable its modulation are key questions to solve in order to design site-selective C-H oxidation reactions.

One of the most important aspects that govern the relative reactivity of a C-H bond is its bond dissociation energy (BDE), which reflects its strength.[23] As a general rule, weak C-H bonds are prone to oxidation. For example, benzylic or allylic C-H bonds are weak because of the stabilization of the corresponding radicals, and are easier to oxidize than unactivated C-H bonds, such as the ones of saturated hydrocarbons (Scheme I.3, top). Additionally, tertiary C-H bonds are usually more reactive than secondary and primary ones, being their strength smaller (Scheme I.3, bottom).
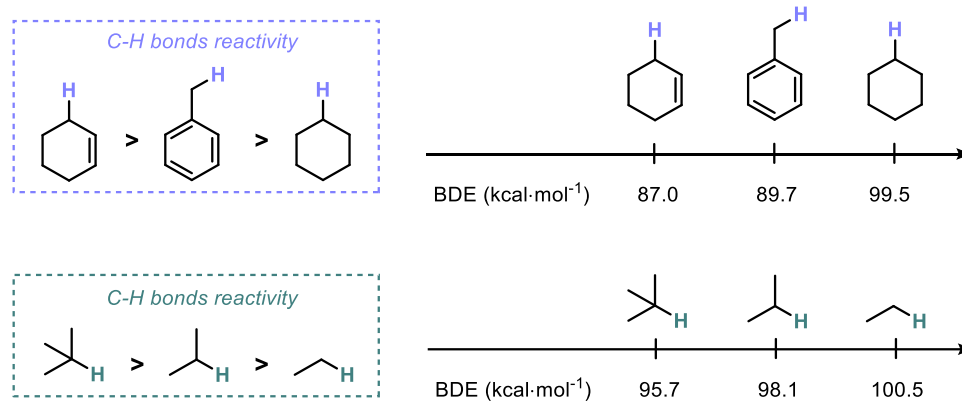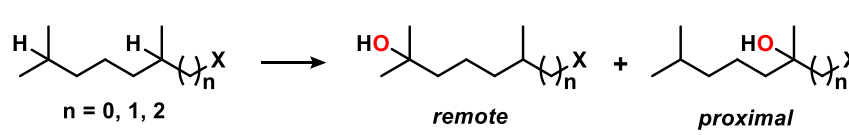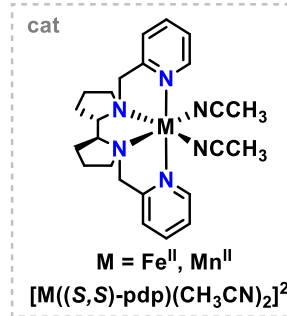
Scheme I.3. BDE of C-H bonds and their relative reactivity.

Nevertheless, to target selectively a specific C-H bond, a part from BDEs other properties have to be considered.[24]

A first element of discrimination among C-H bonds with comparable bond dissociation energies is represented by their relative electronic properties. Accounting for the electrophilic character of high-valent oxometal species,[9] the most electron-rich C-H bond should be preferentially abstracted. On the opposite side, the presence of an electron withdrawing group (EWG) on the substrate may guide the regioselectivity of the reaction, favoring the oxidation in the most remote position with respect to this substituent.

In a milestone work reported by Chen and White in 2007, this trend was observed for hydroxylation reactions catalyzed by $[Fe^{II}((S,S)\text{-pdp})(CH_3CN)_2](SbF_6)_2$, used in combination with hydrogen peroxide and acetic acid (Table I.1).[25] Some years later, the same selectivity trend was also found by Bryliakov and co-workers with manganese based complexes (Table I.1).[26]
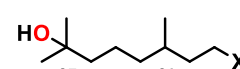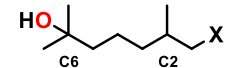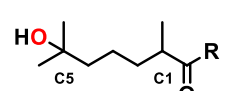
Table I.1. Regioselectivity in C-H bonds hydroxylation depending on electronic properties.[25, 26]

entry	M	substrate	X	yield(%)	remote:proximal
1[a]	Fe		H	48	1:1
2[b]	Mn		H	69	1:1
3[a]	Fe		OAc	43	5:1
4[b]	Mn		OAc	54	7:1
5[a]	Fe		Br	39	9:1
6[b]	Mn		Br	70	34:1
7[a]	Fe		OAc	49	29:1
8[a]	Fe		Br	48	20:1
9[a]	Fe		CH_3	52	>99:1
10[a]	Fe		OCH_3	56	>99:1

[a]3x[cat (5 mol%), H_2O_2 (1.2 equiv), AcOH (50 mol%)], CH_3CN, RT, 30 min.
[b]cat (0.1 mol%), H_2O_2 (1.3 equiv), AcOH (14 equiv), CH_3CN, 0 °C, 3 h.

In the oxidation of dihydrocitronellol derivatives, the most favored oxidation site corresponds to the tertiary C-H bonds, because they are weaker compared to secondary or primary ones. In the absence of a substituent X, the two tertiary C-H bonds are indistinguishable (entries 1 and 2, Table I.1). However, in the presence of a EWG, it is possible to guide the oxidation towards the more electron-rich tertiary C-H bond, which corresponds to the one located far away from the substituent (remote position). Being the electronic an inductive effect, the selectivity towards the remote position is higher as shorter is the distance between the proximal C-H bond and the functional group. This is clearly exemplified by the results shown in Table I.1. When the proximal tertiary C-H bond is located in β with respect to the EWG (entries 7 and 8, Table I.1), the selectivity for the hydroxylation of the remote position is between two and six times higher than when the EWG is located in γ (entries 3 and 5, Table I.1). The situation is even more extreme when the proximal C-H bond is in the α position with respect to the substituent. Indeed, in this case an exclusive remote oxidation is observed (entries 9 and 10, Table I.1). The same phenomenon can also be used to guide the selectivity towards remote methylenic sites in the presence of α or β located weaker tertiary C-H bonds.[27] As shown in the examples in Scheme I.4, the deactivation of the proximal positions, due to the presence

of the ester substituent, minimizes the tertiary C-H bond oxidation at Cα (1% yield, example on the top) or Cβ (9% yield, example on the bottom). Thus, methylenic oxidation of the remote C-H bonds (C4 and C5 in Scheme I.4) is achieved with 99% and 86% selectivity when the tertiary C-H bond is placed, respectively, in the α and β position.
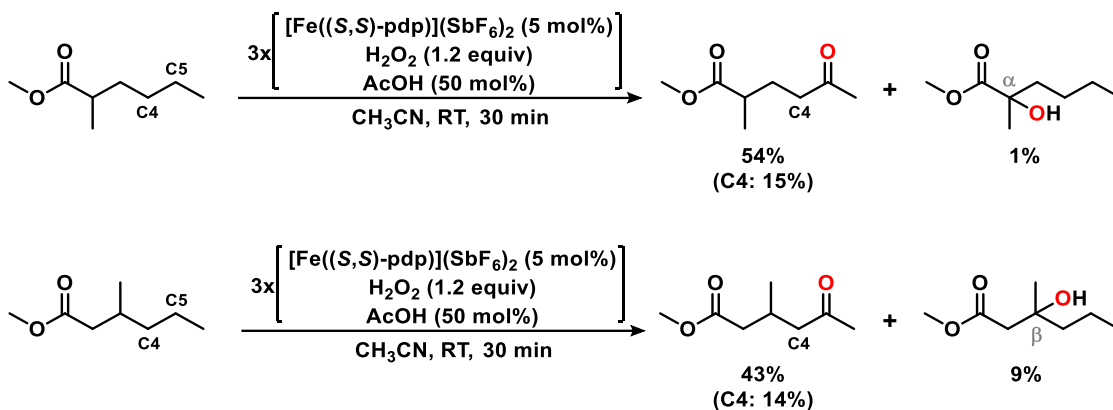
Scheme I.4. Influence of electronic effect on secondary versus tertiary C-H bonds hydroxylation.[27]

Additionally, C-H bonds located at the same distance from a polar group, thus with similar electronic properties, can be discriminated on the basis of their relative steric hindrance. This is illustrated in the oxidation of (−)-acetoxy-*p*-menthane. For this substrate there are two tertiary C-H bonds, located in carbons C1 and C8, which are four bonds away with respect to the acetate group. Theoretical calculations, done through DFT analysis, indicated that these two tertiary C-H bonds have similar electronic density in the most stable conformation of (−)-acetoxy-*p*-menthane. Then, they are electronically indistinguishable. However, the oxidation using $[M((S,S)\text{-pdp})(CH_3CN)_2]^{2+}$ (M = Fe^{II} or Mn^{II}) in combination with hydrogen peroxide and acetic acid occurs preferentially at C1 (Scheme I.5).[25, 26] This is rationalized by taking into account that in the oxidation of C1-H, being less hindered than C8-H, the steric interaction between the substrate and the bulky high-valent oxometal active species is less important.
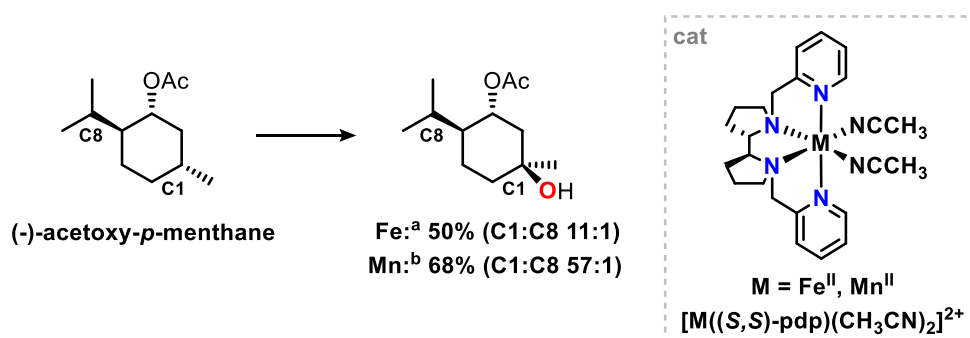
^{a}3x[cat (5 mol%), H_2O_2 (1.2 equiv), AcOH (50 mol%)], CH_3CN, RT, 30 min.
^{b}cat (0.1 mol%), H_2O_2 (1.3 equiv), AcOH (14 equiv), CH_3CN, 0 °C, 4 h.

Scheme I.5. Regioselectivity in C-H bonds hydroxylation depending on steric properties.[25, 26]

Finally, for C-H bonds with similar electronic and steric properties, stereoelectronic factors can be a useful tool of differentiation. Particularly, in cyclic substrates it is possible to discriminate C-H bonds on the basis of strain release.[28] This could be an important aspect for synthetic applications, considering that complex organic molecules are target substrates that often contain fused rings.

The impact of strain release is exemplified for the oxidation of *cis*-4-methylcyclohexyl-1-pivalate, performed with the bulky [Fe^{II}(OTf)$_2$((*S,S,R*)-mcpp)] catalyst (Scheme I.6) in combination with hydrogen peroxide and acetic acid. For this specific case, exclusive tertiary C-H bond oxidation at C1 is observed. However, the oxidation of the corresponding *trans* isomer also affords secondary C-H bond oxidation (Scheme I.6, top).[29] This result can be explained considering that, in the *cis* isomer, HAT from the equatorial tertiary hydrogen (H$_{eq}$) leads to a decrease of 1,3-diaxial interactions, thanks to the movement of the methyl substituent in the newly formed alkyl radical (Scheme I.6, bottom). Conversely, in the *trans* isomer the tertiary hydrogen atom is located in the axial position (H$_{ax}$) and its oxidation is disfavored in terms of strain release. For this reason, for the *trans* isomer the secondary C-H bonds, despite being stronger than the tertiary one, are as well oxidized.
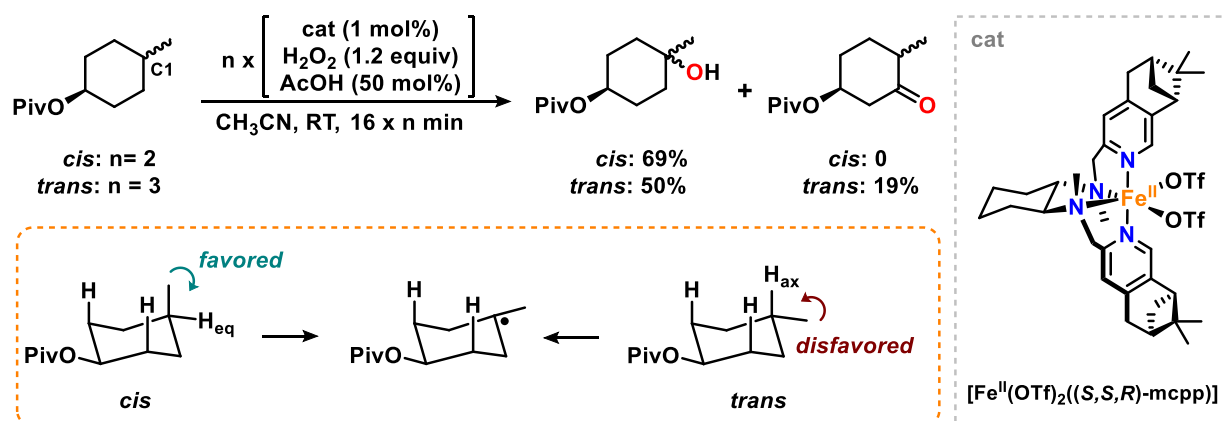
Scheme I.6. Regioselectivity in C-H bonds hydroxylation depending on stereoelectronic properties.[29]

I.2.2 Impact of the catalyst structure on selectivity and catalytic activity

Catalyst design represents another strategy to guide the hydroxylation site selectivity and to improve the efficiency of the system. Most importantly, it may allow to implement selectivities that differ from the innate relative reactivity of C-H bonds towards standard HAT agents.

The influence of the catalyst structure in the outcome of an alkane hydroxylation reaction was first observed by modulating the steric hindrance of the ligand, which impacts the accessibility of the substrate to the metal center. In this regard, in 2009 Gomez et al. reported iron complexes bearing tetradentate N-based ligands with a bulky substituent, namely a pinene group, on the pyridine arms ((*R*)-mepp, (*S,S,R*)-mcpp in Scheme I.7).[29] As shown in Scheme I.7, the introduction of the pinene group improves the catalytic activity, being the yields with [Fe^{II}(OTf)$_2$((*R*)-mepp)] and [Fe^{II}(OTf)$_2$((*S,S,R*)-mcpp)] substantially higher than the ones obtained with the non-substituted

[Fe^{II}(OTf)$_2$(mep)] and [Fe^{II}(OTf)$_2$((*S,S*)-mcp)] counterparts (49-57% vs 36-38%). This result was rationalized considering that the pinene arms construct a defined cavity around the iron center, thus preventing the formation of catalytically inactive dimers that are thermodynamic sinks for catalysts decomposition. As a demonstration, time-profile analysis reveals that [Fe^{II}(OTf)$_2$((*S,S,R*)-mcpp)] is capable to restore its activity upon a second addition of oxidant. Conversely, according to mass spectrometry analysis, with [Fe^{II}(OTf)$_2$((*S,S*)-mcp)] the precursor of the active species is consumed when the first added hydrogen peroxide is depleted and the formation of inactive oxo dimers is identified.
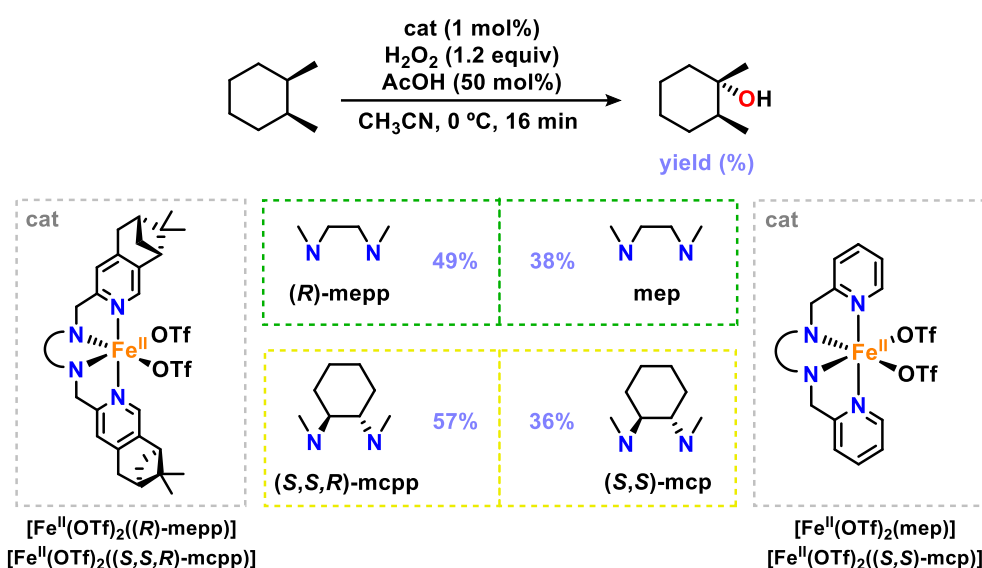
Scheme I.7. Impact of the steric hindrance of the catalyst on its activity.[29]

Additionally, in a subsequent work, the same group showed that changing the backbone of the ligand could have an important impact on the regioselectivity of the hydroxylation.[30] As represented in Scheme I.8, the oxidation of 1,1-dimethylcyclohexane using [Fe^{II}(OTf)$_2$((*S,S,R*)-pdpp)] as catalyst affords products at positions C2, C3 and C4, and relative yields follow the statistical distribution of the number of C-H bonds (C2:C3:C4 40:40:20). However, replacement of the bipyrrolidine ring of the pdpp by the diaminocyclohexane in the mcpp ligand allows to significantly reduce the oxidation at C2, the sterically more stressed site. Thus, with the mcpp ligand it is possible to discriminate among different methylenic sites on the basis of a steric interaction dictated by the diaminocyclohexane backbone. Indeed, the same trend was also observed in the absence of the pinene arms, using [Fe^{II}(OTf)$_2$((*S,S*)-mcp)], [Fe^{II}(OTf)$_2$((*S,S*)-pdp)] and [Fe^{II}(OTf)$_2$(mep)] as catalysts, thus demonstrating that the diaminocyclohexane backbone is the most sensitive to the steric hindrance of the substrate C-H bonds.[31]
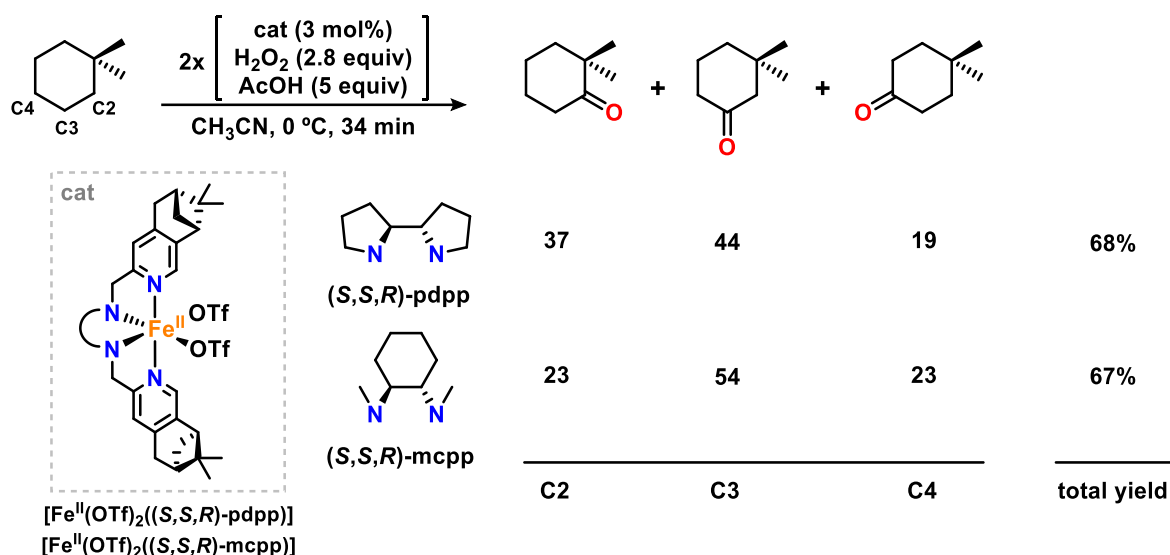
Scheme I.8. Impact of the backbone of the ligand on C-H bond hydroxylation regioselectivity.[30]

Importantly, the sensitivity of the catalyst to the steric properties of the substrate can lead to the preferential oxidation of less sterically hindered methylenic sites in the presence of the inherently weaker tertiary C-H bonds. This is illustrated in the oxidation of *trans*-1,2-dimethylcyclohexane shown in Scheme I.9. The presence of the bulky TIPS substituent (TIPS = tris(isopropyl)silyl) in position 5 of the pyridines allows to improve the secondary over tertiary C-H hydroxylation ratio (2º/3º) from 1 and 3, obtained using non-substituted [Fe^{II}(OTf)$_2$((*S,S*)-pdp)] and [Fe^{II}(OTf)$_2$((*S,S*)-mcp)] catalysts, to 4 and 13, achieved with TIPS-substituted [Fe^{II}(OTf)$_2$((*S,S*)-^{TIPS}pdp)] and [Fe^{II}(OTf)$_2$((*S,S*)-^{TIPS}mcp)] catalysts.[32] Of notice, as mentioned above, the ligands containing the diaminocyclohexane backbone are especially sensitive to steric effects and provide higher levels of regioselectivity.
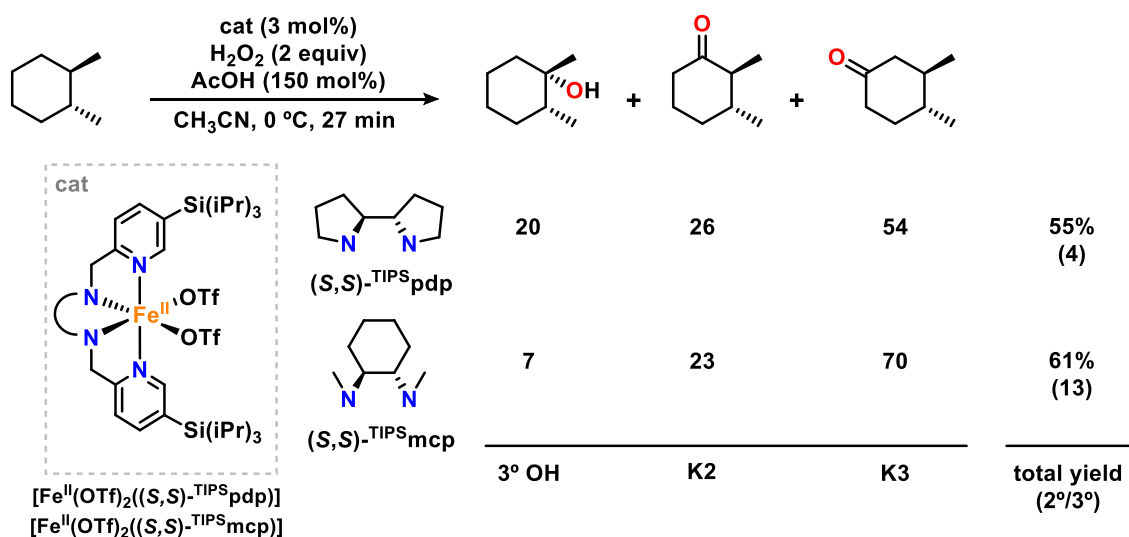
Scheme I.9. Impact of steric interaction on C-H bond hydroxylation regioselectivity.[32]

On the same line, in 2013 Gormisky and White reported a variation of the pdp ligand in which an aryl ring with *ortho*-trifluoromethyl groups was placed in the position 5 of the pyridines ((*R,R*)-^{CF3}pdp in Scheme I.10).[33] The comparison between [Fe^{II}((*R,R*)-pdp)(CH$_3$CN)$_2$]$^{2+}$ and [Fe^{II}((*R,R*)-^{CF3}pdp)(CH$_3$CN)$_2$]$^{2+}$ reinforced the idea that the catalyst structure can dictate the selectivity outcome of C-H bond oxidation reactions. Particularly, the use of [Fe^{II}((*R,R*)-^{CF3}pdp)(CH$_3$CN)$_2$]$^{2+}$ allows to improve the selectivity towards methylenic oxidation, overriding the preference for tertiary C-H bond observed with [Fe^{II}((*R,R*)-pdp)(CH$_3$CN)$_2$]$^{2+}$. For example, in the oxidation of *trans*-4-methylcyclohexyl acetate, the 2º/3º ratio increases by a factor of six employing [Fe^{II}((*R,R*)-^{CF3}pdp)(CH$_3$CN)$_2$]$^{2+}$ as catalyst (Scheme I.10). This indicates that the steric interactions dictated by the bulkiness of the catalyst lead to overcome the electronic bias of the substrate, moving the oxidation from tertiary C-H bonds to the stronger secondary ones.
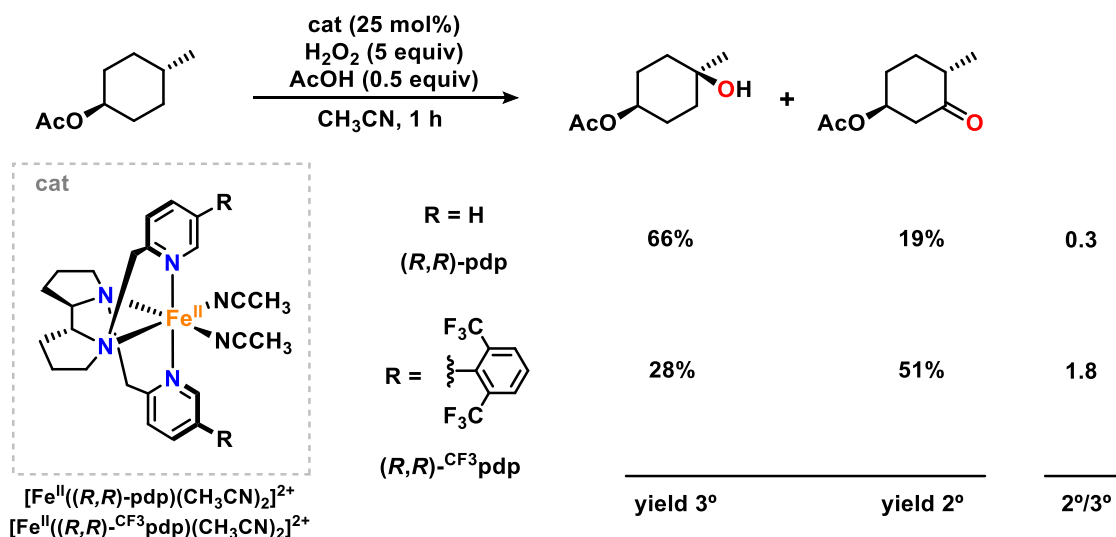
Scheme I.10. Impact of catalyst structure on C-H bond hydroxylation chemoselectivity.[33]

Despite being much less studied, the impact of structural changes on the activity of manganese-based catalysts has also been investigated.[34, 35] Sun and co-workers reported that the substitution of pyridine arms by benzoimidazole groups has a beneficial effect on the catalytic activity in benzylic C-H bond oxidations (Scheme I.11, top).[35] On the other hand, the combination of a pyiridine and a benzoimidazole arm is advantageous for the oxidation of unactivated C-H bonds (Scheme I.11, bottom).[34] Although a systematic study to elucidate the impact of the ligand structure on the catalytic activity of the system has not been reported, it could be noted that the substitution of a pyridine for a benzimidazole affects both the steric and the electronic properties of the manganese complex. Indeed, the introduction of benzimidazole moieties leads to a more rigid and more electron-rich system, compared to the one containing pyridine arms.
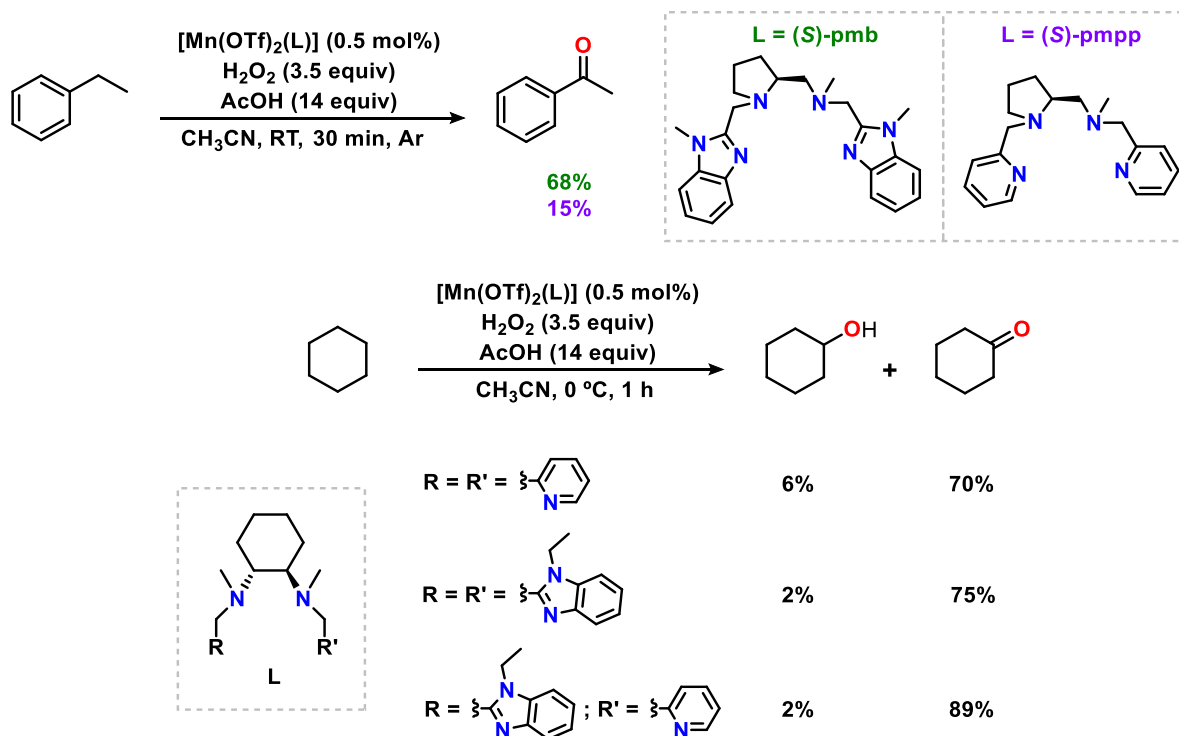
Scheme I.11. Impact of ligand structure on the efficiency of C-H bond hydroxylation.[34, 35]

I.2.3 Solvent effect on reactivity and selectivity

In HAT processes performed with organic radicals the reaction rates can be affected by the media used, due to the presence of hydrogen bond interactions between the solvent and the abstracting species or the substrate.[36-38]

Particularly, it has been observed that in HAT processes by alkoxyl radicals, in hydrogen bond acceptor (HBA) solvents (e.g. benzene or acetonitrile), using phenols as substrates, the reaction rate decreases with the increase of the HBA ability of the solvent (Scheme I.12, top).[39] As example, in the HAT from phenol to the cumoxyl radical (CumO$^{\bullet}$) the reaction rate decreases by a factor of 190 moving from n-octane ($k_2 = 110 \times 10^7$ M$^{-1}\cdot$s^{-1}), which is a non HBA solvent, to acetonitrile ($k_2 = 0.58 \times 10^7$ M$^{-1}\cdot$s^{-1}) (Scheme I.12, top). Conversely, in the same reaction the employment of hydrocarbons as substrates results in no significant changes in reaction rates.[40] As shown on the top of Scheme I.12, in the HAT from cyclohexane to the cumoxyl radical the reaction rate is almost the same independently of the reaction media used.

Then, in these reactions hydrogen bonds have to be formed between the substrate and the solvent, without involving the alkoxyl radical. Indeed, this explains why in the HAT from phenol the reactivity decreases when the HBA ability of the solvent increases. In this case, a desolvation of the substrate prior to its reaction is necessary. Instead, hydrocarbons do not establish hydrogen bonds with the solvent and, for this reason, no changes in reaction rates are observed when HBA solvents are used. In sharp contrast, when hydrogen bond donor (HBD) solvents (e.g. methanol or 2,2,2-

trifluoroethanol) are used in combination with alkanes, reaction rates increase with the increase of the HBD ability of the solvent (Scheme I.12, bottom).[41] Particularly, a significant increase of the rate is obtained using as reaction media 2,2,2-trifluoroethanol (TFE), which is a strong HBD solvent. As shown on the bottom of Scheme I.12, in the HAT from cyclohexane to the cumoxyl radical a four-fold increase in the reaction rate is observed moving from *n*-octane (k_2 = 1.08 x 10^6 M^{-1}·s^{-1}) to TFE (k_2 = 4.39 x 10^6 M^{-1}·s^{-1}). Thus, in this context, the hydrogen bonds have to be established between the alkoxyl radical and the solvent. Taking into account the charge separation arising in the transition state for the HAT from hydrocarbons to alkoxyl radicals, the formation of the above mentioned hydrogen bonds leads to a stabilization of the transition state (Scheme I.13). As a consequence, the reactions are accelerated employing solvents with increased HBD ability.

^{a}T = 23 ºC. ^{b}T = 30 ºC. ^{c}T = 25 ºC.
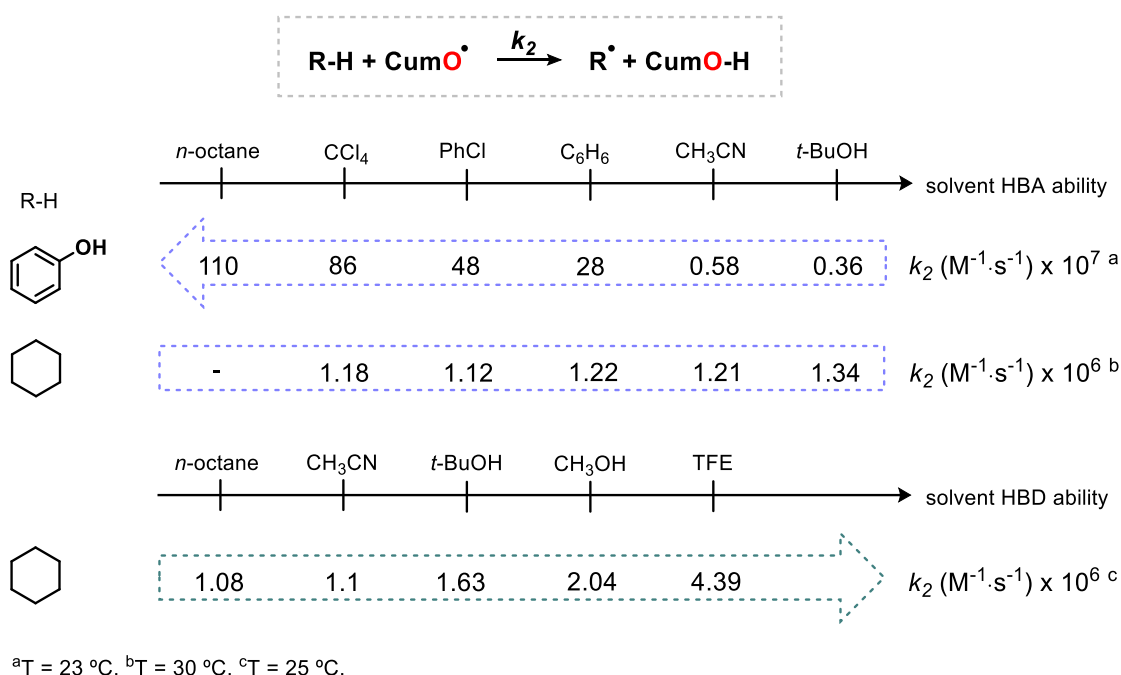
Scheme I.12. Solvent effect on HAT reaction rates.[39-41]
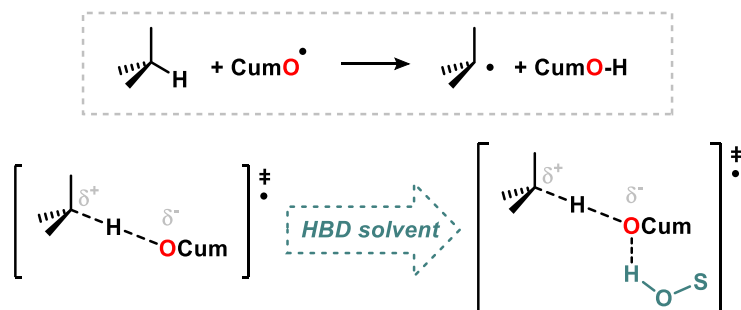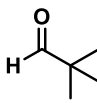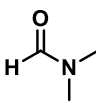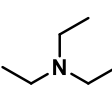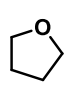
Scheme I.13. Stabilization of the transition state in HAT from hydrocarbons to cumoxyl radical.[13]

In spite of the fact that using TFE as solvent leads to an increase of the rate in HAT processes with hydrocarbons, the reaction of substrates with HBA sites shows the opposite trend (Scheme I.14).[38,

[41-44] Indeed, when aldehydes, amides, amines and ethers are used as substrates, changing isooctane for methanol or TFE as solvent causes a diminishment of one to two order of magnitude in the reaction rates, as shown in Scheme I.14. In these cases hydrogen bonds are established between the HBA site of the substrate and the solvent, resulting in a destabilization of the transition state and a consequent decrease of the reaction rates (Scheme I.15). These hydrogen bonding interactions between the substrate and the solvent also result in the deactivation of the C-H bond in α to the heteroatom towards electrophilic attack, an effect that could be used as a tool to modulate the regioselectivity of these transformations.

isooctane	1.12×10^8	7.7×10^6	2.9×10^8	1.21×10^7	k_2 (M$^{-1}\cdot$s^{-1})
CH$_3$OH	1.7×10^7	9.8×10^5	3.8×10^7	4.9×10^6	k_2 (M$^{-1}\cdot$s^{-1})
TFE	1.04×10^7	$<1 \times 10^4$	-	2.7×10^6	k_2 (M$^{-1}\cdot$s^{-1})

Scheme I.14. Solvent effect on HAT reaction rates for substrates bearing HBA sites.[38, 41-44]
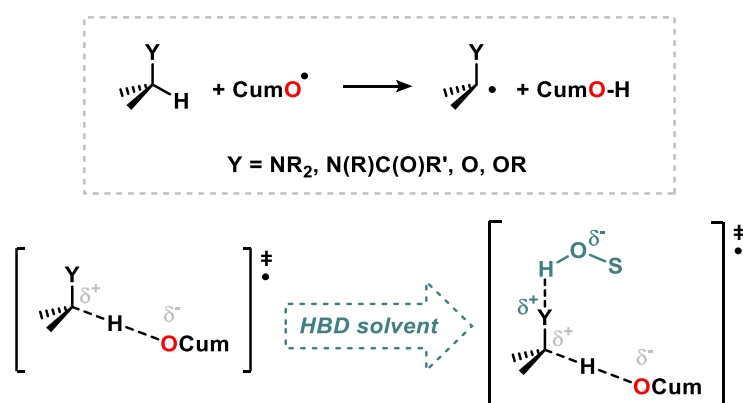
Scheme I.15. Destabilization of the transition state in HAT from HBA substrates to cumoxyl radical.[13]

In addition to the above described HAT processes, the use of fluorinated alcohols, particularly TFE and 1,1,1,3,3,3-hexafluoroisopropanol (HFIP), has been largely explored in the last decades in a variety of chemical transformations. Importantly, it has been observed that the employment of TFE and HFIP can significantly modify the efficiency and the selectivity of a target reaction.[45-49]

In a relevant work reported by Pappo and co-workers in 2017, the chemoselective benzylic C-H bond oxidation of methylarenes to benzaldehydes derivatives could be attained by using TFE or HFIP as reaction media.[50] In particular, the use of HFIP as solvent, a part from preventing the overoxidation of benzaldehydes to benzoic acids, results in highly efficient oxidations (example shown in Scheme I.16).

solvent	t	conversion	selectivity		
TFE	24 h	7%	100	:	0
HFIP	4 h	91%	90	:	1
HFIP[a]	4 h	62%	99	:	1

[a]under air
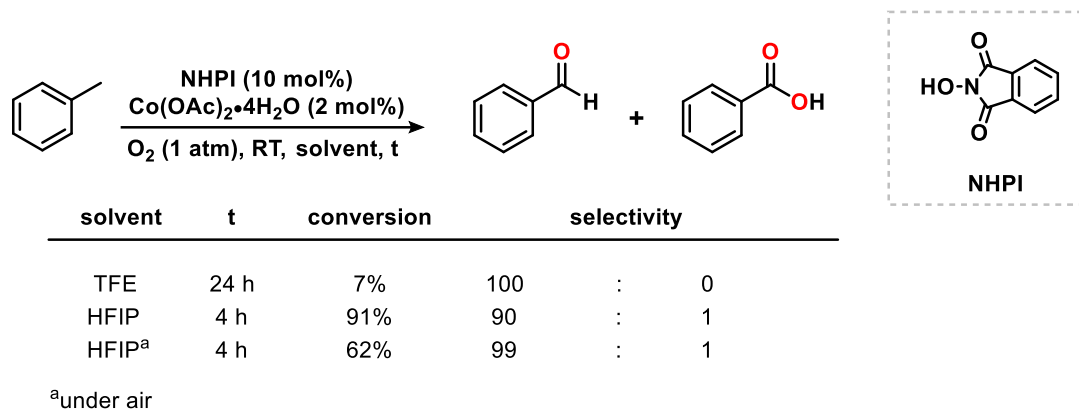
Scheme I.16. Chemoselective oxidation of toluene in fluorinated alcohol solvents.[50]

To elucidate the role of HFIP in the oxidation of methylarenes mechanistic studies have been carried out. Thus, thanks to computational and experimental studies, it has been highlighted that HFIP engages in hydrogen bonds with the carbonyl of the aldehyde, deactivating the α hydrogen. Indeed, the BDE of this hydrogen is 15 kcal·mol⁻¹ higher in the benzaldehyde-HFIP adduct than in the free benzaldehyde. As a consequence, aldehyde can be accumulated in the reaction mixture, conversely to what is observed when acetic acid is employed as solvent. Consequently, chemoselective oxidation of methylarenes can be obtained. Additionally, despite the exposure of benzaldehyde to molecular oxygen leads to its autoxidation to benzoic acid, process that occurs also when up to 1.5 equivalents of acetic acid or acetonitrile are added to the reaction mixture, the addition of HFIP to neat benzaldehyde blocked its autoxidation.

I.3 MECHANISTIC INSIGHT INTO BIOINSPIRED OXIDATION

I.3.1 Oxoiron species in iron-dependent oxygenases

Iron-dependent oxygenases constitute a valuable class of biological catalysts, due to their competence to perform challenging transformations with exquisite efficiency and selectivity.[5, 6] In these enzymes molecular oxygen is reductively activated, the O-O bond is cleaved and this results in the formation of high-valent oxoiron species, which are powerful electrophilic oxidants. As represented in Scheme I.17, in a number of these intermediates, such as for example in hemes and

α-KG-dependent oxygenases, the iron center possesses a formal +4 oxidation state.[51-54] Additionally, oxoiron(V) compounds have been postulated as possible oxidizing agents in the catalytic cycle of Rieske oxygenases.[55]
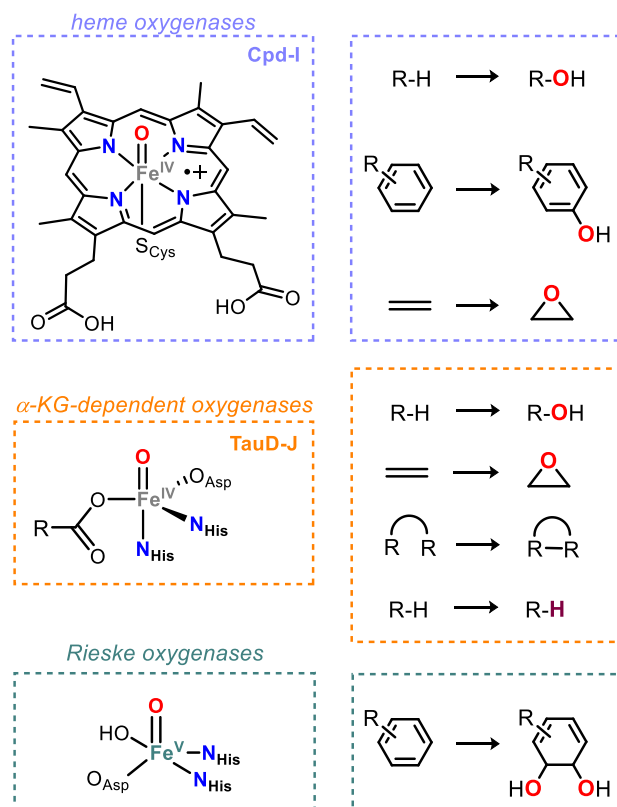
Scheme I.17. Schematic representation of high-valent oxoiron species in heme oxygenases, α-KG-dependent oxygenases and Rieske oxygenases (left) and their biological transformations (right).[10, 56]

Given the powerful oxidative ability of biological oxoiron species, in the last decades efforts have been devoted to the preparation of synthetic complexes capable to reproduce the reactivity and the selectivity found in nature. Thus, several synthetic oxoiron compounds have been reported.[9, 57] The following sections summarize the advances in the synthetic preparation of both oxoiron(IV) and oxoiron(V) compounds.

I.3.2 Synthetic oxoiron(IV) species

The first synthetic oxoiron(IV) fully characterized was reported by Que and co-workers in 2003.[58] By adding stoichiometric amounts of PhIO to a solution of [Fe^{II}(OTf)$_2$(tmc)] in CH$_3$CN at -40 ºC, a green intermediate with an absorption band at 820 nm was obtained in 90% yield within two minutes (Scheme I.18, top). Alternatively, this compound could be generated in three hours by adding 3 equivalents of H$_2$O$_2$. After exhaustive spectroscopic characterization (Scheme I.18, bottom) and the resolution of its X-Ray crystal structure, this species could be identified as a S = 1 oxoiron(IV) with

the general formula $[Fe^{IV}(O)(tmc)(CH_3CN)](OTf)_2$. The doublet in the Mössbauer spectrum showed a chemical shift (δ) of 0.17 mm·s^{-1}, fully consistent with the +4 oxidation state of the iron center, and a quadrupole spitting (ΔE_Q) of 1.24 mm·s^{-1}. The Fe-O distance (r_{Fe-O}) of 1.646 Å measured from the crystal structure analysis is also consistent with an oxoiron(IV) moiety. Unfortunately, the high stability of $[Fe^{IV}(O)(tmc)(CH_3CN)](OTf)_2$, which made possible its characterization and crystallization, compromises its reactivity. Indeed, this species was far from being a strong oxidant and reactivity studies indicated that it was only competent to perform oxygen atom transfer (OAT) to triphenylphosphine and HAT with substrates containing weak C-H bonds.

ESI-MS	UV-vis	MB	FT-IR	X-Ray
exp 184.4	λ_{max} = 820 nm	δ = 0.17 mm·s^{-1}	ν_{Fe-O} = 834 cm^{-1}	r_{Fe-O} = 1.646 Å
(calcd 184.5)	ε = 400 M^{-1}·cm^{-1}	ΔE_Q = 1.24 mm·s^{-1}		
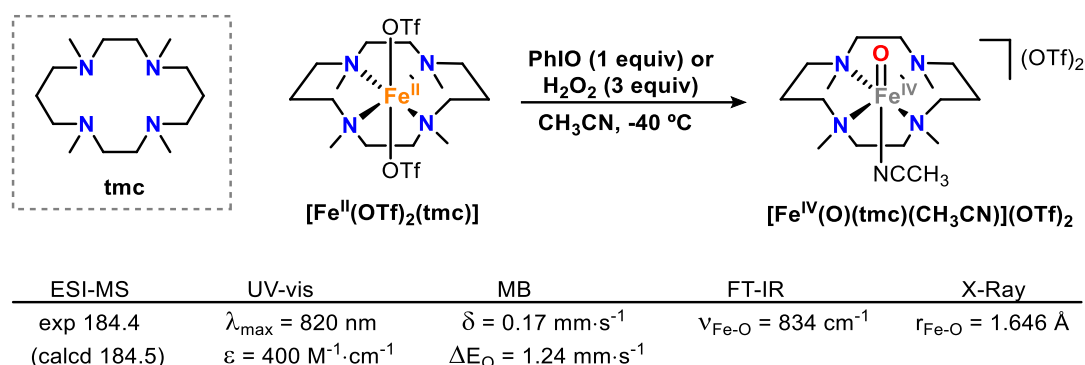
Scheme I.18. Representation of the tmc ligand (top left), generation of $[Fe^{IV}(O)(tmc)(CH_3CN)](OTf)_2$ by oxidation of its iron(II) precursor (top right) and main spectroscopic and spectrometric features of this oxoiron(IV) compound (bottom).[58]

Since this report, a number of oxoiron(IV) species containing tetradentate as well as pentadentate N-based ligands have been synthetized and characterized. Most commonly, these compounds are prepared by oxidation of the iron(II) precursors with the appropriate oxidant, including for example PhIO, H$_2$O$_2$, ^{t}BuOOH, *m*-CPBA, NaOCl and Bu$_4$NIO$_4$.[57, 59] For tetradentate ligands the corresponding oxoiron(IV) complexes present a labile site of coordination, which can be located either *cis* or *trans* to the oxo moiety depending on the manner that the ligand wraps around the iron center. The stability of such compounds is also highly dependent on the ligand architecture. In general, pentadentate and tetradentate systems with a *trans* labile site with respect to the oxo ligand are more stable than tetradentate systems with a labile site in a relative *cis* configuration with respect to the oxo group. In many cases, low temperatures are needed for the generation and stabilization of these oxoiron(IV) compounds. Similarly, the ligand architecture also determines the spin state of the iron center, so that both S = 1 and S = 2 species have been reported. Figure I.1 shows a selection of synthetic oxoiron(IV) compounds, classified depending on the ligand architectures.

Given the relatively large number of synthetic oxoiron(IV) species that have been reported to date, an extensive study of their oxidative reactivity and correlation with their structural and electronic features is possible. Such oxidation reactions have been mainly focused on OAT and HAT

processes.[60-63] The following sections will summarize the main reactivity features of synthetically generated oxoiron(IV) compounds.

tetradentate ligands (S = 1, S = 2)

S = 1: one trans labile site

[Fe^{IV}(O)(L^{8}Py$_2$)(CH$_3$CN)]$^{2+}$
t$_{1/2}$ (-20 °C) ~ 7 h

[Fe^{IV}(O)(L)(CH$_3$CN)]$^{2+}$
R = CH$_3$: L = tmc
t$_{1/2}$ (25 °C) ~ 10 h
R = Bn: L = tbc
t$_{1/2}$ (25 °C) ~ 100 min

[Fe^{IV}(O)(Pymac)(X)]$^{2+}$
X = CH$_3$CN
t$_{1/2}$ (25 °C) ~ 30 min

[Fe^{IV}(taml)(O)]$^{2-}$

S = 1: one cis labile site

[Fe^{IV}(O)(L)(CH$_3$CN)]$^{2+}$
R = R' = H: L = tpa
t$_{1/2}$ (10 °C) ~ 1 h
R = OCH$_3$, R' = CH$_3$: L = tpa*

[Fe^{IV}(O)(^{R}Pytacn)(H$_2$O)]$^{2+}$
R = H, Cl, CO$_2$Et, NO$_2$
t$_{1/2}$ (25 °C) > 90 min

[Fe^{IV}(O)(Me$_3$ntb)(Y)]$^{2+}$
t$_{1/2}$ (-40 °C) ~ 2 min

S = 2

[Fe^{IV}(O)(tpa^{Ph})]$^-$
t$_{1/2}$ (-40 °C) ~ 1h

[Fe^{IV}(O)(tqa)(CH$_3$CN)]$^{2+}$
t$_{1/2}$ (-40 °C) ~ 15 min

[Fe^{IV}(O)(TMG$_3$tren)]$^{2+}$
t$_{1/2}$ (-30 °C) ~ 4.3 h

pentadentate ligands (S = 1)

[Fe^{IV}(O)(L)]$^{2+}$
R = R' = H: L = N4Py
t$_{1/2}$ (25 °C) ~ 60 h
R = OCH$_3$, R' = CH$_3$: L = N4Py*
t$_{1/2}$ (30 °C) ~ 50 h

[Fe^{IV}(O)(MePy$_2$tacn)]$^{2+}$

[Fe^{IV}(O)(dpaq)]$^+$
t$_{1/2}$ (25 °C) ~ 5.8 h

[Fe^{IV}(O)(L)]$^{2+}$
R = CH$_3$: L = Me-tpen
R = Bn: L = Bn-tpen
t$_{1/2}$ (25 °C) ~ 6 h
R = CH$_2$Py: L = tpen
t$_{1/2}$ (25 °C) ~ 30 min

Figure I.1. Examples of reported synthetic oxoiron(IV) species.[57, 64-78]

I.3.2.1 Oxygen atom transfer processes

The first evidence that synthetic oxoiron(IV) species can transfer the oxygen atom to an organic substrate was obtained in 2003, when $[Fe^{IV}(O)(tmc)(CH_3CN)]^{2+}$ was shown capable to quantitatively oxidize triphenylphosphine to triphenylphosphine oxide (Scheme I.19, left).[58] The same year, OAT to sulfides was also accomplished, by using the more reactive $[Fe^{IV}(O)(tpa)(CH_3CN)]^{2+}$ complex (Figure I.19, right).[79]
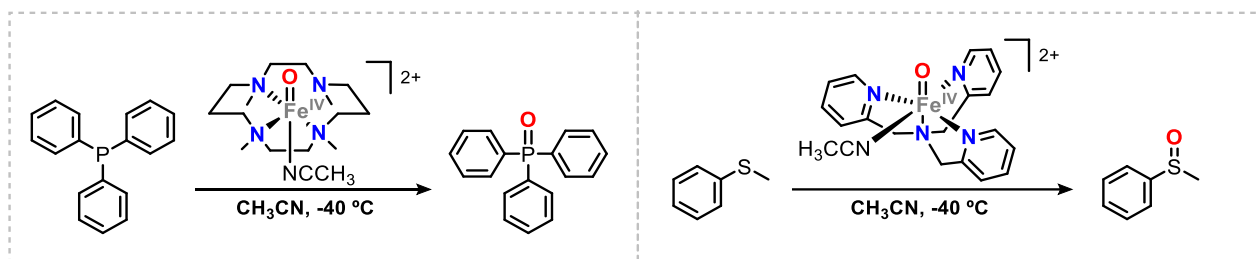
Scheme I.19. OAT from oxoiron(IV) species to organic substrates.[58, 79]

Particularly, Hammett analysis for the oxidation of *para*-subtituted thioanisoles reveals that an increase of the electron density of the substrate is translated in an increase of the OAT rates. Indeed, by correlating the logarithm of the reaction rates ($log(k_2)$) with the Hammett parameters (σ_p) of the target substrates a straight line with a negative slope (ρ) is obtained (Scheme I.20). As example, in the Hammett plot performed using $[Fe^{IV}(O)(tmc)(CH_3CN)]^{2+}$ and $[Fe^{IV}(O)(tpa)(CH_3CN)]^{2+}$ complexes ρ values of -2.5 and -1.6 were reported, respectively.[80] This behavior highlights the electrophilic character of the oxoiron(IV) species, as higher reaction rates are observed for more electron-rich substrates (Scheme I.20).

X	σ_p
OCH_3	-0.27
CH_3	-0.17
H	0.0
Cl	+0.23
C(O)H	+0.42
CN	+0.66
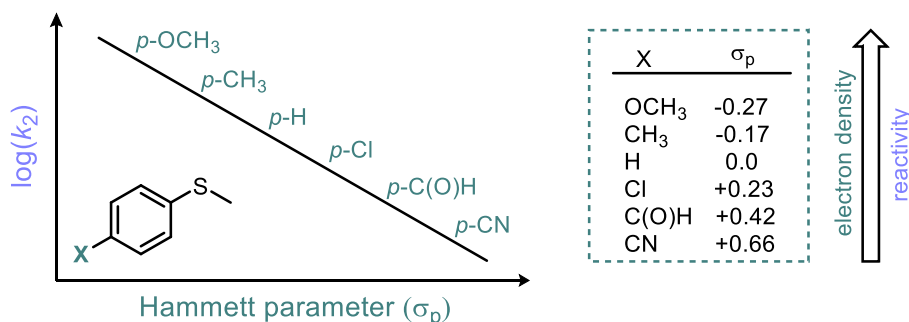
Scheme I.20. Representation of the Hammett plot for OAT from oxoiron(IV) species to *para*-substituted thioanisoles.[81]

The electrophilic character of oxoiron(IV) species, and thus their OAT reactivity, is dictated by the Fe^{IV}/Fe^{III} redox potential, which has been shown to be affected by the ligand topology[82] as well as by the nature of the labile ligand in *trans*[83, 84] or *cis*[85] with respect to the oxo moiety in tetradentate

systems. Additionally, the donor ability of the ligands in *cis* to the oxo moiety (either pyridines or aliphatic amines) was demonstrated to affect the reactivity of oxoiron(IV) species supported by pentadentate ligands.[60]

Compound $[Fe^{IV}(O)(bqcn)(CH_3CN)]^{2+}$ turned out to be an appropriate system to show how the ligand topology influences the reactivity of oxoiron(IV) species.[82] The iron(II) precursor of this compound presented two possible geometries depending on the folding of the bqcn ligand around the metal: *cis*-α and *cis*-β. Thus, $[Fe^{IV}(O)(\alpha\text{-bqcn})(CH_3CN)]^{2+}$ and $[Fe^{IV}(O)(\beta\text{-bqcn})(CH_3CN)]^{2+}$ species could be synthetized and their reactivity could be compared (Scheme I.21). While in the *cis*-α topology the oxo moiety is *trans* to a *N*-CH$_3$ group, according to DFT calculations in the *cis*-β configuration a *N*-quinoline is found in that position. Electrochemical measurements highlighted that $[Fe^{IV}(O)(\alpha\text{-bqcn})(CH_3CN)]^{2+}$ has a redox potential 0.11 V higher than $[Fe^{IV}(O)(\beta\text{-bqcn})(CH_3CN)]^{2+}$, reflecting the decreased donor ability of the *trans* aliphatic amine nitrogen when compared with the *trans* quinolyl unit. As a consequence, $[Fe^{IV}(O)(\alpha\text{-bqcn})(CH_3CN)]^{2+}$ was more active in OAT to sulfides compared to $[Fe^{IV}(O)(\beta\text{-bqcn})(CH_3CN)]^{2+}$. For instance, the rate for the oxidation of *para*-nitrothioanisole performed with $[Fe^{IV}(O)(\alpha\text{-bqcn})(CH_3CN)]^{2+}$ ($k_2 = 6.0$ M$^{-1}\cdot$s^{-1}) was two orders of magnitude higher than the one obtained with $[Fe^{IV}(O)(\beta\text{-bqcn})(CH_3CN)]^{2+}$ ($k_2 = 0.053$ M$^{-1}\cdot$s^{-1}) (Scheme I.21).
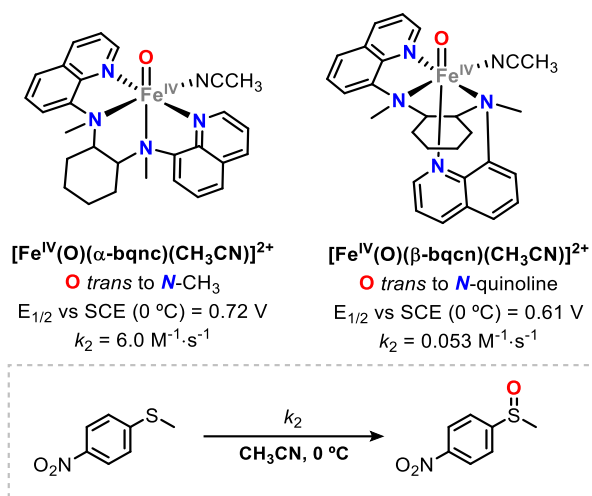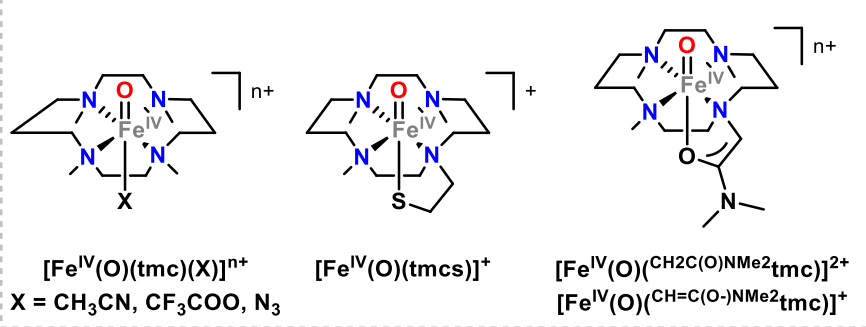
Scheme I.21. Impact of ligand topology on the OAT reactivity of $[Fe^{IV}(O)(bqcn)(CH_3CN)]^{2+}$.[82]

The impact of the nature of the labile ligand on the electrophilicity of oxoiron(IV) species can be established considering the systematic study carried out with a series of $[Fe^{IV}(O)(tmc)(X)]^{n+}$ complexes, containing different anionic ligands *trans* to the oxo ligand. As shown in Table I.2, an increase of the electron donation by the *trans* ligand is translated in a decrease of the redox potential. Consequently, the reaction rates for OAT to triphenylphosphine are diminished. Thus, the reaction rate (k_2) gradually decreases when moving from $[Fe^{IV}(O)(tmc)(CH_3CN)]^{2+}$ ($E_{p,c} = -0.32$ V) to $[Fe^{IV}(O)(^{CH=C(O-)NMe2}tmc)]^+$ ($E_{p,c} = -1.16$ V). With the latter reactivity towards triphenylphosphine was

so slow that reaction rate could not be determined, due to the competition with the self-decay of the intermediate itself.[83, 84]

Table I.2. Impact of the *trans* ligand on the OAT reactivity of $[Fe^{IV}(O)(tmc)(X)]^{n+}$ series of complexes.[83, 84]

$[Fe^{IV}(O)(tmc)(X)]^{n+}$
X = CH$_3$CN, CF$_3$COO, N$_3$ $[Fe^{IV}(O)(tmcs)]^+$ $[Fe^{IV}(O)(^{CH2C(O)NMe2}tmc)]^{2+}$
$[Fe^{IV}(O)(^{CH=C(O-)NMe2}tmc)]^+$

	$E_{p,c}$ (V vs Fc)	Ph$_3$P → Ph$_3$P=O k_2 (M^{-1}·s^{-1})
$[Fe^{IV}(O)(tmc)(CH_3CN)]^{2+}$	-0.32 V	5.9
$[Fe^{IV}(O)(tmc)(CF_3COO)]^+$	-0.50 V	2.9
$[Fe^{IV}(O)(tmc)(N_3)]^+$	-0.60 V	0.61
$[Fe^{IV}(O)(^{CH2C(O)NMe2}tmc)]^{2+}$	-0.63 V	0.19
$[Fe^{IV}(O)(tmcs)]^+$	-1.00 V[a]	0.016[b]
$[Fe^{IV}(O)(^{CH=C(O-)NMe2}tmc)]^+$	-1.16 V	-

Unless otherwise noticed $E_{p,c}$ were measured at 25 ºC and reactivity studies were performed in CH$_3$CN at 0 ºC.
[a]T = -30 ºC. [b]CH$_3$CN:CH$_3$OH 1:1.

Finally, it has been shown that the electrophilic character of oxoiron(IV) compounds can be enhanced by addition of acids or metal cations in the reaction mixture,[62] as well as by the establishment of hydrogen bonds involving the second coordination sphere of the iron.[86] Indeed, when the oxo moiety is coordinated by an acid or a metal ion the reduction potential of the oxoiron(IV) species increases. Consequently, an enhancement of the oxidation reactivity is attained. The same consideration could also be extended to the formation of hydrogen bonds with the oxo moiety.

I.3.2.2 Hydrogen atom transfer processes

In 2004, Que and co-workers reported the first study demonstrating the capability of oxoiron(IV) species to perform HAT from C-H bonds. In this work, $[Fe^{IV}(O)(N4Py)]^{2+}$ (structure in Figure I.1) and $[Fe^{IV}(O)(Bn-tpen)]^{2+}$ (Figure I.2) complexes bearing pentadentate N-based ligands were used.[74] By plotting the logarithm of the normalized oxidation rates (log(k_2')), which considered the number of abstractable protons in each substrate, as a function of the C-H bond dissociation energies, a linear correlation was observed (Figure I.2 shows this correlation determined for $[Fe^{IV}(O)(Bn-tpen)]^{2+}$). This trend indicated that the HAT corresponds to the rate determining step of the reaction,[87] as further

supported by the large kinetic isotope effects (KIE) observed in the oxidation of ethylbenzene-d_{10} ([Fe^{IV}(O)(N4Py)]$^{2+}$: KIE = 30, [Fe^{IV}(O)(Bn-tpen)]$^{2+}$: KIE = 50).
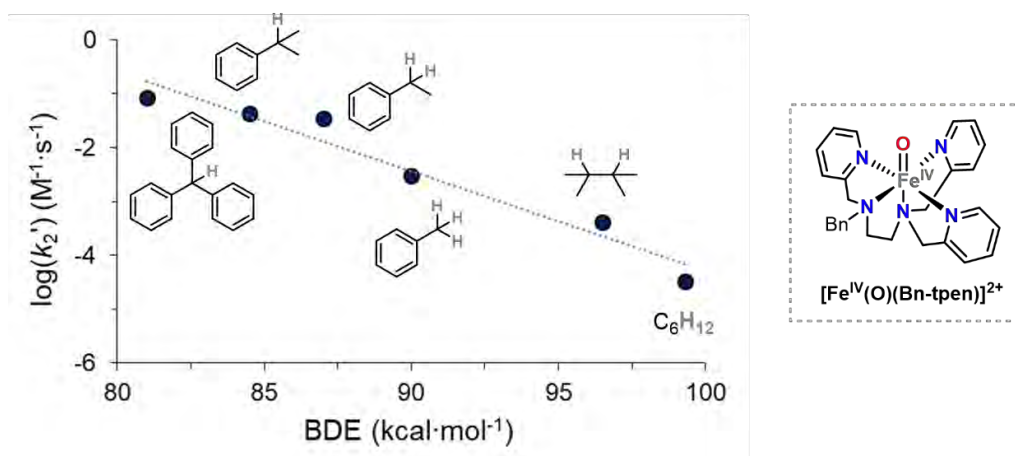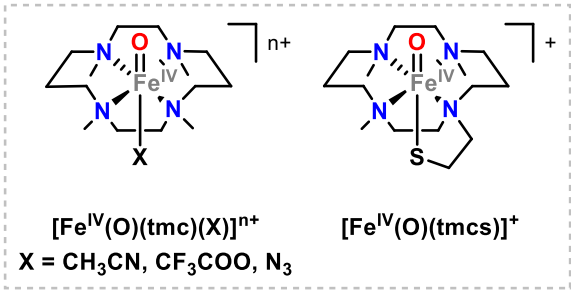
Figure I.2. Correlation of log(k_2') with C-H BDEs for the oxidation of different alkanes by [Fe^{IV}(O)(Bn-tpen)]$^{2+}$. T = 25 ºC. Bn = benzyl.[74]

As discussed above for OAT processes, the HAT reactivity of oxoiron(IV) species can be modulated by modifying the ligand topology or the nature of the *cis/trans* ligands with respect to the oxo moiety, as well as by the addition of metal cations or acids in the reaction mixture.[60, 62, 82-85] Nevertheless, for these transformations the mechanistic scenario is more complicated and cannot always be explained only in terms of electrophilicity of the oxoiron(IV) species.

The study describing the influence of the *trans* ligand on the reactivity of [Fe^{IV}(O)(tmc)(X)]$^{n+}$ species can be taken as an example.[84] As shown above, for OAT processes an electrophilic trend was obtained, so that reaction rates could be directly correlated with the redox potential of the oxoiron(IV) species. Nevertheless, for HAT reactions it was found that an increase in the electrophilic character of oxoiron(IV) species, determined by a higher redox potential, is translated in slower HAT reactions. Thus, the so-called antielectrophilic trend was described. According to Mayer's proposal, being HAT a process that involves the transfer of a proton and an electron, reaction rates are related to both the redox potential and the basicity of the abstracting species. These properties define the energy of the O-H bond formed upon HAT (BDE$_{O-H}$).[88, 89] In this context, the antielectrophilic trend observed in HAT reactions performed by [Fe^{IV}(O)(tmc)(X)]$^{n+}$ complexes could be rationalized considering that the oxoiron(IV) species is more reactive as more basic is the oxo ligand, despite its oxidizing power is lower (see Table I.3). For instance, in the oxidation of 9,10-dihydroanthracene (DHA) the substitution of the CH$_3$CN *trans* ligand ([Fe^{IV}(O)(tmc)(CH$_3$CN)]$^{2+}$: pK$_a$ = -3.0) by a thiolate ([Fe^{IV}(O)(tmcs)]$^+$: pK$_a$ = +8.5) leads to a 54-fold increase of the reaction rate.

Table I.3. Impact of the *trans* ligand on the HAT reactivity of [Fe^{IV}(O)(tmc)(X)]$^{n+}$.[14, 84]

[Fe^{IV}(O)(tmc)(X)]$^{n+}$
X = CH$_3$CN, CF$_3$COO, N$_3$

[Fe^{IV}(O)(tmcs)]$^+$

	E$_{p,c}$ (V vs Fc)	LFe^{IV}(O) → LFe^{IV}(OH) pK$_a$	DHA → A k$_2$ (M^{-1}·s^{-1})
[Fe^{IV}(O)(tmc)(CH$_3$CN)]$^{2+}$	-0.32 V	-3.0[b]	0.14
[Fe^{IV}(O)(tmc)(CF$_3$COO)]$^+$	-0.50 V	+0.2[b]	1.3
[Fe^{IV}(O)(tmc)(N$_3$)]$^+$	-0.60 V	+5.5[b]	2.4
[Fe^{IV}(O)(tmcs)]$^+$	-1.00 V[a]	+8.5[b]	7.5[c]

Unless otherwise noticed E$_{p,c}$ were measured at 25 °C and reactivity studies were performed in CH$_3$CN at 0 °C. [a]T = -30 °C. [b]calculated values. [c]CH$_3$CN:CH$_3$OH 1:1. DHA = 9,10-dihydroanthracene. A = anthracene.

Nonetheless, DFT calculations indicated that the [Fe^{III}(OH)(tmc)(X)]$^{n+}$ species, generated after the HAT event, have all approximately the same BDE$_{O-H}$. Thus, a two state reactivity model was proposed to explain the experimentally observed antielectrophilic trend. Oxoiron(IV) species can have two different spin states, namely the triplet (S = 1) and the quintet (S = 2) one, being the triplet state the ground state for these complexes. However, theoretical studies predicted the excited quintet state to have a lower energy barrier than the triplet state in HAT processes.[90] The energy gap between the quintet and triplet state diminished with the increase of the electron donation by the axial ligand. Then, the increased basicity of [Fe^{IV}(O)(tmc)(X)]$^{n+}$ species led to a higher participation of the quintet state and, as a consequence, to a faster reaction. Therefore, in HAT processes the higher basicity of a given oxoiron(IV) species can compensate its diminished electrophilic character, so that its reactivity is enhanced.

I.3.3 Synthetic oxoiron(V) species

This section was adapted from: "Oxoiron(V) Complexes of Relevance in Oxidation Catalysis of Organic Substrates". Valeria Dantignana, Anna Company,* Miquel Costas*. *Israelian Journal of Chemistry* **2020**, *60*, doi: 10.1002/ijch.201900161. © 2020 Wiley-VCH Verlag GmbH & Co. KGaA, Weinheim. Reuse with permission from John Wiley and Sons.

The first synthetic oxoiron(V) complex was described by Collins and co-workers using the macrocyclic taml ligand (Scheme I.22, left).[91] Thanks to its anionic character, this ligand was

previously used as a platform for stabilizing high-valent iron(IV) compounds.[92] The addition of *m*-CPBA to a solution of [Fe^{III}(taml)(H$_2$O)]$^-$ in *n*-butyronitrile at -60 °C led to the formation of a green intermediate, with absorption bands at 445 and 630 nm, which was proved to be the [Fe^V(taml)(O)]$^-$ species on the basis of a detailed spectroscopic characterization (Scheme I.22, bottom). Alternative synthetic strategies included the generation of [Fe^V(taml)(O)]$^-$ in acetonitrile at -40 °C with stoichiometric amounts of *m*-CPBA in the presence of small amounts of water, pyridine or benzoic acid. The EPR spectrum of [Fe^V(taml)(O)]$^-$ exhibited g_x = 1.99, g_y = 1.97 and g_z = 1.74 values, representative of an S = 1/2 species. According to Mössbauer analyses, this compound could be obtained in ~ 95% yield and it was characterized by a distinctive low isomer shift (δ) of -0.46 mm·s^{-1} and a quadrupole splitting (ΔE_Q) of 4.25 mm·s^{-1}. The observed isomer shift was lower than the one of the parent oxoiron(IV) species (δ = -0.19 mm·s^{-1}),[67] thus supporting the higher oxidation state of this new compound.

UV-vis	EPR	MB	XAS
λ_{max} = 445 nm (ε = 5400 M^{-1}·cm^{-1})	g_x = 1.99	δ = -0.46 mm·s^{-1}	K-edge energy: 7125.3 eV
λ_{max} = 630 nm (ε = 4200 M^{-1}·cm^{-1})	g_y = 1.97	ΔE_Q = 4.25 mm·s^{-1}	pre-edge area: >60 units
	g_z = 1.74		$r_{Fe=O}$ = 1.58 Å
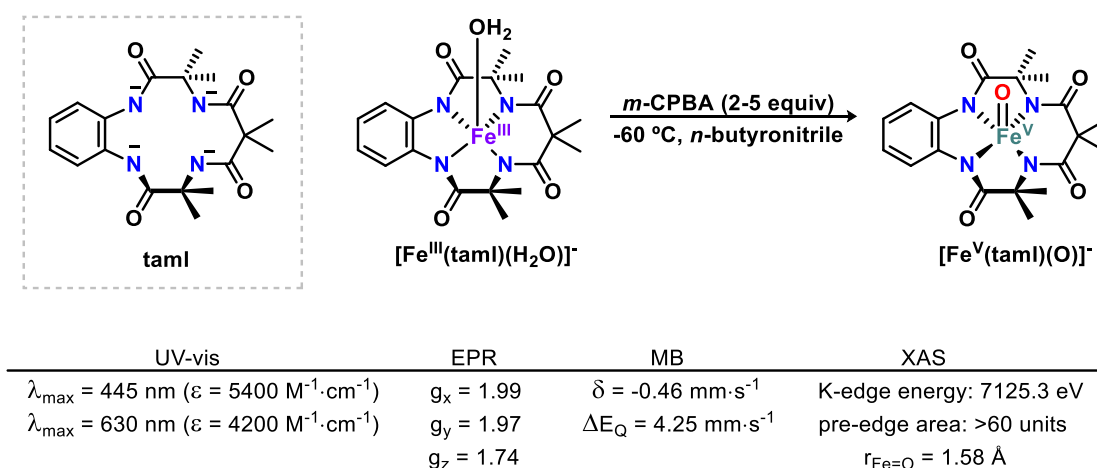
Scheme I.22. Representation of the taml ligand (top left), generation of [Fe^V(taml)(O)]$^-$ by oxidation of its iron(III) precursor (top right) and main spectroscopic features of this oxoiron(V) compound (bottom).[91]

After this pioneering work, several taml derivatives were prepared and studied, so that the spectroscopic characterization of a few more examples of this class of synthetic oxoiron(V) species could be achieved.[93-96] Nevertheless, in most of the cases these intermediates were not efficient catalysts and their reactivity was limited to the oxidation of sulfides, phosphines, alkenes and alkanes in stoichiometric conditions. More efficient systems, capable to act as catalysts, were reported by using iron(II) complexes in combination with hydrogen peroxides or peracids as terminal oxidant. With the latter the in situ generation of an oxoiron(V) species was postulated,[97, 98] although in most of the cases it remains undetected.

I.3.3.1 Oxo-hydroxo-iron(V) species

In 1997, Que and co-workers reported the first example of a stereospecific hydrocarbon hydroxylation catalyzed by a bio-inspired iron complex, namely $[Fe^{II}(tpa)(CH_3CN)_2](ClO_4)_2$, used in combination with H_2O_2 as terminal oxidant under large excess of substrate (Scheme I.23).[99] The C-H bond oxidation was studied with cyclohexane and *cis*- or *trans*-1,2-dimethylcyclohexane at room temperature. These substrates can serve as mechanistic probes to define if the oxidation occurs through a radicalary or a metal-based pathway.[100] In the oxidation of cyclohexane, if HAT is performed by a radical species a long-lived alkyl radical is generated. The latter can be trapped by molecular oxygen giving an alkylperoxyl radical and, as a consequence of Russel type termination reaction,[101] equimolar amounts of cyclohexanol and cyclohexanone are obtained. Thus, in this scenario an alcohol:ketone (A/K) ratio of approximately one would be expected. Instead, in the oxidation of *cis*- or *trans*-1,2-dimethylcyclohexane the generation of a long-lived alkyl radical would result in its epimerization, so that loss of stereochemistry would be observed in the tertiary alcohol product.[102] As shown in Scheme I.23, in the oxidation of cyclohexane catalyzed by $[Fe^{II}(tpa)(CH_3CN)_2](ClO_4)_2$ an A/K ratio higher than one (A/K ~ 4) was obtained, which did not change in the presence of O_2. Furthermore, in the oxidation of *cis*- or *trans*-1,2-dimethylcyclohexane >99% retention of configuration (RC) was observed in the tertiary alcohol products. Moreover, full RC values were also found in the epoxidation of olefins, such as *cis*- or *trans*-2-hexene. These results, together with the KIE of 3.5 obtained in the oxidation of cyclohexane, suggested that the active oxidant was a metal-based species.

^{a}cat: H_2O_2: substrate 1:10:1000; CH_3CN, RT, air
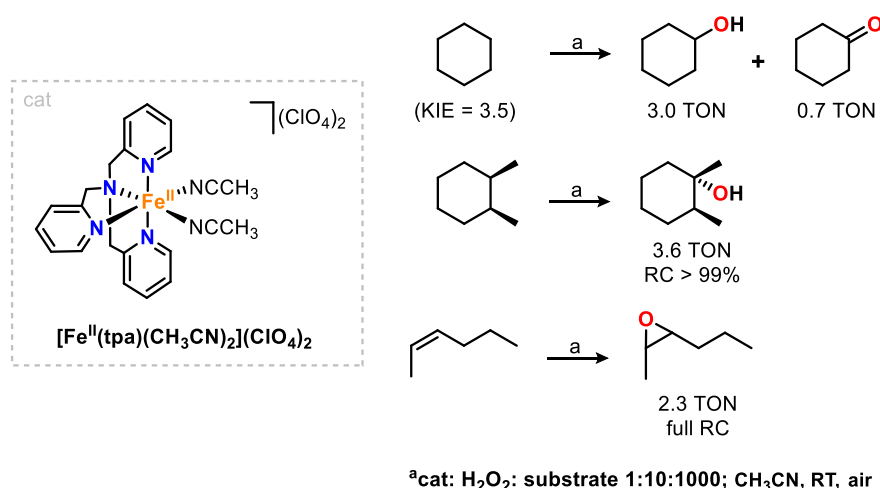
Scheme I.23. Catalytic C-H and C=C bond oxidation by $[Fe^{II}(tpa)(CH_3CN)_2](ClO_4)_2$.[99]

Subsequent mechanistic studies, performed with a series of iron(II) complexes bearing tetradentate aminopyridine ligands derived or similar to tpa, led to propose that the species responsible for the HAT step was an oxo-hydroxo-iron(V) generated through the mechanism shown in Scheme I.24.[103]

The reaction of the starting iron(II) complex with H_2O_2 leads to the rapid formation of $Fe^{III}(OH)$ species, which further evolves to give a low spin $Fe^{III}(OOH)$. Homolytic O-O cleavage would result in the formation of oxoiron(IV) species and a hydroxyl radical. The selective and efficient reactivity observed for these systems is neither consistent with the involvement of hydroxyl radicals[100] not with the slow reactions associated to oxoiron(IV) species with the same or similar ligand architectures.[104] Instead, coordination of water to the *cis* labile site with respect to the hydroperoxo ligand assists the heterolytic O-O bond cleavage, which results in the generation of a $Fe^V(O)(OH)$ species. An oxo-hydroxo tautomerism, analogous to that previously observed in porhyrinic systems,[105] generates an oxo ligand with the oxygen atom originating from water. Hydrogen atom abstraction by the $Fe^V(O)(OH)$ species and posterior fast rebound of the newly formed hydroxyl group with the alkyl radical affords stereospecific hydroxylation of alkanes, while direct oxo transfer by the same species to the olefin functionality affords epoxides. *Syn*-dihydroxylation is accomplished via an asynchronous 3+2 reaction where the hydroxo ligand of $Fe^V(O)(OH)$ initiates the attack in the C=C bond.
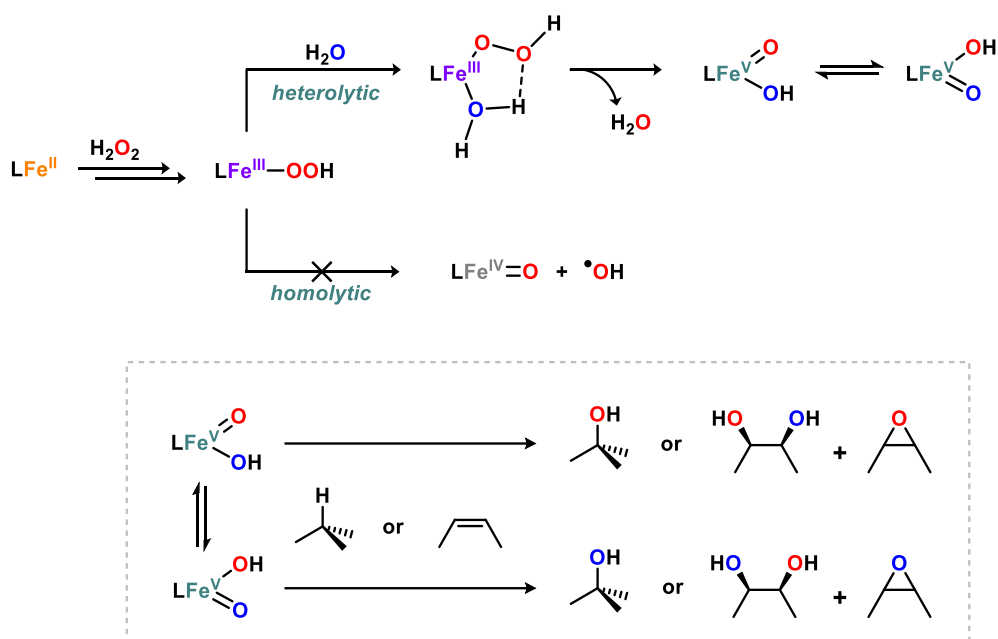
Scheme I.24. Water assisted generation of oxo-hydroxo-iron(V) species (top) and schematic representation of its reactivity (bottom).

The above-described water assisted mechanism not only rationalizes the required presence of two *cis* labile sites to afford efficient catalysts, but also the incorporation of oxygen from water into oxidized products, as ascertained by isotope-labeling experiments carried out using $H_2^{18}O$ both in alkane and olefin oxidations.[103, 106-109]

In spite of the fact that the involvement of an oxo-hydroxo-iron(V) species in oxidation catalysis was early postulated in 1999,[110] the first direct experimental evidence of the formation of such compound was not reported until 2011 by Prat et al.[111] In this work, by means of cryospray variable temperature

mass spectrometry, the authors could identify a transient species in catalytic mixtures upon reaction of [Fe^{II}(OTf)$_2$(Pytacn)] and hydrogen peroxide that could be formulated either as an Fe^{III}(OOH) or an Fe^V(O)(OH) compound (Figure I.3). Isotope-labeling experiments served to support the latter formulation. Thus, experimentally it was observed that the transient species incorporates an ^{18}O-atom when generated in the presence of H$_2^{18}$O. Considering that Fe^{III}(OOH) compounds do not exchange their oxygen atoms with water,[112] the observed intermediate was formulated as an Fe^V(O)(OH) species. Moreover, in the presence of an olefin, ferric glycolate species containing an ^{18}O-atom from H$_2^{18}$O were detected, strongly suggesting that the observed Fe^V(O)(OH) was responsible for olefin dihydroxylation.

[Fe^{II}(OTf)$_2$(Pytacn)] + H$_2$O$_2$ (100 equiv) → m/z = 486.1

{[Fe^{III}(OOH)(Pytacn)](OTf)}$^+$ {[Fe^V(O)(OH)(Pytacn)](OTf)}$^+$
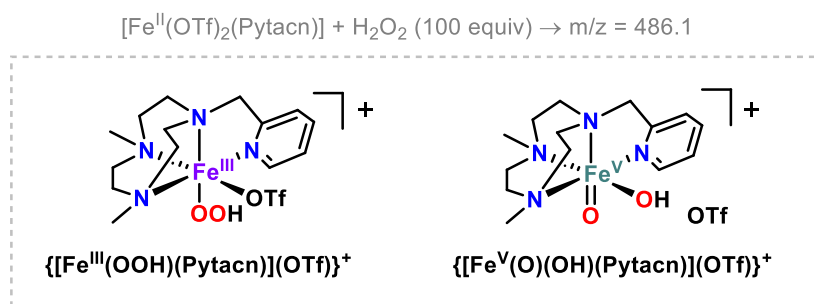
Figure I.3. The two possible structures of the cationic species trapped under catalytic conditions by reaction of [Fe^{II}(OTf)$_2$(Pytacn)] and H$_2$O$_2$.[111]

Later on, making use of mass spectrometry techniques, Kodera and co-workers and Que and co-workers reported the detection of new oxoiron(V) species supported, respectively, by the dpaq and the tpa or tpa* ligands (Figure I.4, left).[113, 114] More recently Borrell et al. reported the first spectroscopic characterization of a Fe^V(O)(OH) intermediate, namely the [Fe^V(O)(OH)($^{5\text{-TIPS3}}$tpa)]$^{2+}$ species (Figure I.4, right), obtained by means of helium tagging infrared photodissociation (IRPD) spectroscopy.[115]

detected

characterized

[Fe^V(O)(dpaq)]$^{2+}$ [Fe^V(O)(OH)(L)]$^{2+}$ [Fe^V(O)(OH)($^{5\text{-TIPS3}}$tpa)]$^{2+}$
                               R = R' = H: L = tpa
                               R = H, R' = CH$_3$: L = tpa*
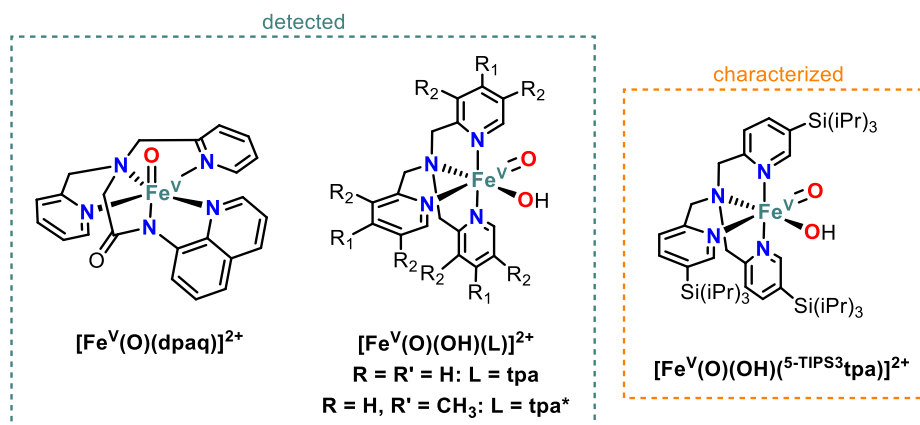
Figure I.4. Structures of the detected [Fe^V(O)(dpaq)]$^{2+}$ and [Fe^V(O)(OH)(L)]$^{2+}$ (L = tpa, tpa*) (left) and of the spectroscopically characterized [Fe^V(O)(OH)($^{5\text{-TIPS3}}$tpa)]$^{2+}$ (right).[113-115]

I.3.3.2 Oxo-carboxylato-iron(V) species

Jacobsen and co-workers were the first to describe that the use of acetic acid, in combination with [Fe^{II}(mep)(CH$_3$CN)$_2$](SbF$_6$)$_2$ and hydrogen peroxide, has a beneficial effect on the catalytic activity in alkene epoxidation.[116] Subsequently, Que and co-workers performed a mechanistic study to clarify the role of acetic acid in these reactions.[117] When the substrate was the limiting reagent (catalyst:H$_2$O$_2$:cyclooctene 1:300:200), an almost quantitative yield of epoxide could be obtained in the oxidation of cyclooctene catalyzed both by [Fe^{II}(mep)(CH$_3$CN)$_2$]$^{2+}$ and [Fe^{II}(tpa)(CH$_3$CN)$_2$]$^{2+}$ complexes in a CH$_3$CN:AcOH 1:2 mixture at 0 ºC. Using the same reaction conditions epoxidation of *cis*-2-heptene proceeded with 99% retention of configuration, thus discarding a free radical path for the reaction. Instead, it was proposed that a high-valent oxoiron species was responsible for the oxidation. The latter was postulated to be an oxo-carboxylato-iron(V) species generated through a carboxylic acid assisted O-O cleavage mechanism, in analogy to the water assisted path (Scheme I.25). This proposal was further supported by the identification of *syn*-1,2-hydroxoacetato derivatives as byproducts of olefin oxidation, formed upon transfer of both the oxo and the acetate ligands to the C=C bond.[118] In the same line, carboxylic acid could be also positively employed in selective C-H bond oxidation reactions, as first described by White and Chen in 2007.[25] The predictable selectivity observed in such transformations supports the involvement of an oxo-carboxylato-iron(V) species as active oxidant.[98]
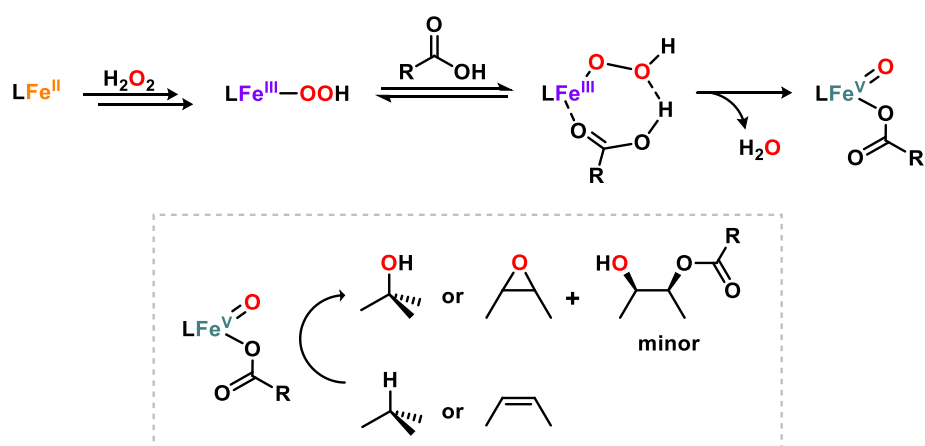
Scheme I.25. Carboxylic acid assisted generation of oxo-carboxylato-iron(V) species (top) and schematic representation of its reactivity (bottom).

The first spectroscopic evidence for the involvement of a Fe^V(O)(OAc) species in a catalytic system was not reported until 2015 by Talsi and co-workers, in the course of a study on the epoxidizing abilities of iron complexes containing tpa* and (*S,S*)-pdp* ligands (Figure I.5, left).[119] In particular, upon mixing the dinuclear [Fe^{III}$_2$(μ-OH)$_2$(tpa*)$_2$]$^{4+}$ complex with H$_2$O$_2$ and acetic acid at -80 ºC, a new iron species with g$_1$ = 2.070, g$_2$ = 2.005 and g$_3$ = 1.956 values appeared in the EPR spectrum

recorded at -196 ºC. Comparable g values were also observed when [Fe$^{III}_2$(μ-OH)$_2$((S,S)-pdp*)$_2$]$^{4+}$ was submitted to a similar treatment (g$_1$ = 2.071, g$_2$ = 2.008 and g$_3$ = 1.960). Interestingly, these new species detected by EPR were kinetically competent to react with olefins such cyclohexene, *cis*-β-methylstyrene or 1-octene. Additionally, they could perform arene oxidation.[120, 121] These compounds were formulated as [Fe^V(O)(OAc)(L)]$^{2+}$ (Figure I.5, right), an assignment that was later reinforced by Que and co-workers through extensive EPR and kinetic analyses performed using iron complexes based on tpa and tpa* ligands.[122] Indeed, g$_1$ = 2.07, g$_2$ = 2.01 and g$_3$ = 1.96 values were reported for the [Fe^V(O)(OAc)(tpa)]$^{2+}$ and [Fe^V(O)(OAc)(tpa*)]$^{2+}$ species. Similar g values were also found for [Fe^V(O)(OC(O)R)((S,S)-pdp)]$^{2+}$.[123]

Nevertheless, in all these studies, these reactive species accumulated in low yields ($\leq$ 10%) precluding a more detailed characterization, beyond the EPR signature, so preventing an unambiguous assignment of the oxidation state of the iron.
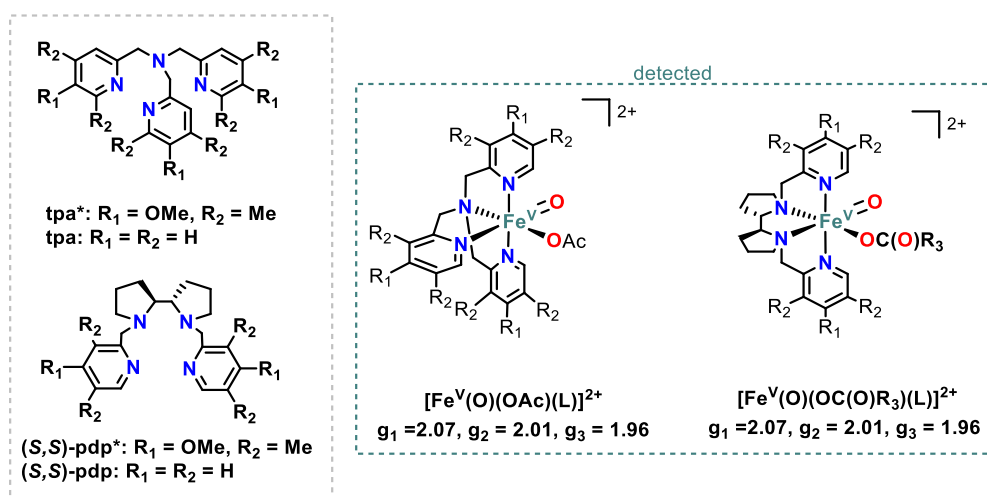
Figure I.5. Representation of the tpa*, tpa, (S,S)-pdp* and (S,S)-pdp ligands (left) and g values of their corresponding oxo-carboxylato-iron(V) species detected by EPR (right).[119, 122, 123]

A system that permits the accumulation of an oxo-carboxylato-iron(V) species was first described by Serrano-Plana et al. in 2015. In this work, the generation of a transient species formulated as [Fe^V(O)(OAc)(PyNMe$_3$)]$^{2+}$ (Scheme I.26) was achieved in a remarkable 40% yield, upon reaction of the iron(II) precursor with peracetic acid (4 equiv) as external oxidant at -41 ºC.[124] This compound, characterized by two visible absorption bands at 490 nm (ε = 4500 M$^{-1}\cdot$s^{-1}) and 660 nm with a 7:1 relative intensity, exhibited an EPR spectrum with g$_1$ = 2.07, g$_2$ = 2.01 and g$_3$ = 1.95 values, very close to those reported by Talsi and Que (see above).[119, 122, 123] Additionally, high-resolution cryospray mass spectrometry analysis showed the presence of a main peak with m/z 528.0893. The latter moved by three units in the presence of deuterated acetic acid, thus corroborating the formulation of the detected intermediate as [Fe^V(O)(OAc)(PyNMe$_3$)]$^{2+}$. Unfortunately, a Mössbauer analysis that could unequivocally establish the oxidation state of the iron center could not be

performed with this system, since the sample contained other iron species that made the analysis unfeasible.
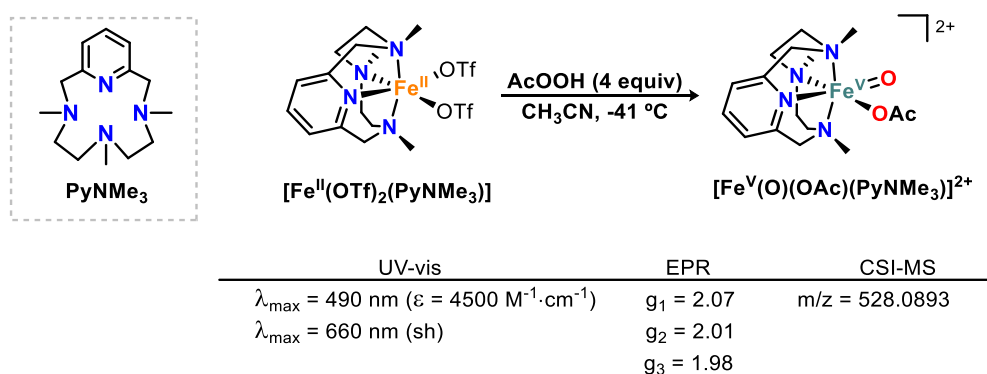
Scheme I.26. Representation of the PyNMe$_3$ ligand (top left), generation of [Fe^V(O)(OAc)(PyNMe$_3$)]$^{2+}$ species by reaction of its iron(II) precursor with peracetic acid (top right) and spectroscopic and spectrometric features of this oxoiron(V) compound (bottom).[124]

Under catalytic conditions, [Fe^V(O)(OAc)(PyNMe$_3$)]$^{2+}$ was highly reactive and even the strong C-H bonds of cyclohexane (BDE = 99.5 kcal·mol^{-1}) could be oxidized with remarkable chemoselectivity for the alcohol product (A/K = 5). Selectivity towards tertiary C-H bonds of adamantane over secondary ones (normalized 3º/2º = 23) and stereoretention in the oxidation of *cis*-1,2-dimethylcycloxane (RC = 92%) were observed. Moreover, a detailed kinetic analysis for the reaction of [Fe^V(O)(OAc)(PyNMe$_3$)]$^{2+}$ with alkyl C-H bonds (BDE = 89.7-99.5 kcal·mol^{-1}) by stopped-flow methods revealed a linear correlation between second order rate constants and BDEs values. This indicates that the HAT is the rate determining step of the reaction, as also suggested by the kinetic isotopic effect observed in the oxidation of cyclohexane-d_{12} (KIE = 5). Moreover, the epoxidation of olefins by [Fe^V(O)(OAc)(PyNMe$_3$)]$^{2+}$ showed that this intermediate behaves as an electrophilic species.[125] Indeed, faster reaction rates were observed as more electron-rich was the double bond. In addition, a negative ρ value was found in the Hammett plot constructed with a series of *para*-substituted styrenes. Remarkably, the reaction rates exhibited by [Fe^V(O)(OAc)(PyNMe$_3$)]$^{2+}$ in C-H and C=C bond oxidation were the highest reported thus far for any synthetic high-valent oxometal species in analogous reactions.

Despite important clues in favor of an [Fe^V(O)(OAc)(PyNMe$_3$)]$^{2+}$ species were collected, due to the complexity of the reaction mixture in which it was generated, the spectroscopic description of this species was basically limited to its EPR and electronic spectra. Extensive experimentation led to the identification of an iron complex derivative and reaction conditions that enabled a complete spectroscopic characterization. By using an electron-rich analogue of the PyNMe$_3$ ligand (^{OMe}PyNMe$_3$) in combination with cyclohexyl peroxycarboxylic acid, the transient intermediate accumulated in 48% yield and low spin ferric components that initially complicated the spectra were not present.[126] In this case, the Mössbauer spectrum of [Fe^V(O)(OC(O)Cy)(^{OMe}PyNMe$_3$)]$^{2+}$ (Cy =

C_6H_{11}) could be extracted, with an isomer shift (δ) of -0.08 mm·s^{-1} and a quadrupole splitting (ΔE_Q) of +1.15 mm·s^{-1}. The isomer shift value is lower than the one of the [Fe^{IV}(O)(PyNMe$_3$)(CH$_3$CN)]$^{2+}$ species (δ = +0.05 mm·s^{-1}), thus supporting the higher oxidation state of the iron center of the detected intermediate. Moreover, the EPR spectrum of the latter exhibited g_x = 2.01, g_y = 2.07 and g_z = 1.94 values, which resembled the ones of the related [Fe^V(O)(OAc)(PyNMe$_3$)]$^{2+}$ species. Through the combination of the collected data, which included also resonance Raman, EXAFS and DFT analyses, the electronic structure of this intermediate was described as ~75% [Fe^V(O)(OC(O)Cy)(^{OMe}PyNMe$_3$)]$^{2+}$ with contribution of [Fe^{IV}(O)($^\bullet$OC(O)Cy)(^{OMe}PyNMe$_3$)]$^{2+}$ (15%) and [Fe^{III}(OOC(O)Cy)(^{OMe}PyNMe$_3$)]$^{2+}$ (10%) species. Nevertheless, the electronic structure of [Fe^V(O)(OAc)(PyNMe$_3$)]$^{2+}$ remains a matter of debate. Ye and co-workers performed an extensive theoretical investigation and formulated this species as an iron(IV) antiferromagnetically coupled to an O-O σ^* radical. In this analysis the compound is proposed to bear a single electron O-O bond.[127] The involvement of an oxoiron(IV) ligand cation radical in hydrocarbon oxidation was previously reported by Chi-Ming Che and co-workers, which identified the [Fe^{IV}(Me$_3$tacn)(Cl-acac)$^{\bullet+}$(O)]$^{2+}$ intermediate through high-resolution ESI mass spectrometry and EPR spectroscopy and corroborated the proposed formulation with DFT analysis.[128]

I.4 CONCLUDING REMARKS

The most recent efforts in the field of catalytic C-H oxidation with bioinspired complexes have disclosed several strategies to target a specific C-H bond within a substrate. In selected cases, electronic, steric and stereoelectronic properties of the substrate can be used to predictably oxidize C-H bonds in a selective manner. Furthermore, selectivity can be modulated by fine tuning the catalyst structure or through establishment of non-covalent interactions. Even so, the discovery of novel methods to alter the relative reactivity of C-H bonds remains an unsolved problem. Additionally, the improvement of the hydroxylation selectivity continues to be an open task.

In a mechanistic perspective, it is nowadays well-known that high-valent oxometal intermediates are the active species involved in the aforementioned reactions. Thus, efforts have been devoted to the understanding of the properties that govern their reactivity. Although the oxidative ability of synthetic oxoiron(IV) compounds has been widely studied, to date only few examples of spectroscopically characterized oxoiron(V) compounds have been reported. As oxoiron(V) species exhibit outstanding activity and selectivity in oxidation reactions, much higher than that observed for oxoiron(IV) species, a deeper understanding of their properties is crucial. Consequently, preparation and isolation of such compounds remains an important challenge.

I.5 References

(1)   Godula, K. D. Sames, C-H Bond Functionalization in Complex Organic Synthesis. *Science* **2006,** *312*, 67-72.

(2)   Hartwig, J. F. M. A. Larsen, Undirected, Homogeneous C–H Bond Functionalization: Challenges and Opportunities. *ACS Cent. Sci.* **2016,** *2*, 281-292.

(3)   Crabtree, R. H., Alkane C–H activation and functionalization with homogeneous transition metal catalysts: a century of progress—a new millennium in prospect. *J. Chem. Soc., Dalton Trans.* **2001**, 2437-2450.

(4)   Pombeiro, A. J. L. M. de Fatima Costa Guedes da Silva (2019). Alkane Functionalization, Wiley.

(5)   Huang, X. J. T. Groves, Oxygen Activation and Radical Transformations in Heme Proteins and Metalloporphyrins. *Chem. Rev.* **2018,** *118*, 2491-2553.

(6)   Kal, S. L. Que, Dioxygen activation by nonheme iron enzymes with the 2-His-1-carboxylate facial triad that generate high-valent oxoiron oxidants. *J. Biol. Inorg. Chem.* **2017,** *22*, 339-365.

(7)   Olivo, G., O. Cussó, M. Borrell M. Costas, Oxidation of alkane and alkene moieties with biologically inspired nonheme iron catalysts and hydrogen peroxide: from free radicals to stereoselective transformations. *J. Biol. Inorg. Chem.* **2017,** *22*, 425-452.

(8)   Talsi, E. P., R. V. Ottenbacher K. P. Bryliakov, Bioinspired oxidations of aliphatic C–H groups with H_2O_2 in the presence of manganese complexes. *J. Organomet. Chem.* **2015,** *793*, 102-107.

(9)   Kal, S., S. Xu L. Que Jr., Bio-inspired Nonheme Iron Oxidation Catalysis: Involvement of Oxoiron(V) Oxidants in Cleaving Strong C−H Bonds. *Angew. Chem. Int. Ed.* **2020,** *59*, 7332-7349.

(10)   Guo, M., T. Corona, K. Ray W. Nam, Heme and Nonheme High-Valent Iron and Manganese Oxo Cores in Biological and Abiological Oxidation Reactions. *ACS Cent. Sci.* **2019,** *5*, 13-28.

(11)   Li, X.-X., M. Guo, B. Qiu, K.-B. Cho, W. Sun W. Nam, High-Spin Mn(V)-Oxo Intermediate in Nonheme Manganese Complex-Catalyzed Alkane Hydroxylation Reaction: Experimental and Theoretical Approach. *Inorg. Chem.* **2019,** *58*, 14842-14852.

(12)   Mayer, J. M., Understanding Hydrogen Atom Transfer: From Bond Strengths to Marcus Theory. *Acc. Chem. Res.* **2011,** *44*, 36-46.

(13)   Salamone, M. M. Bietti, Tuning Reactivity and Selectivity in Hydrogen Atom Transfer from Aliphatic C–H Bonds to Alkoxyl Radicals: Role of Structural and Medium Effects. *Acc. Chem. Res.* **2015,** *48*, 2895-2903.

(14)   Bím, D., M. Maldonado-Domínguez, L. Rulíšek M. Srnec, Beyond the classical thermodynamic contributions to hydrogen atom abstraction reactivity. *Proc. Natl. Acad. Sci. USA* **2018,** *115*, E10287-E10294.

(15)   Nam, W., Y.-M. Lee S. Fukuzumi, Hydrogen Atom Transfer Reactions of Mononuclear Nonheme Metal–Oxygen Intermediates. *Acc. Chem. Res.* **2018,** *51*, 2014-2022.

(16)   Stateman, L. M., K. M. Nakafuku D. A. Nagib, Remote C–H Functionalization via Selective Hydrogen Atom Transfer. *Synthesis* **2018,** *50*, 1569-1586.

(17)   Curci, R., L. D'Accolti C. Fusco, A Novel Approach to the Efficient Oxygenation of Hydrocarbons under Mild Conditions. Superior Oxo Transfer Selectivity Using Dioxiranes. *Acc. Chem. Res.* **2006,** *39*, 1-9.

(18)   D'Accolti, L., C. Annese C. Fusco, Continued Progress towards Efficient Functionalization of Natural and Non-natural Targets under Mild Conditions: Oxygenation by C−H Bond Activation with Dioxirane. *Chem. Eur. J.* **2019,** *25*, 12003-12017.

(19)   Brodsky, B. H. J. Du Bois, Oxaziridine-Mediated Catalytic Hydroxylation of Unactivated 3° C−H Bonds Using Hydrogen Peroxide. *J. Am. Chem. Soc.* **2005,** *127*, 15391-15393.

(20)   Litvinas, N. D., B. H. Brodsky J. Du Bois, C–H Hydroxylation Using a Heterocyclic Catalyst and Aqueous H_2O_2. *Angew. Chem. Int. Ed.* **2009,** *48*, 4513-4516.

(21)   Moteki, S. A., A. Usui, T. Zhang, C. R. Solorio Alvarado K. Maruoka, Site-Selective Oxidation of Unactivated C–H Bonds with Hypervalent Iodine(III) Reagents. *Angew. Chem. Int. Ed.* **2013,** *52*, 8657-8660.

(22)   Moteki, S. A., S. Selvakumar, T. Zhang, A. Usui K. Maruoka, A Practical Approach for the Oxidation of Unactivated C_{sp3}–H Bonds with o-Nitro(diacetoxyiodo)benzene as an Efficient Hypervalent Iodine(III)-Based Oxidizing Agent. *Asian J. Org. Chem.* **2014,** *3*, 932-935.

(23)   Xue, X.-S., P. Ji, B. Zhou J.-P. Cheng, The Essential Role of Bond Energetics in C–H Activation/Functionalization. *Chem. Rev.* **2017,** *117*, 8622-8648.

(24)   Newhouse, T. P. S. Baran, If C–H Bonds Could Talk: Selective C–H Bond Oxidation. *Angew. Chem. Int. Ed.* **2011,** *50*, 3362-3374.

(25)   Chen, M. S. M. C. White, A Predictably Selective Aliphatic C–H Oxidation Reaction for Complex Molecule Synthesis. *Science* **2007,** *318*, 783-787.

(26)   Ottenbacher, R. V., D. G. Samsonenko, E. P. Talsi K. P. Bryliakov, Highly Efficient, Regioselective, and Stereospecific Oxidation of Aliphatic C–H Groups with H_2O_2, Catalyzed by Aminopyridine Manganese Complexes. *Org. Lett.* **2012,** *14*, 4310-4313.

(27)   Chen, M. S. M. C. White, Combined Effects on Selectivity in Fe-Catalyzed Methylene Oxidation. *Science* **2010,** *327*, 566-571.

(28)   Chen, K., A. Eschenmoser P. S. Baran, Strain Release in C–H Bond Activation? *Angew. Chem. Int. Ed.* **2009,** *48*, 9705-9708.

(29)   Gómez, L., I. Garcia-Bosch, A. Company, J. Benet-Buchholz, A. Polo, X. Sala, X. Ribas M. Costas, Stereospecific C–H Oxidation with H_2O_2 Catalyzed by a Chemically Robust Site-Isolated Iron Catalyst. *Angew. Chem. Int. Ed.* **2009,** *48*, 5720-5723.

(30)   Gómez, L., M. Canta, D. Font, I. Prat, X. Ribas M. Costas, Regioselective Oxidation of Nonactivated Alkyl C–H Groups Using Highly Structured Non-Heme Iron Catalysts. *J. Org. Chem.* **2013,** *78*, 1421-1433.

(31)   Canta, M., D. Font, L. Gómez, X. Ribas M. Costas, The Iron(II) Complex [Fe(CF$_3$SO$_3$)$_2$(mcp)] as a Convenient, Readily Available Catalyst for the Selective Oxidation of Methylenic Sites in Alkanes. *Adv. Synth. Catal.* **2014,** *356*, 818-830.

(32)   Font, D., M. Canta, M. Milan, O. Cussó, X. Ribas, R. J. M. Klein Gebbink M. Costas, Readily Accessible Bulky Iron Catalysts exhibiting Site Selectivity in the Oxidation of Steroidal Substrates. *Angew. Chem. Int. Ed.* **2016,** *55*, 5776-5779.

(33)   Gormisky, P. E. M. C. White, Catalyst-Controlled Aliphatic C–H Oxidations with a Predictive Model for Site-Selectivity. *J. Am. Chem. Soc.* **2013,** *135*, 14052-14055.

(34)   Shen, D., C. Miao, S. Wang, C. Xia W. Sun, Efficient Benzylic and Aliphatic C–H Oxidation with Selectivity for Methylenic Sites Catalyzed by a Bioinspired Manganese Complex. *Org. Lett.* **2014,** *16*, 1108-1111.

(35)   Wang, W., D. Xu, Q. Sun W. Sun, Efficient Aliphatic C−H Bond Oxidation Catalyzed by Manganese Complexes with Hydrogen Peroxide. *Chem. Asian J.* **2018,** *13*, 2458-2464.

(36)   Litwinienko, G. K. U. Ingold, Solvent Effects on the Rates and Mechanisms of Reaction of Phenols with Free Radicals. *Acc. Chem. Res.* **2007,** *40*, 222-230.

(37)   Warren, J. J. J. M. Mayer, Predicting organic hydrogen atom transfer rate constants using the Marcus cross relation. *Proc. Natl. Acad. Sci. USA* **2010,** *107*, 5282-5287.

(38)   Salamone, M. M. Bietti, Reaction Pathways of Alkoxyl Radicals. The Role of Solvent Effects on C–C Bond Fragmentation and Hydrogen Atom Transfer Reactions. *Synlett* **2014,** *25*, 1803-1816.

(39)   Snelgrove, D. W., J. Lusztyk, J. T. Banks, P. Mulder K. U. Ingold, Kinetic Solvent Effects on Hydrogen-Atom Abstractions: Reliable, Quantitative Predictions via a Single Empirical Equation. *J. Am. Chem. Soc.* **2001,** *123*, 469-477.

(40)   Avila, D. V., C. E. Brown, K. U. Ingold J. Lusztyk, Solvent effects on the competitive b-scission and hydrogen atom abstraction reactions of the cumyloxyl radical. Resolution of a long-standing problem. *J. Am. Chem. Soc.* **1993,** *115*, 466-470.

(41)   Bietti, M., R. Martella M. Salamone, Understanding Kinetic Solvent Effects on Hydrogen Abstraction Reactions from Carbon by the Cumyloxyl Radical. *Org. Lett.* **2011,** *13*, 6110-6113.

(42)   Salamone, M., I. Giammarioli M. Bietti, Kinetic Solvent Effects on Hydrogen Abstraction Reactions from Carbon by the Cumyloxyl Radical. The Importance of Solvent Hydrogen-Bond Interactions with the Substrate and the Abstracting Radical. *J. Org. Chem.* **2011,** *76*, 4645-4651.

(43)   Salamone, M., L. Mangiacapra M. Bietti, Kinetic Solvent Effects on the Reactions of the Cumyloxyl Radical with Tertiary Amides. Control over the Hydrogen Atom Transfer Reactivity and Selectivity through Solvent Polarity and Hydrogen Bonding. *J. Org. Chem.* **2015,** *80*, 1149-1154.

(44)   Bietti, M. M. Salamone, Kinetic Solvent Effects on Hydrogen Abstraction Reactions from Carbon by the Cumyloxyl Radical. The Role of Hydrogen Bonding. *Org. Lett.* **2010,** *12*, 3654-3657.

(45)   Bégué, J.-P., D. Bonnet-Delpon B. Crousse, Fluorinated Alcohols: A New Medium for Selective and Clean Reaction. *Synlett* **2004,** *2004*, 18-29.

(46)   Shuklov, I. A., N. V. Dubrovina A. Börner, Fluorinated Alcohols as Solvents, Cosolvents and Additives in Homogeneous Catalysis. *Synthesis* **2007,** *2007*, 2925-2943.

(47)   Berkessel, A. (2010). Catalytic Oxidations with Hydrogen Peroxide in Fluorinated Alcohol Solvents. Modern Oxidation Methods. J.-E. Bäckvall (Ed.), Wiley-VCH**:** 117-145.

(48)   Wencel-Delord, J. F. Colobert, A remarkable solvent effect of fluorinated alcohols on transition metal catalysed C–H functionalizations. *Org. Chem. Front.* **2016,** *3*, 394-400.

(49)   Sinha, S. K., T. Bhattacharya D. Maiti, Role of hexafluoroisopropanol in C–H activation. *React. Chem. Eng.* **2019,** *4*, 244-253.

(50)   Gaster, E., S. Kozuch D. Pappo, Selective Aerobic Oxidation of Methylarenes to Benzaldehydes Catalyzed by N-Hydroxyphthalimide and Cobalt(II) Acetate in Hexafluoropropan-2-ol. *Angew. Chem. Int. Ed.* **2017,** *56*, 5912-5915.

(51)   Rittle, J. M. T. Green, Cytochrome P450 Compound I: Capture, Characterization, and C-H Bond Activation Kinetics. *Science* **2010,** *330*, 933-937.

(52)   Ortiz de Montellano, P. R., Hydrocarbon Hydroxylation by Cytochrome P450 Enzymes. *Chem. Rev.* **2010,** *110*, 932-948.

(53)   Price, J. C., E. W. Barr, B. Tirupati, J. M. Bollinger C. Krebs, The First Direct Characterization of a High-Valent Iron Intermediate in the Reaction of an α-Ketoglutarate-Dependent Dioxygenase: A High-Spin Fe(IV) Complex in Taurine/α-Ketoglutarate Dioxygenase (TauD) from Escherichia coli. *Biochemistry* **2003,** *42*, 7497-7508.

(54)   Hoffart, L. M., E. W. Barr, R. B. Guyer, J. M. Bollinger C. Krebs, Direct spectroscopic detection of a C-H-cleaving high-spin Fe(IV) complex in a prolyl-4-hydroxylase. *Proc. Natl. Acad. Sci. USA* **2006,** *103*, 14738-14743.

(55)   Chakrabarty, S., R. N. Austin, D. Deng, J. T. Groves J. D. Lipscomb, Radical Intermediates in Monooxygenase Reactions of Rieske Dioxygenases. *J. Am. Chem. Soc.* **2007,** *129*, 3514-3515.

(56)   Hohenberger, J., K. Ray K. Meyer, The biology and chemistry of high-valent iron–oxo and iron–nitrido complexes. *Nat. Commun.* **2012,** *3*, 720.

(57)   Klein, J.E. and Que, L., Jr (2016). Biomimetic High-Valent Mononuclear Nonheme Iron-Oxo Chemistry. Encyclopedia of Inorganic and Bioinorganic Chemistry, R.A. Scott (Ed.), Wiley**:** 1-22.

(58)   Rohde, J.-U., J.-H. In, M. H. Lim, W. W. Brennessel, M. R. Bukowski, A. Stubna, E. Münck, W. Nam L. Que, Crystallographic and Spectroscopic Characterization of a Nonheme Fe(IV)=O Complex. *Science* **2003,** *299*, 1037-1039.

(59)   McDonald, A. R. L. Que, High-valent nonheme iron-oxo complexes: Synthesis, structure, and spectroscopy. *Coord. Chem. Rev.* **2013,** *257*, 414-428.

(60)   Wang, D., K. Ray, M. J. Collins, E. R. Farquhar, J. R. Frisch, L. Gómez, T. A. Jackson, M. Kerscher, A. Waleska, P. Comba, M. Costas L. Que, Nonheme oxoiron(IV) complexes of pentadentate N5 ligands: spectroscopy, electrochemistry, and oxidative reactivity. *Chem. Sci.* **2013,** *4*, 282-291.

(61)   Company, A., J. Lloret-Fillol M. Costas (2013). Small Molecule Models for Nonporphyrinic Iron and Manganese Oxygenases. Comprehensive Inorganic Chemistry II, Vol. 3, Elsevier: 487-564.

(62)   Nam, W., Y.-M. Lee S. Fukuzumi, Tuning Reactivity and Mechanism in Oxidation Reactions by Mononuclear Nonheme Iron(IV)-Oxo Complexes. *Acc. Chem. Res.* **2014,** *47*, 1146-1154.

(63)   Engelmann, X., I. Monte-Pérez K. Ray, Oxidation Reactions with Bioinspired Mononuclear Non-Heme Metal–Oxo Complexes. *Angew. Chem. Int. Ed.* **2016,** *55*, 7632-7649.

(64)   Zhou, Y., X. Shan, R. Mas-Ballesté, M. R. Bukowski, A. Stubna, M. Chakrabarti, L. Slominski, J. A. Halfen, E. Münck L. Que Jr, Contrasting cis and trans Effects on the Reactivity of Nonheme Oxoiron(IV) Complexes. *Angew. Chem. Int. Ed.* **2008,** *47*, 1896-1899.

(65)   Rohde, J. U. L. Que, Jr., Axial coordination of carboxylate activates the non-heme Fe^{IV}=O unit. *Angew. Chem. Int. Ed.* **2005,** *44*, 2255-2258.

(66)   Ye, W., D. M. Ho, S. Friedle, T. D. Palluccio E. V. Rybak-Akimova, Role of Fe(IV)-Oxo Intermediates in Stoichiometric and Catalytic Oxidations Mediated by Iron Pyridine-Azamacrocycles. *Inorg. Chem.* **2012,** *51*, 5006-5021.

(67)   Chanda, A., X. Shan, M. Chakrabarti, W. C. Ellis, D. L. Popescu, F. Tiago de Oliveira, D. Wang, L. Que, T. J. Collins, E. Münck E. L. Bominaar, (TAML)Fe^{IV}=O Complex in Aqueous Solution: Synthesis and Spectroscopic and Computational Characterization. *Inorg. Chem.* **2008,** *47*, 3669-3678.

(68)   Rohde, J.-U., A. Stubna, E. L. Bominaar, E. Münck, W. Nam L. Que, Nonheme Oxoiron(IV) Complexes of Tris(2-pyridylmethyl)amine with *cis*-Monoanionic Ligands. *Inorg. Chem.* **2006,** *45*, 6435-6445.

(69)   Codolà, Z., I. Garcia-Bosch, F. Acuña-Parés, I. Prat, J. M. Luis, M. Costas J. Lloret-Fillol, Electronic Effects on Single-Site Iron Catalysts for Water Oxidation. *Chem. Eur. J.* **2013,** *19*, 8042-8047.

(70)   Seo, M. S., N. H. Kim, K.-B. Cho, J. E. So, S. K. Park, M. Clémancey, R. Garcia-Serres, J.-M. Latour, S. Shaik W. Nam, A mononuclear nonheme iron(IV)-oxo complex which is more reactive than cytochrome P450 model compound I. *Chem. Sci.* **2011,** *2*, 1039-1045.

(71)   Bigi, J. P., W. H. Harman, B. Lassalle-Kaiser, D. M. Robles, T. A. Stich, J. Yano, R. D. Britt C. J. Chang, A high-spin iron(IV)-oxo complex supported by a trigonal nonheme pyrrolide platform. *J. Am. Chem. Soc.* **2012,** *134*, 1536-1542.

(72)   Biswas, A. N., M. Puri, K. K. Meier, W. N. Oloo, G. T. Rohde, E. L. Bominaar, E. Münck L. Que, Modeling TauD-J: A High-Spin Nonheme Oxoiron(IV) Complex with High Reactivity toward C–H Bonds. *J. Am. Chem. Soc.* **2015,** *137*, 2428-2431.

(73)   England, J., M. Martinho, E. R. Farquhar, J. R. Frisch, E. L. Bominaar, E. Münck L. Que, Jr., A synthetic high-spin oxoiron(IV) complex: generation, spectroscopic characterization, and reactivity. *Angew. Chem. Int. Ed.* **2009,** *48*, 3622-3626.

(74)   Kaizer, J., E. J. Klinker, N. Y. Oh, J.-U. Rohde, W. J. Song, A. Stubna, J. Kim, E. Münck, W. Nam L. Que, Nonheme Fe^{IV}O Complexes That Can Oxidize the C−H Bonds of Cyclohexane at Room Temperature. *J. Am. Chem. Soc.* **2004,** *126*, 472-473.

(75)   Rana, S., A. Dey D. Maiti, Mechanistic elucidation of C–H oxidation by electron rich non-heme iron(IV)–oxo at room temperature. *Chem. Commun.* **2015,** *51*, 14469-14472.

(76)   Hitomi, Y., K. Arakawa M. Kodera, Synthesis, stability and reactivity of the first mononuclear nonheme oxoiron(IV) species with monoamido ligation: a putative reactive species generated from iron-bleomycin. *Chem. Commun.* **2014,** *50*, 7485-7487.

(77)   Martinho, M., F. Banse, J.-F. Bartoli, T. A. Mattioli, P. Battioni, O. Horner, S. Bourcier J.-J. Girerd, New Example of a Non-Heme Mononuclear Iron(IV) Oxo Complex. Spectroscopic Data and Oxidation Activity. *Inorg. Chem.* **2005,** *44*, 9592-9596.

(78)   Seo, M. S., J. Kim W. Nam, Generation of a Nonheme Oxoiron(IV) Intermediate and Its Reactivities

in Oxidation Reactions. *Bull. Korean Chem. Soc.* **2005,** *26*, 971-974.

(79)   Lim, M. H., J.-U. Rohde, A. Stubna, M. R. Bukowski, M. Costas, R. Y. N. Ho, E. Münck, W. Nam L. Que, An Fe^{IV}O complex of a tetradentate tripodal nonheme ligand. *Proc. Natl. Acad. Sci. USA* **2003,** *100*, 3665-3670.

(80)   Park, M. J., J. Lee, Y. Suh, J. Kim W. Nam, Reactivities of Mononuclear Non-Heme Iron Intermediates Including Evidence that Iron(III)−Hydroperoxo Species Is a Sluggish Oxidant. *J. Am. Chem. Soc.* **2006,** *128*, 2630-2634.

(81)   Hansch, C., A. Leo R. W. Taft, A survey of Hammett substituent constants and resonance and field parameters. *Chem. Rev.* **1991,** *91*, 165-195.

(82)   Hong, S., Y.-M. Lee, K.-B. Cho, K. Sundaravel, J. Cho, M. J. Kim, W. Shin W. Nam, Ligand Topology Effect on the Reactivity of a Mononuclear Nonheme Iron(IV)-Oxo Complex in Oxygenation Reactions. *J. Am. Chem. Soc.* **2011,** *133*, 11876-11879.

(83)   England, J., J. O. Bigelow, K. M. Van Heuvelen, E. R. Farquhar, M. Martinho, K. K. Meier, J. R. Frisch, E. Münck L. Que, An ultra-stable oxoiron(IV) complex and its blue conjugate base. *Chem. Sci.* **2014,** *5*, 1204-1215.

(84)   Sastri, C. V., J. Lee, K. Oh, Y. J. Lee, J. Lee, T. A. Jackson, K. Ray, H. Hirao, W. Shin, J. A. Halfen, J. Kim, L. Que, S. Shaik W. Nam, Axial ligand tuning of a nonheme iron(IV)–oxo unit for hydrogen atom abstraction. *Proc. Natl. Acad. Sci. USA* **2007,** *104*, 19181-19186.

(85)   Planas, O., M. Clémancey, J.-M. Latour, A. Company M. Costas, Structural modeling of iron halogenases: synthesis and reactivity of halide-iron(IV)-oxo compounds. *Chem. Commun.* **2014,** *50*, 10887-10890.

(86)   Widger, L. R., C. G. Davies, T. Yang, M. A. Siegler, O. Troeppner, G. N. L. Jameson, I. Ivanović-Burmazović D. P. Goldberg, Dramatically Accelerated Selective Oxygen-Atom Transfer by a Nonheme Iron(IV)-Oxo Complex: Tuning of the First and Second Coordination Spheres. *J. Am. Chem. Soc.* **2014,** *136*, 2699-2702.

(87)   Bryant, J. R. J. M. Mayer, Oxidation of C−H Bonds by [(bpy)$_2$(py)Ru^{IV}O]$^{2+}$ Occurs by Hydrogen Atom Abstraction. *J. Am. Chem. Soc.* **2003,** *125*, 10351-10361.

(88)   Mayer, J. M., Hydrogen Atom Abstraction by Metal−Oxo Complexes: Understanding the Analogy with Organic Radical Reactions. *Acc. Chem. Res.* **1998,** *31*, 441-450.

(89)   Warren, J. J., T. A. Tronic J. M. Mayer, Thermochemistry of Proton-Coupled Electron Transfer Reagents and its Implications. *Chem. Rev.* **2010,** *110*, 6961-7001.

(90)   Hirao, H., L. Que Jr, W. Nam S. Shaik, A Two-State Reactivity Rationale for Counterintuitive Axial Ligand Effects on the C–H Activation Reactivity of Nonheme Fe^{IV}=O Oxidants. *Chem. Eur. J.* **2008,** *14*, 1740-1756.

(91)   de Oliveira, F. T., A. Chanda, D. Banerjee, X. Shan, S. Mondal, L. Que, E. L. Bominaar, E. Münck T. J. Collins, Chemical and Spectroscopic Evidence for an Fe^V-Oxo Complex. *Science* **2007,** *315*, 835-838.

(92)   Chanda, A., D.-L. Popescu, F. T. de Oliveira, E. L. Bominaar, A. D. Ryabov, E. Münck T. J. Collins, High-valent iron complexes with tetraamido macrocyclic ligands: Structures, Mössbauer spectroscopy, and DFT calculations. *J. Inorg. Biochem.* **2006,** *100*, 606-619.

(93)   Ghosh, M., K. K. Singh, C. Panda, A. Weitz, M. P. Hendrich, T. J. Collins, B. B. Dhar S. Sen Gupta, Formation of a Room Temperature Stable Fe^V(O) Complex: Reactivity Toward Unactivated C–H Bonds. *J. Am. Chem. Soc.* **2014,** *136*, 9524-9527.

(94)   Ren, Q., Y. Guo, M. R. Mills, A. D. Ryabov T. J. Collins, On the Iron(V) Reactivity of an Aggressive Tail-Fluorinated Tetraamido Macrocyclic Ligand (TAML) Activator. *Eur. J. Inorg. Chem.* **2015,** *2015*, 1445-1452.

(95)   Mills, M. R., A. C. Weitz, M. P. Hendrich, A. D. Ryabov T. J. Collins, NaClO-Generated Iron(IV)oxo and Iron(V)oxo TAMLs in Pure Water. *J. Am. Chem. Soc.* **2016,** *138*, 13866-13869.

(96)   Pattanayak, S., F. G. Cantú Reinhard, A. Rana, S. S. Gupta S. P. de Visser, The Equatorial Ligand Effect on the Properties and Reactivity of Iron(V) Oxo Intermediates. *Chem. Eur. J.* **2019,** *25*, 8092-8104.

(97)   Lyakin, O. Y., K. P. Bryliakov E. P. Talsi, Non-heme oxoiron(V) intermediates in chemo-, regio- and stereoselective oxidation of organic substrates. *Coord. Chem. Rev.* **2019,** *384*, 126-139.

(98)   Oloo, W. N. L. Que, Bioinspired Nonheme Iron Catalysts for C–H and C=C Bond Oxidation: Insights into the Nature of the Metal-Based Oxidants. *Acc. Chem. Res.* **2015,** *48*, 2612-2621.

(99)   Kim, C., K. Chen, J. Kim L. Que, Stereospecific Alkane Hydroxylation with H_2O_2 Catalyzed by an Iron(II)−Tris(2-pyridylmethyl)amine Complex. *J. Am. Chem. Soc.* **1997,** *119*, 5964-5965.

(100)   Costas, M., K. Chen L. Que, Biomimetic nonheme iron catalysts for alkane hydroxylation. *Coord. Chem. Rev.* **2000,** *200-202*, 517-544.

(101)   Russell, G. A., Deuterium-isotope Effects in the Autoxidation of Aralkyl Hydrocarbons. Mechanism of the Interaction of Peroxy Radicals. *J. Am. Chem. Soc.* **1957,** *79*, 3871-3877.

(102)   Miyajima, S. O. Simamura, The Stereochemistry of Autoxidation of Methylcyclohexanes. *Bull. Chem. Soc. Jpn* **1975,** *48*, 526-530.

(103)   Chen, K. L. Que, Stereospecific Alkane Hydroxylation by Non-Heme Iron Catalysts: Mechanistic Evidence for an Fe^V=O Active Species. *J. Am. Chem. Soc.* **2001,** *123*, 6327-6337.

(104)   Dantignana, V., J. Serrano-Plana, A. Draksharapu, C. Magallón, S. Banerjee, R. Fan, I. Gamba, Y. Guo, L. Que, M. Costas A. Company, Spectroscopic and Reactivity Comparisons between Nonheme Oxoiron(IV) and Oxoiron(V) Species Bearing the Same Ancillary Ligand. *J. Am. Chem. Soc.* **2019,** *141*, 15078-15091.

(105)   Bernadou, J. B. Meunier, 'Oxo-hydroxo tautomerism' as useful mechanistic tool in oxygenation reactions catalysed by water-soluble metalloporphyrins. *Chem. Commun.* **1998**, 2167-2173.

(106)   Chen, K., M. Costas J. L. Que, Spin state tuning of non-heme iron-catalyzed hydrocarbon oxidations: participation of Fe^{III}–OOH and Fe^V=O intermediates. *J. Chem. Soc., Dalton Trans.* **2002**, 672-679.

(107)   Chen, K., M. Costas, J. Kim, A. K. Tipton L. Que, Olefin Cis-Dihydroxylation versus Epoxidation by Non-Heme Iron Catalysts: Two Faces of an Fe^{III}−OOH Coin. *J. Am. Chem. Soc.* **2002,** *124*, 3026-3035.

(108)   Company, A., L. Gómez, X. Fontrodona, X. Ribas M. Costas, A Novel Platform for Modeling Oxidative Catalysis in Non-Heme Iron Oxygenases with Unprecedented Efficiency. *Chem. Eur. J.* **2008,** *14*, 5727-5731.

(109)   Company, A., Y. Feng, M. Güell, X. Ribas, J. M. Luis, L. Que Jr M. Costas, Olefin-Dependent Discrimination between Two Nonheme HO–Fe^{V}=O Tautomeric Species in Catalytic H_2O_2 Epoxidations. *Chem. Eur. J.* **2009,** *15*, 3359-3362.

(110)   Chen, K. L. Que Jr, Evidence for the participation of a high-valent iron–oxo species in stereospecific alkane hydroxylation by a non-heme iron catalyst. *Chem. Commun.* **1999**, 1375-1376.

(111)   Prat, I., J. S. Mathieson, M. Güell, X. Ribas, J. M. Luis, L. Cronin M. Costas, Observation of Fe(V)=O using variable-temperature mass spectrometry and its enzyme-like C–H and C=C oxidation reactions. *Nat. Chem.* **2011,** *3*, 788-793.

(112)   Ho, R. Y. N., G. Roelfes, B. L. Feringa L. Que, Raman Evidence for a Weakened O−O Bond in Mononuclear Low-Spin Iron(III)−Hydroperoxides. *J. Am. Chem. Soc.* **1999,** *121*, 264-265.

(113)   Hitomi, Y., K. Arakawa, T. Funabiki M. Kodera, An Iron(III)–Monoamidate Complex Catalyst for Selective Hydroxylation of Alkane C–H Bonds with Hydrogen Peroxide. *Angew. Chem. Int. Ed.* **2012,** *51*, 3448-3452.

(114)   Xu, S., J. J. Veach, W. N. Oloo, K. C. Peters, J. Wang, R. H. Perry L. Que, Detection of a transient Fe^{V}(O)(OH) species involved in olefin oxidation by a bio-inspired non-haem iron catalyst. *Chem. Commun.* **2018,** *54*, 8701-8704.

(115)   Borrell, M., E. Andris, R. Navrátil, J. Roithová M. Costas, Characterized *cis*-Fe^{V}(O)(OH) intermediate mimics enzymatic oxidations in the gas phase. *Nat. Commun.* **2019,** *10*, 901.

(116)   White, M. C., A. G. Doyle E. N. Jacobsen, A Synthetically Useful, Self-Assembling MMO Mimic System for Catalytic Alkene Epoxidation with Aqueous H_2O_2. *J. Am. Chem. Soc.* **2001,** *123*, 7194-7195.

(117)   Mas-Ballesté, R. L. Que, Iron-Catalyzed Olefin Epoxidation in the Presence of Acetic Acid: Insights into the Nature of the Metal-Based Oxidant. *J. Am. Chem. Soc.* **2007,** *129*, 15964-15972.

(118)   Mas-Balleste, R., M. Fujita J. L. Que, High-valent iron-mediated *cis*-hydroxyacetoxylation of olefins. *Dalton Trans.* **2008**, 1828-1830.

(119)   Lyakin, O. Y., A. M. Zima, D. G. Samsonenko, K. P. Bryliakov E. P. Talsi, EPR Spectroscopic Detection of the Elusive Fe^{V}=O Intermediates in Selective Catalytic Oxofunctionalizations of Hydrocarbons Mediated by Biomimetic Ferric Complexes. *ACS Catal.* **2015,** *5*, 2702-2707.

(120)   Lyakin, O. Y., A. M. Zima, N. V. Tkachenko, K. P. Bryliakov E. P. Talsi, Direct Evaluation of the Reactivity of Nonheme Iron(V)–Oxo Intermediates toward Arenes. *ACS Catal.* **2018,** *8*, 5255-5260.

(121)   Tkachenko, N. V., R. V. Ottenbacher, O. Y. Lyakin, A. M. Zima, D. G. Samsonenko, E. P. Talsi K. P. Bryliakov, Highly Efficient Aromatic C−H Oxidation with H_2O_2 in the Presence of Iron Complexes of the PDP Family. *ChemCatChem* **2018,** *10*, 4052-4057.

(122)   Oloo, W. N., R. Banerjee, J. D. Lipscomb L. Que, Equilibrating (L)Fe^{III}–OOAc and (L)Fe^{V}(O) Species in Hydrocarbon Oxidations by Bio-Inspired Nonheme Iron Catalysts Using H_2O_2 and AcOH. *J. Am. Chem. Soc.* **2017,** *139*, 17313-17326.

(123)   Zima, A. M., O. Y. Lyakin, R. V. Ottenbacher, K. P. Bryliakov E. P. Talsi, Dramatic Effect of Carboxylic Acid on the Electronic Structure of the Active Species in Fe(PDP)-Catalyzed Asymmetric Epoxidation. *ACS Catal.* **2016,** *6*, 5399-5404.

(124)   Serrano-Plana, J., W. N. Oloo, L. Acosta-Rueda, K. K. Meier, B. Verdejo, E. García-España, M. G. Basallote, E. Münck, L. Que, A. Company M. Costas, Trapping a Highly Reactive Nonheme Iron Intermediate That Oxygenates Strong C—H Bonds with Stereoretention. *J. Am. Chem. Soc.* **2015,** *137*, 15833-15842.

(125)   Serrano-Plana, J., A. Aguinaco, R. Belda, E. García-España, M. G. Basallote, A. Company M. Costas, Exceedingly Fast Oxygen Atom Transfer to Olefins via a Catalytically Competent Nonheme Iron Species. *Angew. Chem. Int. Ed.* **2016,** *55*, 6310-6314.

(126)   Fan, R., J. Serrano-Plana, W. N. Oloo, A. Draksharapu, E. Delgado-Pinar, A. Company, V. Martin-Diaconescu, M. Borrell, J. Lloret-Fillol, E. García-España, Y. Guo, E. L. Bominaar, L. Que, M. Costas E. Münck, Spectroscopic and DFT Characterization of a Highly Reactive Nonheme Fe^V–Oxo Intermediate. *J. Am. Chem. Soc.* **2018,** *140*, 3916-3928.

(127)   Mondal, B., F. Neese, E. Bill S. Ye, Electronic Structure Contributions of Non-Heme Oxo-Iron(V) Complexes to the Reactivity. *J. Am. Chem. Soc.* **2018,** *140*, 9531-9544.

(128)   Tse, C.-W., T. W.-S. Chow, Z. Guo, H. K. Lee, J.-S. Huang C.-M. Che, Nonheme Iron Mediated Oxidation of Light Alkanes with Oxone: Characterization of Reactive Oxoiron(IV) Ligand Cation Radical Intermediates by Spectroscopic Studies and DFT Calculations. *Angew. Chem. Int. Ed.* **2014,** *53*, 798-803.

Chapter II

Objectives

Oxidation of strong and unactivated C-H bonds is an important but demanding reaction, which has drawn interest both in academic and industrial contexts. Particularly, efforts have been devoted to the development of sustainable processes with minimum environmental impact. To that purpose, bioinspired complexes have been actively studied as potential catalysts, taking inspiration from the unique capability of metalloenzymes to perform such challenging transformation. Thanks to the advances in the field, it is nowadays accepted that oxidation of C-H bonds, catalyzed by bioinspired complexes, takes place through a HAT process, carried out by a high-valent oxometal intermediate, followed by a rapid hydroxyl rebound that leads to the corresponding alcohol product. Furthermore, selectivity trends that define the relative reactivity of different C-H bonds have been established for such transformation. However, key aspects, as the enhancement of the selectivity and the efficiency of this reaction, remain to be solved before such strategy can be applied in synthetically useful processes.

In this context, the objectives of this thesis are, on one side, to find reaction conditions that permit to accomplish selective catalytic oxidation of unactivated C-H bonds and, on the other side, to investigate the properties affecting the reactivity of high-valent oxoiron species. Elucidation of mechanistic aspects is envisioned to help in improving the reaction.

More in detail, in Chapter III solvent effects in the oxidation of aliphatic C-H bonds catalyzed by bioinspired iron and manganese complexes bearing tetradentate aminopyridine ligands will be studied. Indeed, it has been reported that interaction of the solvent with the oxidant or the substrate can guide the outcome of HAT processes performed by organic radicals, and it has been envisioned that this could be an useful tool to modulate the chemoselectivity and the regioselectivity of C-H bond hydroxylation catalyzed by bioinspired complexes, being HAT the first step of such transformations (Scheme II.1, top).

Subsequently, in Chapter IV and V, attention will be pointed towards the study of high-valent oxoiron species. In Chapter IV, the oxidative ability of an oxoiron(IV) species containing an azamacrocyclic ligand will be investigated in OAT and HAT processes. Then, it will be compared to the one of the oxoiron(V) species bearing the same ligand architecture, previously reported. The direct comparison of these two complexes will allow to shed light on the impact of the oxidation state of the metal center on the reactivity and the selectivity of the studied reactions (Scheme II.1, middle).

In Chapter V, instead, the electronic properties of the azamacrocyclic ligand presented in Chapter IV will be modified, by introduction of polar substituents, with the aim to investigate the relevance of electronic effects on the reactivity of oxoiron(IV) species. Additionally, since these systems can exist as two different geometrical isomers, the influence of the relative orientation of the oxo ligand on the reactivity of the oxoiron(IV) species will be as well investigated (Scheme II.1, bottom).

Chapter III

chemoselective hydroxylations

regioselective hydroxylations

Chapter IV

chemoselectivity

oxidative ability

stereoselectivity

Chapter V

electronic effects

oxo ligand orientation

OAT

HAT
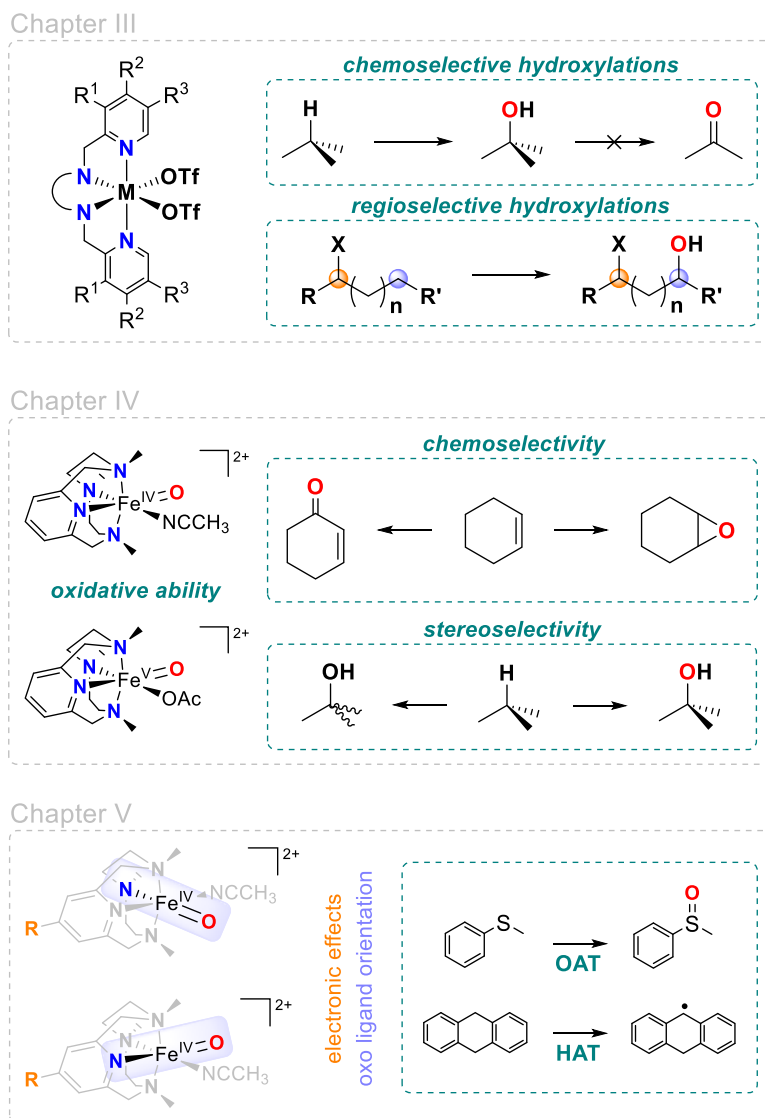
Scheme II.1. Objective of this thesis schematically represented.

Chapter III

Chemoselective aliphatic C−H bond oxidation enabled by polarity reversal

SITE AND PRODUCT SELECTIVE C-H OXIDATION DIRECTED BY SOLVENT HYDROGEN BONDING

selective oxidation — **strong HBD solvents** — **CH₃CN** — *overoxidation*

remote C-H oxidation — **X = OH, OR, NH₂, NHCOR** — *α-C-H oxidation*
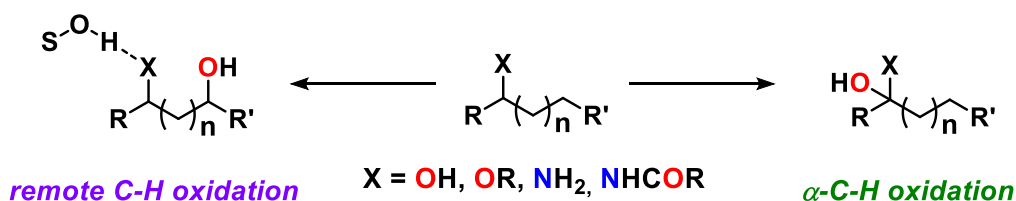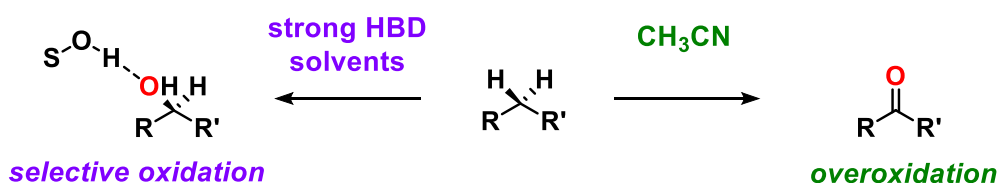
This chapter corresponds to the following publication:

V. Dantignana,‡ M. Milan,‡ O. Cussó, A. Company,* M. Bietti,* M. Costas*

ACS Cent. Sci., **2017**, *3*, 12, 1350-1358

‡both authors contributed equally to this work

For this publication V. D. developed the reaction protocol, synthetized ligands and metal complexes, performed the oxidation of alkanes and alcohols and analyzed the reaction products. Besides, V. D. contributed in writing the manuscript and was involved in argumentations and discussions.

Chemoselective Aliphatic C−H Bond Oxidation Enabled by Polarity Reversal

Valeria Dantignana,[†,‡] Michela Milan,[†,‡] Olaf Cussó,[†] Anna Company,[*,†] Massimo Bietti,[*,§] and Miquel Costas[*,†]

[†]Grup de Química Bioinspirada, Supramolecular i Catàlisi (QBIS-CAT), Institut de Química Computacional i Catàlisi (IQCC) and Departament de Química, Universitat de Girona, Campus Montilivi, Girona E-17071, Catalonia, Spain

[§]Dipartimento di Scienze e Tecnologie Chimiche, Università "Tor Vergata", Via della Ricerca Scientifica, 1, I-00133 Rome, Italy

Ⓢ Supporting Information

ABSTRACT: Methods for selective oxidation of aliphatic C−H bonds are called on to revolutionize organic synthesis by providing novel and more efficient paths. Realization of this goal requires the discovery of mechanisms that can alter in a predictable manner the innate reactivity of these bonds. Ideally, these mechanisms need to make oxidation of aliphatic C−H bonds, which are recognized as relatively inert, compatible with the presence of electron rich functional groups that are highly susceptible to oxidation. Furthermore, predictable modification of the relative reactivity of different C−H bonds within a molecule would enable rapid diversification of the resulting oxidation products. Herein we show that by engaging in hydrogen bonding, fluorinated alcohols exert a polarity reversal on electron rich functional groups, directing iron and manganese catalyzed oxidation toward a priori stronger and unactivated C−H bonds. As a result, selective hydroxylation of methylenic sites in hydrocarbons and remote aliphatic C−H oxidation of otherwise sensitive alcohol, ether, amide, and amine substrates is achieved employing aqueous hydrogen peroxide as oxidant. Oxidations occur in a predictable manner, with outstanding levels of product chemoselectivity, preserving the first-formed hydroxylation product, thus representing an extremely valuable tool for synthetic planning and development.
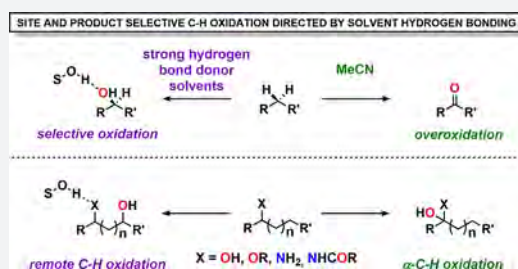
Selective oxidation of unactivated aliphatic C−H bonds constitutes a potentially very useful reaction because it introduces functionality in otherwise inert aliphatic skeletons.[1−4] However, the differentiation among multiple C−H bonds with powerful oxidizing agents and predictability in site selectivity are often unsurmountable problems that prevent the widespread incorporation of these reactions in synthetic planning. Another critical issue is represented by product chemoselectivity because the first formed products are generally more susceptible to oxidation than the starting substrate, and they are thus overoxidized or obtained in relatively low yield, a problem that is commonly encountered in the hydroxylation of methylenic C−H bonds, which in fact constitute the most represented aliphatic unit in organic molecules.[5]

In order to fully develop the power of C−H bond oxidation in organic synthesis, intense research efforts have been devoted to uncover the factors that govern C−H bond reactivity, pointing toward the important role played by bond strengths as well as by steric, electronic, stereoelectronic, and torsional effects in these processes.[2,6,7] On the basis of these elements, C−H bonds are recognized to bear an innate relative reactivity against oxidizing agents,[8] which defines the site selectivity in the oxidation of molecules containing different C−H bonds. However, this is basically unaffected by the nature of the oxidant, a factor that effectively limits the potential of the reaction. Since C−H oxidizing species generally display a strong

electrophilic character, C−H bonds in proximity to electron donating groups such as those of amines, amides, ethers, and alcohols are more reactive toward these reagents than those close to electron withdrawing groups, which are instead deactivated.[9] Efforts have also been devoted to modify the innate relative reactivity of C−H bonds by introducing directing groups.[10−15] Alternatively, interaction of Lewis or Brønsted acids with amines builds up positive charge onto these groups and deactivates via polarity reversal the adjacent C−H bonds, directing oxidation to the most remote and less deactivated C−H bonds.[7,16−18]

Recently, kinetic studies on hydrogen atom transfer (HAT) from aliphatic C−H bonds to the cumyloxy radical (CumO•) have shown that fluorinated alcohols can strongly influence the HAT reactivity.[7,19] With substrates bearing hydrogen bond acceptor (HBA) functional groups, a decrease in the rate constant for HAT from the aliphatic C−H bonds to CumO• was measured on going from acetonitrile to 2,2,2-trifluoroethanol (TFE), with the observed decrease in rate being dependent on the functional group HBA ability. This behavior was explained in terms of solvent hydrogen bonding to the substrate HBA center that, by increasing the extent of positive charge on the functional group, reverses the polarity of the

proximal C−H bonds that are thus deactivated toward HAT to the electrophilic CumO• (Scheme 1a, where Y represents an HBA group, H−D an HBD solvent, and X• = CumO•).

Scheme 1. (a) Schematic Diagram of the Polarity Reversal Concept and (b) Simplified C−H Hydroxylation Mechanism, Entailing Initial Hydrogen Atom Transfer (HAT) from a Substrate C−H Bond to High Valent Metal−Oxo Species II
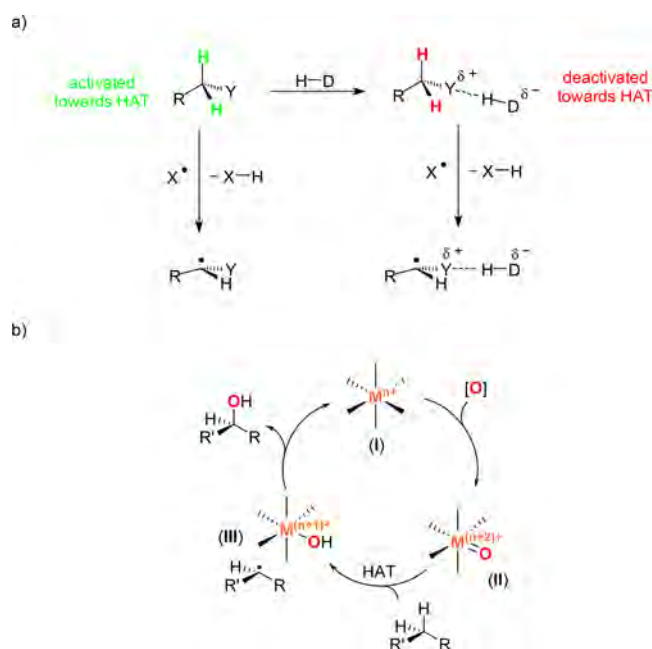
Along similar lines, 1,1,1,3,3,3-hexafluoro-2-propanol (HFIP) was shown to promote selective benzylic C−H oxidation of methylarenes to benzaldehydes via HAT to the phthalimide N-oxyl radical. In this case, hydrogen bonding to the oxygen atom of the first formed aldehyde product deactivates the formylic C−H toward HAT, preventing overoxidation to the carboxylic acid.[20,21]

We envisioned that these effects could offer a tool to manipulate the relative reactivity of aliphatic C−H bonds in metal catalyzed oxidations, where the reaction is initiated by HAT from the substrate to a high valent metal−oxo species (Scheme 1b).[22,23] With these bonds site-selectivity and product chemoselectivity are far more challenging than in the oxidation of benzylic C−H bonds because more powerful oxidants are typically required. With these concepts in hand, herein we show that fluorinated alcohol solvents strongly deactivate electron rich functional groups by virtue of hydrogen bonding interactions directing iron and manganese catalyzed oxidation toward a priori stronger and unactivated C−H bonds. As a result, selective hydroxylation of methylenic sites in hydrocarbons and remote C−H oxidation of alcohol, ether, amide, and amine substrates can be accomplished. Oxidations occur in a predictable manner, with outstanding levels of product chemoselectivity, preserving the first-formed hydroxylated product, thus representing an extremely valuable tool for synthetic planning.

■ **RESULTS AND DISCUSSION**

We initiated our study by analyzing the oxidation of a model alkane substrate (hexane, **1**) with H$_2$O$_2$ (0.2 equiv) using 1 mol

% of catalyst [Fe(CF$_3$SO$_3$)$_2$(pdp)] (**Fe(pdp)**) and [Mn-(CF$_3$SO$_3$)$_2$(pdp)] (**Mn(pdp)**) (Scheme 2a).[24,25] Reactions were performed in MeCN, TFE, and HFIP as solvents. Results are collected in Scheme 2b. In all cases, mixtures of 2-hexanol (**1a**), 3-hexanol (**1b**), 2-hexanone (**1c**), and 3-hexanone (**1d**) were obtained, but most interestingly, the relative alcohol to ketone ratios are largely dependent on the solvent. In MeCN, the reaction with **Fe(pdp)** (entry 1) provides oxidation products with an overall 54% yield, and the sum of the two alcohols (**1a** and **1b**) represents 46% of the products. Related values were observed with **Mn(pdp)** (entry 4, 52% yield, 38% selectivity toward the alcohols). The product pattern observed under these experimental conditions is in good agreement with literature precedents and can be rationalized considering the easier oxidation of the alcohol as compared to the hydrocarbon substrate.[24,25] When the same reactions were performed in TFE or HFIP (entries 2 and 3 for **Fe(pdp)** and 5 and 6 for **Mn(pdp)**), selectivity patterns changed in a very remarkable manner. In TFE, selectivity toward the alcohol products increases up to 86% and 92% for the iron and manganese catalyst (entries 2 and 5), and to an outstanding 98−99% in HFIP (entries 3 and 6). Remarkably, the use of a typical oxidation catalyst such as the porphyrin-based [Mn(TCPP)Cl] in combination with iodosylbenzene as oxidant, commonly used together with these complexes,[26] exhibits an analogous reactivity pattern. [Mn(TCPP)Cl] afforded the alcohol and ketone products in a 3:2 ratio and an overall 14% yield in MeCN, and only alcohol products (6% yield) in HFIP (see Table S1).

Further optimizations were performed in TFE and involved the screening of different catalysts structurally related to Fe- and Mn-based pdp complexes (see Scheme 2a and Tables S2 and S3).[12] **Fe(mcp)** and **Mn(mcp)** provide slightly reduced yields, while retaining or further improving the high chemoselectivity toward the alcohol products. Iron catalysts bearing electron rich pyridine ligands (**Fe(^{dMM}pdp)** and **Fe(^{dMM}mcp)**) exhibit improved selectivities toward the alcohol (93 and 91%), while the opposite effect is observed when an electron withdrawing group is installed on the pyridine ligand (80% for **Fe(^{Cl}pdp)**). Of notice, selectivities toward the alcohols observed with the manganese catalysts are less sensitive to analogous changes in the electronic properties of the pyridines, and remain high (≥93%) in all cases. Finally, catalysts bearing pyridines with sterically bulky silyl groups were explored.[12,27] Gratifyingly, **Fe(^{TIPS}mcp)** and **Mn(^{TIPS}mcp)** provided the highest product yields of the series (entries 7 and 8, 63 and 58%, respectively) while retaining very high chemoselectivity toward the alcohols (91 and 96%). With the optimal catalysts in hand, the impact of the solvent was further analyzed (entries 9−14, reactions run at 0 °C), employing lower catalyst loading (0.5 mol % was chosen after optimization) and a larger amount of H$_2$O$_2$ (0.5 equiv), which represents a more challenging condition because the larger amount of oxidant should favor overoxidation. For both catalysts, in MeCN, alcohols were obtained as minor products: 16% for **Fe(^{TIPS}mcp)** (entry 9) and 19% for **Mn(^{TIPS}mcp)** (entry 12). Instead, in TFE (entries 10 and 13), chemoselectivities were high: 86 and 89% for **Fe(^{TIPS}mcp)** and **Mn(^{TIPS}mcp)**, respectively. Most remarkably, in HFIP (entries 11 and 14) alcohols were obtained with outstanding selectivities (97%). Considering the slightly improved performance of **Mn(^{TIPS}mcp)**, this catalyst was chosen for further development of the reaction. Control

Scheme 2. (a) Catalysts Employed in This Work and (b) Optimization of Reaction Conditions for the Oxidation of Hexane (1)
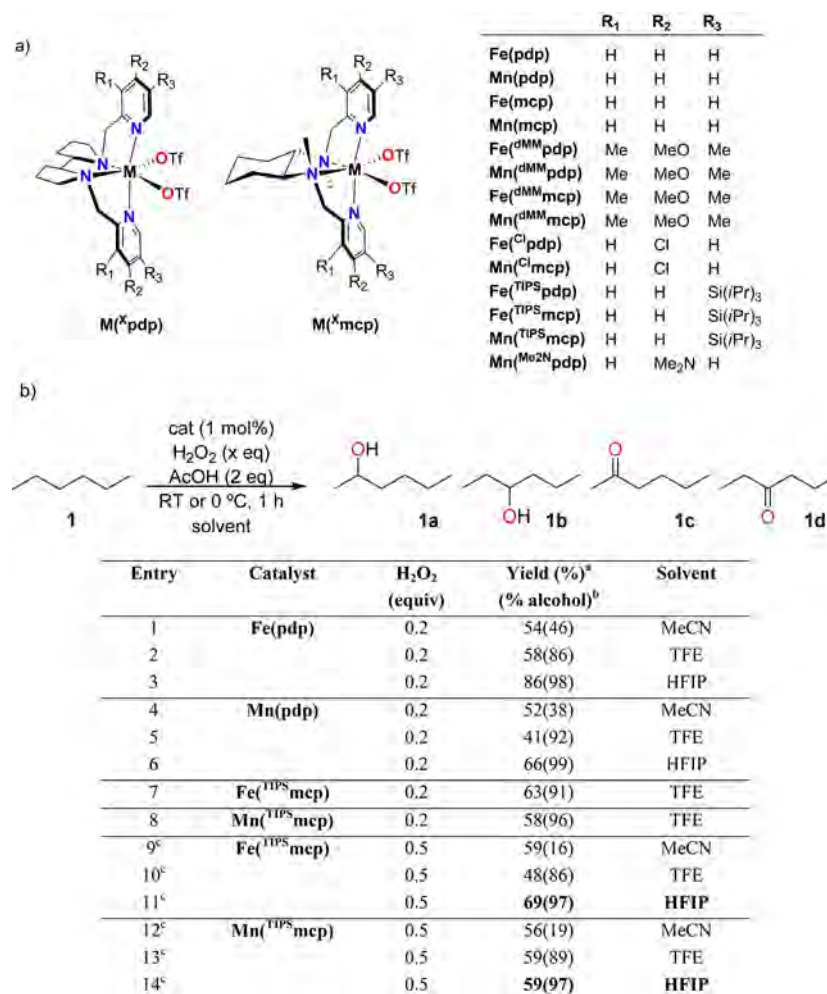
	R_1	R_2	R_3
Fe(pdp)	H	H	H
Mn(pdp)	H	H	H
Fe(mcp)	H	H	H
Mn(mcp)	H	H	H
Fe(^{dMM}pdp)	Me	MeO	Me
Mn(^{dMM}pdp)	Me	MeO	Me
Fe(^{dMM}mcp)	Me	MeO	Me
Mn(^{dMM}mcp)	Me	MeO	Me
Fe(^{Cl}pdp)	H	Cl	H
Mn(^{Cl}mcp)	H	Cl	H
Fe(^{TIPS}pdp)	H	H	Si(iPr)$_3$
Fe(^{TIPS}mcp)	H	H	Si(iPr)$_3$
Mn(^{TIPS}mcp)	H	H	Si(iPr)$_3$
Mn(^{Me2N}pdp)	H	Me$_2$N	H

Entry	Catalyst	H_2O_2 (equiv)	Yield (%)^a (% alcohol)^b	Solvent
1	Fe(pdp)	0.2	54(46)	MeCN
2		0.2	58(86)	TFE
3		0.2	86(98)	HFIP
4	Mn(pdp)	0.2	52(38)	MeCN
5		0.2	41(92)	TFE
6		0.2	66(99)	HFIP
7	Fe(^{TIPS}mcp)	0.2	63(91)	TFE
8	Mn(^{TIPS}mcp)	0.2	58(96)	TFE
9^c	Fe(^{TIPS}mcp)	0.5	59(16)	MeCN
10^c		0.5	48(86)	TFE
11^c		0.5	**69(97)**	**HFIP**
12^c	Mn(^{TIPS}mcp)	0.5	56(19)	MeCN
13^c		0.5	**59(89)**	TFE
14^c		0.5	**59(97)**	**HFIP**

^{a}With respect to H_2O_2, determined by GC-FID against an internal standard. Yields are calculated considering that 2 equiv of H_2O_2 are necessary for the formation of the ketone products (**1c** and **1d**). ^{b}100 × ([**1a**] + [**1b**]/([**1a**] + [**1b**] + [**1c**] + [**1d**]). ^{c}0.5 mol % catalyst was used; oxidations performed at 0 °C. Full details on the product distributions are provided in Table S1.

experiments indicated that no oxidation products were formed in the absence of the catalysts (see Table S4).

The high preference for the alcohol product in the oxidation of hexane in fluorinated alcohols is outstanding and unprecedented. Indeed, the hydroxylation of methylenic sites with high product chemoselectivity is a long-standing goal in C−H oxidations, because the resulting secondary alcohol is usually oxidized to the corresponding ketone under the reaction conditions, a process that can lead to loss of stereochemistry.[5,28,29] TFE and HFIP engage in hydrogen bonding with the first formed alcohol product, thus preventing overoxidation to the ketone via polarity reversal and consequent deactivation of the α-C−H bond (Scheme 1a, Y = OH, H−D = TFE or HFIP, X• = high valent metal−oxo species (**II** in Scheme 1b)). This picture is nicely supported by the stronger HBD ability of HFIP as compared to TFE (quantified on the basis of Abraham's α_2^H parameter: α_2^H = 0.771 and 0.567 for HFIP and TFE, respectively),[30] that accordingly leads in all cases to significantly higher selectivities for the alcohol product in HFIP. Thus, the current reaction provides a unique entry into highly chemoselective hydrocarbon hydroxylation.

A series of cyclic and bicyclic alkane substrates containing methylenic sites were then submitted to the optimized conditions. Results are collected in Table 1 and highlight the generality of the above-described observations. Oxidation of cyclohexane (**2**, entry 1) in MeCN gives preferentially cyclohexanone **2b** over cyclohexanol **2a** (**2a**:**2b** = 0.7) in 67% yield. Instead, in TFE the product chemoselectivity toward the alcohol is dramatically altered (**2a**:**2b** = 23, entry 2), and the effect is further enhanced in HFIP (entry 3), where **2a** accounts for 97% of the oxidation products. Analogous observations are noted in the oxidation of cyclooctane (**3**), where cyclooctanol **3a** is obtained as the major product in MeCN, with a modest selectivity over cyclooctanone **3b** (55%, entry 4), that increases in TFE (77%, entry 5) and HFIP (85%, entry 6). Oxidation of norbornane **4** is particularly interesting. In MeCN (entry 7) oxidation produces the *exo* alcohol **4a**$_{exo}$, with >99% selectivity over the *endo* alcohol **4a**$_{endo}$, along with the corresponding ketone **4b** (**4a**$_{exo}$:**4b** = 1.3). Reactions in TFE and HFIP increase both yield (entries 8 and 9, 82 and 80%, respectively) and chemoselectivity for **4a**$_{exo}$ (**4a**$_{exo}$:**4b** = 14.4 and 18 for TFE and HFIP, respectively), without altering the selectivity over **4a**$_{endo}$. Of notice, the large **4a**$_{exo}$/**4a**$_{endo}$ ratio reflects the hydroxylation stereospecificity, in good agreement with

Table 1. Oxidation of Methylenic C–H Bonds of Hydrocarbons in Different Solvents

Mn(^{TIPS}mcp) (0.5 mol%)
H$_2$O$_2$ (0.5 eq)
AcOH (2 eq)
solvent, 0 °C, 1 h

Entry	Substrate	Products	Solvent	Product yields (%)[a]	Yield (%)[a]	Hydroxylation selectivity (%)
				2a/2b		
1	**2**	**2a** **2b**	MeCN	17/50	67	40
2			TFE	68/6	74	96
3			HFIP	68/4	72	97
				3a/3b[b]		
4	**3**	**3a** **3b**	MeCN	24/28	58	55
5			TFE	48/4	64	77
6			HFIP	47/2	56	85
				4a[c]**/4b**		
7	**4**	**4a** **4b**	MeCN	24/36	60	57
8			TFE	72/10	82	94
9			HFIP	72/8	80	95
				5a[d]**/5b**[e]**/5c/5d**		
10	**5**	**5a** **5b** **5c** **5d**	MeCN	13/5/36/12	66	44
11			TFE	51/18/4/2	75	96
12			HFIP	62/23/2/2	89	98
				6a[f]**/6b**[g]**/6c/6d**		
13	**6**	**6a** **6b** **6c** **6d**	MeCN	8/13/12/26	59	53[c]
14			TFE	23/33/4/2	62	95[c]
15			HFIP	28/36/2/2	68	97[c]

[a]With respect to H$_2$O$_2$, determined by GC-FID against an internal standard. Yields are calculated considering that 2 equiv of H$_2$O$_2$ are necessary for the formation of the ketone products. [b]6–12% cyclooctene oxide formed. [c]**4a$_{exo}$** is obtained with >99 selectivity over **4a$_{endo}$** in all solvents. [d]**5a** is obtained as a mixture of axial and equatorial alcohol products. **5a$_{ax}$**:**5a$_{eq}$** ratios are 1:5, 1:3, and 1:3 for MeCN, TFE, and HFIP, respectively. [e]**5b** is obtained as a mixture of axial and equatorial alcohol products. **5b$_{ax}$**:**5b$_{eq}$** ratio is 2:3 in all solvents. [f]**6a** is obtained as a mixture of axial and equatorial alcohol products. **6a$_{ax}$**:**6a$_{eq}$** ratios are 1:3, 1:5, and 1:2 for MeCN, TFE, and HFIP, respectively. [g]**6b** is obtained as a mixture of axial and equatorial alcohol products. **6b$_{ax}$**:**6b$_{eq}$** ratios are 1:2, 1:2, and 2:5 for MeCN, TFE, and HFIP, respectively.

previous mechanistic studies in MeCN for these types of catalysts.[31,32]

Oxidation of *tert*-butylcyclohexane (**5**) is also very interesting. Products resulting from oxidation at C1, C2, and the *t*Bu moiety are not observed, reflecting a combination of steric, stereoelectronic, torsional, and bond strength contributions. As expected, oxidation concentrates at C3 and C4 and in HFIP provides alcohols **5a** and **5b** over ketones **5c** and **5d** with 98% selectivity (entry 12), in sharp contrast with the results obtained in MeCN (entry 10) and those of previous studies on the oxidation of **5** by HAT reagents where predominant formation of the ketone products was observed.[5,12,33] The ratio for oxidation at C3 (**5a** + **5c**) and C4 (**5b** + **5d**) is ~3. By taking into account the different number of C–H bonds at C3 and C4, these values denote a slight preference for oxidation at

the former site, in line with previous findings.[5,12,33] Equatorial alcohols are formed preferentially over axial ones (**5a$_{eq}$**:**5a$_{ax}$** = 3 and **5b$_{eq}$**:**5b$_{ax}$** = 1.5 in HFIP), a behavior that reasonably reflects the higher reactivity of equatorial C–H bonds toward HAT reagents.[34,35]

Finally, oxidation of *trans*-decalin (**6**) yields a mixture of alcohol (**6a** and **6b**) and ketone (**6c** and **6d**) products from oxidation at C2 and C3 methylenic sites (entries 13–15). In HFIP, **6a** and **6b** account for 97% of the oxidation products, and are obtained in 64% yield. Oxidation at C3 appears to be slightly favored over C2, presumably because the latter is sterically more encumbered. Most interestingly, hydroxylation occurs preferentially at the equatorial over the axial C–H bond (**6a$_{eq}$**:**6a$_{ax}$** = 2 and **6b$_{eq}$**:**6b$_{ax}$** = 2.5).

The unique chemoselectivity attained in fluorinated alcohols suggests that enantioselective hydroxylation of methylenic sites may be possible in these solvents without requiring large excess of the substrate due to the chiral nature of the catalysts. Oxidation of propylbenzene (**7**) with 1 mol % catalyst, 0.5 equiv of H_2O_2, and 2 equiv of AcOH in TFE led to the formation of the corresponding benzylic alcohol (**7a**) in 92% selectivity but with a modest 8% ee (Scheme 3). However,

Scheme 3. Oxidation of Propylbenzene (7) in TFE with Different Catalysts[a]

Mn(^{TIPS}mcp) / AcOH / 0 °C	12% (8% ee)	2%
Mn(^{dMM}pdp) / 2-eha / -35 °C	24% (66% ee)	2%
Mn(^{Me2N}pdp) / 2-eha / -35°C	44% (60% ee)	7%
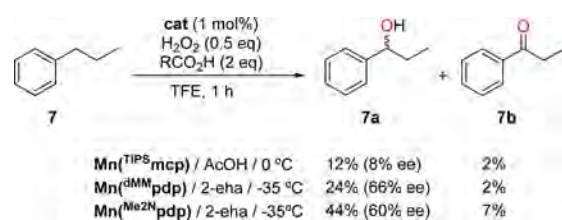
[a]Yields (with respect to H_2O_2) are shown below each of the products (**7a** and **7b**), and the enantiomeric excess of **7a** is written in parentheses.

catalyst screening using different Mn(^{X}mcp) and Mn(^{X}pdp) complexes and optimization of both the nature of the carboxylic acid additive and the temperature enabled the ee to be significantly increased while the selectivity for the alcohol product was kept above 90% (see Table S7). The best results were obtained with 2-ethylhexanoic acid in combination with Mn(^{dMM}pdp) or Mn(^{Me2N}pdp) at −35 °C, which afforded 1-phenyl-1-propanol with an enantiomeric excess of 66% and 60%, respectively (Scheme 3 and Table S8). Under identical experimental conditions, comparable ee's were also observed in the oxidation of ethylbenzene and *p*-methylethylbenzene (Table S7). For comparison, when the same reaction was performed in MeCN with the Mn(^{Me2N}pdp) catalyst under analogous reaction conditions, the ketone is the largely dominant product (7% of **7a** (10% ee) and 39% of **7b**).

Most importantly, as compared to previous examples of HAT based enantioselective benzylic oxidation,[36] the results obtained in this study clearly indicate that the use of fluorinated alcohols preserves the first formed chiral alcohol from overoxidation, avoiding moreover the use of relatively large substrate/oxidant ratios.

Intermolecular competition experiments were also carried out, in order to evaluate the relative reactivity of the substrate C−H and product HOC−H bonds under the reaction conditions. For this purpose, oxidation of a 1:1 mixture of cyclohexane (**2**) and cyclooctanol (**3a**) was carried out in MeCN, TFE, and HFIP (Scheme 4). In MeCN, the main

product (47% yield) corresponded to cyclooctanone (**3b**), derived from oxidation of **3a**, while smaller amounts of cyclohexane oxidation products (**2a** and **2b**) were obtained (8% combined yield). In fluorinated alcohols, the reactivity trend was completely reversed and the hydroxylation of **2** was preferential so that 31% and 34% yield of **2a** was obtained in TFE and HFIP, respectively. Product **3b** was obtained in only 10% and 4% yield, along with trace amounts of cyclooctanediol products **3c** and **3d** (*vide infra*). The complementary experiment using cyclohexanol (**2a**) and cyclooctane (**3**) as substrates (see Scheme S2) led to similar results, confirming that in fluorinated solvents C−H bonds are preferentially oxidized over HOC−H bonds. These results further demonstrate that by deactivating the C−H bond α to the OH group fluorinated alcohols exert a protective role, thus making oxidation of the first formed alcohol product much more difficult than in non-HBD or weaker HBD solvents.

Further studies investigated the impact of TFE and HFIP on the intramolecular selectivity in the oxidation of alcohol substrates, i.e., in modulating the relative reactivity of unactivated aliphatic C−H bonds versus secondary and primary alcohol functionalities placed on the same molecule (Scheme 5 and Scheme S4). Oxidation of 3-hexanol (**8**) in MeCN forms 3-hexanone (**8a**) in 76% yield as the only detectable product, but oxidation at the most remote methylenic site to form 2,4-hexanediol (**8b**) becomes a competitive path in the fluorinated alcohols, accounting for 20% of the oxidation products in HFIP. Oxidation of alcohols with longer alkyl chains evidence more substantial changes in the reaction selectivity. Thus, 1-hexanol (**9**) is oxidized in MeCN to hexanal (**9a**) and hexanoic acid (**9b**) in 66% combined yield. However, in HFIP, remote methylenic oxidation produces 1,5-hexanediol (**9c**) with 82% selectivity. Oxidations of 2-heptanol (**10**) and 2-octanol (**11**) follow an analogous pattern. Exclusive formation of 2-heptanone (**10a**) and 2-octanone (**11a**) is obtained in MeCN, while 2,6-heptanediol (**10b**) and 2,7-octanediol (**11b**) are the major products (75% and 93% selectivity, respectively) in HFIP. Of notice, in fluorinated alcohols, yields and selectivities for oxidation at the remote methylenic positions increase on going from **8** to **11**. In addition to the above-mentioned α-C−H bond deactivation via solvent hydrogen bonding, this trend also reflects remote C−H deactivation that decreases with increasing distance from the hydroxyl group.

Oxidation of cycloalkanols further illustrates the α-C−H bond deactivation determined by fluorinated alcohols. Oxidation of cyclohexanol (**2a**) in MeCN provides cyclohexanone (**2b**) with excellent chemoselectivity. However, competitive hydroxylation at the most remote C4-methylenic site takes place in HFIP, producing approximately a 1:1 mixture of *cis*- and *trans*-1,4-cyclohexanediols (**2c**), accounting for 45%

Scheme 4. Competitive Oxidation of Cyclohexane (2) and Cyclooctanol (3a) in Different Solvents[a]

	2a	2b	3b
MeCN	4%	4%	47%
TFE	31%	6%	10%
HFIP	34%	2%	4%
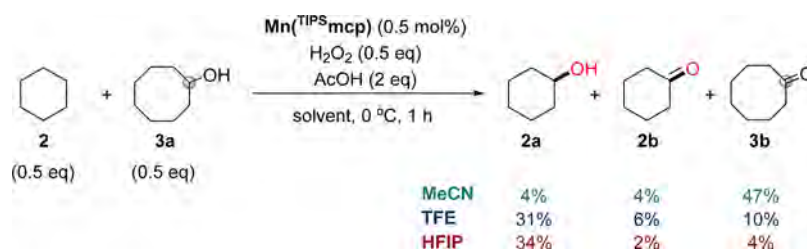
[a]Yields (with respect to H_2O_2) are shown below each of the products (**2a**, **2b**, and **3b**).

Scheme 5. Impact of the Solvent on the Catalytic Oxidation of Alkanols[a]
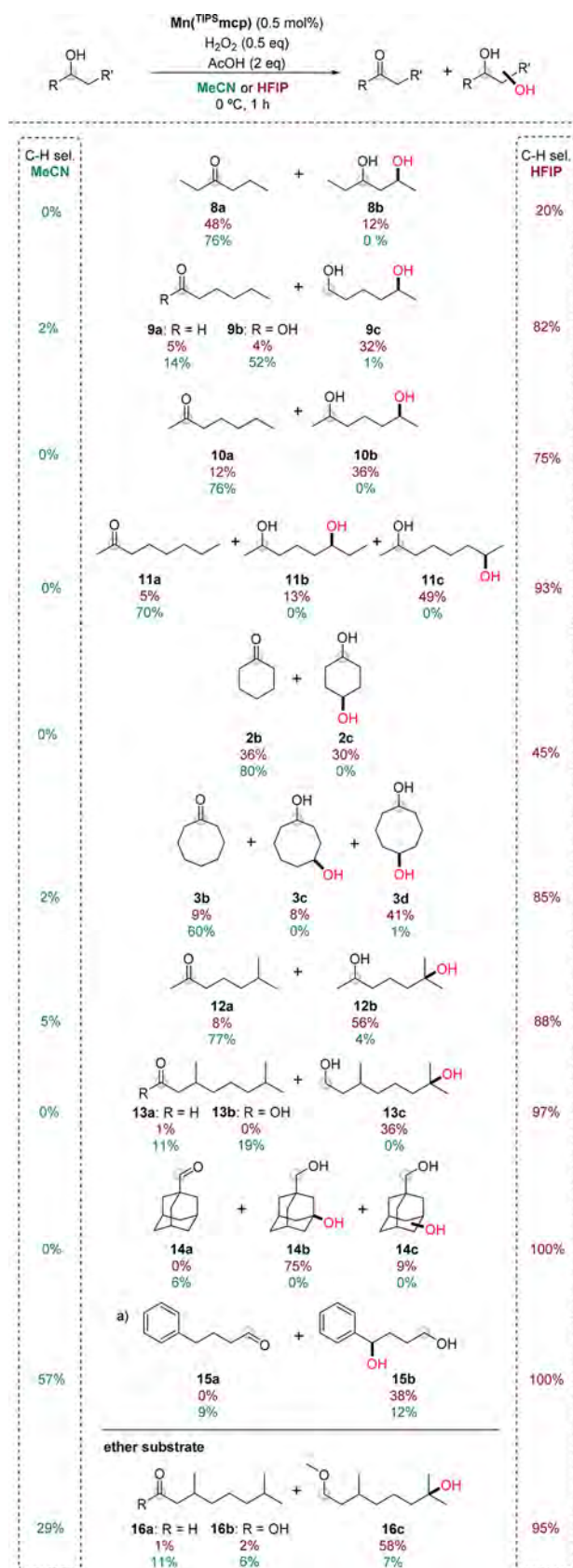
of the oxidation products. As observed with the linear alcohols, deactivation determined by solvent hydrogen bonding decreases with increasing distance from the hydroxyl group and, accordingly, the most remote methylenic sites become the preferred competitive oxidation sites. Thus, oxidation of cyclooctanol (**3a**) changes from nearly exclusive formation of cyclooctanone (**3b**) in MeCN to selective formation of 1,5-cyclooctanediol (**3c**), along with minor amounts of 1,4-cyclooctanediol in HFIP (85% selectivity).

Alkanols containing more reactive remote tertiary C–H bonds exhibit even higher hydroxylation selectivities. 6-Methyl-2-heptanol (**12**) afforded 2-methylheptane-2,6-diol (**12b**) as the predominant product in HFIP (88% selectivity), while in MeCN it only represented 5% of oxidized products, which were mainly represented by 6-methyl-2-heptanone (**12a**). The primary alcohol **13**, containing two tertiary C–H bonds, in MeCN gave exclusively the corresponding aldehyde (**13a**) or carboxylic acid (**13b**) products derived from the oxidation of the alcohol functionality. In contrast, oxidation at the tertiary C–H bond located further away from the alcohol was almost exclusively observed in HFIP (97% selectivity). A similar situation was found when 1-adamantanemethanol (**14**) was used as substrate: exclusive formation of the aldehyde product was observed in MeCN whereas only products deriving from hydroxylation of the adamantane C–H bonds were detected in HFIP. In the latter case and as expected, hydroxylation of tertiary C–H bonds (**14b**) was preferred over secondary ones (**14c**) in a combined 84% yield. With 4-phenyl-1-butanol (**15**), reaction in MeCN afforded an almost equimolar mixture of the aldehyde (**15a**) and 4-phenyl-1,4-butanediol (**15b**) products in a 21% combined yield. Benzylic hydroxylation was exclusively observed in HFIP to give diol **15b** in moderate yield (38%). In this case, **Mn(^{Me2N}pdp)** was used as catalyst because, as described above for the oxidation of **7**, in benzylic C–H hydroxylations, this complex affords significantly higher yields as compared to **Mn(^{TIPS}mcp)**. Finally, oxidation of substrate **16**, containing a methyl ether functionality instead of an alcohol, in MeCN yielded the corresponding aldehyde and carboxylic acid (**16a** and **16b**) as major products, presumably formed via the initial hydroxylation of the activated α-C–H bonds of the methyl ether moiety. Hydrolysis of the resulting α-hydroxy ether will produce the corresponding aldehyde (**16a**), which can be further oxidized to the carboxylic acid (**16b**). The ether functionality was instead preserved in HFIP, and hydroxylation at the remote tertiary C–H bond (**16c**) was accomplished in 58% yield and 95% selectivity.

Finally, we considered the use of fluorinated alcohols as a tool for deactivating C–H bonds that are adjacent to other HBA groups, directing oxidation toward remote C–H bonds (Scheme 6). Interestingly, oxidation of amides also evidences a powerful role of the fluorinated solvents in dictating site selectivity in line with the results obtained previously on the reactions of alkanamides with CumO[•],[19] where strong deactivation toward HAT of the C–H bonds that are α to the amide nitrogen was observed in TFE. Oxidation of amides was carried out using a large excess of acetic acid (13 equiv), which was necessary to maximize product yields as previously reported by some of us.[12] Oxidation of N-pentylacetamide (**17**) in MeCN occurs preferentially at the activated methylenic site α to the amide nitrogen providing hydroxylated product **17a**.[37]

[a]Yields (with respect to H₂O₂) are shown below each of the products (purple: yields obtained in HFIP, green: yields obtained in MeCN). [a]**Mn(^{Me2N}pdp)** was used as catalyst in this case.

Scheme 6. Impact of the Fluorinated Alcohols on the Catalytic Oxidation of Amides[a]

[a]Yields (calculated with respect to the substrate) are shown below each of the products (green: yields obtained in MeCN, purple: yields obtained in HFIP). [a]Isolated yield. Reaction conditions: [b]**Mn-**(^{dMM}**pdp**) (1 mol %), H_2O_2 (3.5 eq), AcOH (13 eq), MeCN, −40 °C. [c]**Mn**(^{TIPS}**mcp**) (1 mol %), H_2O_2 (3.5 eq), AcOH (13 eq). HFIP, 0 °C. [d]**Mn**(^{dMM}**pdp**) (1 mol %), H_2O_2 (1.0 eq), AcOH (13 eq), MeCN or HFIP, 0 °C. [e]**Mn**(^{TIPS}**mcp**) (1 mol %), H_2O_2 (1.0 eq), AcOH (13 eq), MeCN or HFIP, 0 °C.

When the same reaction is performed in HFIP, ketoamide **17b** resulting from oxidation of the most remote methylenic site is also formed as the major product in 51% yield. In this case, formation of the δ-C=O in **17b** instead of the hydroxyl group is not understood and, indeed, lowering the amount of oxidant to prevent overoxidation did not change the outcome of the reaction. Oxidation of amide **18** features competition between the α-C−H bond and a remote tertiary γ-C−H bond. In MeCN, oxidation occurs almost exclusively at the most activated α-C−H bond to form product **18a** in 65% yield.[37] A complete reversal in site selectivity is observed in HFIP, where **18b** is exclusively formed in 62% yield. Similary, in MeCN, amide **19**, bearing a remote tertiary C−H bond in the ε position with respect to the amide group,[16] almost exclusively afforded formyl amide **19a** following ring opening of the first formed product deriving from hydroxylation of the secondary α-C−H bond. In HFIP, exclusive formation of product **19b** deriving from hydroxylation of the remote tertiary C−H bond was instead observed. Furthermore, the oxidation of *N*-1-adamantylmethyl pivalamide **20** in MeCN results in a mixture of products deriving from hydroxylation of two (**20b**) and three (**20c**) tertiary C−H bonds of the adamantane core. Instead, when the reaction is performed in HFIP, exclusive formation of monohydroxylated product **20a** is observed in 55% yield. This result evidences a synergistic deactivating role of the amide and

hydroxyl groups upon hydrogen bonding to the fluorinated alcohol.

Selective hydroxylation of lactam **21** at the remote tertiary C−H bond, which has been recently accomplished through oxygen methylation,[38] was successfully achieved in HFIP to form **21a** in 49% yield, without the need of covalent modification of the substrate (Scheme 7).

Scheme 7. Oxidation of Lactam 21 in HFIP, without Covalent Modification
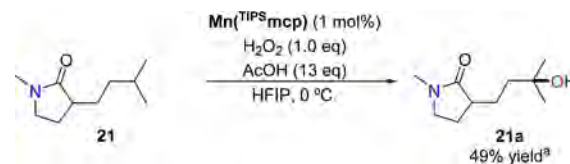
[a]Isolated yield.

Primary and secondary amines could also be successfully hydroxylated in fluorinated solvents (Scheme 8). Most

Scheme 8. Impact of Fluorinated Solvents on the Catalytic Oxidation of Amines[a]
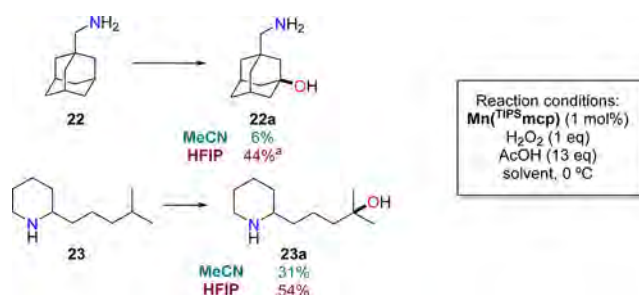
[a]Yields (calculated with respect to the substrate) are shown below each of the products (green, MeCN; purple, HFIP). [a]Isolated yield

remarkably, in HFIP, 1-admantylmethylamine (**22**) and 2-(4-methylpentyl)piperidine (**23**) were hydroxylated at the tertiary adamantane C−H bonds and most remote tertiary C−H bond, respectively, to furnish the corresponding aminoalcohols (**22a** and **23a**) in 44% and 54% yield, respectively, again without the need to deactivate the amine functionality via a covalent modification.

■ CONCLUSIONS

The origin of the effect of fluorinated alcohols in modulating the relative reactivity of aliphatic C−H bonds deserves some final discussion. These alcohols are strong HBD solvents and display a non-nucleophilic character, which endows them with the ability to stabilize charged intermediates. These solvents have been recently shown to strongly impact on a number of aliphatic C−H functionalizations.[28,39−45] However, as pointed out in two recent reviews,[46,47] the accurate role of HFIP and TFE in these processes has not been fully elucidated and tentative explanations associated with their strong HBD ability have been generally proposed. The current work provides, on the other hand, solid evidence that fluorinated alcohols induce a polarity reversal to HBA groups, strongly deactivating proximal C−H bonds toward oxidation by high valent metal oxo species, which proceeds via an initial HAT. By virtue of this effect, alcohols, ethers, amines, and amides, commonly understood as

critical functional groups in C−H oxidations, and able moreover to strongly activate adjacent C−H bonds toward electrophilic HAT reagents, become oxidatively robust functionalities that can be used to direct C−H oxidation toward remote positions in a predictable manner. A synthetically relevant consequence of this effect is that efficient hydroxylation of methylenic sites can be accomplished with outstanding product chemoselectivity. Therefore, the current reactions open novel paths for C−H bond oxidation with orthogonal chemoselectivity to that occurring in conventional solvents. Finally, the current work focuses on metal catalyzed oxidations, but it is envisioned that the effects described herein, being substrate based, will have general applicability in HAT promoted functionalization reactions, and therefore will have a very important and rapidly implemented impact in synthetically useful C−H functionalization procedures.

ASSOCIATED CONTENT

Ⓢ Supporting Information

The Supporting Information is available free of charge on the ACS Publications website at DOI: 10.1021/acscentsci.7b00532.

> Synthesis of complexes and substrates, experimental details, product characterization, results of screening, oxidation of alcohols in TFE, and control experiments (PDF)

AUTHOR INFORMATION

Corresponding Authors
*E-mail: anna.company@udg.edu.
*E-mail: bietti@uniroma2.it.
*E-mail: miquel.costas@udg.edu.

ORCID Ⓘ
Massimo Bietti: 0000-0001-5880-7614
Miquel Costas: 0000-0001-6326-8299

Author Contributions
[‡]V.D. and M.M. contributed equally to this work.

Notes
The authors declare no competing financial interest.

ACKNOWLEDGMENTS

REFERENCES

(1) Cernak, T.; Dykstra, K. D.; Tyagarajan, S.; Vachal, P.; Krska, S. W. The medicinal chemist's toolbox for late stage functionalization of drug-like molecules. *Chem. Soc. Rev.* **2016**, *45*, 546−576.

(2) Newhouse, T.; Baran, P. S. If C-H Bonds Could Talk: Selective C-H Bond Oxidation. *Angew. Chem., Int. Ed.* **2011**, *50*, 3362−3374.

(3) White, M. C. Adding Aliphatic C-H Bond Oxidations to Synthesis. *Science* **2012**, *335*, 807−809.

(4) Genovino, J.; Sames, D.; Hamann, L. G.; Touré, B. B. Accessing Drug Metabolites via Transition-Metal Catalyzed C−H Oxidation: The Liver as Synthetic Inspiration. *Angew. Chem., Int. Ed.* **2016**, *55*, 14218−14238.

(5) Chen, M. S.; White, M. C. Combined Effects on Selectivity in Fe-Catalyzed Methylene Oxidation. *Science* **2010**, *327*, 566−571.

(6) Mayer, J. M. Understanding Hydrogen Atom Transfer: From Bond Strengths to Marcus Theory. *Acc. Chem. Res.* **2011**, *44*, 36−46.

(7) Salamone, M.; Bietti, M. Tuning Reactivity and Selectivity in Hydrogen Atom Transfer from Aliphatic C−H Bonds to Alkoxyl Radicals: Role of Structural and Medium Effects. *Acc. Chem. Res.* **2015**, *48*, 2895−2903.

(8) Brückl, T.; Baxter, R. D.; Ishihara, Y.; Baran, P. S. Innate and Guided C−H Functionalization Logic. *Acc. Chem. Res.* **2012**, *45*, 826−839.

(9) Roberts, B. P. Polarity-reversal catalysis of hydrogen-atom abstraction reactions: concepts and applications in organic chemistry. *Chem. Soc. Rev.* **1999**, *28*, 25−35.

(10) Bigi, M. A.; Reed, S. A.; White, M. C. Directed Metal (Oxo) Aliphatic C−H Hydroxylations: Overriding Substrate Bias. *J. Am. Chem. Soc.* **2012**, *134*, 9721−9726.

(11) Das, S.; Incarvito, C. D.; Crabtree, R. H.; Brudvig, G. W. Molecular Recognition in the Selective Oxygenation of Saturated C-H Bonds by a Dimanganese Catalyst. *Science* **2006**, *312*, 1941−1943.

(12) Milan, M.; Bietti, M.; Costas, M. Highly Enantioselective Oxidation of Nonactivated Aliphatic C-H Bonds with Hydrogen Peroxide Catalyzed by Manganese Complexes. *ACS Cent. Sci.* **2017**, *3*, 196−204.

(13) Simmons, E. M.; Hartwig, J. F. Catalytic functionalization of unactivated primary C−H bonds directed by an alcohol. *Nature* **2012**, *483*, 70−73.

(14) Chen, K.; Richter, J. M.; Baran, P. S. 1,3-Diol Synthesis via Controlled, radical-Mediated C-H Functionalization. *J. Am. Chem. Soc.* **2008**, *130*, 7247−7249.

(15) Frost, J. R.; Huber, S. M.; Breitenlechner, S.; Bannwarth, C.; Bach, T. Enantiotopos-Selective C-H Oxygenation Catalyzed by a Supramolecular Ruthenium Complex. *Angew. Chem., Int. Ed.* **2015**, *54*, 691−695.

(16) Howell, J. M.; Feng, K. B.; Clark, J. R.; Trzepkowski, L. J.; White, M. C. Remote Oxidation of Aliphatic C-H Bonds in Nitrogen-Containing Molecules. *J. Am. Chem. Soc.* **2015**, *137*, 14590−14593.

(17) Lee, M.; Sanford, M. S. Platinum-Catalyzed, Terminal-Selective C(sp³)−H Oxidation of Aliphatic Amines. *J. Am. Chem. Soc.* **2015**, *137*, 12796−12799.

(18) Mbofana, C. T.; Chong, E.; Lawniczak, J.; Sanford, M. S. Iron-Catalyzed Oxyfunctionalization of Aliphatic Amines at Remote Benzylic C−H Sites. *Org. Lett.* **2016**, *18*, 4258−4261.

(19) Salamone, M.; Mangiacapra, L.; Bietti, M. Kinetic Solvent Effects on the Reactions of the Cumyloxyl Radical with Tertiary Amides. Control over the Hydrogen Atom Transfer Reactivity and Selectivity through Solvent Polarity and Hydrogen Bonding. *J. Org. Chem.* **2015**, *80*, 1149−1154.

(20) Lumb, J.-P. Stopping Aerobic Oxidation in Its Tracks: Chemoselective Synthesis of Benzaldehydes from Methylarenes. *Angew. Chem., Int. Ed.* **2017**, *56*, 9276−9277.

(21) Gaster, E.; Kozuch, S.; Pappo, D. Selective Aerobic Oxidation of Methylarenes to Benzaldehydes Catalyzed by N-Hydroxyphthalimide and Cobalt(II) Acetate in Hexafluoropropan-2-ol. *Angew. Chem., Int. Ed.* **2017**, *56*, 5912−5915.

(22) Oloo, W. N.; Que, L. Bioinspired Nonheme Iron Catalysts for C−H and C≡C Bond Oxidation: Insights into the Nature of the Metal-Based Oxidants. *Acc. Chem. Res.* **2015**, *48*, 2612−2621.

(23) Huang, X.; Groves, J. T. Beyond ferryl-mediated hydroxylation: 40 years of the rebound mechanism and C−H activation. *J. Biol. Inorg. Chem.* **2017**, *22*, 185−207.

(24) Gomez, L.; Garcia-Bosch, I.; Company, A.; Benet-Buchholz, J.; Polo, A.; Sala, X.; Ribas, X.; Costas, M. Stereospecific CH Oxidation with H2O2 Catalyzed by a Chemically Robust Site-Isolated Iron Catalyst. *Angew. Chem., Int. Ed.* **2009**, *48*, 5720−5723.

(25) Ottenbacher, R. V.; Samsonenko, D. G.; Talsi, E. P.; Bryliakov, K. P. Highly Efficient, Regioselective, and Stereospecific Oxidation of Aliphatic C-H Groups with H2O2, Catalyzed by Aminopyridine Manganese Complexes. *Org. Lett.* **2012**, *14*, 4310−4313.

(26) Gómez, L. PhD thesis; University of Girona: 2010.

(27) Font, D.; Canta, M.; Milan, M.; Cusso, O.; Ribas, X.; Klein Gebbink, R. J. M.; Costas, M. Readily Accessible Bulky Iron Catalysts exhibiting Site Selectivity in the Oxidation of Steroidal Substrates. *Angew. Chem., Int. Ed.* **2016**, *55*, 5776−5779.

(28) Kawamata, Y.; Yan, M.; Liu, Z.; Bao, D.-H.; Chen, J.; Starr, J. T.; Baran, P. S. Scalable, Electrochemical Oxidation of Unactivated C−H Bonds. *J. Am. Chem. Soc.* **2017**, *139*, 7448−7451.

(29) Curci, R.; D'Accolti, L.; Fusco, C. A Novel Approach to the Efficient Oxygenation of Hydrocarbons under Mild Conditions. Superior Oxo Transfer Selectivity Using Dioxiranes. *Acc. Chem. Res.* **2006**, *39*, 1−9.

(30) Abraham, M. H.; Grellier, P. L.; Prior, D. V.; Duce, P. P.; Morris, J. J.; Taylor, P. J. Hydrogen Bonding. Part 7. A Scale of Solute Hydrogen-bond Acidity based on log *K* Values for Complexation in Tetrachloromethane. *J. Chem. Soc., Perkin Trans. 2* **1989**, 699−711.

(31) Ottenbacher, R. V.; Talsi, E. P.; Bryliakov, K. P. Mechanism of Selective C-H Hydroxylation Mediated by Manganese Aminopyridine Enzyme Models. *ACS Catal.* **2015**, *5*, 39−44.

(32) Chen, K.; Que, L. Stereospecific alkane hydroxylation by non-heme iron catalysts: Mechanistic evidence for an Fe^v=O active species. *J. Am. Chem. Soc.* **2001**, *123*, 6327−6337.

(33) Canta, M.; Font, D.; Gómez, L.; Ribas, X.; Costas, M. The Iron(II) Complex [Fe(CF$_3$SO$_3$)$_2$(mcp)] as a Convenient, Readily Available Catalyst for the Selective Oxidation of Methylenic Sites in Alkanes. *Adv. Synth. Catal.* **2014**, *356*, 818−830.

(34) Chen, K.; Eschenmoser, A.; Baran, P. S. Strain Release in C-H Bond Activation? *Angew. Chem., Int. Ed.* **2009**, *48*, 9705−9708.

(35) Salamone, M.; Ortega, V. B.; Bietti, M. Enhanced Reactivity in Hydrogen Atom Transfer from Tertiary Sites of Cyclohexanes and Decalins via Strain Release: Equatorial C-H Activation vs Axial C-H Deactivation. *J. Org. Chem.* **2015**, *80*, 4710−4715.

(36) Talsi, E. P.; Samsonenko, D. G.; Bryliakov, K. P. Asymmetric Autoamplification in the Oxidative Kinetic Resolution of Secondary Benzylic Alcohols Catalyzed by Manganese Complexes. *ChemCatChem* **2017**, *9*, 2599−2607.

(37) Milan, M.; Carboni, G.; Salamone, M.; Costas, M.; Bietti, M. Tuning Selectivity in Aliphatic C−H Bond Oxidation of *N*-Alkylamides and Phthalimides Catalyzed by Manganese Complexes. *ACS Catal.* **2017**, *7*, 5903−5911.

(38) Nanjo, T.; de Lucca, E. C.; White, M. C. Remote, Late-Stage Oxidation of Aliphatic C−H Bonds in Amide-Containing Molecules. *J. Am. Chem. Soc.* **2017**, *139*, 14586−14591.

(39) Gutekunst, W. R.; Baran, P. S. Total Synthesis and Structural Revision of the Piperarborenines via Sequential Cyclobutane C−H Arylation. *J. Am. Chem. Soc.* **2011**, *133*, 19076−19079.

(40) Rodriguez, N.; Romero-Revilla, J. A.; Fernandez-Ibanez, M. A.; Carretero, J. C. Palladium-catalyzed *N*-(2-pyridyl)sulfonyl-directed C(sp^3)-H [γ]-arylation of amino acid derivatives. *Chem. Sci.* **2013**, *4*, 175−179.

(41) Fan, M.; Ma, D. Palladium-Catalyzed Direct Functionalization of 2-Aminobutanoic Acid Derivatives: Application of a Convenient and Versatile Auxiliary. *Angew. Chem., Int. Ed.* **2013**, *52*, 12152−12155.

(42) Gong, W.; Zhang, G.; Liu, T.; Giri, R.; Yu, J.-Q. Site-Selective C(sp^3)−H Functionalization of Di-, Tri-, and Tetrapeptides at the *N*-Terminus. *J. Am. Chem. Soc.* **2014**, *136*, 16940−16946.

(43) Sambiagio, C.; Sterckx, H.; Maes, B. U. W. Electrosynthesis: A New Frontier in Aerobic Oxidation? *ACS Cent. Sci.* **2017**, *3*, 686−688.

(44) Wang, D.; Shuler, W. G.; Pierce, C. J.; Hilinski, M. K. An Iminium Salt Organocatalyst for Selective Aliphatic C−H Hydroxylation. *Org. Lett.* **2016**, *18*, 3826−3829.

(45) Adams, A. M.; Du Bois, J. Organocatalytic C-H hydroxylation with Oxone enabled by an aqueous fluoroalcohol solvent system. *Chem. Sci.* **2014**, *5*, 656−659.

(46) Wencel-Delord, J.; Colobert, F. A remarkable solvent effect of fluorinated alcohols on transition metal catalysed C-H functionalizations. *Org. Chem. Front.* **2016**, *3*, 394−400.

(47) Colomer, I.; Chamberlain, A. E. R.; Haughey, M. B.; Donohoe, T. J. Hexafluoroisopropanol as a highly versatile solvent. *Nat. Rev. Chem.* **2017**, *1*, 0088.

Chapter IV

Spectroscopic and reactivity comparisons between nonheme oxoiron(IV) and oxoiron(V) species bearing the same ancillary ligand
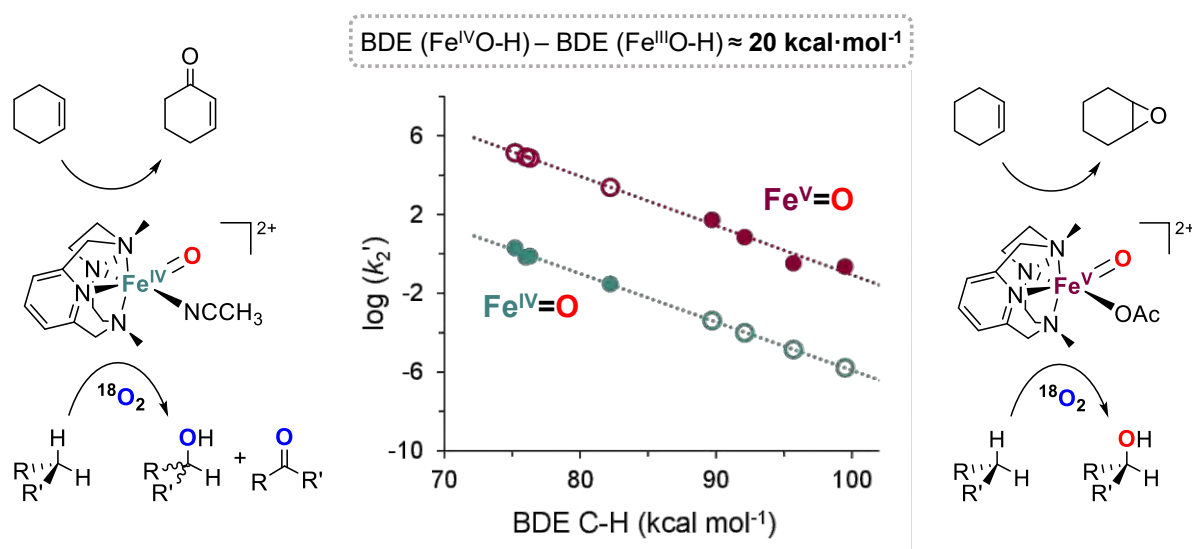
This chapter corresponds to the following publication:

V. Dantignana, J. Serrano-Plana, A. Draksharapu, C. Magallón, S. Banerjee, R. Fan, I. Gamba, Y. Guo, L. Que Jr.,* M. Costas,* A. Company*

J. Am. Chem. Soc. **2019**, *141*, 38*, 15078-15091*

For this publication V. D. synthetized ligand PyNMe$_3$ and the related iron(II) and oxoiron complexes and performed the reactivity studies with the oxoiron species. Besides, V. D. contributed in writing the manuscript and was involved in argumentations and discussions.

Spectroscopic and Reactivity Comparisons between Nonheme Oxoiron(IV) and Oxoiron(V) Species Bearing the Same Ancillary Ligand

Valeria Dantignana,[†] Joan Serrano-Plana,[†,||] Apparao Draksharapu,[‡,⊥] Carla Magallón,[†] Saikat Banerjee,[‡] Ruixi Fan,[§] Ilaria Gamba,[†] Yisong Guo,[§] Lawrence Que, Jr.,[*,‡] Miquel Costas,[*,†] and Anna Company[*,†]

[†]Institut de Química Computacional i Catàlisi (IQCC), Departament de Química, Universitat de Girona, C/M. Aurèlia Capmany 69, 17003 Girona, Catalonia, Spain

[‡]Department of Chemistry and Center for Metals in Biocatalysis, University of Minnesota, Minneapolis, Minnesota 55455, United States

[§]Department of Chemistry, Carnegie Mellon University, 4400 Fifth Avenue, Pittsburgh, Pennsylvania 15213, United States

Ⓢ *Supporting Information*

ABSTRACT: This work directly compares the spectroscopic and reactivity properties of an oxoiron(IV) and an oxoiron(V) complex that are supported by the same neutral tetradentate N-based PyNMe$_3$ ligand. A complete spectroscopic characterization of the oxoiron(IV) species (**2**) reveals that this compound exists as a mixture of two isomers. The reactivity of the thermodynamically more stable oxoiron(IV) isomer (**2b**) is directly compared to that exhibited by the previously reported 1e$^−$-oxidized analogue $[Fe^V(O)(OAc)(PyNMe_3)]^{2+}$ (**3**). Our data indicates that **2b** is 4 to 5 orders of magnitude slower than **3** in hydrogen atom transfer (HAT) from C−H

bonds. The origin of this huge difference lies in the strength of the O−H bond formed after HAT by the oxoiron unit, the O−H bond derived from **3** being about 20 kcal·mol^{-1} stronger than that from **2b**. The estimated bond strength of the Fe^{IV}O−H bond of 100 kcal·mol^{-1} is very close to the reported values for highly active synthetic models of compound I of cytochrome P450. In addition, this comparative study provides direct experimental evidence that the lifetime of the carbon-centered radical that forms after the initial HAT by the high valent oxoiron complex depends on the oxidation state of the nascent Fe−OH complex. Complex **2b** generates long-lived carbon-centered radicals that freely diffuse in solution, while **3** generates short-lived caged radicals that rapidly form product C−OH bonds, so only **3** engages in stereoretentive hydroxylation reactions. Thus, the oxidation state of the iron center modulates not only the rate of HAT but also the rate of ligand rebound.
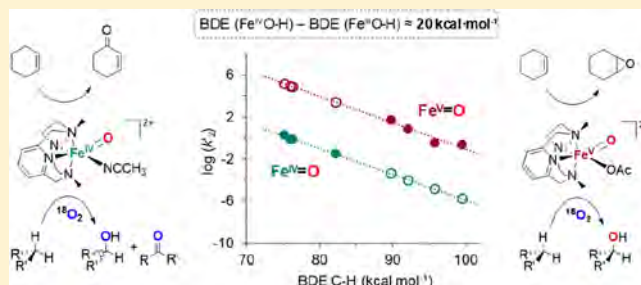
INTRODUCTION

High valent oxoiron species are the oxidizing agents in a variety of iron-dependent oxygenases. For example, in the heme enzyme cytochrome P450, a high-valent oxoiron(IV)-porphyrin radical (Cpd I) is responsible for the hydroxylation of aliphatic C−H bonds and of arene moieties,[1] as well as the epoxidation of olefins, among other reactions.[2−4] In Rieske oxygenases, a family of bacterial nonheme iron enzymes,[5,6] a yet undetected oxoiron(V) species has been proposed as the oxidizing agent,[7] while an $S = 2$ oxoiron(IV) species breaks strong C−H bonds via hydrogen atom transfer (HAT) in other nonheme oxygenases[8] such as taurine hydroxylase,[9] prolyl hydroxylase,[10] tyrosine hydroxylase,[11] phenyl alanine hydroxylase,[12] as well as in α-ketoglutarate dependent halogenases.[13−15] Due to the biological relevance of these high valent oxoiron compounds, intense research efforts have been devoted to the preparation of synthetic analogues that can reproduce both the structural properties and the reactivity of the biological systems. These synthetic models aim to provide detailed insight into the enzymatic mechanisms, and helpful information for the design of catalysts with potential application in environmentally friendly oxidation technologies.[16−20]

Resulting from these research efforts, a large number of synthetic oxoiron(IV) complexes has been described.[16] The reported systems typically consist of iron complexes based on tetra- and pentadentate nitrogen-based ligands, although complexes incorporating O atom donors[16,18] or organometallic moieties are also known.[21] Reactivity studies have disclosed that in most cases these synthetic oxoiron(IV) complexes are competent to perform hydrogen-atom abstraction of weak C−

H bonds and oxygen atom transfer (OAT) to sulfides. Examples in which such species can break stronger C—H bonds are scarce, and moderate reaction rates are observed in most of these cases.[22]

In sharp contrast to the plentiful examples of well-defined synthetic oxoiron(IV) species, the preparation of the one-electron oxidized oxoiron(V) analogues has remained elusive. This can be attributed to the higher oxidizing abilities of these species that make them especially reactive and thus difficult to trap. The first example of a nonporphyrinic oxoiron(V) complex was reported by Collins and co-workers using a tetraanionic macrocyclic tetramide ligand (TAML).[23] $[Fe^V(TAML)(O)]^-$ was characterized by several spectroscopic means, and reactivity studies demonstrated that it was competent in OAT to sulfides and alkenes and in HAT from alkanes.[23,24] The structurally related compound $[Fe^V(bTAML)(O)]^-$ was reported a few years later, and it exhibited remarkably higher stability at room temperature.[25] Nevertheless, these oxoiron(V) species are far less reactive than cytochrome P450 Cpd I,[26] which is considered as their biological heme analogue, suggesting that the tetraanionic character of TAML and related ligands attenuate the electrophilicity of the complex, significantly limiting their oxidation reactivity. More recently, oxoiron(V) species have been generated, and chemically and spectroscopically characterized in the gas phase.[27]

It was recently reported that the reaction of peracids with the iron(II) complex bearing a neutral N-based PyNMe3 ligand, $[Fe^{II}(PyNMe_3)(CH_3CN)_2]^{2+}$ (1, Scheme 1), generates

Scheme 1. Structure for Complex 1 and Synthesis of the Corresponding Oxoiron(IV) (2b) and Oxoiron(V) (3) Complexes
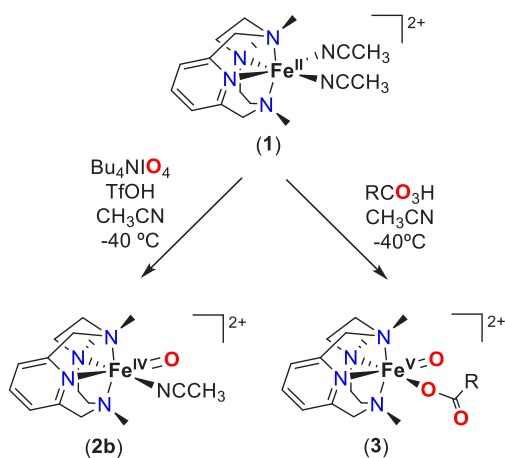
an oxoiron(V) species, $[Fe^V(O)(OAc)(PyNMe_3)]^{2+}$ (3, Scheme 1),[22,28] which exhibits fast reaction rates in the stereoretentive hydroxylation of unactivated C—H bonds of alkanes and in the epoxidation of olefins, even approaching the values reported for P450 Cpd I. The exact electronic structure of 3 has been a matter of debate. Münck, Costas and Que, on the basis of a thorough spectroscopic data, describe the species as an oxoiron(V) core attached to carboxylate ligand, generated after heterolytic O—O cleavage of a cyclic iron-(III)-peracetate moiety.[28] In contrast, Ye, Neese, and co-workers claim that the compound is best characterized as an iron(IV) center antiferromagnetically coupled to an O—O

radical, so that O—O bond has not been completely broken.[29] Thus, this is a fascinating molecule with a very intriguing electronic structure. However, the interest in compound 3 goes beyond its unique bonding structure, as it shows reaction rates and selectivity patterns fully congruent with those of related iron complexes used as efficient catalysts in C—H and C═C oxidation reactions. Indeed, low temperature EPR studies performed along the catalytic reactions of some of these related systems during catalysis display the transient formation of small (<2%) amounts of species with the characteristic spectroscopic features of 3.[30−33] These data strongly suggest that 3 may constitute a representative example of the oxidizing agents operating with these catalysts.[20,34]

In this work, the spectroscopic and reactivity properties of 3 are compared with those of its oxoiron(IV) counterpart $[Fe^{IV}(O)(PyNMe_3)(CH_3CN)]^{2+}$ (2). This oxoiron(IV) species has been characterized by several spectroscopic techniques and, remarkably, two isomers can be identified. The HAT and OAT reactivity of the more thermodynamically stable isomer (2b, Scheme 1) has been studied and compared to 3. By comparing the reactivity of these two complexes with the same tetradentate ligand architecture, the current work provides valuable insight into the impact of the iron oxidation state in defining the unusual reactivity properties of 3.

■ RESULTS AND DISCUSSION

Synthesis and Characterization of 2. The oxoiron(IV) complex $[Fe^{IV}(O)(PyNMe_3)(CH_3CN)]^{2+}$ (2) can be prepared by reaction of the iron(II) precursor $[Fe^{II}(PyNMe_3)-(CH_3CN)_2]^{2+}$ (1) in CH_3CN with either 1.1 equiv Bu_4NIO_4 or 4 equiv 2-tBuSO_2—C_6H_4IO, albeit with low yields (∼40%) as previously determined by Mössbauer spectroscopy.[28] However, the addition of 0.8 equiv triflic acid (TfOH) or 1 equiv $HClO_4$ together with 1.1 equiv Bu_4NIO_4 to 1 affords the target complex 2 with significantly higher yields, as determined by the increased intensity of the two absorption bands characteristic of 2 at ∼800 and ∼980 nm.[35]

UV−vis spectral monitoring of the generation of 2 shows that the relative intensities of these two low energy bands change over time (Figure 1). Thus, the initially more intense ∼800 nm band decreases concomitantly with the increase in
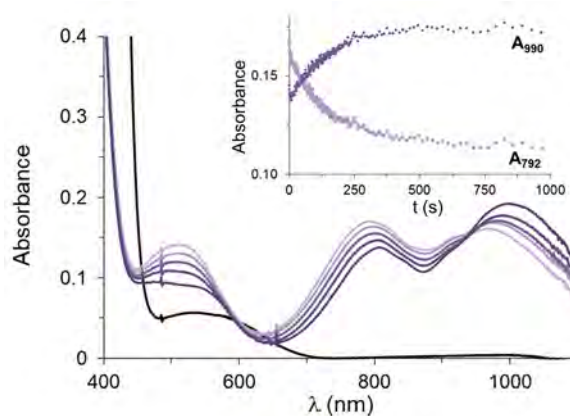
Figure 1. Spectral changes occurring upon reaction of a solution of 1 (1 mM, black line) in CH_3CN with 1.1 equiv Bu_4NIO_4 and 0.8 equiv TfOH at −40 °C. Two bands at ∼800 and ∼980 nm are immediately formed upon mixing the reactants, but their relative intensities changes over time. Inset: kinetic traces at 792 and 990 nm.

Table 1. Summary of Spectroscopic Data for 2a, 2b, and 3

		2a	2b	3[c]
UV−vis−NIR	λ_{max}, nm (ε, M^{-1}cm^{-1})	792 (−)[a]	805 (230)[b]	490 (4500)[b]
		970 (−)[a]	990 (320)[b]	680 (sh)
Mössbauer	δ, mm/s (ΔE_Q, mm/s)	0.07 (0.98)	0.09 (0.24)	−0.06 (1.00)
rRaman	ν (Fe−O), cm^{-1}	822	829	815[e]
XAS	K-edge energy, eV	7124.8	7124.4	7124.8
	pre-edge energy, eV	7114.1	7114.0	7114.4
	pre-edge area, units	20.9	19.6	15.6
	r(Fe=O), Å	1.66	1.65	1.63
	average r(Fe−N), Å	2.00	2.00	1.97[d]

[a]Reliable extinction coefficient for **2a** could not be obtained due to the unavoidable contamination of this compound by **2b**. [b]Extinction coefficient values (ε) determined from the purity calculated by Mössbauer (for **2b**) or EPR analyses (for **3**). [c]Spectroscopic data for **3** was obtained from refs 22, 28. Mössbauer and XAS parameters were obtained from samples of **3** generated using cyclohexyl peroxycarboxylic acid instead of peracetic acid. [d]A second Fe−N subshell is observed at 2.17 Å, which we assign to Fe−N bonds of the diferric byproduct, that represents 50% of the Fe in samples of **3**. [e]This vibration corresponds to the main vibrational frequency of a Fermi doublet.

the intensity of the ~980 nm band, which then becomes the more intense of the two near-IR bands (Figure 1). These observations suggest that two species are formed along the reaction pathway and an isosbestic point at 940 nm becomes apparent in the conversion between them. Interestingly, when the reaction of **1** with IO$_4^-$/TfOH is performed at −60 °C using a 1:1 CH$_3$CN:CH$_2$Cl$_2$ solvent mixture, the initial compound (**2a**) remains stable at this temperature. However, when the same reaction is carried out at −20 °C, the direct formation of the second species (**2b**) is observed (Figure S8).

Spectroscopic analyses have been carried out in order to validate the iron oxidation states of **2a** and **2b** and characterize their electronic structures (Table 1). Mössbauer samples of the two species were prepared by freezing the reaction mixture of ^{57}Fe-enriched **1** and the oxidant in CD$_3$CN at −40 °C to obtain samples of the initial and final species (**2a** and **2b**, Figure 2). Besides unavoidable high-spin ferric impurities that represented ~35% of the samples, the Mössbauer spectra showed time-dependent patterns for the two species that can be clearly characterized by two doublets with different quadrupole splittings. While the sample obtained at reaction time t = 2 min consists of 35% of the kinetically favored species **2a** and 30% of the thermodynamically favored species **2b**, **2a** eventually converts into **2b** at t = 30 min. The Mössbauer parameters of species **2b** (δ = 0.09 mm/s, ΔE_Q = 0.24 mm/s) are fully consistent with its assignment to an S = 1 oxoiron(IV) species previously reported by some of us.[28] Interestingly, the initial species formed with λ_{max} at ~800 nm (**2a**) exhibits different Mössbauer parameters that are also consistent with an oxoiron(IV) species (δ = 0.07 mm/s, ΔE_Q = 0.98 mm/s) with a larger ΔE_Q relative to **2b**. Several attempts to avoid contamination of **2a** by **2b** were carried out, but they all proved unsuccessful, perhaps because of the relatively low energy barrier for conversion of **2a** to **2b**.

Resonance Raman experiments (λ_{exc} = 457 nm) of frozen acetonitrile solutions at 77 K also showed distinct parameters for **2a** and **2b** (Figure 3). A resonantly enhanced band at 822 cm^{-1} was observed for **2a**, while a Raman band at 829 cm^{-1} was observed for **2b**. Both values fall in the range of the ν(Fe=O) modes (798−862 cm^{-1}) previously measured for oxoiron(IV) species.[36]

X-ray absorption spectroscopy (XAS) at 10 K was also used to characterize samples of **2a** and **2b** (Figure 4). The K-edge energies and pre-edge areas for samples of **2a** and **2b** were found to be 7124.8 eV and 20.9 units and 7124.4 eV and 19.6
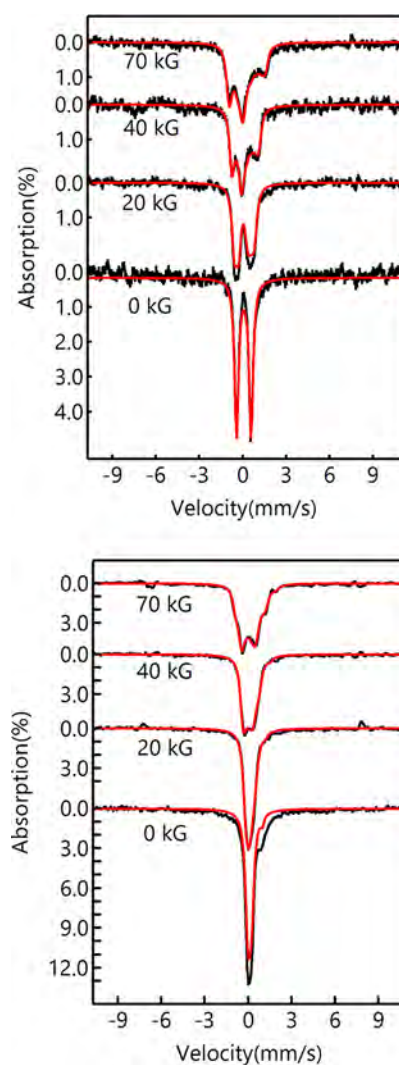
Figure 2. Mössbauer spectra of **2a** and **2b** at various temperatures and magnetic fields. The stacked spectra in the top panel were recorded from the sample frozen at t = 2 min. The high-spin ferric species and species **2b** have been removed to highlight the pattern for species **2a** (35% of total iron). The stacked spectra on the bottom panel were recorded from the sample frozen at t = 30 min. The high-spin ferric species has been removed to highlight the pattern of species **2b** (60% of total iron). Raw Mössbauer data can be found in Figure S6.
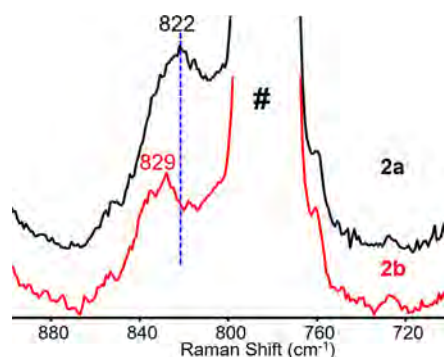
Figure 3. Resonance Raman spectra of **2a** (black line) and **2b** (red line) in frozen acetonitrile solutions at 77 K (λ_{exc} = 457 nm). Band marked with # corresponds to solvent.
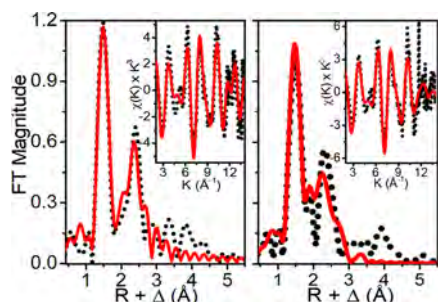
Figure 4. Fourier-transformed k-space EXAFS data of **2a** (left) and **2b** (right) in acetonitrile at 10 K. Insets show the k-space spectra.

units, respectively, in the typical range reported for S = 1 Fe^{IV}=O complexes.[36] The Fourier transformed EXAFS spectrum of **2b** shows two major features at $R + \Delta \sim$ 1.5 and 2.4 Å (Figure 4). The shell at $R + \Delta \sim$ 1.5 is best fit with a 0.8 O scatterer at 1.65 Å that is typical for an Fe=O unit and 5 N/O scatterers at 2.0 Å arising from the ligand PyNMe₃ and probably from a coordinated CH_3CN. The latter shell is best fit with C scatterers at 2.9 and 3.04 Å that typically arise from pyridine containing ligands. The average Fe−N distance of 2.0 Å is as expected to an S = 1 Fe^{IV}=O species.[37] Species **2a** exhibits bond metrics similar to **2b** and the results are summarized in Table S3. Not surprisingly, XAS spectroscopy does not distinguish between the different compounds.

The two oxoiron(IV) complexes **2a** and **2b** may differ only in the nature of the ligand bound *cis* to the oxo atom, which may be the CH_3CN solvent, a $CF_3SO_3^-$ anion or IO_3^-/IO_4^- derived from the oxidant (Scheme 2a). In order to test the likelihood of anion binding, the reactants for the generation of the oxoiron(IV) species were modified: in one experiment the starting iron(II) complex **1** was replaced by $[Fe^{II}(PyNMe_3)$-$(CH_3CN)_2](SbF_6)_2$ (**1·SbF₆**), which does not provide any coordinating anion, and in another experiment 2-tBuSO₂−C_6H_4IO was used as an oxidant instead of Bu_4NIO_4. In both cases, isomer **2a** is still initially formed and then evolves to **2b** in CH_3CN at −40 °C (Figures S10 and S11). Thus, $CF_3SO_3^-$, IO_3^- or IO_4^- coordination can be ruled out as the rationale for having two different oxoiron(IV) species, and a CH_3CN solvent molecule is the most likely to be bound to the labile site in **2a** and **2b**. The inequivalence of the two positions available for oxo coordination to the iron center, one *trans* to the pyridine and the other *trans* to an N-methyl group (see Scheme 2b) easily rationalizes the existence of two geometrical isomers. Thus, **2a** would be the kinetically favored geometric

Scheme 2. (a) Different Ligands (X) Can Be Coordinated *cis* to the Oxo Group in 2a and 2b; (b) Possible Structure of the Two Geometrical Isomers of the Oxoiron(IV) Species, 2a and 2b
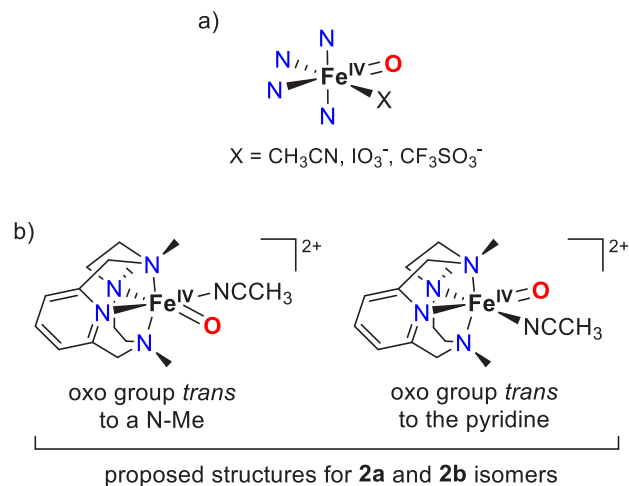
isomer that then evolves to the thermodynamic product **2b**. The existence of two geometrical isomers of oxoiron(IV) compounds with tetradentate ligands has been discussed in previous systems, but spectroscopic characterization of the two species has only been achieved with the equatorially bound tetramethylcyclam (TMC) ligand.[38−40]

Studies have shown that ¹H NMR spectroscopy can be a useful method for determining how the pyridine donors are bound relative to the Fe=O unit.[41−43] They could be coordinated either *cis* or *trans* to the oxo unit, and in the case of the *cis*-bound mode, the ring may be oriented parallel or perpendicular relative to the Fe=O axis or somewhere in between (Table 2). Indeed we show below that this technique can distinguish between the two geometrical isomers of **2**, as the orientation of the pyridine with respect to the Fe=O unit is different in the two options (Scheme 2b).

The ¹H NMR spectrum of the more stable **2b** isomer recorded at −65 °C in 1:1 CD_3CN/CD_2Cl_2 exhibits relatively sharp and well-resolved paramagnetically shifted signals due to the S = 1 Fe^{IV}=O center (Figure 5). The number of signals observed is consistent with the presence of a mirror plane of symmetry that bisects the pyridine ring. Due to their longer distances from the Fe center, the pyridine protons give rise to the sharpest signals in the spectrum of **2b**, which are found at −25 ppm (1H) and 15 ppm (2H) (Figure 5). These peaks can be assigned respectively to the single γ and the two β protons of the pyridine based on their relative intensities. The remaining broader spectral features can be reasonably associated with benzylic CH_2 (46 and −63 ppm), N−CH_2 (−39, −147 ppm) and N−CH_3 (−67 ppm) hydrogens, based on relative integrations of the resonances and by comparison to the ¹H NMR spectrum for the corresponding oxoiron(IV) species supported by the macrocyclic ligand with deuterated benzylic protons (**2b**-d_4) (Figure S7).

The chemical shift pattern observed for the pyridine β and γ protons of **2b** can shed light on the orientation of the pyridine ligand relative to the Fe=O unit, based on comparisons with the patterns associated with structurally well characterized Fe^{IV}=O complexes in the literature.[43] Most published examples have pyridines bound *cis* to the Fe=O unit and oriented parallel to the Fe=O axis, namely [$Fe^{IV}(O)$-

Table 2. ^{1}H NMR Paramagnetic Shifts Observed for Pyridine Protons of Oxoiron(IV) Complexes[a]

compound	T (K)	β	β'	γ	ref
$[Fe^{IV}(O)(N4Py)]^{2+}$	298	$\beta_{\parallel}$ 37	$\beta'_{\parallel}$ −24	$\gamma_{\parallel}$ 2.5	41
		$\beta_{\parallel}$ 23	$\beta'_{\parallel}$ −18	$\gamma_{\parallel}$ 1.3	
$[Fe^{IV}(O)(BnTPEN)]^{2+}$	298	$\beta_{\parallel}$ 36	$\beta'_{\parallel}$ −22.3	$\gamma_{\parallel}$ 3.6	41
		$\beta_{\parallel}$ 33	$\beta'_{\parallel}$ −21.7	$\gamma_{\parallel}$ 3.0	
		$\beta_{\perp}$ −7.3	$\beta'_{\perp}$ −8.5	$\gamma_{\perp}$ 1.4	
$[Fe^{IV}(O)(Py_2MeTACN)]^{2+}$	298	$\beta_{\parallel}$ 39	$\beta'_{\parallel}$ −20	$\gamma_{\parallel}$ 6.3	42
		$\beta_{\perp}$ −8.4	$\beta'_{\perp}$ −5.5	$\gamma_{\perp}$ 4.2	
$[Fe^{IV}(O)(TMC\text{-}py)]^{2+}$	298	β_{trans} 3.6, −0.5		γ_{trans} −11.6	44
$[Fe^{IV}(O)(PyNMe_3)(CH_3CN)]^{2+}$ (2a)	208	−26		5	this work
$[Fe^{IV}(O)(PyNMe_3)(CH_3CN)]^{2+}$ (2b)	208	8		−32	this work

[a]Relative to pyridine at 7 ppm.
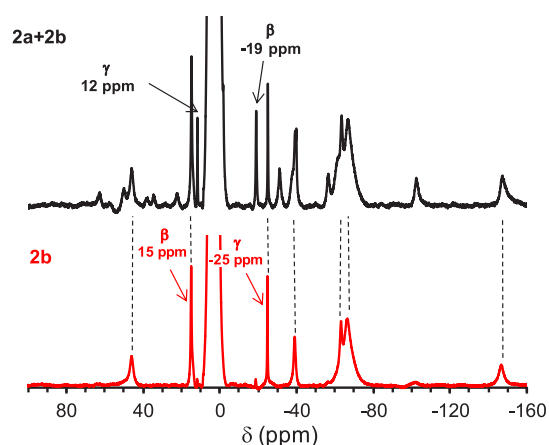
Figure 5. ^{1}H NMR spectra of a mixture of **2a** and **2b** (top) and **2b** (bottom) in 1:1 CD$_3$CN/CD$_2$Cl$_2$ at −65 °C. Pyridine β (2H) and γ (1H) protons are labeled in the figure. Other broader peaks for **2b** are assigned as follows: benzylic protons at 46 ppm (2H) and −63 ppm (2H), aliphatic CH$_2$ peaks at −39 ppm (2H) and −147 ppm (2H), and CH$_3$ protons at −67 ppm (9H).

$(N4Py)]^{2+}$, $[Fe^{IV}(O)(BnTPEN)]^{2+}$ and $[Fe^{IV}(O)$-$(MePy_2tacn)]^{2+}$ (N4Py = N,N-bis(2-pyridyl-methyl)-N-bis(2-pyridyl)methylamine; BnTPEN = N-benzyl-N,N',N'-tris(2-pyridylmethyl)-1,2-diaminoethane; MePy$_2$tacn = N-methyl-N',N''-bis(2-pyridylmethyl)-1,4,7-triazacyclononane).[41,42,45] Such pyridine rings exhibit β and β' protons respectively downfield and upfield shifted by 30−40 ppm and γ protons slightly downfield shifted from their respective diamagnetic positions. Besides having equatorial pyridines bound parallel to the Fe═O unit, both $[Fe^{IV}(O)(BnTPEN)]^{2+}$ and $[Fe^{IV}(O)$-$(Py_2MeTACN)]^{2+}$ have an additional pyridine bound *cis* to the Fe═O unit but with the ring perpendicular to the Fe═O unit. These pyridine donors exhibit smaller paramagnetic shifts of ~10 ppm upfield for the β protons and 4−14 ppm downfield for the γ proton.

Neither of the shift patterns described above matches that observed for **2b**, which exhibits a relatively small downfield paramagnetic shift of 8 ppm for the β protons and a larger upfield paramagnetic shift of 32 ppm for the γ proton. Such a pattern is associated with a pyridine bound *trans* to the oxo atom, as reported for the pendant pyridine ligand *trans* to the Fe═O unit in $[Fe^{IV}(O)(TMC\text{-}py)]^{2+}$ (TMC-py = 1-(pyridyl-2-methyl)-4,8,11-trimethyl-1,4,8,11-tetrazacyclotetradecane).[44] For the latter complex, the two pyridine β protons exhibit quite small paramagnetic shifts of −0.5 and +3.6 ppm (actual peaks observed at 6.5 and 10.6 ppm) and a larger paramagnetic shift

of nearly −11.6 ppm for the γ proton found at −4.6 ppm. Although there is a difference in the magnitudes of the paramagnetic shifts of the pyridine protons between these two complexes, the directions of the shifts agree. The larger paramagnetic shifts observed for **2b** versus $[Fe^{IV}(O)(TMC\text{-}py)]^{2+}$ (Table 2) likely arise from two factors: (a) the 90 °C difference in temperature at which the NMR data were obtained, which will decrease when this difference is taken into account, and (b) the shorter Fe−N$_{py}$ bond length of 2.03 Å calculated for **2b** (see Supporting Information, Figure S27, for more details) versus the 2.118(3) Å value determined crystallographically for $[Fe^{IV}(O)(TMC\text{-}py)]^{2+}$, which results in greater unpaired spin density delocalized onto the pyridine in the former.[46]

The ^{1}H NMR spectrum of **2a** in 1:1 CD$_3$CN:CD$_2$Cl$_2$ at −65 °C shows significant contamination from the more stable **2b** isomer, as shown by the Mössbauer results discussed earlier (Figure 2). On the basis of the above assignment of **2b** as the *trans* isomer, **2a** should correspond to the *cis* isomer with the pyridine perpendicular to the Fe═O axis. From a careful inspection of the composite **2a** + **2b** spectrum and comparison with the spectrum of pure **2b**, we can identify sharper features with a relative 2:1 intensity ratio at −19 and 12 ppm that we assign to the β and γ protons of **2a**, respectively. The shift pattern with upfield shifted β protons and a downfield shifted γ proton is fully consistent with a *cis*-bound pyridine perpendicular to the Fe═O unit (Scheme 2b), as found for the pyridines perpendicular to the Fe═O units of $[Fe^{IV}(O)$-$(BnTPEN)]^{2+}$ and $[Fe^{IV}(O)(Py_2MeTACN)]^{2+}$ (Table 2).[41,42]

Interestingly, in line with the experimental observations, DFT calculations predict that the isomer with the oxo group *trans* to the pyridine ring is slightly energetically favored (by 0.9 kcal/mol) over the isomer with the oxo group *cis* to the pyridine (see Supporting Information for more details). This further supports the NMR results pointing out that the most stable isomer **2b** contains the pyridine *trans* to the oxo group, and they show a relative *cis* orientation in the kinetically favored geometric isomer **2a**.

Oxidative Reactivity of 2a versus 2b and Comparison to 3. The oxidizing abilities of **2a** and **2b** were compared at −60 °C. Isomer **2a** was directly synthesized at −60 °C in 1:1 CH$_3$CN:CH$_2$Cl$_2$. Of note, this compound is obtained together with approximately equimolar amounts of isomer **2b** according to spectroscopic studies (see above). Compound **2b** was first generated at −40 °C and then cooled down to −60 °C for reactivity comparisons with **2a**. Reaction rates were determined by monitoring the decay of the near-IR absorption bands characteristic of **2a** and **2b** (at 792 and 990 nm,

respectively) upon addition of an excess of a particular substrate (Figure S12 and S13). In the case of **2b**, its decay at 990 nm could be fitted to single exponential functions, from which observed reaction rates (k_{obs}) and the corresponding second order rate constants (k_2) could be extracted. Reactions of **2a** with substrates were "contaminated" by the presence of approximately equimolar quantities of **2b**. Thus, the contribution of **2b** to the decay of the most intense absorption band of **2a** at 792 nm was subtracted to obtain the decay of "pure" compound **2a**. Gratifyingly, the reaction of this species with substrates could also be nicely fitted to a single exponential function and reaction rates for **2a** could be extracted (see Supporting Information for more details). Both species exhibited hydrogen-atom transfer (HAT) and oxygen atom transfer (OAT) reactivity typically observed for most S = 1 oxoiron(IV) complexes but they showed different reactivity trends. Isomer **2a** reacted approximately 18 times faster than **2b** in HAT reactions with 9,10-dihydroanthracene (k_2 = 9.5 M^{-1} s^{-1} for **2a** and 0.53 M^{-1} s^{-1} for **2b**) but was about 4 times less reactive than **2b** in OAT reactions with thioanisole (k_2 = 0.038 M^{-1} s^{-1} for **2a** and 0.14 M^{-1} s^{-1} for **2b**). These results further support the notion that **2a** and **2b** correspond to two different oxoiron(IV) species that exhibit different relative reactivity.

Further reactivity studies of the oxoiron(IV) species were carried out using isomer **2b**. On the one hand, this compound corresponds to the thermodynamic product, so that it can be obtained without contamination from **2a** and is thermally stable at −40 °C, which makes it easier to manipulate. On the other hand, the relative disposition of the oxo group *trans* to the pyridine in **2b** is also observed in **3**. For the latter, spectroscopic analysis did not show the presence of two different isomers,[28] and the detected signals were assigned to the isomer with the oxo group *trans* to the pyridine as it was slightly more stable than the corresponding *cis* isomer on the basis of DFT calculations. Thus, **2b** and **3** likely represent the same geometric isomer making reactivity comparisons more straightforward.

First, the reactivity of **2b** with thioanisole and its *para*-substituted derivatives (X = OMe, Me, Cl, CN) at −40 °C was evaluated. Upon substrate addition, the absorption bands associated with **2b** disappeared (Figure S14), and this decay was also accompanied by the recovery of the UV−vis spectroscopic features of **1** (Figure S16), which was ascertained by MS (Figure S17). Moreover, analysis of the oxidized products in the reaction with thioanisole revealed the formation of the corresponding sulfoxide in 54% yield with respect to **2b**. Under conditions of excess substrate, the decay of the absorption band of **2b** at 990 nm could be fitted to a single exponential and second-order rate constants could be extracted. As expected, the Hammett analysis supported the electrophilic character of **2b** (ρ = −1.77, Figure S15) as previously observed for other well-defined oxoiron(IV) complexes[38,47] (see SI for more details). The reaction of the oxoiron(V) species **3** with sulfides is exceedingly fast, and reaction rates could not be determined even when analyzed at −45 °C by stopped flow methods.

Therefore, a direct comparison between the OAT ability of **2b** and **3** cannot be made, but the accumulated data indicate that **2b** behaves like a common oxoiron(IV) complex, while under the same reaction conditions **3** exhibits extraordinarily fast OAT rates. Under the assumption that the possible contributions of spin state changes to these reactions are either

(i) insignificant or (ii) are very similar for the two compounds, the comparison highlights the extreme electrophilicity of the Fe^V=O unit.

The HAT ability of **2b** was also measured by studying its reaction with hydrocarbons. In this case, kinetic studies were carried out at −40 °C in order to establish a direct comparison with the reaction rates reported for **3** at this temperature (see below).[22] Substrates with relatively weak C−H bonds (BDE = 75−85 kcal·mol^{-1}) were used, because substrates with stronger bonds turned out to be unreactive toward **2b** at this temperature. Due to the limited solubility of the chosen substrates (xanthene, 1,4-cyclohexadiene, 9,10-dihydroanthracene, and fluorene) in CH_3CN at −40 °C, reactions were run in a 1:1 $CH_3CN:CH_2Cl_2$ mixture. Reactions produce $[Fe^{III}(OH)(CF_3SO_3)(PyNMe_3)]^+$ (ascertained by MS, Figure S19) and organic products. Reactions were monitored by UV−vis absorption spectroscopy by following the decay of the band at 990 nm characteristic of **2b** upon addition of the substrate (Figure S18). Under these experimental conditions reactions showed pseudo-first-order behavior and second-order reaction rates (k_2) could be extracted by plotting the observed rate constants (k_{obs}) as a function of the substrate concentration (Figure S20). These rate constants were then adjusted for the reaction stoichiometry to yield k_2' based on the number of abstractable hydrogen atoms of substrates. As expected, reaction rates decreased with the increase of the C−H BDE and more interestingly the $\log(k_2')$ values correlated linearly with the C−H BDE values, giving a slope of approximately −0.25 (kcal/mol)$^{-1}$ (Figure S21).

HAT reactions with compound **2b** also exhibit a large kinetic isotope effect (KIE), so deuterated substrates react more slowly than their protio analogues. Using xanthene-d_2 and 9,10-dihydroanthracene-d_4, KIE values of 24 and 28 were obtained, respectively (Figure S23).[48] These high values are commonly observed in HAT processes carried out by oxoiron(IV) complexes. For example, a KIE value of 36 (at -40 °C) was reported for the oxidation of xanthene with the oxoiron(IV) complex bearing the 13-TMC ligand[49] and a KIE value of 27 (at −15 °C) was described for the oxidation of 9,10-dihydroanthracene using the $[Fe^{IV}(O)(CH_3CN)(Pytacn)]^{2+}$ complex.[38] Interestingly, these high KIE values are comparable to the large KIE determined for the S = 2 oxoiron(IV) intermediate J in TauD (KIE ∼50).[50,51] Altogether, the good correlation between reaction rates and C−H BDE values and the large KIE values provides strong evidence for a rate-determining HAT process in the reactions of hydrocarbons with **2b**.

Activation parameters for HAT reactions of **2b** with xanthene and cyclohexadiene were determined by measuring reaction rates between 273 and 233 K. The corresponding Eyring plot for xanthene afforded $\Delta H^{\ddagger}$ = 6.4 ± 0.6 kcal·mol^{-1} and $\Delta S^{\ddagger}$ = −27.2 ± 2.6 cal·K^{-1}·mol^{-1}, while $\Delta H^{\ddagger}$ = 7.3 ± 0.5 kcal·mol^{-1} and $\Delta S^{\ddagger}$ = −25.6 ± 2.1 cal·K^{-1}·mol^{-1} were determined for cyclohexadiene (Figure S24). These values are very close to the ones previously reported for the reaction of a tetracarbene ligated oxoiron(IV) with 1,4-cyclohexadiene and 9,10-dihydroanthracene.[52]

It has been observed that the reactivity of oxoiron(IV) complexes depends dramatically on the ligand set.[53−55] The combination of the above-described data for **2b** and the recently described reactivity of **3**[22] represents a unique opportunity to compare the oxidizing abilities of a pair of oxoiron(IV) and oxoiron(V) compounds bearing exactly the

same ligand architecture. A first notable observation is that reactions with substrates bearing strong C−H bonds (BDE ∼89−100 kcal·mol^{-1}) can only be studied for **3** because **2b** does not appear to be powerful enough to carry out HAT reactions with these strong C−H bonds. On the other hand, rates for HAT reactions with substrates containing weak C−H bonds can only be measured for **2b**, because the reaction with **3** exhibited extremely fast reaction rates, too fast even at −40 °C to be extracted by stopped flow methods.[22] Therefore, reaction rates for a common substrate are not available.

In order to establish a quantitative comparison between reaction rates, we performed regression analyses of the log(k_2') vs BDE correlations experimentally determined for **2b** and **3**. Regression analyses provide correlation lines with a slope of −0.25 (kcal/mol)$^{-1}$ in both cases (using a linear free energy relationship a unitless slope of 0.34 is obtained in both cases. Figures S22). This coincidence in the slopes of these correlations strongly suggests that HAT of **2b** and **3** proceed via very similar transition states. Extrapolation of the straight lines obtained in these correlations permitted us to estimate hypothetical second order reaction rates for substrates containing strong C−H bonds in the case of **2b**, and for the fast reactions of **3** against substrates with weak C−H bonds. Results are shown in Figure 6 and Table 3. As anticipated, the
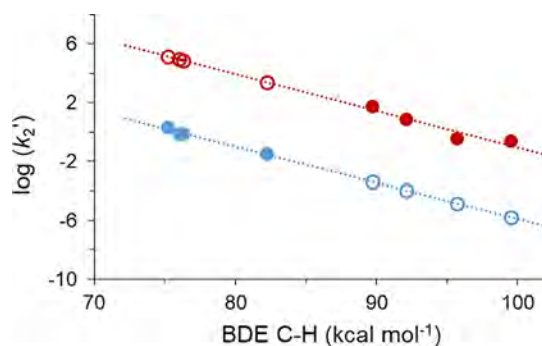

Figure 6. Correlation of log(k_2') with the BDE of different substrates at −40 °C for **2b** (blue line) and **3** (red line). Filled circles correspond to experimentally determined data and empty circles correspond to extrapolated values. The extrapolation made for compound **3** should be taken with a caveat, since a loss of linearity is likely to occur at BDE values below 90 kcal·mol^{-1}, as previously reported for other highly reactive HAT reagents (see text for more details).

Table 3. Experimental and Extrapolated k_2' Values for 2b and 3[a] at −40 °C

substrate	BDE (kcal mol^{-1})	compound **2b** k_2' (M^{-1} s^{-1})	compound **3** k_2' (M^{-1} s^{-1})
xanthene	75.2	2.1 ± 0.2	*1.4 × 10^5*
cyclohexadiene	76.0	0.70 ± 0.05	*8.7 × 10^4*
9,10-dihydroanthracene	76.3	0.77 ± 0.05	*7.4 × 10^4*
fluorene	82.2	0.030 ± 0.004	*2.5 × 10^3*
toluene	89.7	*4.2 × 10^{-4}*	55 ± 1[b]
tetrahydrofuran	92.1	*1.0 × 10^{-4}*	7.2 ± 0.2[b]
cyclooctane	95.7	*1.4 × 10^{-5}*	0.34 ± 0.01[b]
cyclohexane	99.5	*1.7 × 10^{-6}*	0.23 ± 0.01[b]

[a]Extrapolated values are shown in italics. [b]Ref 22.

gathered data show that **3** is 4 to 5 orders of magnitude more reactive than **2b**. It is important to note that extrapolation of the log(k_2') vs BDE correlations must be done with caution.

While linear correlations over a wide range of BDEs have been reported for several oxoiron(IV) complexes with moderate reactivities,[25,38,55,56] a loss of linearity below 90 kcal/mol has been observed for a highly reactive peroxygenase compound I and *t*-butoxyl radicals.[27,57,58] Such a loss of linearity might not be discarded for the highly reactive oxoiron(V) species **3** for substrates with low BDEs, thus challenging the direct extrapolation at low BDEs for this compound. Thus, while loss of linearity may happen for compound **3** at low BDE values, this is not likely to occur at high BDEs for **2b** according to literature precedents. This way, extrapolation of the straight line is reliable for **2b** and the statement that **3** is 4 to 5 orders of magnitude more reactive than **2b** can be more strongly defended for strong C−H bonds.

Reactivity comparisons between oxoiron(IV) and oxoiron-(V) species have been reported in very few systems. In fact, the only precedent for nonheme iron systems is for the complexes of the tetraanionic bTAML ligand. In this case, the reaction of [Fe^V(O)(bTAML)]$^-$ toward benzyl alcohol (BDE < 80 kcal·mol^{-1}) at pH 7 was found to be 2500 times faster than for its 1-e$^-$-reduced counterpart [Fe^{IV}(O)(bTAML)]$^{2-}$ at pH 12.[59] Of note, reactions toward stronger C−H bonds were precluded due to the attenuated electrophilicity of this system. In contrast, van Eldik and co-workers found that a Cpd I mimic, [(TMPS$^{•+}$)Fe^{IV}(O)(H$_2$O)]$^{3-}$, reacted with benzyl alcohols only a hundred times faster than its 1-e$^-$-reduced counterpart [(TMPS)Fe^{IV}(O)(OH)]$^{5-}$. The different degrees of protonation of the OH/OH$_2$ ligand in these two compounds should be noted.[60] Even more interestingly, a Cpd I model compound reported by Groves [(4-TMPyP$^{•+}$)-Fe^{IV}(O)]$^+$ exhibited a very high second order rate constant of 3.6 × 10^6 M^{-1} s^{-1} for the oxidation of xanthene, but negligible reactivity was observed when the 1-e$^-$-reduced analogue [(4-TMPyP)Fe^{IV}(O)] was used.[61] Indeed, the extrapolated reaction rate for the oxidation of xanthene calculated for **3** (Table 3) is only 10 times slower than that observed for Groves' model compound without accounting for the 50 °C difference in the measurements (reaction rates in the Groves' system were measured at +10 °C, while reactions for **3** were recorded at −40 °C), thus suggesting that **3** compares well in HAT reactivity with the most active cytochrome P450 mimics.

The KIE's determined for **2b** and **3** are also significantly different. **2b** exhibits very large KIE's (∼28), in agreement with the large values observed for synthetic and enzymatic oxoiron(IV) species, which are commonly rationalized on the basis of large tunneling contributions.[15,50,62,63] In contrast, KIE's determined for **3** of ∼5−6 are significantly smaller than those determined for **2b**, so they can still be accommodated by a classical treatment of the C−H cleavage. Notably, these "classical" values resemble those obtained for catalytic C−H oxidation systems with bioinspired iron catalysts.[64]

Activation parameters in representative HAT reactions performed by **2b** and **3** are collected in Table 4. Activation entropies are large and negative, consistent with a bimolecular process, and those determined for **2b** are systematically more negative. This pattern reflects a later and more ordered transition state for the less reactive **2b**. This provides some clues about the origin of the differences in the magnitude of the KIE's; tunneling contributions require close proximity between the hydrogen-donor and the hydrogen-acceptor and activation parameters indeed provide evidence for the necessary closer contact between the oxoiron(IV) (**2b**) and

Table 4. Activation Parameters for the Reactions of 2b and 3 with C−H Bonds

compound	substrate	BDE (kcal mol^{-1})	$\Delta H^{\ddagger}$ (kcal mol^{-1})	$\Delta S^{\ddagger}$ (cal K^{-1} mol^{-1})	ref
2b	xanthene	75.2	6.4 ± 0.6	−27.2 ± 2.6	this work
	cyclohexadiene	76.0	7.3 ± 0.5	−25.6 ± 2.1	this work
3	toluene	89.7	6.5 ± 0.2	−19.6 ± 1.2	22
	cyclohexane	99.5	8.8 ± 0.7	−18.2 ± 1.9	22

the substrate C−H bond with respect to the same situation in the more reactive oxoiron(V) (**3**).

The linear free energy correlation between $\log(k_2')$ and differences in enthalpy observed for the present system (Figure 6) provides interesting insights into the origin of the fast HAT reactivity of **3**. With few exceptions,[57,58,65] such a correlation is commonly observed for HAT reactions as described by the Bell−Evans−Polyani model.[66] The enthalpy change of the present reactions corresponds to the difference between the energy that is required to break the C−H bond (BDE$_{C-H}$) and the energy provided by the formation of the FeO−H bond (BDE$_{FeO-H}$) (eq 2). Considering that cyclohexadiene reacts with **2b** at a reaction rate ($k_2' = 0.70$ M^{-1} s^{-1}) that is only 2.05 times the rate of reaction of **3** with cyclooctane ($k_2' = 0.34$ M^{-1} s^{-1}), we can estimate that both reactions have similar activation free energies given the observed Bell−Evans−Polyani correlation (Figure 6). Therefore, the 20 kcal·mol^{-1} difference in BDE$_{C-H}$ between these two substrates (76.0 kcal·mol^{-1} for cyclohexadiene and 95.7 kcal·mol^{-1} for cyclooctane) should approximately correspond to the difference in energy between the BDE of Fe^{III}O−H and Fe^{IV}O−H.

$$\text{Fe}^{n+}\!=\!\text{O} + \text{C}-\text{H} \xrightarrow[\text{reaction}]{\text{HAT}} \text{Fe}^{n-1}-\text{O}-\text{H} + \text{C}\cdot$$

$$\Delta H^{O} = H^{O}_{FeO-H} - H^{O}_{FeO} + H^{O}_{C\bullet} - H^{O}_{C-H} \qquad (1)$$

()
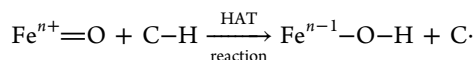
$$\Delta H^{O} = \text{BDE}_{C-H} - \text{BDE}_{FeO-H} \qquad (2)$$

()

BDE's for nonheme Fe^{III}O−H complexes with neutral N-rich ligands have been estimated to be between 78−87 kcal·mol^{-1},[67,68] and therefore, the BDE for the Fe^{IV}O−H should be around 100 kcal·mol^{-1}. This number falls between the 103 kcal·mol^{-1} value estimated for the heme-thiolate peroxygenase Cpd I[27] and the 95 kcal·mol^{-1} value recently determined by a combination of experimental and theoretical methods in horseradish peroxidase and in an aromatic peroxidase as reported by Green and co-workers.[69] The Fe^{IV}O−H value estimated for the present nonheme system constitutes one of the strongest described so far, attesting for the extraordinarily high HAT reactivity of **3**. Remarkably, this estimation of the BDE for the Fe^{IV}O−H bond is in line with the value that we previously estimated on the basis of the reactivity of **3** toward toluene (estimated BDE$_{O-H} = 101$ kcal·mol^{-1}).[22] Interestingly, the ∼20 kcal·mol^{-1} difference in FeO−H strength between **2b** and **3** parallels the difference between the Fe^{IV}O−H strength of Cpd I and Fe^{III}O−H in Cpd II from an aromatic peroxidase described by Groves.[27] Instead, Green has deduced a reduced impact of oxidation state in FeO−H bond dissociation energies in a P450 mutant (CYP158) by a combination of redox titrations and theoretical methods; values of 95 and 90 kcal mol^{-1} for the Fe^{IV}O−H and Fe^{III}O−H bonds, respectively, were determined.[69]

The different nature of the sixth ligand in **2b** (CH$_3$CN) and **3** (carboxylate anion) deserves some comment. Acetonitrile is a neutral, π-acceptor ligand and stabilizes low oxidation states. On the other hand, acetate is an anionic sigma donor ligand that should favor higher oxidation states. Therefore, the extraordinarily higher reactivity of **3** when compared with **2b** is likely to be even tamed by the different ligand. In other words, if the two complexes would share exactly the same ligand set, differences in reaction rates are expected to be even larger.

It is also remarkable that the hydrogen-atom abstraction reactions carried out by **2b** and **3** entail changes in the spin state along the reaction. HAT reactions from **3** (which has a $S = 1/2$ ground state) form an iron(IV)-hydroxo species, which possesses a $S = 1$ or $S = 2$ spin state, together with an alkyl radical. After the hydroxyl ligand rebound, an iron(III) complex with a $S = 5/2$ is formed concomitantly with the hydroxylated product. Thus, a change in the spin state occurs along this reaction path. Indeed, we and others have investigated the spin state changes along the reaction of oxoiron(V) with alkanes by computational methods[70,71] and disclosed that reactions usually occur at the $S = 1/2$ or $S = 3/2$ surfaces, depending on which of the two spin states has the lower energy barriers. In some instances, a spin crossover before reaching the first transition state is necessary to access the most energetically favored path. The $S = 5/2$ reaction path is usually much higher in energy with larger kinetic barriers. However, this is the most stable spin state for the reaction products, so that a spin crossover is necessary after the ligand rebound. A similar situation occurs with the HAT reactions carried out by oxoiron(IV) species analogous to **2b**. In this case, most frequently reaction takes place at the quintet spin state ($S = 2$) even though the most stable spin configuration of the oxoiron(IV) species is the triplet ($S = 1$)[72,73] (for a notable exception see ref 52). Thus, a spin crossover occurs before the transition state. In spite of the fact that spin-state changes are involved along the course of the reaction, spin−orbit couplings and spin−spin interactions remove the associated forbiddance. Thus, the feasibility of the HAT reactions carried out by oxoiron(IV) and oxoiron(V) species appears to be dictated by ground state thermodynamics rather than by multiple state reactivities.

Differences in Chemoselectivity between 2b and 3. The oxidation of cyclohexene constitutes a very informative mechanistic probe. Indeed, cyclohexene has been used as a substrate probe to study the reaction mechanism of oxidation reactions in enzymes and model systems.[74,75] This molecule provides the oxidant with two possible channels of reactivity: abstraction of an allylic C−H bond and OAT to the C=C bond. Analysis of the oxidized products formed upon reaction of **2b** or **3** with 100 equiv cyclohexene at −40 °C in CH$_3$CN showed completely different outcomes (Scheme 3). Under aerobic conditions, the oxoiron(IV) complex **2b** afforded mainly allylic oxidation (31% yield of allylic ketone and 5% yield of allylic alcohol with traces of epoxide), while the oxoiron(V) compound **3** afforded mainly cyclohexene oxide

Scheme 3. Product Distribution in the Reaction of 2b and 3 with Cyclohexene at −40 °C in CH₃CN under Aerobic Conditions
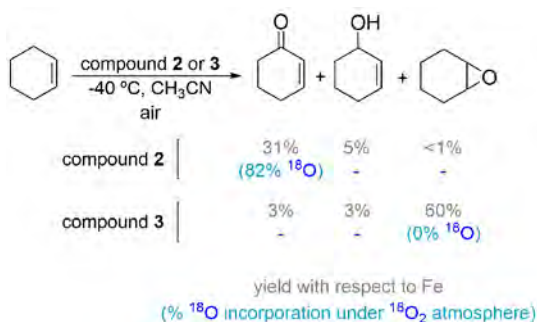
(60% yield) with minor amounts of allylic products (6% combined yield of allylic alcohol and ketone products). This comparison clearly indicates that **2b** is a sluggish OAT reagent toward olefins, as previously observed for other oxoiron(IV) species,[75] and instead favors one-electron processes, such as hydrogen atom abstraction at the allylic position. In contrast, **3** is an excellent two-electron oxidant, epoxidizing C=C bonds instead of abstracting H atoms.

Interestingly, when these reactions were carried out under a $^{18}O_2$ atmosphere the allylic ketone product derived from the reaction of **2b** with cyclohexene incorporated 82% ^{18}O (Figure S25), which indicates that after hydrogen atom abstraction by **2b** the newly formed alkyl radical does not undergo rapid rebound and has a long enough lifetime to interact with gaseous dioxygen (Scheme 4). In contrast, no isotope labeling

Scheme 4. Hydrogen Atom Transfer from C−H Bonds by Oxoiron(IV) and Oxoiron(IV) Species
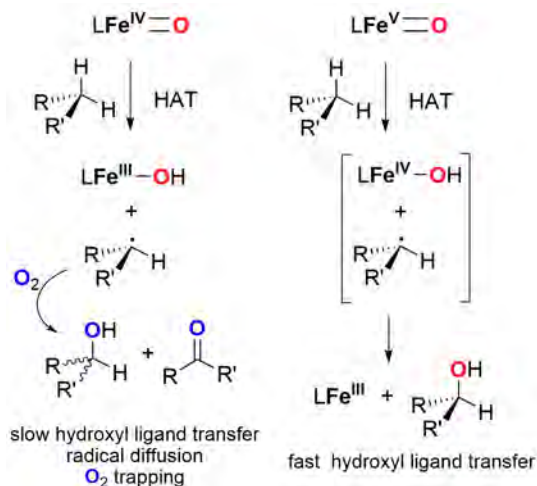
into the epoxide was detected in the same experiment carried out by **3** (Figure S25), which agrees with a direct OAT from the oxoiron(V) to the C=C bond. Of note, cyclohexene oxidation by **2b** under a N₂ atmosphere afforded the allylic alcohol as the major product (28% yield), while the production of allylic ketone was minimal (5% yield), which contrasts with the preferential formation of ketone in the presence of O₂. Finally, control experiments in the presence of triphenylphosphine have been done to exclude the formation of hydro-

peroxides under the different conditions tested (see Experimental Section).[76]

Differences in the Lifetimes of the Carbon-Centered Radicals between 2b and 3. The outcome in the oxidation of cyclohexene with **2b** performed under $^{18}O_2$ atmosphere indicates that the hydroxyl ligand formed after HAT inefficiently rebounds with the newly formed carbon-centered radical, which diffuses out of the solvent cage, producing long-lived carbon-centered radicals that can interact with dioxygen, to give rise to the observed ^{18}O-labeling of the allylic ketone (Scheme 4). In striking contrast, **3** hydroxylates alkanes with stereoretention, as demonstrated by the hydroxylation of the tertiary C−H bonds of *cis*-1,2-dimethylcyclohexane by **3**, which occurs with 96% stereoretention.[22] This result excludes the formation of long-lived carbon-centered radicals and indicates that the formed alkyl radicals after HAT rapidly recombine with the hydroxyl bound to the iron(IV) with no time for stereoscrambling. To further demonstrate this idea, we have carried out the oxidation of cyclohexane with **3** under a $^{18}O_2$ atmosphere, which mainly affords cyclohexanol.[22] Conversely to what was observed in the oxidation of cyclohexene by **2b**, analysis of the cyclohexanol product showed no ^{18}O incorporation (Figure S26), further supporting the idea that the organic radicals formed along the reaction are very short-lived and do not have time to escape from the solvent cage and interact with atmospheric dioxygen.

Overall, the comparison between **2b** and **3** constitutes a unique case in nonheme systems providing convincing evidence that the lifetime of the carbon-centered radical formed after the initial hydrogen-atom transfer (HAT) is dependent on the oxidation state of the iron center (Scheme 4). The data indicates that the putative hydroxoiron(IV) intermediate, formed after initial HAT by the oxoiron(V) species **3**, can rapidly transfer the hydroxyl ligand (oxygen rebound) to the carbon-centered radical at reaction rates that exceed diffusion rates ($10^9 \, s^{-1}$). This observation is in line with the short lifetime of carbon-centered radicals formed by the heme enzyme cytochrome P450 (rate ~10^{10} to $10^{11} \, s^{-1}$).[77] On the other hand, the reaction of the hydroxoiron(III) species, formed after HAT by the oxoiron(IV) species **2b**, with the carbon-centered radical is slower than diffusion out of the reaction pocket, so that the latter process dominates the outcome. Again, this observation finds wide precedent in previous studies on the C−H oxidation activity of nonheme oxoiron complexes[78] and in more recent reports in which the rebound rates of ferric-methoxide and ferric-hydroxide complexes with carbon-centered radicals have been directly measured.[79,80] The origin of this dichotomy may be tentatively traced to the redox nature of the rebound step, which entails a one-electron reduction of the iron center.

■ CONCLUSIONS

In this work we have described the synthesis and characterization of an oxoiron(IV) species with a neutral tetradentate N-based ligand, $[Fe^{IV}(O)(PyNMe_3)(CH_3CN)]^{2+}$, that according to our spectroscopic studies exists as a mixture of two isomers (**2a** and **2b**). The reactivity of the thermodynamically more stable isomer (**2b**) toward C−H bonds has been directly compared to that exhibited by the previously reported 1e⁻ oxidized species $[Fe^V(O)(OAc)(PyNMe_3)]^{2+}$ (**3**).[22] Our data show that the oxoiron(IV) species **2b** is 4 to 5 orders of magnitude slower than **3** in hydrogen atom abstraction reactions from C−H bonds. Analysis of the collected kinetic

data indicates that the origin of this huge difference lies in the strength of the O−H bond formed after hydrogen-atom abstraction by the oxoiron unit and we estimate that the O−H bond formed upon reaction of **3** with a C−H bond is about 20 kcal·mol^{-1} stronger than that derived from **2b**. On the basis of literature reports on the energy of the Fe^{III}O−H bond of similar complexes, we estimate that the value of the Fe^{IV}O−H bond derived from **3** is around 100 kcal·mol^{-1}, which is close to the reported values for highly active synthetic models of compound I of cytochrome P450. Overall, we have made a direct comparison between the oxidizing abilities of two nonheme oxoiron species with relevance in synthetic catalytic oxidation reactions, and we have established that the strength of the O−H bond formed after hydrogen atom abstraction is the key factor that determines their dramatic difference in HAT reactivity. In addition, our comparative study provides direct experimental evidence that the outcome of the carbon centered radical that forms after the initial HAT by the high valent oxo-iron complex is sensitive to the oxidation state of the complex. While **3** generates caged, short-lived radicals, **2** generates carbon-centered radicals that freely diffuse in solution. The most obvious consequence is that only **3** engages in stereoretentive hydroxylation reactions. Thus, the oxidation state of the iron center not only modulates the rate of HAT but also the rate of ligand rebound.

■ EXPERIMENTAL SECTION

Materials. Reagents and solvents used were of commercially available reagent quality unless otherwise stated. Solvents were purchased from Scharlab, Acros or Sigma-Aldrich and used without further purification. Preparation and handling of air-sensitive materials were carried out in an N$_2$ drybox (Jacomex) with O$_2$ and H$_2$O concentrations <1 ppm. PyNMe$_3$, [Fe^{II}(CF$_3$SO$_3$)$_2$(PyNMe$_3$)] (**1·CF$_3$SO$_3$**) and **3** were prepared following previously described procedures.[22,81] [Fe^{II}(PyNMe$_3$)(CH$_3$CN)$_2$]$^{2+}$ (**1**) is obtained by exchange of the CF$_3$SO$_3$ anions by CH$_3$CN upon dissolving **1·CF$_3$SO$_3$** in this solvent. Xanthene-d_2 (>99% D enrichment) and 9,10-dihydroanthracene-d_4 (98% D enrichment) were prepared according to literature protocols.[82,83]

Physical Methods. UV−vis absorption spectroscopy was performed with an Agilent 50 Scan (Varian) UV−vis spectrophotometer with 1 cm quartz cells. Low temperature control was achieved with a cryostat from Unisoku Scientific Instruments, Japan. GC product analyses were performed on an Agilent 7820A gas chromatograph equipped with a HP-5 capillary column 30m × 0.32 mm × 0.25 mm and a flame ionization detector. GC−MS analyses were performed on an Agilent 7890A gas chromatograph equipped with an HP-5 capillary column interfaced with an Agilent 5975C mass spectrometer. For electron ionization (EI) the source was set at 70 eV, while a 50/50 NH$_3$:CH$_4$ mix was used as the ionization gas for chemical ionization (CI) analyses. High resolution mass spectra (HRMS) were recorded on a Bruker MicroTOF-Q IITM instrument using ESI or Cryospray ionization sources at Serveis Tècnics of the University of Girona. Samples were introduced into the mass spectrometer ion source by direct infusion using a syringe pump and were externally calibrated using sodium triflate. The instrument was operated in positive ion mode.

Fe K-edge X-ray absorption spectra on the frozen solution of **2a** and **2b** were collected at 10 K in the energy range 6900 to 8000 eV on beamline 9−3 of the Stanford Synchrotron Radiation Lightsource (SSRL) of SLAC National Accelerator Laboratory. A 100-element solid-state Ge detectors (Canberra) were used to obtain the XAS data. An iron foil was used for the energy calibration of the beam and the first inflection point of the edge was assigned to 7112.0 eV. Seven scans of the fluorescence mode XAS spectra were collected on **2a** and **2b**. To increase the signal-to-noise ratio of the spectra, a 6-μm Mn filter along with the Soller slit was placed in between detector and the

sample. Data reduction, averaging, and normalization were performed using the program EXAFSPAK.[84] The pre-edge features were fitted using the Fityk software[85] with pseudo-Voigt functions composed of 50:50 Gaussian/Lorentzian functions.

Resonance Raman spectra were obtained on frozen samples of **2a** and **2b** at 77 K with excitation at 457 nm laser (50 mW at source, Cobolt Lasers) through the sample in an NMR tube using a 135° scattering arrangement (parallel to the slit direction). The collimated Raman scattering was collected using two Plano convex lenses ($f = 10$ cm, placed at an appropriate distance) through appropriate long pass edge filters (Semrock) into an Acton AM-506M3 monochromator equipped with a Princeton Instruments ACTON PyLON LN/CCD-1340 × 400 detector. The detector was cooled to −120 °C prior to the experiments. Spectral calibration was performed using the Raman spectrum of acetonitrile/toluene 50:50 (v:v).[86] Each spectrum was accumulated, typically 60 times with 5 s acquisition time, resulting in a total acquisition time of 5 min per spectrum. The collected data was processed using Spectragryph,[87] and a multipoint baseline correction was performed for all spectra.

NMR spectra were recorded on a Bruker Avance III HD nanobay 400 MHz spectrometer or on a Bruker Ultrashield Avance III400. Temperatures for low temperature experiments were determined by calibration using a solution of methanol and TMS as the standard. 0.5 mL 4-mM solution of **1** was prepared for NMR experiments and the corresponding oxoiron(IV) samples were prepared by adding 1.1 equiv tBuNIO$_4$ and 1 equiv HClO$_4$ to this solution in an NMR tube at 253 K.

Mössbauer spectra were recorded with two spectrometers using Janis Research (Wilmington, MA) SuperVaritempdewars that allow studies in applied magnetic fields up to 8 T in the temperature range from 1.5 to 200 K. Mössbauer spectral simulations were performed using the WMOSS software package (SEE Co, Edina,MN). The figures of Mössbauer spectra were plotted in SpinCount (provided by Prof. M. P. Hendrich of Carnegie Mellon University).

Synthesis of [Fe^{II}(PyNMe$_3$)(CH$_3$CN)$_2$](SbF$_6$)$_2$ (1·SbF$_6$). In the glovebox, PyNMe$_3$ (41.3 mg, 0.17 mmol) was dissolved in CH$_3$CN (2 mL). Afterward FeCl$_2$ (21.1 mg, 0.17 mmol) was added directly as a solid and the mixture was stirred for 24 h. A color change from pale yellow to deep orange was observed. Then, AgSbF$_6$ (121 mg, 0.34 mmol) was added, which caused the immediate formation of a white precipitate corresponding to AgCl and the solution turned dark green. After stirring for 2 h the solution was filtered over Celite to remove precipitated AgCl. Then, direct addition of diethyl ether (10 mL) caused the precipitation of the complex which was separated and dried. Finally, the resulting solid was dissolved using a mixture of CH$_2$Cl$_2$ (1.5 mL) and CH$_3$CN (0.5 mL). Slow diethyl ether diffusion over the resulting solution in the anaerobic box afforded 41.8 mg (0.05 mmol, 32% yield) of dark brown crystals corresponding to **1·SbF$_6$** suitable for X-ray diffraction (see SI). ^{1}H NMR (CD$_3$CN, 400 MHz, 298 K) δ, ppm 114, 99, 87, 77, 66, 56, 55, 12, −24, −35. ESI-QTOF-MS (m/z) calcd for [Fe(PyNMe$_3$)(CH$_3$CN)]$^{2+}$172.5802, found 172.5806; calcd for [Fe(PyNMe$_3$)](SbF$_6$)]$^+$ 539.0287, found 539.0290. Anal. Calcd for C$_{18}$H$_{30}$F$_{12}$FeN$_6$Sb$_2$: C, 25.20; H, 3.53; N: 9.80. Found: C, 25.18; H, 3.21; N, 9.72.

Synthesis of PyNMe$_3$-d_4. PyNMe$_3$ (96.6 mg, 0.39 mmol) and NaH (39.3 mg, 1.56 mmol) were suspended in CD$_3$CN (2.5 mL) in a two-necked round flask inside the glovebox. The mixture was taken out the glovebox and stirred at 50 °C under an inert atmosphere for 24 h. Then D$_2$O (2 mL) was added to quench the reaction. Upon removal of CD$_3$CN under vacuum, the residue was extracted with CH$_2$Cl$_2$ (4 × 10 mL) and the organic layer was dried with MgSO$_4$ and filtered. The solvent was removed under reduced pressure obtaining a brown oil. The product was further purified by column chromatography over silica using an initial mixture of CH$_2$Cl$_2$:MeOH:NH$_3$ 80:20:4 and slowly raising the polarity to 60:40:4 to ensure the complete elution of PyNMe$_3$-d_4. 53.2 mg (0.21 mmol, 54% yield) of the pure deuterated ligand were obtained. ^{1}H NMR (CDCl$_3$, 400 MHz, 298 K) δ, ppm 7.58 (t, $J = 7.7$ Hz, 1H), 7.10 (d, $J = 7.7$ Hz, 2H), 2.55−2.46 (m, 14H), 2.21 (s, 3H). ^{13}C

NMR (CDCl$_3$, 100 MHz, 298 K) δ, ppm 157.4, 136.8, 122.2, 61.9 (m), 53.1, 52.4, 45.1 (2C).

Synthesis of [Fe^{II}(CF$_3$SO$_3$)$_2$(PyNMe$_3$-d_4)] (1·CF$_3$SO$_3$-d_4). [Fe^{II}(CF$_3$SO$_3$)$_2$(CH$_3$CN)$_2$] (91.9 mg, 0.21 mmol) was added directly as a solid to a vigorously stirred solution of PyNMe$_3$-d_4 (53.2 mg, 0.21 mmol) in tetrahydrofuran (2 mL). The solution turned from a pale color to an intense yellow color. The mixture was stirred overnight and then the obtained precipitate was separated, washed with tetrahydrofuran and dried under vacuum. Finally, the solid was redissolved in the minimum amount of CH$_2$Cl$_2$ and a few drops of acetonitrile were added to ensure the complete dissolution of the complex. After filtration over Celite, slow diethyl ether diffusion over the resulting solution afforded 63.9 mg (0.11 mmol, 52%) of yellow crystals. ^{1}H NMR (CD$_3$CN, 243 MHz, 298 K) δ, ppm = 44.8, 34.1, 24.5, 18.7, 10.5, −10.7. ESI-QTOF-MS (m/z) calcd for [Fe(PyNMe$_3$-d_4)(OH$_2$)]$^{2+}$ 163.0848, found 163.0856; calcd for [Fe(PyNMe$_3$-d_4)](OTf)]$^+$ 457.1116, found 457.1125.

Generation of 2 with Bu$_4$NIO$_4$ and TfOH. A 1 mM solution of **1** in CH$_3$CN (or in a 1:1 mixture of CH$_3$CN:CH$_2$Cl$_2$) was prepared into the glovebox. Two mL of this solution (2 μmol of **1**) were introduced in a UV−vis cuvette, that was capped with a septum, taken out from the glovebox, placed in the cryostat of the UV−vis spectrophotometer and cooled down to the set temperature (−20, −40, or −60 °C). Once the desired temperature was reached, an initial UV−vis absorption spectrum of **1** was recorded. Then 60 μL of a solution containing 1.1 equiv Bu$_4$NIO$_4$ and 0.8 equiv TfOH in CH$_3$CN were added in the cuvette. The formation of two bands at ∼800 and ∼980 nm was immediately observed. When the generation of **2** was carried out at −20 °C, the band at ∼980 nm (**2b**) was the most intense. Conversely, at −60 °C the band at ∼800 nm was the highest in intensity (corresponding to a mixture of **2a** and **2b**). Finally, at −40 °C the band at ∼800 nm was the most intense right after addition of the oxidant (mixture of **2a** and **2b**) but it decreased over time in favor of the one at ∼980 nm (**2b**) that became the major one.

The oxoiron(IV) complexes **2b**-d_4 and **2·SbF$_6$** were generated following the above-described method for the preparation of **2** but using **1·CF$_3$SO$_3$-d_4** or **1·SbF$_6$** as starting material.

Generation of 2 with 2-tBuSO$_2$−C$_6$H$_4$IO. A 1 mM solution of **1** in CH$_3$CN was prepared into the glovebox. Two mL of this solution (2 μmol of **1**) were introduced in a UV−vis cuvette that was capped with a septum, taken out from the glovebox, placed in the cryostat of the UV−vis spectrophotometer and cooled down to −40 °C. Once the desired temperature was reached, an initial UV−vis absorption spectrum of **1** was recorded. Then 100 μL of a solution containing 2-tBuSO$_2$−C$_6$H$_4$IO (2.2 μmol) in CH$_2$Cl$_2$ were added in the cuvette. As previously observed in the generation of **2** with 1.1 equiv Bu$_4$NIO$_4$ and 0.8 equiv TfOH, the intensity of the band at ∼800 nm decreased over time in favor of the one at ∼980 nm, which became the most intense.

Reaction of 2 with Substrates. For the reactivity studies, **2** was generated as described above using Bu$_4$NIO$_4$ and TfOH.

Oxidation of p-X-thioanisole by 2b at −40 °C. Once **2b** was fully formed in CH$_3$CN, 50 or 100 μL of a solution of the substrate in CH$_3$CN containing the desired amount of substrate (10−100 equiv) were added. The characteristic absorption band at 990 nm of **2b** decayed following a single exponential function from which kinetic data could be extracted. In the case of thioanisole, after total decay of the UV−vis absorption band of **2b**, biphenyl was added as internal standard and the reaction mixture was rapidly filtered through a silica plug, which was washed with ethyl acetate. This solution was then analyzed with GC to calculate the product yield.

Oxidation of Hydrocarbons by 2b at −40 °C. Once **2b** was fully formed in a 1:1 mixture of CH$_3$CN:CH$_2$Cl$_2$, between 100 and 250 μL of a solution containing the desired amount of substrate (10−70 equiv) in a 1:1 mixture of CH$_3$CN:CH$_2$Cl$_2$ were added. The characteristic absorption band at 990 nm of **2b** decayed following a single exponential function from which kinetic data could be extracted.

Oxidation of Sulfides and Hydrocarbons by 2a at −60 °C. To a solution of compound **2a** + **2b**, generated in a 1:1 mixture of CH$_3$CN:CH$_2$Cl$_2$ at −60 °C (see above for more details), 100 μL of a solution containing the desired amount of substrate (10−46 equiv) in a 1:1 mixture of CH$_3$CN:CH$_2$Cl$_2$ were added. Disappearance of the UV−vis absorption band at 792 nm was monitored upon substrate addition and the decay was fitted to a single exponential function after subtraction of the contribution from **2b** (see Supporting Information for more details)

Oxidation of Sulfides and Hydrocarbons with 2b at −60 °C. A solution of **2b** was obtained at −40 °C in a 1:1 mixture of CH$_3$CN:CH$_2$Cl$_2$ (see above for more details) after isomerization of **2a**. The solution of **2b** was cooled down to -60 °C and 100 μL of a solution containing the desired amount of substrate (10−46 equiv) in a 1:1 mixture of CH$_3$CN:CH$_2$Cl$_2$ were added. Disappearance of the UV−vis absorption band characteristic of **2b** at 990 nm was monitored upon substrate addition and the decay was fitted to a single exponential function from which the reaction rate could be extracted.

Oxidation of Cyclohexene with 2b and 3 at −40 °C. Once **2b** or **3** were fully formed in pure CH$_3$CN, 200 μL of a solution containing 100 equiv of cyclohexene in CH$_3$CN were added. After total decay of the UV−vis absorption band of **2b** at 990 nm or **3** at 490 nm, biphenyl was added as internal standard and the reaction mixture was rapidly filtered through a silica plug and subsequently washed with ethyl acetate. At this point an aliquot of the solution was analyzed by GC and GC−MS. To the remaining solution, an excess of solid PPh$_3$ was added and analyzed by GC to exclude the formation of hydroperoxides, as previously reported.[76] This experiment was carried out under different atmospheres, namely N$_2$, air and ^{18}O$_2$.

Oxidation of Cyclohexane by 3 at −40 °C. Once **3** was fully formed in CH$_3$CN, 100 μL of a solution containing 45 equiv of cyclohexane in CH$_3$CN were added. After total decay of the UV−vis absorption band of **3** at 490 nm, the reaction mixture was rapidly filtered through a silica plug and subsequently washed with ethyl acetate. At this point an aliquot of the solution was analyzed by GC and GC−MS. This experiment was carried out under N$_2$ and ^{18}O$_2$ atmospheres.

Eyring Plot for the Reaction of 2b with Cyclohexadiene and Xanthene. Once **2b** was fully formed in a 1:1 mixture of CH$_3$CN:CH$_2$Cl$_2$, 100 μL of a solution containing 10 equiv of cyclohexadiene or xanthene in a 1:1 mixture of CH$_3$CN:CH$_2$Cl$_2$ were added. The decay of the absorption band of **2b** at 990 nm was monitored and fitted to a single exponential function from which the observed rate constant (k_{obs}) could be extracted. This experiment was repeated at five different temperatures (233−273 K) for each substrate, in order to calculate the activation parameters ($\Delta H^{\ddagger}$ and $\Delta S^{\ddagger}$) by plotting the $\ln(k_2/T)$ values as a function of $1/T$.

■ ASSOCIATED CONTENT

Ⓢ Supporting Information

The Supporting Information is available free of charge on the ACS Publications website at DOI: 10.1021/jacs.9b05758.

> Characterization of **PyNMe$_3$-d_4**, **1·CF$_3$SO$_3$-d_4**, and **1·SbF$_6$**, XAS analysis for **2a** and **2b**, raw Mössbauer spectra for **2a** and **2b**, ^{1}H NMR characterization of **2b** and **2b**-d_4, UV−vis spectroscopy of the conversion of **2a** to **2b** and comparison of their reactivities in OAT and HAT processes, UV−vis spectroscopy of the reaction of **2b** in OAT and HAT processes, MS spectra for the reactions of **2b** and **3** with cyclohexene and cyclohexane, DFT calculations for the structure of **2a** and **2b** including predicted ^{1}H NMR chemical shifts and geometry coordinates (PDF)

> Crystal data (CIF)

■ AUTHOR INFORMATION

Corresponding Authors

*E-mail: larryque@umn.edu.
*E-mail: miquel.costas@udg.edu.
*E-mail: anna.company@udg.edu.

ORCID

Valeria Dantignana: 0000-0002-0799-5800
Joan Serrano-Plana: 0000-0003-2735-0943
Apparao Draksharapu: 0000-0001-7897-3230
Saikat Banerjee: 0000-0003-0013-8037
Ruixi Fan: 0000-0002-6996-4276
Ilaria Gamba: 0000-0001-9136-7227
Yisong Guo: 0000-0002-4132-3565
Lawrence Que, Jr.: 0000-0002-0989-2813
Miquel Costas: 0000-0001-6326-8299
Anna Company: 0000-0003-4845-4418

Present Addresses

∥J. Serrano-Plana: Department of Chemistry, University of Basel, Mattenstrasse 24a, BPR 1096, Switzerland.
⊥A. Draksharapu: SL-208A, Department of Chemistry, Indian Institute of Technology Kanpur, Kanpur 208016, India.

Notes

The authors declare no competing financial interest.

■ REFERENCES

(1) Rittle, J.; Green, M. T. Cytochrome P450 Compound I: Capture, Characterization, and C-H Bond Activation Kinetics. *Science* **2010**, *330*, 933−937.

(2) Huang, X.; Groves, J. T. Oxygen Activation and Radical Transformations in Heme Proteins and Metalloporphyrins. *Chem. Rev.* **2018**, *118*, 2491−2553.

(3) Ortiz de Montellano, P. R. Hydrocarbon Hydroxylation by Cytochrome P450 Enzymes. *Chem. Rev.* **2010**, *110*, 932−948.

(4) Shaik, S.; Cohen, S.; Wang, Y.; Chen, H.; Kumar, D.; Thiel, W. P450 Enzymes: Their Structure, Reactivity, and Selectivity-Modeled by QM/MM Calculations. *Chem. Rev.* **2010**, *110*, 949−1017.

(5) Perry, C.; de los Santos; Emmanuel, L. C.; Alkhalaf, L. M.; Challis, G. L. Rieske non-heme iron-dependent oxygenases catalyse diverse reactions in natural product biosynthesis. *Nat. Prod. Rep.* **2018**, *35*, 622−632.

(6) Kovaleva, E. G.; Lipscomb, J. D. Versatility of biological non-heme Fe(II) centers in oxygen activation reactions. *Nat. Chem. Biol.* **2008**, *4*, 186.

(7) Chakrabarty, S.; Austin, R. N.; Deng, D.; Groves, J. T.; Lipscomb, J. D. Radical Intermediates in Monooxygenase Reactions of Rieske Dioxygenases. *J. Am. Chem. Soc.* **2007**, *129*, 3514−3515.

(8) Krebs, C.; Galonić Fujimori, D.; Walsh, C. T.; Bollinger, J. M. Non-Heme Fe(IV)−Oxo Intermediates. *Acc. Chem. Res.* **2007**, *40*, 484−492.

(9) Price, J. C.; Barr, E. W.; Tirupati, B.; Bollinger, J. M.; Krebs, C. The First Direct Characterization of a High-Valent Iron Intermediate in the Reaction of an α-Ketoglutarate-Dependent Dioxygenase: A High-Spin Fe(IV) Complex in Taurine/α-Ketoglutarate Dioxygenase (TauD) from Escherichia coli. *Biochemistry* **2003**, *42*, 7497−7508.

(10) Hoffart, L. M.; Barr, E. W.; Guyer, R. B.; Bollinger, J. M.; Krebs, C. Direct spectroscopic detection of a C-H-cleaving high-spin Fe(IV) complex in a prolyl-4-hydroxylase. *Proc. Natl. Acad. Sci. U. S. A.* **2006**, *103*, 14738−14743.

(11) Eser, B. E.; Barr, E. W.; Frantom, P. A.; Saleh, L.; Bollinger, J. M.; Krebs, C.; Fitzpatrick, P. F. Direct Spectroscopic Evidence for a High-Spin Fe(IV) Intermediate in Tyrosine Hydroxylase. *J. Am. Chem. Soc.* **2007**, *129*, 11334−11335.

(12) Panay, A. J.; Lee, M.; Krebs, C.; Bollinger, J. M.; Fitzpatrick, P. F. Evidence for a High-Spin Fe(IV) Species in the Catalytic Cycle of a Bacterial Phenylalanine Hydroxylase. *Biochemistry* **2011**, *50*, 1928−1933.

(13) Wong, S. D.; Srnec, M.; Matthews, M. L.; Liu, L. V.; Kwak, Y.; Park, K.; Bell, C. B., III; Alp, E. E.; Zhao, J.; Yoda, Y.; Kitao, S.; Seto, M.; Krebs, C.; Bollinger, J. M.; Solomon, E. I. Elucidation of the Fe(IV)=O intermediate in the catalytic cycle of the halogenase SyrB2. *Nature* **2013**, *499*, 320.

(14) Galonić Fujimori, D.; Barr, E. W.; Matthews, M. L.; Koch, G. M.; Yonce, J. R.; Walsh, C. T.; Bollinger, J. M.; Krebs, C.; Riggs-Gelasco, P. J. Spectroscopic Evidence for a High-Spin Br-Fe(IV)-Oxo Intermediate in the α-Ketoglutarate-Dependent Halogenase CytC3 from Streptomyces. *J. Am. Chem. Soc.* **2007**, *129*, 13408−13409.

(15) Galonić, D. P.; Barr, E. W.; Walsh, C. T.; Bollinger, J. M., Jr; Krebs, C. Two interconverting Fe(IV) intermediates in aliphatic chlorination by the halogenase CytC3. *Nat. Chem. Biol.* **2007**, *3*, 113.

(16) McDonald, A. R.; Que, L. High-valent nonheme iron-oxo complexes: Synthesis, structure, and spectroscopy. *Coord. Chem. Rev.* **2013**, *257*, 414−428.

(17) Ray, K.; Pfaff, F. F.; Wang, B.; Nam, W. Status of Reactive Non-Heme Metal−Oxygen Intermediates in Chemical and Enzymatic Reactions. *J. Am. Chem. Soc.* **2014**, *136*, 13942−13958.

(18) Guo, M.; Corona, T.; Ray, K.; Nam, W. Heme and Nonheme High-Valent Iron and Manganese Oxo Cores in Biological and Abiological Oxidation Reactions. *ACS Cent. Sci.* **2019**, *5*, 13−28.

(19) Oloo, W. N.; Que, L. Bioinspired Nonheme Iron Catalysts for C−H and C=C Bond Oxidation: Insights into the Nature of the Metal-Based Oxidants. *Acc. Chem. Res.* **2015**, *48*, 2612−2621.

(20) Olivo, G.; Cussó, O.; Borrell, M.; Costas, M. Oxidation of alkane and alkene moieties with biologically inspired nonheme iron catalysts and hydrogen peroxide: from free radicals to stereoselective transformations. *JBIC, J. Biol. Inorg. Chem.* **2017**, *22*, 425−452.

(21) Meyer, S.; Klawitter, I.; Demeshko, S.; Bill, E.; Meyer, F. A Tetracarbene−Oxoiron(IV) Complex. *Angew. Chem., Int. Ed.* **2013**, *52*, 901−905.

(22) Serrano-Plana, J.; Oloo, W. N.; Acosta-Rueda, L.; Meier, K. K.; Verdejo, B.; García-España, E.; Basallote, M. G.; Münck, E.; Que, L.; Company, A.; Costas, M. Trapping a Highly Reactive Nonheme Iron

Intermediate That Oxygenates Strong C–H Bonds with Stereo-retention. *J. Am. Chem. Soc.* **2015**, *137*, 15833−15842.

(23) de Oliveira, F. T.; Chanda, A.; Banerjee, D.; Shan, X.; Mondal, S.; Que, L.; Bominaar, E. L.; Münck, E.; Collins, T. J. Chemical and Spectroscopic Evidence for an Fe^V-Oxo Complex. *Science* **2007**, *315*, 835−838.

(24) Kwon, E.; Cho, K.-B.; Hong, S.; Nam, W. Mechanistic insight into the hydroxylation of alkanes by a nonheme iron(V)−oxo complex. *Chem. Commun.* **2014**, *50*, 5572−5575.

(25) (a) Ghosh, M.; Singh, K. K.; Panda, C.; Weitz, A.; Hendrich, M. P.; Collins, T. J.; Dhar, B. B.; Sen Gupta, S. Formation of a Room Temperature Stable Fe^V(O) Complex: Reactivity Toward Unactivated C−H Bonds. *J. Am. Chem. Soc.* **2014**, *136*, 9524−9527. (b) Collins, T. J.; Ryabov, A. D. Targeting of High-Valent Iron-TAML Activators at Hydrocarbons and Beyond. *Chem. Rev.* **2017**, *117*, 9140−9162.

(26) Wang, X.; Peter, S.; Kinne, M.; Hofrichter, M.; Groves, J. T. Detection and Kinetic Characterization of a Highly Reactive Heme−Thiolate Peroxygenase Compound I. *J. Am. Chem. Soc.* **2012**, *134*, 12897−12900.

(27) Borrell, M.; Andris, E.; Navratil, R.; Roithova, J.; Costas, M. Characterized cis-Fe^V(O)(OH) intermediate mimics enzymatic oxidations in the gas phase. *Nat. Commun.* **2019**, *10*, 901.

(28) Fan, R.; Serrano-Plana, J.; Oloo, W. N.; Draksharapu, A.; Delgado-Pinar, E.; Company, A.; Martin-Diaconescu, V.; Borrell, M.; Lloret-Fillol, J.; García-España, E.; Guo, Y.; Bominaar, E. L.; Que, L.; Costas, M.; Münck, E. Spectroscopic and DFT Characterization of a Highly Reactive Nonheme Fe^V−Oxo Intermediate. *J. Am. Chem. Soc.* **2018**, *140*, 3916−3928.

(29) Mondal, B.; Neese, F.; Bill, E.; Ye, S. Electronic Structure Contributions of Non-Heme Oxo-Iron(V) Complexes to the Reactivity. *J. Am. Chem. Soc.* **2018**, *140*, 9531−9544.

(30) Lyakin, O. Y.; Zima, A. M.; Samsonenko, D. G.; Bryliakov, K. P.; Talsi, E. P. EPR Spectroscopic Detection of the Elusive Fe^V=O Intermediates in Selective Catalytic Oxofunctionalizations of Hydrocarbons Mediated by Biomimetic Ferric Complexes. *ACS Catal.* **2015**, *5*, 2702−2707.

(31) Zima, A. M.; Lyakin, O. Y.; Ottenbacher, R. V.; Bryliakov, K. P.; Talsi, E. P. Dramatic Effect of Carboxylic Acid on the Electronic Structure of the Active Species in Fe(PDP)-Catalyzed Asymmetric Epoxidation. *ACS Catal.* **2016**, *6*, 5399−5404.

(32) Zima, A. M.; Lyakin, O. Y.; Ottenbacher, R. V.; Bryliakov, K. P.; Talsi, E. P. Iron-Catalyzed Enantioselective Epoxidations with Various Oxidants: Evidence for Different Active Species and Epoxidation Mechanisms. *ACS Catal.* **2017**, *7*, 60−69.

(33) Oloo, W. N.; Banerjee, R.; Lipscomb, J. D.; Que, L. Equilibrating (L)Fe^{III}−OOAc and (L)Fe^V(O) Species in Hydrocarbon Oxidations by Bio-Inspired Nonheme Iron Catalysts Using H$_2$O$_2$ and AcOH. *J. Am. Chem. Soc.* **2017**, *139*, 17313−17326.

(34) White, M. C.; Zhao, J. Aliphatic C−H Oxidations for Late-Stage Functionalization. *J. Am. Chem. Soc.* **2018**, *140*, 13988−14009.

(35) Serrano-Plana, J.; Acuña-Parés, F.; Dantignana, V.; Oloo, W. N.; Castillo, E.; Draksharapu, A.; Whiteoak, C. J.; Martin-Diaconescu, V.; Basallote, M. G.; Luis, J. M.; Que, L.; Costas, M.; Company, A. Acid-Triggered O−O Bond Heterolysis of a Nonheme Fe^{III}(OOH) Species for the Stereospecific Hydroxylation of Strong C−H Bonds. *Chem. - Eur. J.* **2018**, *24*, 5331−5340.

(36) Klein, J. E. M. N.; Que, L. Biomimetic High-Valent Mononuclear Nonheme Iron-Oxo Chemistry. In *Encyclopedia of Inorganic and Bioinorganic Chemistry*; Scott, R. A., Ed.; John Wiley & Sons, 2016; pp 1−22.

(37) Rasheed, W.; Draksharapu, A.; Banerjee, S.; Young, V. G., Jr.; Fan, R.; Guo, Y.; Ozerov, M.; Nehrkorn, J.; Krzystek, J.; Telser, J.; Que, L., Jr. Crystallographic Evidence for a Sterically Induced Ferryl Tilt in a Non-Heme Oxoiron(IV) Complex that Makes it a Better Oxidant. *Angew. Chem., Int. Ed.* **2018**, *57*, 9387−9391.

(38) Company, A.; Prat, I.; Frisch, J. R.; Mas-Ballesté, D. R.; Güell, M.; Juhász, G.; Ribas, X.; Münck, D. E.; Luis, J. M.; Que, L.; Costas, M. Modeling the cis-Oxo-Labile Binding Site Motif of Non-Heme Iron Oxygenases: Water Exchange and Oxidation Reactivity of a Non-Heme Iron(IV)-Oxo Compound Bearing a Tripodal Tetradentate Ligand. *Chem. - Eur. J.* **2011**, *17*, 1622−1634.

(39) Anastasi, A. E.; Comba, P.; McGrady, J.; Lienke, A.; Rohwer, H. Electronic Structure of Bispidine Iron(IV) Oxo Complexes. *Inorg. Chem.* **2007**, *46*, 6420−6426.

(40) Prakash, J.; Rohde, G. T.; Meier, K. K.; Münck, E.; Que, L. Upside Down! Crystallographic and Spectroscopic Characterization of an [Fe^{IV}(O$_{syn}$)(TMC)]$^{2+}$ Complex. *Inorg. Chem.* **2015**, *54*, 11055−11057.

(41) Klinker, E. J.; Kaizer, J.; Brennessel, W. W.; Woodrum, N. L.; Cramer, C. J.; Que, L., Jr. Structures of Nonheme Oxoiron(IV) Complexes from X-ray Crystallography, NMR Spectroscopy, and DFT Calculations. *Angew. Chem., Int. Ed.* **2005**, *44*, 3690−3694.

(42) Company, A.; Sabenya, G.; González-Béjar, M.; Gómez, L.; Clémancey, M.; Blondin, G.; Jasniewski, A. J.; Puri, M.; Browne, W. R.; Latour, J.-M.; Que, L.; Costas, M.; Pérez-Prieto, J.; Lloret-Fillol, J. Triggering the Generation of an Iron(IV)-Oxo Compound and Its Reactivity toward Sulfides by RuII Photocatalysis. *J. Am. Chem. Soc.* **2014**, *136*, 4624−4633.

(43) Rasheed, W.; Fan, R.; Abelson, C. S.; Peterson, P. O.; Ching, W. M.; Guo, Y.; Que, L., Jr. Structural Implications of the Paramagnetically Shifted NMR Signals from Pyridine H-Atoms on Synthetic Nonheme Fe^{IV}=O Complexes. *JBIC, J. Biol. Inorg. Chem.* **2019**, *24*, 533−545.

(44) Ching, W.-M.; Zhou, A.; Klein, J. E. M. N.; Fan, R.; Knizia, G.; Cramer, C. J.; Guo, Y.; Que, L. Characterization of the Fleeting Hydroxoiron(III) Complex of the Pentadentate TMC-py Ligand. *Inorg. Chem.* **2017**, *56*, 11129−11140.

(45) Duban, E. A.; Bryliakov, K. P.; Talsi, E. P. The Active Intermediates of Non-Heme-Iron-Based Systems for Catalytic Alkene Epoxidation with H$_2$O$_2$/CH$_3$COOH. *Eur. J. Inorg. Chem.* **2007**, *2007*, 852−857.

(46) Thibon, A.; England, J.; Martinho, M.; Young, V. G., Jr.; Frisch, J. R.; Guillot, R.; Girerd, J.-J.; Münck, E.; Que, L., Jr.; Banse, F. Proton- and Reductant-Assisted Dioxygen Activation by a Nonheme Iron(II) Complex to Form an Oxoiron(IV) Intermediate. *Angew. Chem., Int. Ed.* **2008**, *47*, 7064−7067.

(47) Park, M. J.; Lee, J.; Suh, Y.; Kim, J.; Nam, W. Reactivities of Mononuclear Non-Heme Iron Intermediates Including Evidence that Iron(III)−Hydroperoxo Species Is a Sluggish Oxidant. *J. Am. Chem. Soc.* **2006**, *128*, 2630−2634.

(48) Notice that 9,10-dihydroanthracene-d_4 could be synthesized with only a 98% D enrichment. If this is taken into account, a much higher KIE should have been obtained.

(49) Hong, S.; So, H.; Yoon, H.; Cho, K.-B.; Lee, Y.-M.; Fukuzumi, S.; Nam, W. Reactivity comparison of high-valent iron(IV)-oxo complexes bearing N-tetramethylated cyclam ligands with different ring size. *Dalton Trans.* **2013**, *42*, 7842−7845.

(50) Price, J. C.; Barr, E. W.; Glass, T. E.; Krebs, C.; Bollinger, J. M. Evidence for Hydrogen Abstraction from C1 of Taurine by the High-Spin Fe(IV) Intermediate Detected during Oxygen Activation by Taurine:α-Ketoglutarate Dioxygenase (TauD). *J. Am. Chem. Soc.* **2003**, *125*, 13008−13009.

(51) Bollinger, J. M.; Krebs, C. Stalking intermediates in oxygen activation by iron enzymes: Motivation and method. *J. Inorg. Biochem.* **2006**, *100*, 586−605.

(52) Kupper, C.; Mondal, B.; Serrano-Plana, J.; Klawitter, I.; Neese, F.; Costas, M.; Ye, S.; Meyer, F. Nonclassical Single-State Reactivity of an Oxo-Iron(IV) Complex Confined to Triplet Pathways. *J. Am. Chem. Soc.* **2017**, *139*, 8939−8949.

(53) Monte Pérez, I.; Engelmann, X.; Lee, Y.-M.; Yoo, M.; Kumaran, E.; Farquhar, E. R.; Bill, E.; England, J.; Nam, W.; Swart, M.; Ray, K. A Highly Reactive Oxoiron(IV) Complex Supported by a Bioinspired N$_3$O Macrocyclic Ligand. *Angew. Chem., Int. Ed.* **2017**, *56*, 14384−14388.

(54) Mitra, M.; Nimir, H.; Demeshko, S.; Bhat, S. S.; Malinkin, S. O.; Haukka, M.; Lloret-Fillol, J.; Lisensky, G. C.; Meyer, F.; Shteinman, A. A.; Browne, W. R.; Hrovat, D. A.; Richmond, M. G.;

Costas, M.; Nordlander, E. Nonheme Fe(IV) Oxo Complexes of Two New Pentadentate Ligands and Their Hydrogen-Atom and Oxygen-Atom Transfer Reactions. *Inorg. Chem.* **2015**, *54*, 7152−7164.

(55) Kaizer, J.; Klinker, E. J.; Oh, N. Y.; Rohde, J.-U.; Song, W. J.; Stubna, A.; Kim, J.; Münck, E.; Nam, W.; Que, L. Nonheme Fe^{IV}O Complexes That Can Oxidize the C−H Bonds of Cyclohexane at Room Temperature. *J. Am. Chem. Soc.* **2004**, *126*, 472−473.

(56) Biswas, A. N.; Puri, M.; Meier, K. K.; Oloo, W. N.; Rohde, G. T.; Bominaar, E. L.; Münck, E.; Que, L. Modeling TauD-J: A High-Spin Nonheme Oxoiron(IV) Complex with High Reactivity toward C−H Bonds. *J. Am. Chem. Soc.* **2015**, *137*, 2428−2431.

(57) Tanko, J. M.; Friedline, F.; Suleman, N. K.; Castagnoli, N., Jr. tert-Butoxyl as a Model for Radicals in Biological Systems: Caveat Emptor. *J. Am. Chem. Soc.* **2001**, *123*, 5808−5809.

(58) Finn, M.; Friedline, R.; Suleman, N. K.; Wohl, C. J.; Tanko, J. M. Chemistry of the t-Butoxyl Radical: Evidence that Most Hydrogen Abstractions from Carbon are Entropy-Controlled. *J. Am. Chem. Soc.* **2004**, *126*, 7578−7584.

(59) Pattanayak, S.; Jasniewski, A. J.; Rana, A.; Draksharapu, A.; Singh, K. K.; Weitz, A.; Hendrich, M.; Que, L.; Dey, A.; Sen Gupta, S. Spectroscopic and Reactivity Comparisons of a Pair of bTAML Complexes with Fe^V=O and Fe^{IV}=O Units. *Inorg. Chem.* **2017**, *56*, 6352−6361.

(60) Oszajca, M.; Franke, A.; Drzewiecka-Matuszek, A.; Brindell, M.; Stochel, G.; van Eldik, R. Temperature and Pressure Effects on C−H Abstraction Reactions Involving Compound I and II Mimics in Aqueous Solution. *Inorg. Chem.* **2014**, *53*, 2848−2857.

(61) Bell, S. R.; Groves, J. T. A Highly Reactive P450 Model Compound I. *J. Am. Chem. Soc.* **2009**, *131*, 9640−9641.

(62) Krebs, C.; Price, J. C.; Baldwin, J.; Saleh, L.; Green, M. T.; Bollinger, J. M., Jr. Rapid Freeze-Quench ^{57}Fe Mössbauer Spectroscopy: Monitoring Changes of an Iron-Containing Active Site during a Biochemical Reaction. *Inorg. Chem.* **2005**, *44*, 742−757.

(63) Sastri, C. V.; Lee, J.; Oh, K.; Lee, Y. J.; Lee, J.; Jackson, T. A.; Ray, K.; Hirao, H.; Shin, W.; Halfen, J. A.; Kim, J.; Que, L.; Shaik, S.; Nam, W. Axial ligand tuning of a nonheme iron(IV)−oxo unit for hydrogen atom abstraction. *Proc. Natl. Acad. Sci. U. S. A.* **2007**, *104*, 19181−19186.

(64) Company, A.; Gómez, L.; Costas, M. Bioinspired Non-heme Iron Catalysts in C−H and C=C Oxidation Reactions. In *Iron-Containing Enzymes*; Visser, S. P. d., Kumar, D., Eds.; RSC Publishing: Cambridge, 2011.

(65) Mader, E. A.; Davidson, E. R.; Mayer, J. M. Large Ground-State Entropy Changes for Hydrogen Atom Transfer Reactions of Iron Complexes. *J. Am. Chem. Soc.* **2007**, *129*, 5153−5166.

(66) Evans, M. G.; Polanyi, M. Inertia and driving force of chemical reactions. *Trans. Faraday Soc.* **1938**, *34*, 11−24.

(67) Wang, D.; Zhang, M.; Bühlmann, P.; Que, L. Redox Potential and C−H Bond Cleaving Properties of a Nonheme Fe^{IV}=O Complex in Aqueous Solution. *J. Am. Chem. Soc.* **2010**, *132*, 7638−7644.

(68) Usharani, D.; Lacy, D. C.; Borovik, A. S.; Shaik, S. Dichotomous Hydrogen Atom Transfer vs Proton-Coupled Electron Transfer During Activation of X−H Bonds (X = C, N, O) by Nonheme Iron−Oxo Complexes of Variable Basicity. *J. Am. Chem. Soc.* **2013**, *135*, 17090−17104.

(69) Mittra, K.; Green, M. T. Reduction Potentials of P450 Compounds I and II: Insight into the Thermodynamics of C−H Bond Activation. *J. Am. Chem. Soc.* **2019**, *141*, 5504−5510.

(70) Postils, V.; Company, A.; Solà, M.; Costas, M.; Luis, J. M. Computational Insight into the Mechanism of Alkane Hydroxylation by Non-heme Fe(PyTACN) Iron Complexes. Effects of the Substrate and Solvent. *Inorg. Chem.* **2015**, *54*, 8223−8236.

(71) Wang, Y.; Janardanan, D.; Usharani, D.; Han, K.; Que, L.; Shaik, S. Nonheme Iron Oxidant Formed in the Presence of H2O2 and Acetic Acid Is the Cyclic Ferric Peracetate Complex, Not a Perferryloxo Complex. *ACS Catal.* **2013**, *3*, 1334−1341.

(72) Chen, H.; Lai, W.; Shaik, S. Exchange-Enhanced H-Abstraction Reactivity of High-Valent Nonheme Iron(IV)-Oxo from Coupled Cluster and Density Functional Theories. *J. Phys. Chem. Lett.* **2010**, *1*, 1533−1540.

(73) Hirao, H.; Kumar, D.; Que, L.; Shaik, S. Two-State Reactivity in Alkane Hydroxylation by Non-Heme Iron−Oxo Complexes. *J. Am. Chem. Soc.* **2006**, *128*, 8590−8606.

(74) Groves, J. T.; Adhyam, D. V. Hydroxylation by cytochrome P-450 and metalloporphyrin models. Evidence for allylic rearrangement. *J. Am. Chem. Soc.* **1984**, *106*, 2177−2181.

(75) Oloo, W. N.; Feng, Y.; Iyer, S.; Parmelee, S.; Xue, G.; Que, L. Cyclohexene as a substrate probe for the nature of the high-valent iron-oxo oxidant in Fe(TPA)-catalyzed oxidations. *New J. Chem.* **2013**, *37*, 3411−3415.

(76) Shul'pin, G. B.; Süss-Fink, G.; Smith, J. R. L. Oxidations by the System "Hydrogen Peroxide - Manganese(IV) Complex - Acetic Acid" - Part II. *Tetrahedron* **1999**, *55*, 5345−5358.

(77) Jiang, Y.; He, X.; Ortiz de Montellano, P. R. Radical Intermediates in the Catalytic Oxidation of Hydrocarbons by Bacterial and Human Cytochrome P450 Enzymes. *Biochemistry* **2006**, *45*, 533−542.

(78) Cho, K.-B.; Hirao, H.; Shaik, S.; Nam, W. To rebound or dissociate? This is the mechanistic question in C−H hydroxylation by heme and nonheme metal−oxo complexes. *Chem. Soc. Rev.* **2016**, *45*, 1197−1210.

(79) Pangia, T. M.; Davies, C. G.; Prendergast, J. R.; Gordon, J. B.; Siegler, M. A.; Jameson, G. N. L.; Goldberg, D. P. Observation of Radical Rebound in a Mononuclear Nonheme Iron Model Complex. *J. Am. Chem. Soc.* **2018**, *140*, 4191−4194.

(80) Drummond, M. J.; Ford, C. L.; Gray, D. L.; Popescu, C. V.; Fout, A. R. Radical Rebound Hydroxylation Versus H-Atom Transfer in Non-Heme Iron(III)-Hydroxo Complexes: Reactivity and Structural Differentiation. *J. Am. Chem. Soc.* **2019**, *141*, 6639−6650.

(81) Serrano-Plana, J.; Aguinaco, A.; Belda, R.; García-España, E.; Basallote, M. G.; Company, A.; Costas, M. Exceedingly Fast Oxygen Atom Transfer to Olefins via a Catalytically Competent Nonheme Iron Species. *Angew. Chem., Int. Ed.* **2016**, *55*, 6310−6314.

(82) Sankaralingam, M.; Lee, Y.-M.; Jeon, S. H.; Seo, M. S.; Cho, K.-B.; Nam, W. A mononuclear manganese(III)−hydroperoxo complex: synthesis by activating dioxygen and reactivity in electrophilic and nucleophilic reactions. *Chem. Commun.* **2018**, *54*, 1209−1212.

(83) Kim, S. J.; Latifi, R.; Kang, H. Y.; Nam, W.; de Visser, S. P. Activation of hydrocarbon C−H bonds by iodosylbenzene: how does it compare with iron(IV)−oxo oxidants? *Chem. Commun.* **2009**, 1562−1564.

(84) George, G. N. *EXAFSPAK*; Stanford Synchrotron Radiation Laboratory, Stanford Linear Accelerator Center: Stanford, CA, 2000.

(85) Wojdyr, M. Fityk: a general-purpose peak fitting program. *J. Appl. Crystallogr.* **2010**, *43*, 1126−1128.

(86) ASTM E1840−96: Standard Guide for Raman Shift Standards for Spectrometer Calibration; ASTM International, 2007; DOI: 10.1520/E1840-96R07.

(87) Menges, F. *Spectragryph*, Version 1.2.10; 2018. http://www.effemm2.de/spectragryph/ (accessed on March 24, 2019).

Chapter V

Ligand effects on the reactivity of oxoiron(IV)
species supported by electronically
tuned azamacrocycles
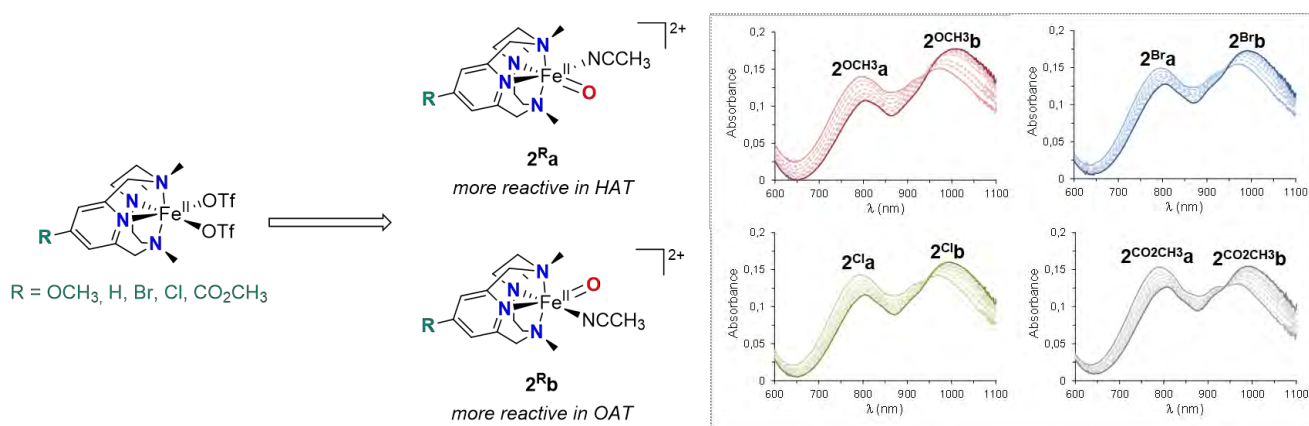
V. Dantignana, J. Serrano-Plana, Á. Martínez Camarena,

E. García-España, Anna Company,* M. Costas*

manuscript in preparation

For this publication V. D. synthetized and characterized the iron(II) and oxoiron(IV) complexes and performed the reactivity studies with the oxoiron(IV) species. Besides, V. D. contributed in writing the manuscript and was involved in argumentations and discussions.

Ligand effects on the reactivity of oxoiron(IV) species supported by electronically tuned azamacrocycles

Valeria Dantignana,[a] Joan Serrano-Plana,[a] Álvaro Martínez Camarena,[b] Enrique García-España,[b] Anna Company,*[a] Miquel Costas*[a]

[a]   Institut de Química Computacional i Catàlisi (IQCC), Departament de Química, Universitat de Girona. C/ M. Aurèlia Capmany 69, 17003 Girona (Catalonia, Spain).
      E-mail: anna.company@udg.edu, miquel.costas@udg.edu
[b]   Instituto de Ciencia Molecular (ICMol), Universidad de Valencia, 46980, Paterna, Spain

Abstract

In this work, a series of iron(II) complexes ([$Fe^{II}(CF_3SO_3)_2(^RPyNMe_3)$], 1^R) bearing $PyNMe_3$ ligands containing a 4-R-substituted pyridine ($^RPyNMe_3$) has been described. The modulation of the electronic properties of the ligand affects the redox potential and the magnetic moment of the 1^R complexes, thus this is envisioned to tune the reactivity of the related oxoiron species. 1^R compounds have been employed in the synthesis of the corresponding oxoiron(IV) species ([$Fe^{IV}(O)(^RPyNMe_3)(CH_3CN)$]$^{2+}$, 2^R). Remarkably, with the whole series of 2^R compounds two different geometrical isomers, differing in the ligand moiety in *trans* to the oxo group (2^Ra and 2^Rb), can be experimentally observed and spectroscopically characterized. Oxidative abilities of 2^Ra and 2^Rb have been studied in OAT and HAT processes. Electronic effects, modulated by changing the nature of the pyridine donor, present a modest impact on the oxoiron(IV) reactivity. Reaction rates decrease gradually with the improvement of the ligand donor character, but the decrease of rates in the series are smaller than one order of magnitude. Most interestingly, comparison between the reactivity of 2^Ra and 2^Rb shows more important differences. The compound having an aliphatic amine moiety in *trans* to the oxo group (2^Ra) is up to 30 times more reactive than its isomer (2^Rb) in the oxidation of 9,10-dihydroanthracene via HAT, whereas 2^Rb reacted up to 11 times faster than 2^Ra in the oxidation of thioanisole via OAT. The inverted relative reactivity of 2^Ra and 2^Rb, which overcomes the electronic effects imparted by the tetradentate ligand and depends on the nature of the oxidation reaction, is unprecedented and highlights a novel mechanistic aspect that could be helpfully employed to modulate the oxidative ability of oxoiron(IV) species.

V. Dantignana, J. Serrano-Plana, Á. Martínez Camarena, E. García-España, A. Company,

M. Costas. "Ligand effects on the reactivity of oxoiron(IV) species supported by electronically tuned

azamacrocycles". (2020). Manuscript in preparation.

Chapter VI

Results and discussion

VI.1 CHEMOSELECTIVE ALIPHATIC C-H BOND OXIDATION ENABLED BY POLARITY REVERSAL

Oxygenated compounds are common skeletons in natural and bioactive products; therefore, selective oxidation of C-H bonds represents an interesting transformation in synthetic chemistry.[1] For C-H bond oxidations catalyzed by bioinspired complexes general trends in the selectivity outcome have been established, which are dictated by the nature of the substrate itself or by the interaction of the substrate with the catalyst.[2-4] Even so, progresses are still needed to accomplish minimization of overoxidation processes as well as oxidation of specific C-H bonds in the presence of unprotected polar groups. In that regard, it was shown that the use of hydrogen bond donor solvents could be useful to enhance the chemo- and the regioselectivity in HAT processes.[5, 6] Thus, with the aim to address the above mentioned challenges, we have studied the solvent effect in aliphatic C-H bond oxidations catalyzed by bioinspired iron and manganese complexes (Figure VI.1)
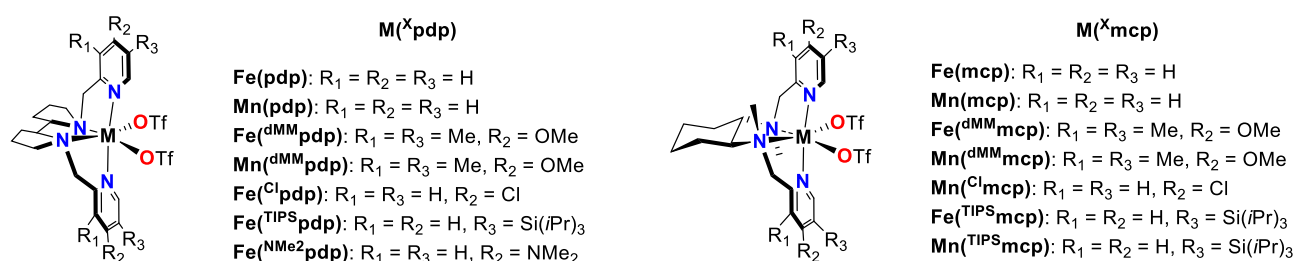

M(^{X}pdp)

Fe(pdp): $R_1 = R_2 = R_3 = H$
Mn(pdp): $R_1 = R_2 = R_3 = H$
Fe(^{dMM}pdp): $R_1 = R_3 = Me$, $R_2 = OMe$
Mn(^{dMM}pdp): $R_1 = R_3 = Me$, $R_2 = OMe$
Fe(^{Cl}pdp): $R_1 = R_3 = H$, $R_2 = Cl$
Fe(^{TIPS}pdp): $R_1 = R_2 = H$, $R_3 = Si(iPr)_3$
Fe(^{NMe2}pdp): $R_1 = R_3 = H$, $R_2 = NMe_2$

M(^{X}mcp)

Fe(mcp): $R_1 = R_2 = R_3 = H$
Mn(mcp): $R_1 = R_2 = R_3 = H$
Fe(^{dMM}mcp): $R_1 = R_3 = Me$, $R_2 = OMe$
Mn(^{dMM}mcp): $R_1 = R_3 = Me$, $R_2 = OMe$
Mn(^{Cl}mcp): $R_1 = R_3 = H$, $R_2 = Cl$
Fe(^{TIPS}mcp): $R_1 = R_2 = H$, $R_3 = Si(iPr)_3$
Mn(^{TIPS}mcp): $R_1 = R_2 = H$, $R_3 = Si(iPr)_3$

**Figure VI.1.** Complexes used in this chapter.

At first oxidation on hexane (**1**) was studied, employing the iron and manganese pdp complexes as catalysts (Figure VI.1), hydrogen peroxide as terminal oxidant and acetic acid as additive. As expected,[7, 8] in acetonitrile the first formed alcohol products (**1a** and **1b**) were further oxidized to the related ketones (**1c** and **1d**), despite low conversion conditions that should limit overoxidation processes were used (0.2 equiv of H_2O_2 with respect to the substrate). As a consequence, 2-hexanone (**1c**) and 3-hexanone (**1d**) were obtained as main products, in up to 40% combined yield (entries 1 and 2, Table VI.1). Instead, 2-hexanol (**1a**) and 3-hexanol (**1b**) were obtained in up to 16% combined yield, which translated in a 46% hydroxylation selectivity (defined as: 100x([**1a**]+[**1b**])/([**1a**]+[**1b**]+[**1c**]+[**1d**])). In sharp contrast, when the oxidations were performed in the same conditions but using 2,2,2-trifluoroethanol (TFE) as solvent, instead of acetonitrile, up to 92% hydroxylation selectivity was observed, being **1a** and **1b** formed in up to 44% combined yield (entries 3 and 4 in Table VI.1). Furthermore, overoxidation of **1a** and **1b** could be almost suppressed by using 1,1,3,3-hexafluoroisopropanol (HFIP) as reaction media, so that 98-99% hydroxylation selectivity was achieved in this solvent (entries 5 and 6, Table VI.1). Interestingly, a similar trend was also found using a manganese porphyrin complex as catalyst and iodosylbenzene as oxidant (see Table S1 in Annex 1).

Table VI.1. Solvent screening for the oxidation of hexane (**1**).
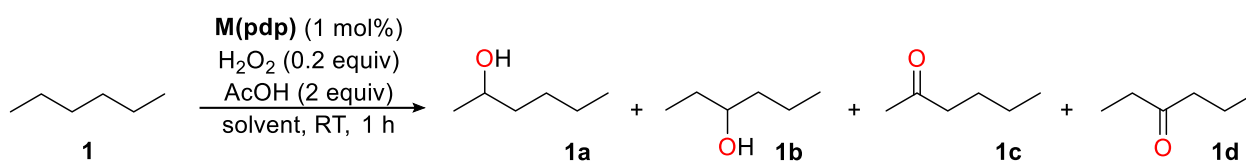
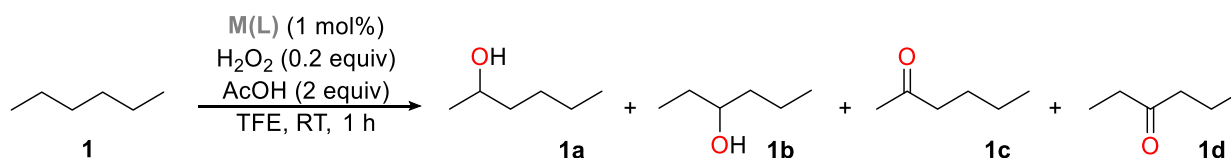| entry	M	solvent	1a (%)[a]	1b (%)[a]	1c (%)[a]	1d (%)[a]	yield (%)[a] (% alcohol)[b]
1	Fe	MeCN	8	8	24	14	54 (46)
2	Mn	MeCN	7	5	26	14	52 (38)
3	Fe	TFE	26	18	8	6	58 (86)
4	Mn	TFE	21	14	4	2	41 (92)
5	Fe	HFIP	49	33	2	2	86 (98)
6	Mn	HFIP	39	25	1	1	66 (99)

[a]Yields with respect to H_2O_2, determined by GC-FID against an internal standard. Yields are calculated considering that 2 equivalents of H_2O_2 are necessary for the formation of the ketone products (**1c** and **1d**). [b]$100 \times ([\mathbf{1a}]+[\mathbf{1b}])/([\mathbf{1a}]+[\mathbf{1b}]+[\mathbf{1c}]+[\mathbf{1d}])$.

The outstanding chemoselectivity found in the oxidation performed in fluorinated alcohols (TFE and HFIP) can be rationalized considering their hydrogen bond donor ability.[9] Upon hydroxylation of hexane, hexanol is obtained. The latter contains a polar group that makes the hydrogen atom in α to the substituent activated towards the attack of an electrophilic oxidant, being it more electron-rich with respect to the other C-H bonds of the molecule. Thus, in acetonitrile the C-H bond in α to the hydroxyl group of the hexanol is prone to be oxidized and, as a consequence, hexanone is obtained as main product (Scheme VI.1, top). Nevertheless, in fluorinated alcohols a polarity reversal occurs, thanks to the establishment of hydrogen bonds between the solvent and the polar group of the first formed alcohol product. As a result, the C-H bond in α to the hydroxyl functionality is deactivated and the alcohol to ketone overoxidation is prevented (Scheme VI.1, bottom). In that view, additionally, the enhanced chemoselectivity found in the oxidations performed in HFIP with respect to the ones carried out in TFE can be explained bearing in mind its higher hydrogen bond donor ability.[10]
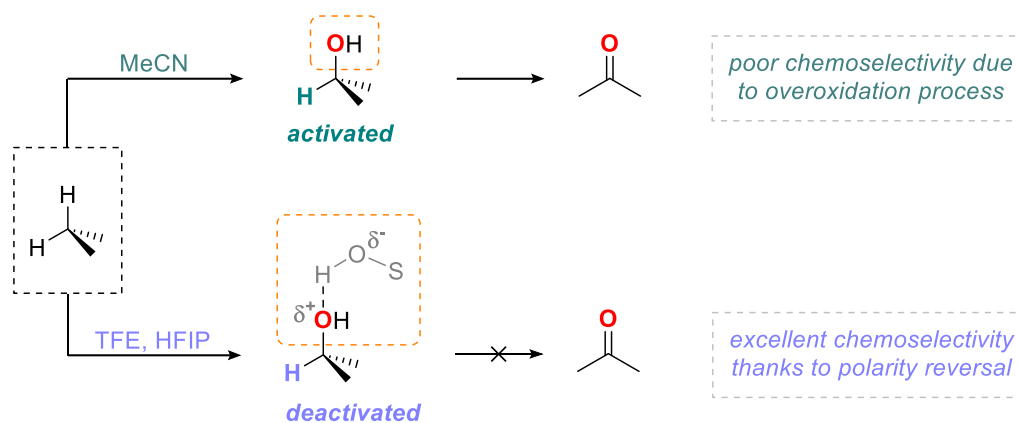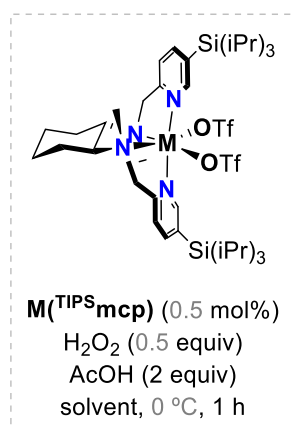
Scheme VI.1. Schematic representation of the chemoselectivity outcome in C-H bond oxidations performed in acetonitrile (MeCN) or hydrogen bond donor solvents (TFE, HFIP).

Afterwards, a screening of iron and manganese complexes, bearing tetradentate aminopyridine ligands with different electronic and steric properties as well as a different backbone, was performed in TFE (Scheme VI.2, top; see Table S2 and Table S3 in Annex 1 for the yield of each product; see Figure VI.1 for complexes structure). Among the catalysts tested, the M(^{TIPS}mcp) complexes afforded the highest total yield (63% and 58% with Fe(^{TIPS}mcp) and Mn(^{TIPS}mcp), respectively), together with an excellent degree of chemoselectivity (91% and 96% with Fe(^{TIPS}mcp) and Mn(^{TIPS}mcp), respectively). Thus, optimization of the reaction conditions was carried out with these catalysts. The optimized conditions (Scheme VI.2, bottom) included lower catalyst loading (from 1 to 0.5 mol%) and lower temperature (from room temperature to 0 °C). Additionally, higher amounts of hydrogen peroxide (from 0.2 to 0.5 equiv with respect to the substrate) could be used maintaining outstanding degrees of chemoselectivity (Scheme VI.2, bottom; see Table S2 in Annex 1 for the yield of each product). Since the manganese catalyst generally exhibits a slightly better chemoselectivity than iron, the former was selected for further studies.
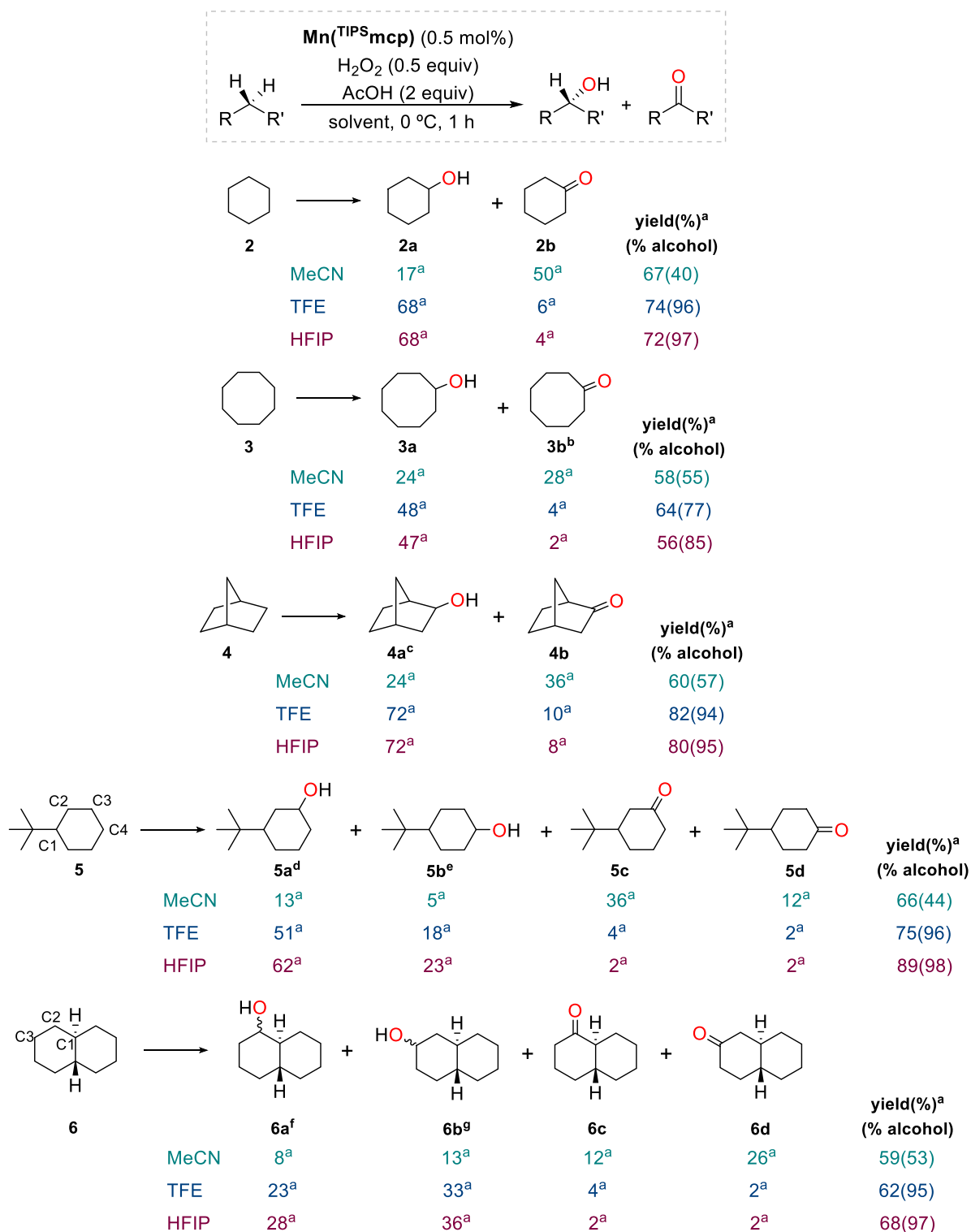
Scheme VI.2. Catalyst screening (top) and optimized reaction conditions (bottom) for the oxidation of hexane (**1**).

[a]Total yield. Yields with respect to H_2O_2, determined by GC-FID against an internal standard. Yields are calculated considering that 2 equivalents of H_2O_2 are necessary for the formation of the ketone products (**1c** and **1d**). [b]$100\times([\mathbf{1a}]+[\mathbf{1b}])/([\mathbf{1a}]+[\mathbf{1b}]+[\mathbf{1c}]+[\mathbf{1d}])$.

The solvent effect observed with hexane was also found for different cyclic and bicyclic alkane substrates, as shown in Scheme VI.3. In the oxidation of cyclohexane (**2**), the yield of cyclohexanol (**2a**) improved from 17% (40% hydroxylation selectivity) in acetonitrile, to 69% (96-97% hydroxylation selectivity) in TFE and HFIP. Similarly, for cyclooctane (**3**) hydroxylation selectivity towards cyclooctanol (**3a**) improved from 55% (yield **3a** = 24%) in acetonitrile, to 77% (yield **3a** = 48%) and 85% (yield **3a** = 47%) in TFE and HFIP, respectively. Subsequently, oxidation of more elaborated substrates, such as norbornane (**4**), *tert*-butylcyclohexane (**5**) and *trans*-decalin (**6**), was studied. Oxidation of norbornane (**4**) permitted to observe that, in line with literature precedents,[11, 12] the target hydroxylation is stereospecific. Indeed, the *exo* alcohol product (**4a**$_{exo}$) was obtained with a >99% selectivity over the *endo* one (**4a**$_{endo}$) with all the solvents tested. Additionally, total yield and

hydroxylation selectivity improved going from acetonitrile (60% yield, 57% hydroxylation selectivity) to TFE (82% yield, 94% hydroxylation selectivity) and HFIP (80% yield, 95% hydroxylation selectivity).

In the oxidation of *tert*-butylcyclohexane (**5**) more aspects could be considered. First, oxidation occurred only at C3 and C4, as oxidation at C1 and C2 is prevented by steric and torsional effects and the primary C-H bonds of the *tert*-butyl group are too strong to be reactive under the conditions used. Then, comparing the combined yield of **5a** and **5c** (oxidation at C3) with the one of **5b** and **5d** (oxidation at C4) it could be noted that oxidation at C3 was slightly favored (normalized C3/C4 ratio: 1.3 in HFIP, 1.4 in TFE and MeCN). This could be ascribed to electronic effects, being C3 closer than C4 to the electrondonating *tert*-butyl substituent.[13-15] Moreover, it should be noted that the alcohol products **5a** and **5b** could derive by HAT of either the equatorial or the axial hydrogen. Nevertheless, previous studies showed that the equatorial hydrogen is preferentially abstracted due to the consequent diminishment of 1,3-diaxial interactions.[16, 17] Accordingly, despite products **5a** and **5b** were obtained as a mixture of equatorial (**5a**$_{eq}$ and **5b**$_{eq}$) and axial alcohols (**5a**$_{ax}$ and **5b**$_{ax}$), **5a**$_{eq}$ and **5b**$_{eq}$ dominated over **5a**$_{ax}$ and **5b**$_{ax}$ in all the solvents tested. Furthermore, as in the case of norbornane, besides the increased total yield (75 and 89% in TFE and HFIP, respectively, vs 66% in acetonitrile) an outstanding hydroxylation selectivity was attained using fluorinated alcohols as reaction media (96 and 98% inTFE and HFIP, respectively, vs 44% in acetonitrile).
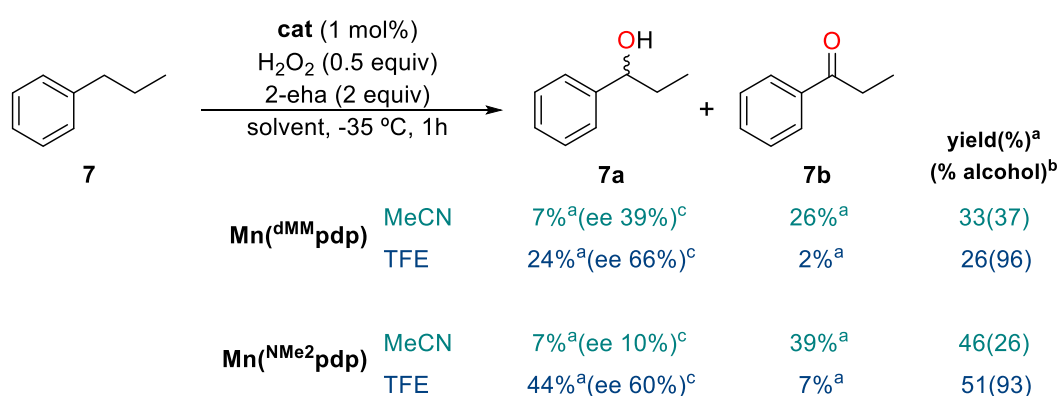
Lastly, in the oxidation of *trans*-decalin (**6**) products deriving from the oxidation of the tertiary C-H bond at C1 were not observed in any solvent, even though this bond is weaker than the secondary ones. This is due to its limited accessibility and its axial position.[18] Instead, products at C2 (**6a** and **6c**) and C3 (**6b** and **6d**) were formed. As in the case of *tert*-butyl cyclohexane, considering the alcohol products **6a** and **6b** equatorial over axial hydroxylation was favored (**6a**$_{ax}$:**6a**$_{eq}$ up to 1:5; **6b**$_{ax}$:**6b**$_{eq}$ up to 2:5). Furthermore, also with this substrate extremely high degrees of hydroxylation selectivity were reached using TFE and HFIP as solvents (95% and 97% in TFE and HFIP, respectively, vs 53% in MeCN).

Mn(TIPSmcp) (0.5 mol%)
H$_2$O$_2$ (0.5 equiv)
AcOH (2 equiv)
solvent, 0 °C, 1 h

Compound 2

	2a	2b	yield(%)[a] (% alcohol)
MeCN	17[a]	50[a]	67(40)
TFE	68[a]	6[a]	74(96)
HFIP	68[a]	4[a]	72(97)

Compound 3

	3a	3b[b]	yield(%)[a] (% alcohol)
MeCN	24[a]	28[a]	58(55)
TFE	48[a]	4[a]	64(77)
HFIP	47[a]	2[a]	56(85)

Compound 4

	4a[c]	4b	yield(%)[a] (% alcohol)
MeCN	24[a]	36[a]	60(57)
TFE	72[a]	10[a]	82(94)
HFIP	72[a]	8[a]	80(95)

Compound 5

	5a[d]	5b[e]	5c	5d	yield(%)[a] (% alcohol)
MeCN	13[a]	5[a]	36[a]	12[a]	66(44)
TFE	51[a]	18[a]	4[a]	2[a]	75(96)
HFIP	62[a]	23[a]	2[a]	2[a]	89(98)

Compound 6

	6a[f]	6b[g]	6c	6d	yield(%)[a] (% alcohol)
MeCN	8[a]	13[a]	12[a]	26[a]	59(53)
TFE	23[a]	33[a]	4[a]	2[a]	62(95)
HFIP	28[a]	36[a]	2[a]	2[a]	68(97)

[a]Yields with respect to H$_2$O$_2$, determined by GC-FID against an internal standard. Yields are calculated considering that 2 equivalents of H$_2$O$_2$ are necessary for the formation of the ketone products. [b]6-12% cyclooctene oxide formed. [c]**4a$_{exo}$** is obtained with >99% selectivity over **4a$_{endo}$** in all solvents. [d]**5a** is obtained as a mixture of axial and equatorial alcohol products. **5a$_{ax}$:5a$_{eq}$** ratios are 1:5, 1:3, and 1:3 for MeCN, TFE, and HFIP, respectively. [e]**5b** is obtained as a mixture of axial and equatorial alcohol products. **5b$_{ax}$:5b$_{eq}$** ratio is 2:3 in all solvents. [f]**6a** is obtained as a mixture of axial and equatorial alcohol products. **6a$_{ax}$:6a$_{eq}$** ratios are 1:3, 1:5, and 1:2 for MeCN, TFE, and HFIP, respectively. [g]**6b** is obtained as a mixture of axial and equatorial alcohol products. **6b$_{ax}$:6b$_{eq}$** ratios are 1:2, 1:2, and 2:5 for MeCN, TFE, and HFIP, respectively.

Scheme VI.3. Oxidation of hydrocarbons in MeCN, TFE and HFIP.

The excellent chemoselectivity found in the hydroxylation of aliphatic methylenic sites could be advantageous in the hydroxylation of prochiral substrates. As the first formed alcohol product is a chiral compound, preventing overoxidation is crucial to avoid the formation of achiral ketones and, consequently, to attain enantioselective transformations. Thus, asymmetric oxidation of benzylic C-H bonds in TFE was also investigated. As expected, oxidation of propylbenzene (**7**) in TFE was extremely chemoselective. Under the optimized reaction conditions shown in Scheme VI.4 (see Table S7 and S8 in Annex 1 for optimization details), 1-phenyl-1-propanol (**7a**) was obtained in 24% and 44% yield with Mn(dMMpdp) and Mn(NMe2pdp), respectively. Importantly, the hydroxylation selectivity (defined as: 100x[**7a**]/([**7a**]+[**7b**])) increased from 37% and 26%, in acetonitrile, to 96% and 93%, in TFE, with Mn(dMMpdp) and Mn(NMe2pdp), respectively. Remarkably, the employment of TFE instead of acetonitrile also afforded higher enantiomeric excess (ee) for **7a**: a 1.7 and 6-fold increase of the ee was observed in TFE with Mn(dMMpdp) and Mn(NMe2pdp), respectively. Analogous results were as well achieved in the oxidation of ethylbenzene and *p*-methylethylbenzene (see Table S7 in Annex 1).

		7a	**7b**	**yield(%)[a]** (% alcohol)[b]
Mn(dMMpdp)	MeCN	7%[a](ee 39%)[c]	26%[a]	33(37)
	TFE	24%[a](ee 66%)[c]	2%[a]	26(96)
Mn(NMe2pdp)	MeCN	7%[a](ee 10%)[c]	39%[a]	46(26)
	TFE	44%[a](ee 60%)[c]	7%[a]	51(93)

[a]Yields with respect to H_2O_2, determined by GC-FID against an internal standard. Yields are calculated considering that 2 equivalents of H_2O_2 are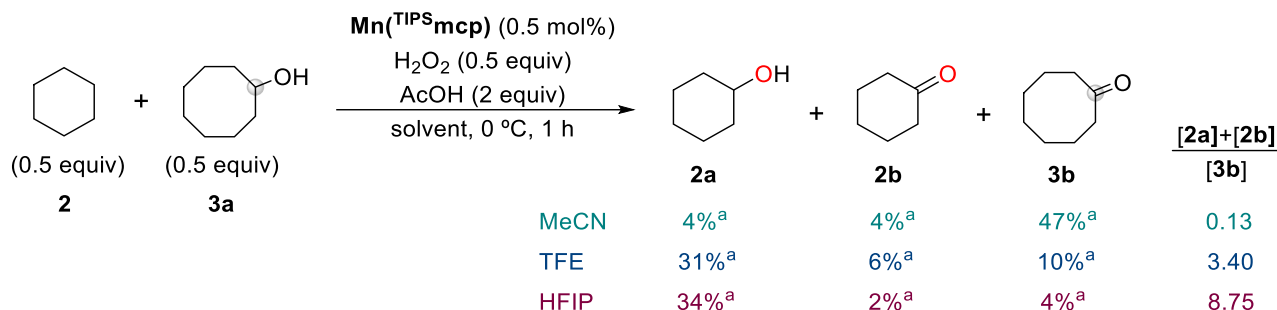 necessary for the formation of **7b**. [b]100x[**7a**]/([**7a**]+[**7b**]). [c]ee of **7a** determined by GC with a chiral stationary phase.

Scheme VI.4. Enantioselective oxidation of benzylic C-H bonds in MeCN and TFE. Scheme adapted from ref [19].

Overall, the collected data suggests that deactivation of the C-H bond in α to the hydroxyl group of the alcohol product (HOC-H) occurs when fluorinated alcohols are used as solvents, as demonstrated by the minimization of overoxidation processes. Then, with the aim of studying the changes in the relative reactivity of C-H and HOC-H bonds as a function of the reaction media, competitive oxidation of an equimolar mixture of cyclohexane (**2**) and cyclooctanol (**3a**) was performed (Scheme VI.5).

In acetonitrile cyclooctanone (**3b**) was obtained (47% yield), upon oxidation of the HOC-H bond of cyclooctanol, along with minor amount of cyclohexanol and cyclohexanone (combined yield **2a+2b**: 8%). Conversely, in TFE and HFIP cyclohexanol (**2a**) and cyclohexanone (**2b**) were formed in a

combined 36-37% yield, while cyclooctanone (**3b**) was obtained in up to 10% yield. Thus, these results further support the above explained concept of polarity reversal, which allows to rationalize the inverted relative reactivity of C-H and HOC-H bonds observed in fluorinated alcohol solvents.

Mn(^{TIPS}mcp) (0.5 mol%)
H$_2$O$_2$ (0.5 equiv)
AcOH (2 equiv)
solvent, 0 °C, 1 h

(0.5 equiv)   (0.5 equiv)
2   **3a**

	2a	2b	3b	[2a]+[2b] / [3b]
MeCN	4%[a]	4%[a]	47%[a]	0.13
TFE	31%[a]	6%[a]	10%[a]	3.40
HFIP	34%[a]	2%[a]	4%[a]	8.75

[a]Yields with respect to H$_2$O$_2$, determined by GC-FID against an internal standard. Yields are calculated considering that 2 equivalents of H$_2$O$_2$ are necessary for the formation of **2b**.

Scheme VI.5. Competitive oxidation of cyclohexane (**2**) and cyclooctanol (**3a**) in MeCN, TFE and HFIP. Scheme adapted from ref [19].

The identification of a protocol that permits to deactivate C-H bonds in α to an electron donating group might be useful to achieve alternative selectivity outcomes in the oxidation of alcohols, ethers, amines and amides.

Oxidation of alcohols in acetonitrile, as shown above in the competitive oxidation of **2** and **3a**, leads to the formation of the corresponding ketones. However, we envisioned that in TFE and HFIP, being the relative reactivity of unactivated C-H bonds higher than the one of the HOC-H bond, preparation of diols could be feasible. Thus, oxidation of linear and cyclic alcohols was investigated (Scheme VI.6, see Scheme S4 in Annex 1 for the oxidation in TFE).

In line with our predictions, oxidation of 3-hexanol (**8**) in acetonitrile only afforded 3-hexanone (**8a,** 76% yield). Instead, the employment of HFIP allowed to get, along with 48% yield of **8a**, 2,4-hexanediol (**8b**) in 12% yield (20% selectivity, defined as: [8a]/([8a]+[8b])). As shown in Scheme VI.6, in HFIP selectivity towards C-H bonds could be enhanced by increasing the distance between the hydroxyl group and the remote C-H bonds. Oxidation of 1-hexanol (**9**) in HFIP afforded 1,5-hexanediol (**9c**) in 32% yield (82% selectivity), while products deriving from the oxidation of the HOC-H bonds (aldehyde **9a** and its overoxidized product **9b**) were obtained in a 9% combined yield. The diol products derived from the oxidation of 2-heptanol (**10**) and 2-octanol (**11**) were obtained in 36% (**10b**, 75% selectivity) and 62% (**11b**+**11c**, 93% selectivity) yield, respectively, togheter with minor amounts of the corresponding ketones **10a** and **11a**.

These results highlighted that the deactivation achieved in HFIP by estabilism of hydrogen bonds between the solvent and the hydroxyl substituent not only involved the α C-H bond. Instead, this effect propagated along the alkyl chain, so that methylenic sites are more reactive as larger is their distance from the polar group. For example, in the oxidation of 2-octanol (**11**) the methylenic site

placed five bonds away to the hydroxyl group, which oxidation affoded product **11c**, is preferentially oxidized over the one at four bond distance, which gave product **11b** (**11c**: 49% yield; **11b**: 13% yield).

The just described trend could also be extended to cyclic alkanols, such as cyclohexanol (**2a**) and cyclooctanol (**3a**) (Scheme VI.6). Indeed, while in acetonitrile diols were formed in up to 1% yield, in HFIP 1,4-cyclohexanediol (**2c**) and 1,x-cyclooctanediol (**3c**: x = 4, **3d**: x = 5) were obtained in 30% (**2c**, 45% selectivity) and 49% yield (**3c**+**3d**, selectivity 85%), respectively. Additionally, in the oxidation of **3a** the yield of 1,5-cyclooctanediol (**3d**: 41% yield) was approximately 5 times higher that the one of 1,4-cyclooctanediol (**3c**: 8% yield). Thus, as in the case of 2-octanol (**11**), the most activated methylenic site is the one located farther away from the hydroxyl group.

aYields with respect to H_2O_2, determined by GC-FID against an internal standard.
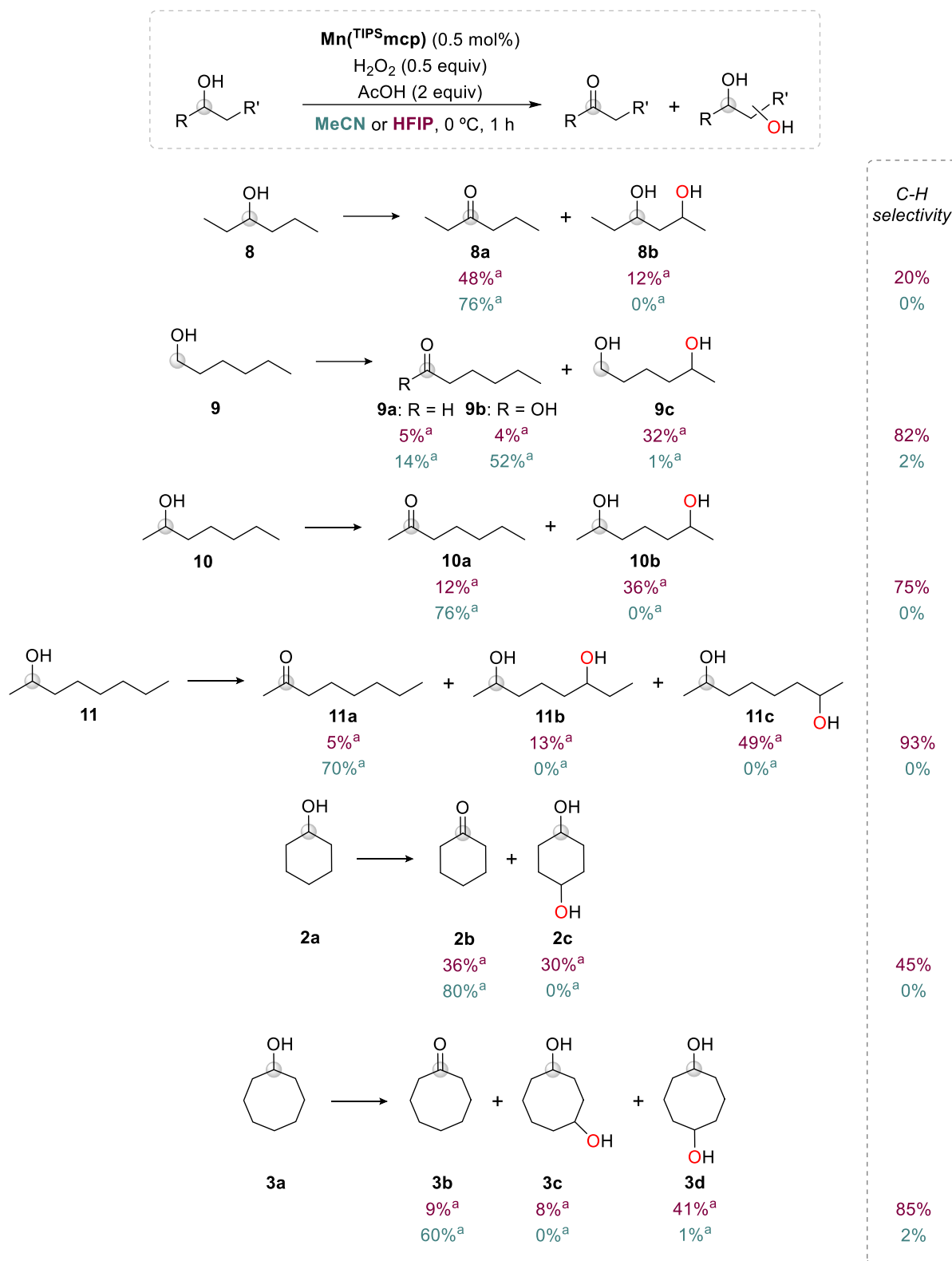
Scheme VI.6. Oxidation of alcohols in MeCN and HFIP. Scheme adapted from ref [19].

Finally, alcohols bearing activated C-H bonds, such as tertiary or benzylic ones, were tested (Scheme VI.7). In the oxidation of 6-methyl-2-heptanol (**12**) selectivity towards the formation of 2-

methylheptane-2,6-diol (**12b**) improved from 5% (4% yield) to 88% (56% yield) by using HFIP instead of acetonitrile, in which 6-methyl-2-heptanone (**12a**) was obtained as main product (77% yield).

In the reaction of 3,7-dimethyl-1-octanol (**13**), oxidation in HFIP occurred at the remote tertiary C-H bond, whereas the proximal one was unreactive. Then, the diol product **13c** was formed in 36% yield (97% selectivity), along with only 1% of the aldehyde **13a**. Conversely, in acetonitrile the diol **13c** was not observed; instead, aldehyde **13a** (11% yield) and its overoxidation product **13b** (19% yield) were obtained. Finally, in the oxidation of 1-adamantanemethanol (**14**), albeit in acetonitrile aldehyde **14a** (6% yield) was formed as single product, diol products (**14b**: 75% yield; **14c**: 9% yield) were obtained with 100% selectivity in HFIP. A 100% selectivity was also observed in the oxidation of 4-phenyl-1-butanol (**15**) performed in HFIP, which afforded 4-phenyl-1,4-butanediol (**15b**) as a single product in 38% yield. The latter was also obtained as the main product in acetonitrile (**15b**: 12% yield), but in an 1.3:1 ratio with the aldehyde **15a** (9% yield).
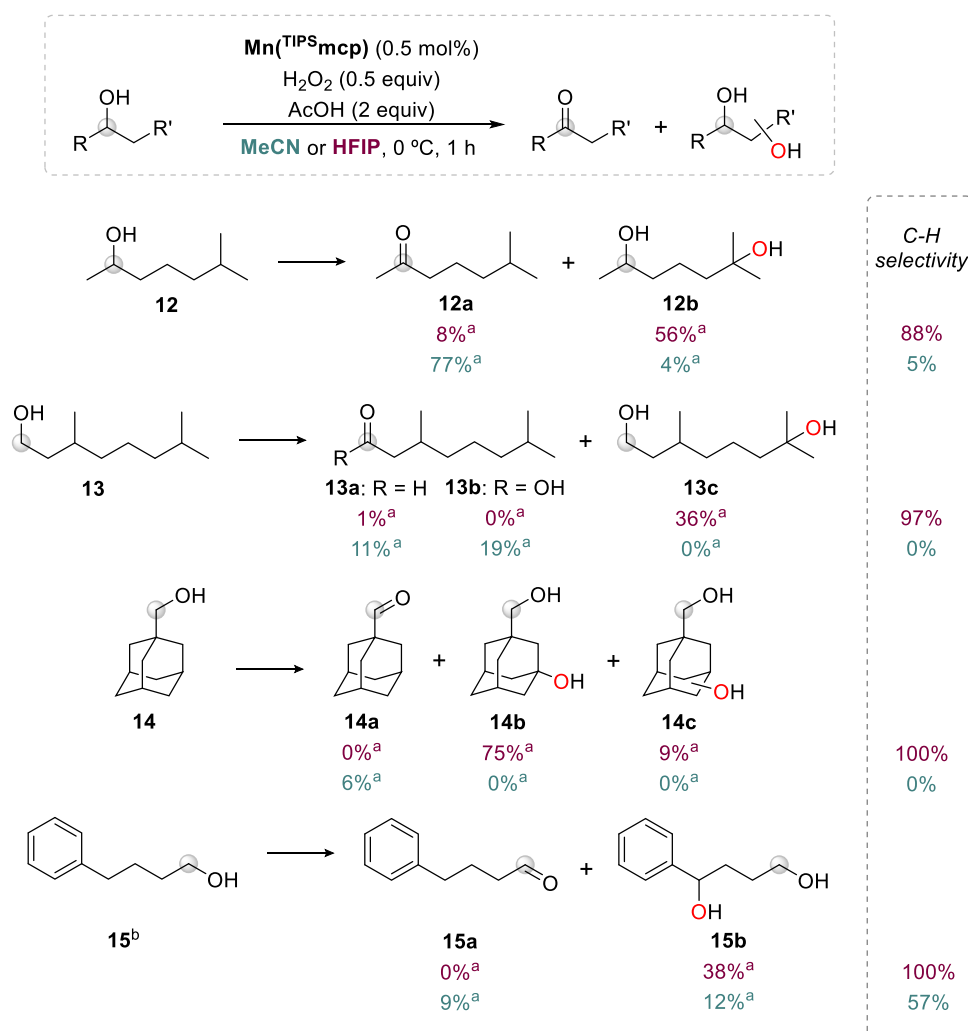
[a]Yields with respect to H_2O_2, determined by GC-FID against an internal standard.
[b]**Mn(NMe2pdp)** was used as catalyst in this oxidation.

Scheme VI.7. Oxidation of alcohols with activated C-H bonds in MeCN and HFIP. Scheme adapted from ref [19].

Interestingly, besides the hydroxyl group, also an ether functionality can be protected in HFIP. For example, oxidation of substrate **16** (Scheme VI.8) afforded alcohol **16c** in 58% yield (95% selectivity), with only minor amounts of products deriving from the oxidation of the C-H bond α to the ether group (**16a**: 1% yield; **16b**: 2% yield). Conversely, in acetonitrile aldehyde **16a** was obtained in 11% yield, along with 6% of its overoxidized product **16b**, wherease alcohol **16c** was formed in only 7% yield (29% selectivity).
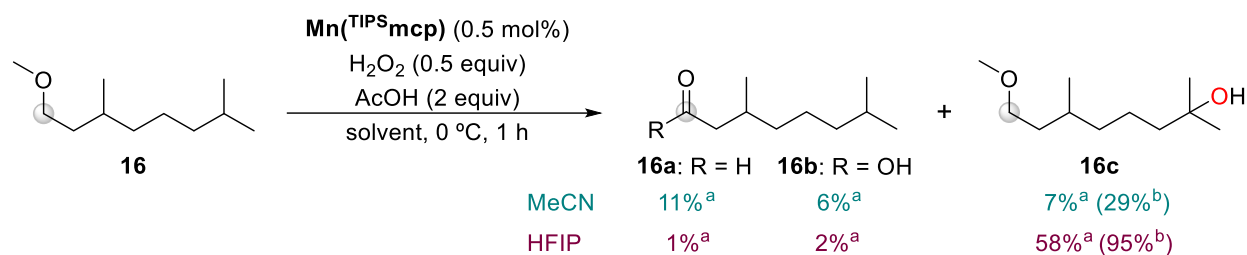
	16a: R = H	**16b**: R = OH	**16c**
MeCN	11%[a]	6%[a]	7%[a] (29%[b])
HFIP	1%[a]	2%[a]	58%[a] (95%[b])

[a]Yields with respect to H_2O_2, determined by GC-FID against an internal standard. Yields are calculated considering that 2 equivalents of H_2O_2 are necessary for the formation of **16b**.[b]100x[**16c**]/([**16a**]+[**16b**]+[**16c**]).

Scheme VI.8. Oxidation of ether **16** in MeCN and HFIP.

Lastly, the impact of fluorinated alcohols on the regioselectivity was investigated employing amides and amines as substrates.[5] Literature precedents and the alcohol oxidations described above suggest that the use of fluorinated solvents may move the oxidation site from proximal to remote positions in amide and amine containing substrates.

In acetonitrile, oxidation of *N*-pentylacetamide (**17**)[20] (Scheme VI.9) afforded **17a**, deriving from proximal oxidation, as single product in 35% yield. Instead, in HFIP remote oxidation dominantly occured, so that ketoamide **17b** was obtained in 51% yield (75% remote regioselectivity, defined as: [**17b**]/([**17a**]+[**17b**])). Inverted regioselectivity was also observed in the oxidation of amides **18** and **19** (Scheme VI.9). In the oxidation of **18**,[20] in acetonitrile proximal oxidation occurred affording product **18a** in 65% yield, along with only 1% of remote oxidation product **18b**. Instead, in HFIP 100% selectivity towards oxidation of the remote tertiary C-H bond was found (62% yield of **18b**). In the same line, oxidation of the α C-H bond was totally suppressed in the reaction of **19** in HFIP, which afforded only product **19b** in 46% yield. Nevertheless, in acetonitrile product **19a** was obtained as main product (22% yield), along with only 3% of **19b** (12% remote regioselectivity). Finally, in the oxidation of *N*-1-adamantylmethyl pivalamide (**20**) the use of HFIP allowed to obtain as unique product the monohydroxylated compound **20c** (55% yield), while in acetonitrile it was formed in 19% yield (76% selectivity) togheter with the bis and tris hydroxylated products **20a** (2% yield) and **20b** (4% yield) (Scheme VI.9). Thus, in HFIP the estabilishment of hydrogen bonds between the solvent and the hydroxyl group of the first formed product **20c** prevents further C-H bond oxidations.

Scheme VI.9. Oxidation of amides in MeCN and HFIP. Scheme adapted from ref [19].

Finally, oxidation of lactam **21** and amines **22** and **23** was carried out (Scheme VI.10). Remarkably, conversely to literature precedents,[21, 22] selective hydroxylation was accomplished in HFIP without a priori protection of the polar group of the substrate. Thus, oxidation of **21** and **23** in HFIP afforded the remote hydroxylated products **21a** and **23a** in 49% and 54% yield, respectively. The monohyhdroxylated product **22a** was formed in 44% yield upon oxidation of **22**.
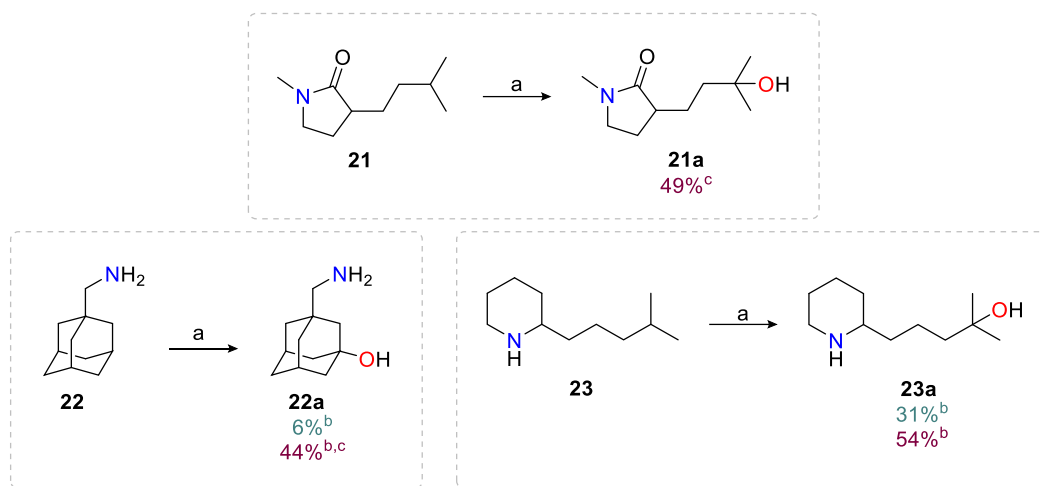
Reaction conditions: **Mn(^{TIPS}mcp)** (1 mol%), H_2O_2 (1.0 equiv), AcOH (13 equiv), **MeCN** or **HFIP,** 0 °C, 30 min. [b]Yields with respect to the substrate, determined by GC-FID against an internal standard. [c]Isolated yield.

Scheme VI.10. Oxidation of a lactam (**21**) and amines (**22**, **23**) in MeCN and HFIP. Scheme adapted from ref [19].

VI.2 SPECTROSCOPIC AND REACTIVITY COMPARISONS BETWEEN NONHEME OXOIRON(IV) AND OXOIRON(V) SPECIES BEARING THE SAME ANCILLARY LIGAND

High-valent oxoiron species are the active oxidants involved in the catalytic cycle of iron-dependent oxygenases and bioinspired synthetic models.[23, 24] Thus, their preparation and reactivity have been largely investigated to shed light on mechanistic details. Oxoiron(IV) species generally exhibit poorer oxidative ability and higher stability than oxoiron(V) intermediates, so their isolation has been accomplished with several synthetic complexes.[25, 26] On the contrary, the elusive character of oxoiron(V) species has limited their characterization, which to date has been achieved with only few systems.[27, 28] As a consequence, there is a lack of reports in which oxoiron(IV) and oxoiron(V) species have been directly compared using the same system.[29, 30] To the best of our knowledge, the only example in the literature for non-heme oxoiron compounds was described by Gupta and co-workers.[29] Albeit an exhaustive spectroscopic characterization was accomplished for the two species bearing the bTAML ligand, reactivity studies were limited to the oxidation of benzyl alcohol. For this system, the oxoiron(V) species reacted approximately three orders of magnitude faster than the related oxoiron(IV).

In this view, we envisioned to compare the oxoiron(IV) and oxoiron(V) species bearing the PyNMe$_3$ ligand (Scheme VI.11), which is capable of supporting high-valent oxoiron compounds in the two oxidation states. Indeed, one of the few reported oxoiron(V) species described to date is the [Fe^V(O)(OC(O)R)(PyNMe$_3$)]$^{2+}$.[31, 32]
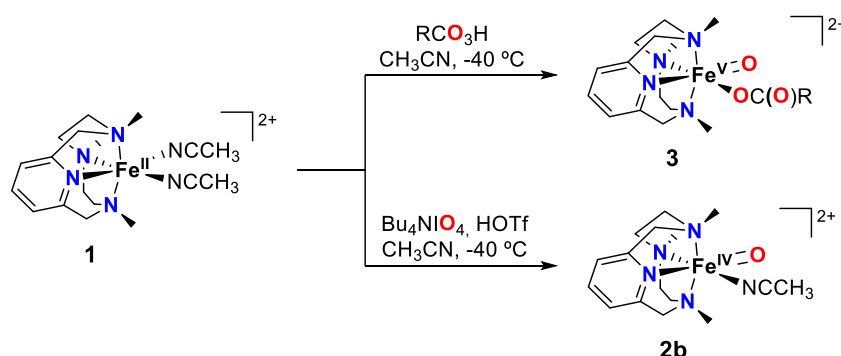
Scheme VI.11. Synthesis of [Fe^V(O)(OC(O)R)(PyNMe$_3$)]$^{2+}$ (**3**) and [Fe^{IV}(O)(PyNMe$_3$)(CH$_3$CN)]$^{2+}$ (**2b**) from the [Fe^{II}(PyNMe$_3$)(CH$_3$CN)$_2$]$^{2+}$ (**1**) complex.

Synthesis of the [Fe^V(O)(OAc)(PyNMe$_3$)]$^{2+}$ (**3**) compound and its oxidative reactivity were previously reported by our group.[31-33] Thus, we focused our attention to the study of the corresponding oxoiron(IV) species, namely [Fe^{IV}(O)(PyNMe$_3$)(CH$_3$CN)]$^{2+}$ (**2**). In a previous work, synthesis of **2** was achieved in 40% yield by oxidation of the [Fe^{II}(PyNMe$_3$)(CH$_3$CN)$_2$]$^{2+}$ complex (**1**) with four equivalents of 2-tBuSO$_2$-C$_6$H$_4$IO at -40 ºC in acetonitrile.[32] Nonetheless, we could optimize this yield and we

found that the use of Bu$_4$NIO$_4$ (1.1 equiv) in the presence of triflic acid (0.8 equiv) permitted to obtain **2** in significantly higher yields. These optimized conditions were employed to prepare **2** and its generation was followed by UV-vis spectroscopy. Addition of the Bu$_4$NIO$_4$/TfOH mixture to an acetonitrile solution of **1** (1 mM) at -40 ºC caused the immediate disappearance of the characteristic absorption band at 380 nm of the iron(II) complex **1** and the formation of two new absorption bands centered at 792 and 990 nm (Figure VI.2). As shown in Figure VI.2, the intensity of the band at 792 nm decreased over time, while the one of the band at 990 nm simultaneously increased. Along with these changes in absorbance, an isosbestic point appeared at 940 nm. Consequently, the 792 nm and 990 nm bands should correspond to two different species that directly interconvert. Additionally, it was found that generation of **2** at higher or lower temperatures (in this case using a 1:1 CH$_3$CN:CH$_2$Cl$_2$ solvent mixture) afforded a different scenario. Particularly, no variation in the relative intensity of the two bands was observed. On one side, conversion of the 792 nm band, associated to a first species **2a**, to the 990 nm band, corresponding to a second species **2b**, could be blocked at -60 ºC (see Figure S8 in Annex 2). On the other side, at -20 ºC the band at 990 nm was instantaneously obtained as the main one (see Figure S8 in Annex 2).

$$[Fe^{II}(PyNMe_3)(CH_3CN)_2]^{2+} \xrightarrow[CH_3CN, -40 \text{ ºC}]{\substack{Bu_4NI\textbf{O}_4 \text{ (1.1 equiv.)} \\ HOTf \text{ (0.8 equiv.)}}} [Fe^{IV}(\textbf{O})(PyNMe_3)(CH_3CN)]^{2+}$$

$$\textbf{1} \qquad\qquad\qquad\qquad\qquad\qquad\qquad\qquad\qquad \textbf{2}$$
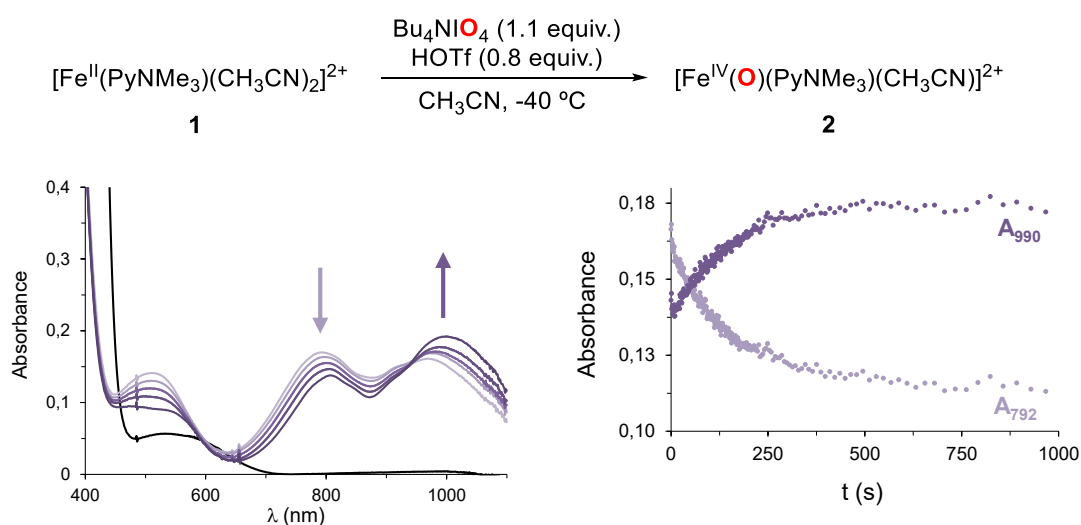
Figure VI.2. Left: spectral changes occurring upon addition of Bu$_4$NIO$_4$ (1.1 equiv) and TfOH (0.8 equiv) to an acetonitrile solution of **1** (1 mM, black line) at -40 ºC. Right: changes over time of the 792 nm and 990 nm bands. Figure adapted from ref [34].

With the aim to shed light on the nature of **2a** and **2b**, a detailed spectroscopic characterization was performed. The Mössbauer spectrum recorded at t = 30 min, which corresponds to the one of the final species **2b**, exhibited a doublet characterized by an isomer shift (δ) of 0.09 mm·s^{-1} and a quadrupole splitting (ΔE_Q) of 0.24 mm·s^{-1}. These parameters are in line with the ones previously reported for [Fe^{IV}(O)(PyNMe$_3$)(CH$_3$CN)]$^{2+}$.[32] Therefore **2b**, which represented the 60% of the total iron content, was assigned to an S = 1 oxoiron(IV) compound. Instead, the spectrum obtained at t = 2 min contained two different species: 35% of the initial species **2a** along with 30% of **2b**. An isomer

shift (δ) of 0.07 mm·s^{-1} and a quadrupole splitting (ΔE_Q) of 0.98 mm·s^{-1} characterized the doublet of **2a**. Thus, as in the case of **2b**, the δ and the ΔE_Q are indicative of the presence of an S = 1 oxoiron(IV) compound. Then, **2a** was associated to the kinetic isomer, which over time converts to the thermodynamic isomer **2b**. In contrast to **2b**, which can be obtained in a pure form, **2a** was obtained in a mixture with **2b**. Resonance Raman and X-ray absorption (XAS) spectroscopy supported the assignment of **2a** and **2b** to oxoiron(IV) species. Raman bands at 822 cm^{-1} and 829 cm^{-1}, ascribed to a ν(Fe=O) mode,[26] were found in the spectra of **2a** and **2b**, respectively. Instead, K-edge energies of 7124.8 eV and 7124.4 eV and pre-edge areas of 20.9 units and 19.6 units were respectively observed in the XAS spectra of **2a** and **2b**. Additionally, EXAFS analysis for **2a** and **2b** showed a Fe=O distance of 1.65-1.66 Å and an average Fe-N distance (4 N from the ligand and 1 N from an acetonitrile solvent molecule) of 2.0 Å. The collected spectroscopic data are gathered in Table VI.2.

Table VI.2. Spectroscopic data collected for **2a** and **2b**.

		2a	**2b**
UV-visible	λ_{max}, nm (ε, M^{-1}·cm^{-1})	792 (-)[a] 970 (-)[a]	805 (230)[b] 990 (320)[b]
Mössbauer	δ, mm·s^{-1} (ΔE_Q, mm·s^{-1})	0.07 (0.98)	0.09 (0.24)
resonance Raman	ν (Fe-O), cm^{-1}	822	829
XAS	K-edge energy, eV	7124.8	7124.4
	pre-edge energy, eV	7114.1	7114.0
	pre-edge area, units	20.9	19.6
	r(Fe=O), Å	1.66	1.65
	average r(Fe–N), Å	2.00	2.00

[a] Reliable ε value for **2a** could not be determined due to the contamination by **2b**.
[b] ε value determined from the purity calculated by Mössbauer.
.

Further investigations were then carried out to get insight into the difference between **2a** and **2b**. The first aspect considered was the possibility to have, in the two species, a distinct labile ligand occupying the available coordination site of **2** (Figure VI.3, left). Bearing in mind the reaction conditions used for the generation of such complex, that position could be plausibly occupied by a triflate anion, deriving from the [Fe^{II}(PyNMe$_3$)(CF$_3$SO$_3$)$_2$] precursor, an IO$_3^-$ or IO$_4^-$ anion, related to the Bu$_4$NIO$_4$, or a molecule of the acetonitrile solvent. To identify the labile ligand, **2** was generated employing [Fe^{II}(PyNMe$_3$)(CH$_3$CN)$_2$](SbF$_6$)$_2$ as a precursor or 2-*t*BuSO$_2$-C$_6$H$_4$IO as the oxidant. The use of [Fe^{II}(PyNMe$_3$)(CH$_3$CN)$_2$](SbF$_6$)$_2$ resulted in no changes in the outcome of the reaction: conversion from **2a** to **2b** was observed, so that the presence of a triflate anion in the labile coordination site of **2** was discarded (see Figure S10 in Annex 2). Similarly, the use of 2-*t*BuSO$_2$-C$_6$H$_4$IO did not prevent the **2a** to **2b** conversion, excluding the possible coordination of IO$_3^-$ or IO$_4^-$ anions (see Figure S11 in Annex 2). Thus, the sixth ligand in **2** is presumably a molecule of

acetonitrile. Assuming that the iron(IV) center in **2a** and **2b** has the same coordination environment, these species were assigned to two geometrical isomers having a different ligand moiety *trans* to the oxo group (Figure VI.3, right).
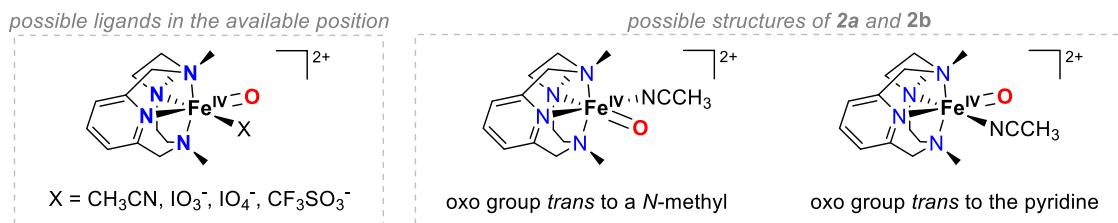

possible ligands in the available position   *possible structures of 2a and 2b*

X = CH$_3$CN, IO$_3^-$, IO$_4^-$, CF$_3$SO$_3^-$ oxo group *trans* to a *N*-methyl   oxo group *trans* to the pyridine

Figure VI.3. Ligands that could occupy the available coordination site (left) and geometrical isomers of **2** (right).

Then, paramagnetic ^{1}H-NMR spectroscopy was used to determine the relative orientation of the oxo ligand in **2a** and **2b**.[35, 36] Spectra of **2a** and **2b** were taken at -65 ºC in a 1:1 CD$_3$CN:CD$_2$Cl$_2$ solvent mixture. In the spectrum of **2b**, shown on the bottom of Figure VI.4, two sharp signals were observed at -25 ppm (1H) and 15 ppm (2H). Considering that the protons of the pyridine are the ones farther away from the paramagnetic iron(IV) center, these signals were attributed to its γ (1H) and β (2H) protons. Then, comparing the paramagnetic ^{1}H-NMR spectrum of **2b** with the one of the analogous species bearing the d_4-PyNMe$_3$ ligand, in which the benzylic hydrogens were replaced by deuterium atoms, the broad signals at -63 ppm (2H) and 46 ppm (2H) were assigned to the benzylic protons (see Figure S7 in Annex 2). Finally, the remaining signals at -39 ppm (2H), -147 ppm (2H) and -67 ppm (9H) were respectively attributed to the *N*-CH$_2$ and *N*-CH$_3$ protons. In the spectrum of **2a** signals corresponding to **2b** could be easily observed (Figure VI.4, top). Once the signals corresponding to **2b** were identified, β and γ protons of the pyridine in **2a** could be assigned to the sharp signals at -19 ppm (2H) and 12 ppm (1H), respectively.
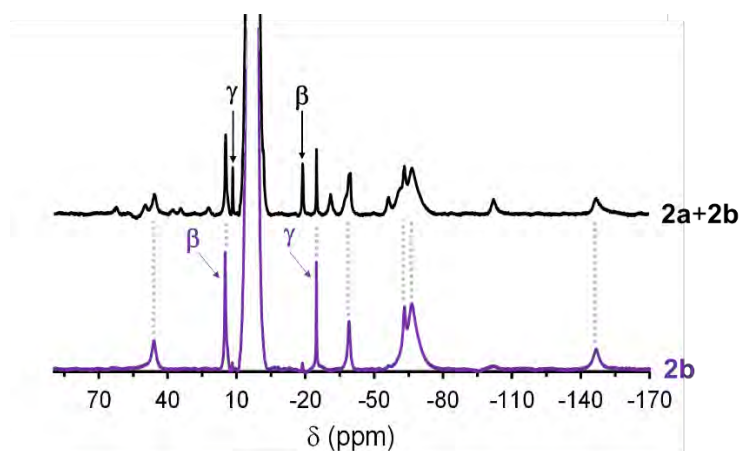
Figure VI.4. ^{1}H-NMR spectra recorded at -65 ºC, in a 1:1 CD$_3$CN:CD$_2$Cl$_2$ solvent mixture, for the **2a+2b** mixture (top) and the **2b** species (bottom). Figure adapted from ref [34].

Comparison of the two spectra highlighted that in **2a**, conversely to **2b**, the β protons of the pyridine were shielded, with respect to their chemical shift in the diamagnetic ligand (PyNMe₃: δ(H_β) = 7.09 ppm), whereas the γ one was unshielded (PyNMe₃: δ(H_γ) = 7.57 ppm). This different trend allowed to clarify the orientation of the pyridine moiety with respect to the oxo ligand in **2a** and **2b** (Figure VI.5, top). The shift pattern found for the β and γ protons in **2a** resembled the one observed in oxoiron(IV) species having the oxo ligand bound *cis* to a pyridine (Figure VI.5, middle). Instead, the one of **2b** suggested the oxo ligand to be bound *trans* to the pyridine (Figure VI.5, bottom).[36] Consequently, this analysis corroborates the existence of two different geometrical isomers and reveals that **2b** is more stable than **2a**, as further confirmed by DFT calculations (see Annex 2 for details).
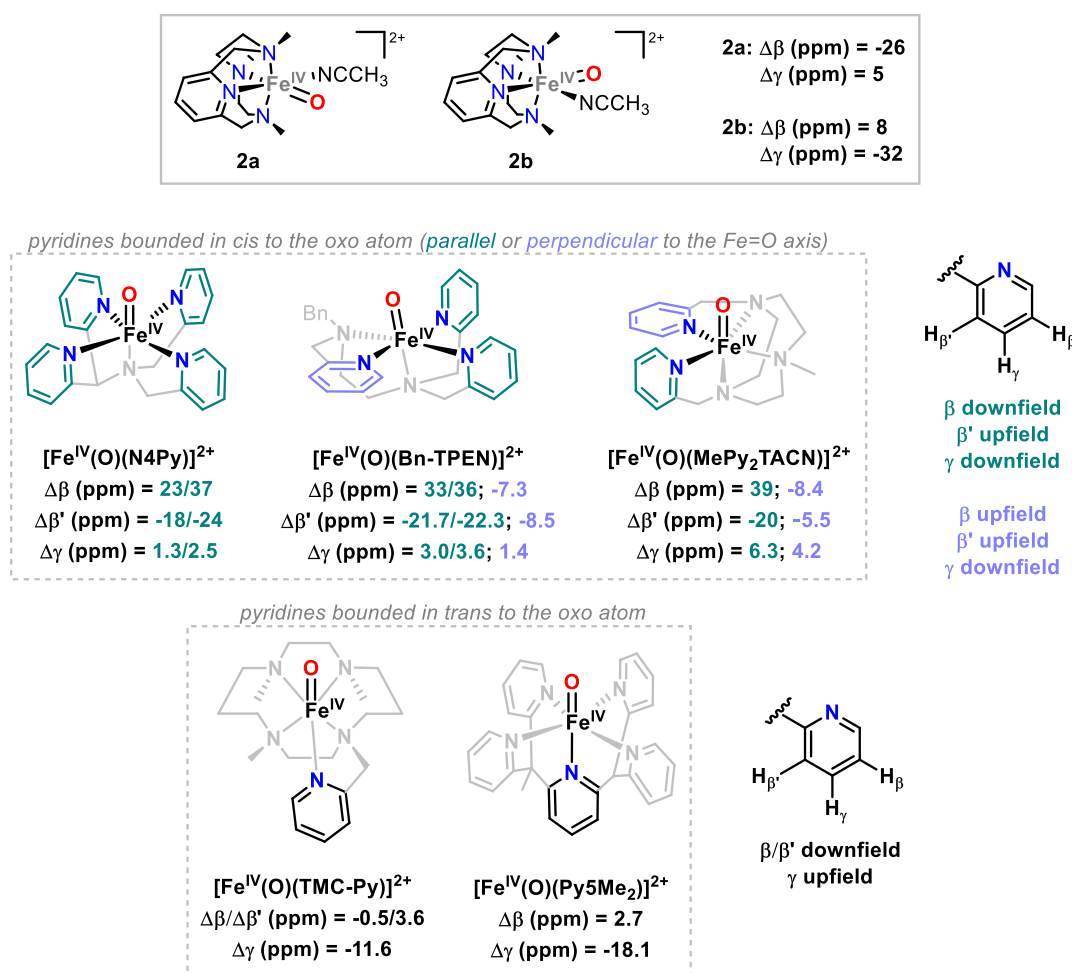
Figure VI.5. Paramagnetic shift observed for the pyridine protons in oxoiron(IV) species. Δx (ppm) corresponds to the shift of the considered hydrogen atom with respect to its chemical shift in the diamagnetic ligand.[36]

Once the nature and the geometry of **2a** and **2b** were defined, their reactivity was compared in the oxidation of 9,10-dihydroanthracene and thioanisole. Reaction rates were measured using UV-vis spectroscopy, by following the decay of the bands at 792 nm and 990 nm for **2a** and **2b**, respectively. As **2a** converts into **2b** at -40 ºC but this isomerization process is blocked at -60 ºC, oxidations were

performed using the latter temperature, in a 1:1 CH$_3$CN:CH$_2$Cl$_2$ solvent mixture, with the aim to study the reactivity of **2a**. In order to carry out the reaction with **2b** under the same conditions, **2b** was formed at -40 ºC and, upon isomerization, the solution was cooled down to -60 ºC. Addition of the target substrate to a solution of **2a** resulted in a double exponential decay, which can be rationalized considering that **2a** is formed in a mixture with **2b**. Instead, upon addition of the target substrate to a solution of **2b** a single exponential decay was obtained, according to the fact that this species is obtained in a pure form. Then, observed kinetic constants (k_{obs}) for the oxidation performed with **2b** were extracted from the fitting of its single exponential decay. In contrast, with **2a** a different approach was required. On one side, the k_{obs} value extracted in the reaction with **2b** could be fixed as one of the two exponential factors in the double exponential fitting function for the same reaction with **2a**, in order to get the k_{obs} value for the latter. On the other side, the k_{obs} value for **2a** could be extracted by fitting the single exponential curve obtained upon subtraction of the **2b** contribution to the **2a** decay at 792 nm (see figures S12 and S13 in Annex 2). Comparison of the second order reaction rates (k_2) found with the two isomers, calculated from the extracted k_{obs} values, highlighted differences in their relative reactivity. As shown in Table VI.3, in HAT processes **2a** (k_2 = 9.5 M^{-1}·s^{-1}) reacted faster than **2b** (k_2 = 0.53 M^{-1}·s^{-1}), whereas an opposite trend was observed in OAT processes (k_2 (**2a**) = 0.038 M^{-1}·s^{-1}; k_2 (**2b**) = 0.14 M^{-1}·s^{-1}).

Table VI.3. Rate constant values (k_2) for the reaction of **2a** and **2b** with 9,10-dihydroanthracene and thioanisole, measured at -60 ºC in a 1:1 CH$_3$CN:CH$_2$Cl$_2$ solvent mixture.

	substrate	k_2 (**2a**) (M^{-1}·s^{-1})	k_2 (**2b**) (M^{-1}·s^{-1})
HAT	9,10-dihydroanthracene	9.5	0.53
OAT	thioanisole	0.038	0.14

More extensive studies were then performed to get insight into the impact of the oxidation state of the metal center on the oxidative ability of high-valent oxoiron species. To that end, reactivity studies were performed at -40 ºC, as this temperature was previously used to measure the reactivity in HAT processes carried out by the oxoiron(V) analogue [Fe^V(O)(OAc)(PyNMe$_3$)]$^{2+}$ (**3**).[31] Thus, the reactivity of **3** was exclusively compared to that of **2b**, since at -40 ºC **2a** undergoes isomerization to **2b**. Apart from the fact that **2b** is obtained in its pure form, the *trans* orientation of the oxo ligand with respect to the pyridine moiety determined for this isomer is the same found in **3** by means of computational studies.[32]

The reactivity of **2b** in OAT processes was investigated using as substrates a series of *para*-substituted thioanisoles (R = OMe, Me, H, Cl, CN). The employment of electronically different substrates allowed to define the electronic character of **2b**, either electrophilic or nucleophilic, as the changes of the reaction rates in response to the electron density of the substrate used could be evaluated. Decay of the **2b** band at 990 nm upon addition of an excess of the target substrate was

followed by UV-vis spectroscopy (see Figure S14 in Annex 2). Observed kinetic constants (k_{obs}) were obtained by fitting the decay to a single exponential function, and the corresponding second order reaction rates (k_2) were then calculated. By plotting the logarithm of the k_2 values as a function of the Hammett parameters a straight line with a negative slope of -1.77 was found (see Figure S15 in Annex 2). Thus, according to literature precedents,[37-39] **2b** exhibited an electrophilic character, being the reaction faster as more electron-rich is the substrate. Moreover, during depletion of **2b** due to its reaction with the substrate the characteristic UV-vis band of the iron(II) precursor $[Fe^{II}(PyNMe_3)(CH_3CN)_2]^{2+}$ (**1**, λ_{max}= 380 nm) was gradually recovered (see Figure S16 in Annex 2). This was further confirmed by the presence of mass peaks corresponding to **1** in the high resolution mass spectra recorded at the end of the reaction (see Figure S17 in Annex 2). Additionally, gas chromatography analysis of the final reaction mixture showed the formation of sulfoxide as the oxidation product, confirming the occurrence of an OAT process.

Unfortunately, OAT reactivity of **2b** cannot be quantitatively compared with the one of **3**, as with the latter sulfide oxidation reactions were so fast that kinetic measurements were not feasible. Additionally, despite **3** was shown capable to oxidize alkenes,[33] **2b** was not competent to perform such transformation. Nevertheless, it could be qualitatively concluded that **3** was much more reactive than **2b** in OAT reaction and, as a consequence, it is a much more powerful electrophilic oxidant.

Subsequently, reactivity of **2b** in HAT processes was evaluated. Initial substrate screening, performed in a 1:1 $CH_3CN:CH_2Cl_2$ solvent mixture instead of CH_3CN for solubility reasons, showed that **2b** only reacts with substrates having weak C-H bonds (xanthene, 1,4-cyclohexadiene, 9,10-dihydroanthracene, fluorene). Addition of an excess of the target substrate to a **2b** solution caused the decay of its characteristic absorption band at 990 nm, which was followed by UV-vis spectroscopy (see Figure S18 in Annex 2). Kinetic traces showed an exponential decay, which fitting afforded the observed kinetic constants (k_{obs}). The latter were then plotted versus the substrate concentration (see Figure S20 in Annex 2) to obtain second order reaction rates (k_2) (Table VI.4). Moreover, at the end of the reaction the crude was analyzed by high resolution mass spectrometry and gas chromatography. It was found that as a consequence of the HAT from the substrate to the oxoiron(IV) species a hydroxoiron(III) species was formed (see Figure S19 in Annex 2), along with oxygenated products.

Table VI.4. Rate constant values (k_2) for the reaction of **2b** with hydrocarbons, measured at -40 ºC in a 1:1 $CH_3CN:CH_2Cl_2$ solvent mixture.

substrate	BDE (kcal·mol^{-1})	k_2 (**2b**) (M^{-1}·s^{-1})
xanthene	75.2	4.09
cyclohexadiene	76.0	2.81
9,10-dihydroanthracene	76.3	3.09
fluorene	82.2	0.06

To define if the HAT process was the rate determining step of the oxidation, Bell-Evans-Polanyi plot and kinetic isotope effect (KIE) were evaluated.

The Bell-Evans-Polanyi plot, in which the logarithm of the normalized k_2' values (k_2' = k_2/number of abstractable hydrogen atoms) was plotted as a function of the C-H bond dissociation energy (BDE), afforded a straight line with a negative slope of -0.25 mol·kcal^{-1} (see Figure S21 in Annex 2). Thus, reaction rates were affected by the strength of the target C-H bond, being them higher for less energetic C-H bonds, suggesting HAT to be the rate determining step of the oxidation. Additionally, oxidations of 9,10-dihydroanthracene-d_4 and xanthene-d_2 proceeded at significantly lower rates than the ones of 9,10-dihydroanthracene and xanthene (see Figure S23 in Annex 2), so that KIE values of 28 and 24 were found, respectively. These values, which are similar to the ones previously reported for other oxoiron(IV) species (examples shown in Table VI.5), further supported the HAT as the kinetically relevant step.

Table VI.5. KIE values for the reaction of **2b** with 9,10-dihydroanthracene and xanthene, measured at -40 ºC in a 1:1 CH$_3$CN:CH$_2$Cl$_2$ solvent mixture, and comparison with previously reported systems.

substrate	compound	T (ºC)	KIE
9,10-dihydroanthracene	[Fe^{IV}(O)(PyTACN)]$^{2+}$	-15	27[a]
	2b	-40	28
xanthene	[Fe^{IV}(O)(13-TCM)]$^{2+}$	-40	36[b]
	2b	-40	24

[a]Data from ref [38]. [b]Data from ref [40].

Since the KIE values determined for the HAT reactions of **2b** are higher than 20, well above the classic limit of 7, it can be concluded that reactions proceed with substantial tunneling contribution. Instead, the competitive oxidation of cyclohexane and its perdeuterated analogue performed by **3** has been described to proceed with a KIE value of 5. The observed difference could be understood assuming that in the HAT carried out with **2b** the two species that gave rise to the transition state are closer than with **3**. This hypothesis could be supported by comparing the activation entropy for the HAT processes carried out by **2b** and **3**. To this aim, Eyring analyses were performed for the oxidation of xanthene and cyclohexadiene by **2b**, in a temperature range from 273 to 233 K. Activation parameters obtained from the Eyring plot (see Figure S24 in Annex 2) are shown in Table VI.6, together with the ones previously reported for the oxidation of toluene and cyclohexane by **3**.[31] In the oxidation of xanthene and cyclohexadiene performed with **2b** activation entropy of -27.2 cal·K^{-1}·mol^{-1} and -25.6 cal·K^{-1}·mol^{-1} were found, respectively. Instead, for the reaction carried out with **3** less negative values were determined ($\Delta S^{\neq}$ = -19.6 cal·K^{-1}·mol^{-1} and -18.2 cal·K^{-1}·mol^{-1} for toluene and cyclohexane, respectively).[31] Albeit in both cases a bimolecular process takes place ($\Delta S^{\neq}$ < 0), with **2b** a more ordered and associated transition state had to be formed during the oxidation. As a

consequence, tunneling should be favored, with respect to **3**, due to the minor distance between the oxoiron(IV) and the substrate in the transition state. This explain the higher KIE values measured for **2b**.

Table VI.6. Activation parameters for C-H bond oxidation reaction by **2b** and **3**.

substrate	compound	BDE (kcal·mol^{-1})	$\Delta H^{\neq}$ (kcal·mol^{-1})	$\Delta S^{\neq}$ (cal·K^{-1}·mol^{-1})
xanthene	**2b**	75.2	6.4±0.6	-27.2±2.6
cyclohexadiene	**2b**	76.0	7.3±0.5	-25.6±2.1
toluene[a]	**3**	89.7	6.5±0.2	-19.6±1.2
cyclohexane[a]	**3**	99.5	8.8±0.7	-18.2±1.9

[a]Data from ref [31].

Finally, the rate constants measured with **2b** were compared with the ones previously reported with **3** under analogous reaction conditions.[31] The substrates used in the reactivity studies carried out with **3** contain stronger C-H bonds (BDE = 89.7-99.5 kcal·mol^{-1}) than those used to study the reactivity with **2b**. Unfortunately, a common substrate for the two species could not be found. Indeed, **2b** resulted unreactive towards the substrates employed with **3**. On the contrary, the significantly fast reaction of **3** with the substrates used with **2b** prevented the proper measurement of reaction rates. Then, rate constants for the reaction of **2b** with substrates containing strong C-H bonds were estimated by using the regression analysis from the Bell-Evans-Polanyi plot obtained for substrates containing weak C-H bonds (Figure VI.6). The same analysis was performed by **3**, but in this case using the correlation established for the experimental rates for substrates containing strong C-H bonds (Figure VI.6). From this correlation, rates for hypothetical reactions with the substrates containing weak C-H bonds could be estimated. It is worth mentioning that, according to literature precedents, it can be confidently assumed that in the reaction performed by **2b** linearity in the correlation between log(k_2') and C-H BDE is maintained in the considered range of BDEs (75-100 kcal·mol^{-1}).[38, 41-43] However, in the case of **3** a loss of linearity could not be excluded for the substrates with weaker C-H bonds of the series.[44-46]

Remarkably, as shown in Table VI.7, compound **3** is significantly a stronger oxidant than **2b**, being the difference in reactivity of four to five orders of magnitude. Considering that **3** has a carboxylate ligand in the labile site of coordination, that is expected to stabilize it, the reactivity of this compound could be even higher. Finally, the linearity observed in the Bell-Evans-Polanyi plot for the oxidation performed by **2b** and **3** allowed to exclude the presence of kinetic barriers associated to spin changes in these transformations.
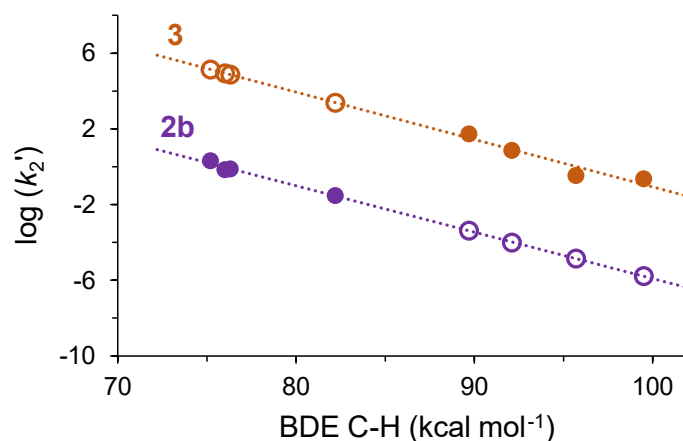
Figure VI.6. Correlation between log(k_2') and C-H BDEs for the reaction of **2b** (purple circle) and **3** (orange circle) with hydrocarbons at -40 ºC. Experimental data correspond to the filled circles, whereas extrapolated data obtained from the regression analysis are shown as empty circles. Figure adapted from ref [34].

Table VI.7. Experimental and extrapolated (shown in italic) normalized rate constant values (k_2') for the reaction of **2b** and **3** with hydrocarbons at -40 ºC.

substrate	BDE (kcal·mol^{-1})	k_2'(**2b**) (M^{-1}·s^{-1})	k_2'(**3**) (M^{-1}·s^{-1})	$\dfrac{k_2'(3)}{k_2'(2b)}$
xanthene	75.2	2.1±0.2	*1.4 x 10^5*	6.8 x 10^4
cyclohexadiene	76.0	0.70±0.05	*8.7 x 10^4*	1.2 x 10^5
9,10-dihydroanthracene	76.3	0.77±0.05	*7.4 x 10^4*	9.6 x 10^4
fluorene	82.2	0.030±0.004	*2.5 x 10^3*	8.3 x 10^4
toluene	89.7	*4.2 x 10^{-4}*	55±1[a]	1.3 x 10^5
tetrahydrofuran	92.1	*1.0 x 10^{-4}*	7.2±0.2 [a]	7.2 x 10^4
cyclooctane	95.7	*1.4 x 10^{-5}*	0.34±0.01 [a]	2.4 x 10^4
cyclohexane	99.5	*1.7 x 10^{-6}*	0.23±0.01 [a]	1.4 x 10^5

[a]Data from ref [31].

Overall, the collected data indicate that oxidations performed by **2b** present a higher activation energy with respect to the ones carried out by **3**. According to the Bell-Evans-Polanyi principle, the activation energy of the aforementioned transformations is proportional to the reaction enthalpy.[47] The latter is defined as the difference between the energy consumed to cleave a bond and the one liberated in the formation of a new bond. In the target transformations, the C-H bond of the substrate is cleaved, thus a carbon centered radical (C$^{\bullet}$) is generated. The hydrogen is transferred to the oxo moiety, so that the oxoiron (Fe^{n+}=O) species is converted into a hydroxide bound iron species (Fe$^{(n-1)+}$-O-H) through the formation of an O-H bond. Therefore, the reaction enthalpy for a HAT process can be expressed as shown in equation 1. Taking into account that the reaction of **2b** with cyclohexadiene and the one of **3** with cyclooctane have comparable reaction rates (see Table VI.7),

it could be assumed that the activation energy for these two reactions are similar. As a consequence, in view of the linear correlation found in the Bell-Evans-Polanyi plot, the reaction enthalpy of the two reactions should be approximately the same (respectively left and right site in equation 2). Then, equation 3 could be derived and the difference between the BDE of the O-H bond formed upon HAT by **3** ($Fe^{IV}O$-H) and **2b** ($Fe^{III}O$-H) can be estimated to be ~ 20 $kcal \cdot mol^{-1}$. Hence, the much higher reactivity of **3** with respect to **2b** can be ascribed to the greater thermodynamic driving force associated with the formation of a stronger O-H bond upon HAT from the substrate. The BDE of the $Fe^{III}O$-H bond in iron complexes bearing N4Py and H_3buea ligands has been estimated to be 78 $kcal \cdot mol^{-1}$ and 87 $kcal \cdot mol^{-1}$, respectively.[48, 49] Consequently, the BDE of the $Fe^{IV}O$-H can be estimated to be ~ 100 $kcal \cdot mol^{-1}$. This value is in agreement with the one previously proposed for **3**, estimated by interpolating the reaction rates found in the oxidation of toluene by **3** with the values determined for a series of oxidants differing in their respective O-H bonds.[31]

$$Fe^{n+}=O + C\text{-}H \rightarrow Fe^{(n-1)+}\text{-}O\text{-}H + C^{\bullet}$$
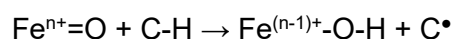
$$\Delta H^O = BDE_{C-H} - BDE_{FeO-H} \qquad \text{(equation 1)}$$

$$BDE_{cyclohexadiene} - BDE_{Fe(III)O-H} = BDE_{cyclooctane} - BDE_{Fe(IV)O-H} \qquad \text{(equation 2)}$$

$$BDE_{Fe(IV)O-H} - BDE_{Fe(III)O-H} = BDE_{cyclooctane} - BDE_{cyclohexadiene} = 19.7 \frac{kcal}{mol} \qquad \text{(equation 3)}$$

Besides the impact of the oxidation state of the metal center in **2b** and **3** on the reactivity, the possibility to have a different selectivity outcome was also considered.

To evaluate the oxidation chemoselectivity, cyclohexene was taken as model susbtrate.[50] This substrate possesses a C=C bond and a weak allylic C-H bond. Then, oxidation could afford either the corresponding epoxide, through OAT from the oxoiron species to the C=C bond, or hydroxylated products, via HAT from the allylic C-H bond to the oxoiron compound. Oxidation of cyclohexene was carried out at -40 ºC under aerobic conditions using **2b** and **3**. Analysis of the reaction crude revealed the formation of different oxidation products with the two species, as shown in Scheme VI.12.

In the reaction performed with **2b** the allylic ketone was obtained as the largely dominant product in 31% yield, along with 5% yield of the allylic alcohol. When the same oxidation with **2b** was performed under a nitrogen atmosphere, the allylic alcohol became the main product (28% yield) and the corresponding ketone was obtained in 5% yield. In sharp contrast, oxidation performed with **3** gave the epoxide as the major product in 60% yield, whereas the two allylic products were formed in only 6% combined yield.

2b:	31%^{a}	5%^{a}	<1^a
	^{18}O: 82%^{b}		
3:	3%^{a}	3%^{a}	60%^{a}
		^{18}O: 0%^{b}	
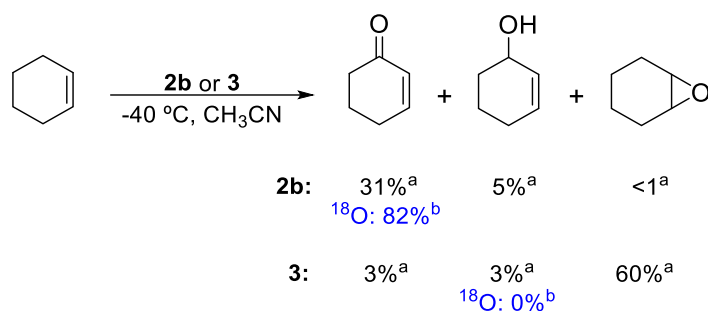
^{a}yield with respect to the iron(II) content.
^{b}% ^{18}O incorporation under ^{18}O$_2$ atmosphere.

Scheme VI.12. Oxidation of cyclohexene by **2b** and **3**. Scheme adapted from ref [34].

These results higlighted that, according to literature precedents,[50] **2b** resulted almost unreactive toward alkenes and instead it engages in HAT with the allylic C-H bond. Additionally, oxidation of cyclohexene by **2b** performed under ^{18}O$_2$ atmosphere revealed an 82% of ^{18}O incorporation in the ketone product (see Figure S25 in Annex 2). This result suggests that the alkyl radical generated upon HAT is a long-lived radical, denoting a scarce capability of Fe^{III}-OH to rebound with it. The alkyl radical can then escape from the cage and is trapped by molecular oxygen. On the contrary, in the labeling experiment performed with **3** no incorporation of ^{18}O was found into the epoxide product (see Figure S25 in Annex 2), in line with a concerted OAT. Interestingly, the outcome of the labeling experiments in the oxidation performed by **2b** suggests that the oxidation state of the metal center affects the lifetime of the alkyl radical generated upon the HAT process. Indeed, opposite to **2b**, when **3** undergoes HAT a short-lived alkyl radical is formed. This conclusion is based on the stereospecific nature of the hydroxylation reactions performed by **3**.[31] Consistent with this interpretation, in the oxidation of cyclohexane by **3**, performed under ^{18}O$_2$ atmosphere, cyclohexanol was obtained as the main product and no incorporation of ^{18}O was observed (see Figure S26 in Annex 2). Thus, upon HAT from cyclohexane to **3** a fast hydroxyl rebound between the Fe^{IV}-OH and the alkyl radical must occur, preventing the diffusion of the latter and its subsequent trapping by molecular oxygen (Scheme VI.13). As a consequence, only **3** is capable to engage in hydroxylation reactions via short-lived carbon centered radicals.
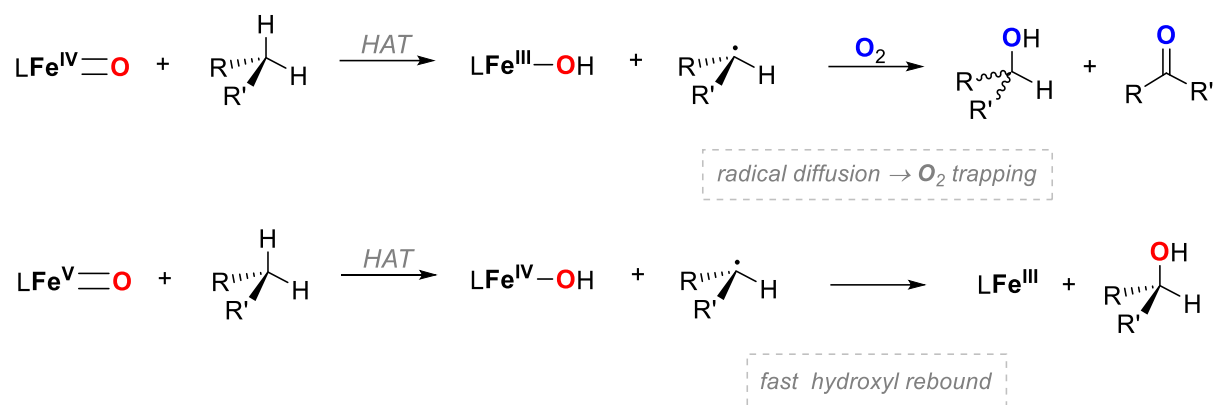
Scheme VI.13. Outcome of C-H bond hydroxylation performed with oxoiron(IV) and oxoiron(V) species. Scheme adapted from ref [34].

PAGES TEMPORARILY EXTRACTED FROM THE THESIS
UNTIL THE ARTICLE WILL BE PUBLISHED IN A JOURNAL

V. Dantignana, J. Serrano-Plana, Á. Martínez Camarena, E. García-España, A. Company, M. Costas. "Ligand effects on the reactivity of oxoiron(IV) species supported by electronically tuned azamacrocycles". (2020). Manuscript in preparation.

VI.4 References

(1)   Genovino, J., D. Sames, L. G. Hamann B. B. Touré, Accessing Drug Metabolites via Transition-Metal Catalyzed C−H Oxidation: The Liver as Synthetic Inspiration. *Angew. Chem. Int. Ed.* **2016,** *55*, 14218-14238.

(2)   Newhouse, T. P. S. Baran, If C−H Bonds Could Talk: Selective C−H Bond Oxidation. *Angew. Chem. Int. Ed.* **2011,** *50*, 3362-3374.

(3)   Olivo, G., O. Cussó, M. Borrell M. Costas, Oxidation of alkane and alkene moieties with biologically inspired nonheme iron catalysts and hydrogen peroxide: from free radicals to stereoselective transformations. *J. Biol. Inorg. Chem.* **2017,** *22*, 425-452.

(4)   White, M. C. J. Zhao, Aliphatic C–H Oxidations for Late-Stage Functionalization. *J. Am. Chem. Soc.* **2018,** *140*, 13988-14009.

(5)   Salamone, M. M. Bietti, Reaction Pathways of Alkoxyl Radicals. The Role of Solvent Effects on C–C Bond Fragmentation and Hydrogen Atom Transfer Reactions. *Synlett* **2014,** *25*, 1803-1816.

(6)   Gaster, E., S. Kozuch D. Pappo, Selective Aerobic Oxidation of Methylarenes to Benzaldehydes Catalyzed by N-Hydroxyphthalimide and Cobalt(II) Acetate in Hexafluoropropan-2-ol. *Angew. Chem. Int. Ed.* **2017,** *56*, 5912-5915.

(7)   Gómez, L., I. Garcia-Bosch, A. Company, J. Benet-Buchholz, A. Polo, X. Sala, X. Ribas M. Costas, Stereospecific C−H Oxidation with H_2O_2 Catalyzed by a Chemically Robust Site-Isolated Iron Catalyst. *Angew. Chem. Int. Ed.* **2009,** *48*, 5720-5723.

(8)   Ottenbacher, R. V., D. G. Samsonenko, E. P. Talsi K. P. Bryliakov, Highly Efficient, Regioselective, and Stereospecific Oxidation of Aliphatic C–H Groups with H2O2, Catalyzed by Aminopyridine Manganese Complexes. *Org. Lett.* **2012,** *14*, 4310-4313.

(9)   Salamone, M. M. Bietti, Tuning Reactivity and Selectivity in Hydrogen Atom Transfer from Aliphatic C–H Bonds to Alkoxyl Radicals: Role of Structural and Medium Effects. *Acc. Chem. Res.* **2015,** *48*, 2895-2903.

(10)   Abraham, M. H., P. L. Grellier, D. V. Prior, P. P. Duce, J. J. Morris P. J. Taylor, Hydrogen bonding. Part 7. A scale of solute hydrogen-bond acidity based on log K values for complexation in tetrachloromethane. *J. Chem. Soc., Perkin Trans. 2* **1989**, 699-711.

(11)   Ottenbacher, R. V., E. P. Talsi K. P. Bryliakov, Mechanism of Selective C–H Hydroxylation Mediated by Manganese Aminopyridine Enzyme Models. *ACS Catal.* **2015,** *5*, 39-44.

(12)   Chen, K. L. Que, Stereospecific Alkane Hydroxylation by Non-Heme Iron Catalysts: Mechanistic Evidence for an Fe^VO Active Species. *J. Am. Chem. Soc.* **2001,** *123*, 6327-6337.

(13)   Chen, M. S. M. C. White, Combined Effects on Selectivity in Fe-Catalyzed Methylene Oxidation. *Science* **2010,** *327*, 566-571.

(14)   Shen, D., C. Miao, S. Wang, C. Xia W. Sun, Efficient Benzylic and Aliphatic C–H Oxidation with Selectivity for Methylenic Sites Catalyzed by a Bioinspired Manganese Complex. *Org. Lett.* **2014,** *16*, 1108-1111.

(15)   Milan, M., M. Bietti M. Costas, Highly Enantioselective Oxidation of Nonactivated Aliphatic C–H Bonds with Hydrogen Peroxide Catalyzed by Manganese Complexes. *ACS Cent. Sci.* **2017,** *3*, 196-204.

(16)   Chen, K., A. Eschenmoser P. S. Baran, Strain Release in C-H Bond Activation? *Angew. Chem. Int. Ed.* **2009,** *48*, 9705-9708.

(17)   Salamone, M., V. B. Ortega M. Bietti, Enhanced Reactivity in Hydrogen Atom Transfer from Tertiary Sites of Cyclohexanes and Decalins via Strain Release: Equatorial C–H Activation vs Axial C–H Deactivation. *J. Org. Chem.* **2015,** *80*, 4710-4715.

(18)   Gómez, L., M. Canta, D. Font, I. Prat, X. Ribas M. Costas, Regioselective Oxidation of Nonactivated Alkyl C–H Groups Using Highly Structured Non-Heme Iron Catalysts. *J. Org. Chem.* **2013,** *78*, 1421-1433.

(19)   Dantignana, V., M. Milan, O. Cussó, A. Company, M. Bietti M. Costas, Chemoselective Aliphatic C–H Bond Oxidation Enabled by Polarity Reversal. *ACS Cent. Sci.* **2017,** *3*, 1350-1358.

(20)   Milan, M., G. Carboni, M. Salamone, M. Costas M. Bietti, Tuning Selectivity in Aliphatic C–H Bond Oxidation of N-Alkylamides and Phthalimides Catalyzed by Manganese Complexes. *ACS Catal.* **2017,** *7*, 5903-5911.

(21)   Nanjo, T., E. C. de Lucca M. C. White, Remote, Late-Stage Oxidation of Aliphatic C–H Bonds in Amide-Containing Molecules. *J. Am. Chem. Soc.* **2017,** *139*, 14586-14591.

(22)   Lee, M. M. S. Sanford, Platinum-Catalyzed, Terminal-Selective C(sp$_3$)–H Oxidation of Aliphatic Amines. *J. Am. Chem. Soc.* **2015,** *137*, 12796-12799.

(23)   Huang, X. J. T. Groves, Oxygen Activation and Radical Transformations in Heme Proteins and Metalloporphyrins. *Chem. Rev.* **2018,** *118*, 2491-2553.

(24)   Kal, S. L. Que, Dioxygen activation by nonheme iron enzymes with the 2-His-1-carboxylate facial triad that generate high-valent oxoiron oxidants. *J. Biol. Inorg. Chem.* **2017,** *22*, 339-365.

(25)   McDonald, A. R. L. Que, High-valent nonheme iron-oxo complexes: Synthesis, structure, and spectroscopy. *Coord. Chem. Rev.* **2013,** *257*, 414-428.

(26)   Klein, J.E. and Que, L., Jr. (2016). Biomimetic High-Valent Mononuclear Nonheme Iron-Oxo Chemistry. Encyclopedia of Inorganic and Bioinorganic Chemistry, R.A. Scott (Ed.) Wiley**:** 1-22.

(27)   Kal, S., S. Xu L. Que Jr., Bio-inspired Nonheme Iron Oxidation Catalysis: Involvement of Oxoiron(V) Oxidants in Cleaving Strong C−H Bonds. *Angew. Chem. Int. Ed.* **2020,** *59*, 7332-7349.

(28)   Lyakin, O. Y., K. P. Bryliakov E. P. Talsi, Non-heme oxoiron(V) intermediates in chemo-, regio- and stereoselective oxidation of organic substrates. *Coord. Chem. Rev.* **2019,** *384*, 126-139.

(29)   Pattanayak, S., A. J. Jasniewski, A. Rana, A. Draksharapu, K. K. Singh, A. Weitz, M. Hendrich, L. Que, A. Dey S. Sen Gupta, Spectroscopic and Reactivity Comparisons of a Pair of bTAML Complexes with Fe^V=O and Fe^{IV}=O Units. *Inorg. Chem.* **2017,** *56*, 6352-6361.

(30)   Oszajca, M., A. Franke, A. Drzewiecka-Matuszek, M. Brindell, G. Stochel R. van Eldik, Temperature and Pressure Effects on C–H Abstraction Reactions Involving Compound I and II Mimics in Aqueous Solution. *Inorg. Chem.* **2014,** *53*, 2848-2857.

(31)   Serrano-Plana, J., W. N. Oloo, L. Acosta-Rueda, K. K. Meier, B. Verdejo, E. García-España, M. G. Basallote, E. Münck, L. Que, A. Company M. Costas, Trapping a Highly Reactive Nonheme Iron Intermediate That Oxygenates Strong C—H Bonds with Stereoretention. *J. Am. Chem. Soc.* **2015,** *137*, 15833-15842.

(32)   Fan, R., J. Serrano-Plana, W. N. Oloo, A. Draksharapu, E. Delgado-Pinar, A. Company, V. Martin-Diaconescu, M. Borrell, J. Lloret-Fillol, E. García-España, Y. Guo, E. L. Bominaar, L. Que, M. Costas E. Münck, Spectroscopic and DFT Characterization of a Highly Reactive Nonheme Fe^V–Oxo Intermediate. *J. Am. Chem. Soc.* **2018,** *140*, 3916-3928.

(33)   Serrano-Plana, J., A. Aguinaco, R. Belda, E. García-España, M. G. Basallote, A. Company M. Costas, Exceedingly Fast Oxygen Atom Transfer to Olefins via a Catalytically Competent Nonheme Iron Species. *Angew. Chem. Int. Ed.* **2016,** *55*, 6310-6314.

(34)   Dantignana, V., J. Serrano-Plana, A. Draksharapu, C. Magallón, S. Banerjee, R. Fan, I. Gamba, Y. Guo, L. Que, M. Costas A. Company, Spectroscopic and Reactivity Comparisons between Nonheme Oxoiron(IV) and Oxoiron(V) Species Bearing the Same Ancillary Ligand. *J. Am. Chem. Soc.* **2019,** *141*, 15078-15091.

(35)   Klinker, E. J., J. Kaizer, W. W. Brennessel, N. L. Woodrum, C. J. Cramer L. Que Jr., Structures of Nonheme Oxoiron(IV) Complexes from X-ray Crystallography, NMR Spectroscopy, and DFT Calculations. *Angew. Chem. Int. Ed.* **2005,** *44*, 3690-3694.

(36)   Rasheed, W., R. Fan, C. S. Abelson, P. O. Peterson, W.-M. Ching, Y. Guo L. Que, Structural implications of the paramagnetically shifted NMR signals from pyridine H atoms on synthetic nonheme Fe^{IV}=O complexes. *J. Biol. Inorg. Chem.* **2019,** *24*, 533-545.

(37)   Park, M. J., J. Lee, Y. Suh, J. Kim W. Nam, Reactivities of Mononuclear Non-Heme Iron Intermediates Including Evidence that Iron(III)−Hydroperoxo Species Is a Sluggish Oxidant. *J. Am. Chem. Soc.* **2006,** *128*, 2630-2634.

(38)   Company, A., I. Prat, J. R. Frisch, D. R. Mas-Ballesté, M. Güell, G. Juhász, X. Ribas, D. E. Münck, J. M. Luis, L. Que Jr. M. Costas, Modeling the *cis*-Oxo-Labile Binding Site Motif of Non-Heme Iron Oxygenases: Water Exchange and Oxidation Reactivity of a Non-Heme Iron(IV)-Oxo Compound Bearing a Tripodal Tetradentate Ligand. *Chem. Eur. J.* **2011,** *17*, 1622-1634.

(39)   Nam, W., High-Valent Iron(IV)–Oxo Complexes of Heme and Non-Heme Ligands in Oxygenation Reactions. *Acc. Chem. Res.* **2007,** *40*, 522-531.

(40)   Hong, S., H. So, H. Yoon, K.-B. Cho, Y.-M. Lee, S. Fukuzumi W. Nam, Reactivity comparison of high-valent iron(IV)-oxo complexes bearing N-tetramethylated cyclam ligands with different ring size. *Dalton Trans.* **2013,** *42*, 7842-7845.

(41)   Ghosh, M., K. K. Singh, C. Panda, A. Weitz, M. P. Hendrich, T. J. Collins, B. B. Dhar S. Sen Gupta, Formation of a Room Temperature Stable Fe^{V}(O) Complex: Reactivity Toward Unactivated C–H Bonds. *J. Am. Chem. Soc.* **2014,** *136*, 9524-9527.

(42)   Kaizer, J., E. J. Klinker, N. Y. Oh, J.-U. Rohde, W. J. Song, A. Stubna, J. Kim, E. Münck, W. Nam L. Que, Nonheme Fe^{IV}O Complexes That Can Oxidize the C−H Bonds of Cyclohexane at Room Temperature. *J. Am. Chem. Soc.* **2004,** *126*, 472-473.

(43)   Biswas, A. N., M. Puri, K. K. Meier, W. N. Oloo, G. T. Rohde, E. L. Bominaar, E. Münck L. Que, Modeling TauD-J: A High-Spin Nonheme Oxoiron(IV) Complex with High Reactivity toward C–H Bonds. *J. Am. Chem. Soc.* **2015,** *137*, 2428-2431.

(44)   Wang, X., S. Peter, M. Kinne, M. Hofrichter J. T. Groves, Detection and Kinetic Characterization of a Highly Reactive Heme–Thiolate Peroxygenase Compound I. *J. Am. Chem. Soc.* **2012,** *134*, 12897-12900.

(45)   Tanko, J. M., R. Friedline, N. K. Suleman N. Castagnoli, *tert*-Butoxyl as a Model for Radicals in Biological Systems: Caveat Emptor. *J. Am. Chem. Soc.* **2001,** *123*, 5808-5809.

(46)   Finn, M., R. Friedline, N. K. Suleman, C. J. Wohl J. M. Tanko, Chemistry of the *t*-Butoxyl Radical: Evidence that Most Hydrogen Abstractions from Carbon are Entropy-Controlled. *J. Am. Chem. Soc.* **2004,** *126*, 7578-7584.

(47)   Evans, M. G. M. Polanyi, Inertia and driving force of chemical reactions. *Trans. Faraday Soc.* **1938,** *34*, 11-24.

(48)   Wang, D., M. Zhang, P. Bühlmann L. Que, Redox Potential and C−H Bond Cleaving Properties of a Nonheme Fe^{IV}=O Complex in Aqueous Solution. *J. Am. Chem. Soc.* **2010,** *132*, 7638-7644.

(49)   Usharani, D., D. C. Lacy, A. S. Borovik S. Shaik, Dichotomous Hydrogen Atom Transfer vs Proton-Coupled Electron Transfer During Activation of X–H Bonds (X = C, N, O) by Nonheme Iron–Oxo Complexes of Variable Basicity. *J. Am. Chem. Soc.* **2013,** *135*, 17090-17104.

(50)   Oloo, W. N., Y. Feng, S. Iyer, S. Parmelee, G. Xue L. Que, Cyclohexene as a substrate probe for the nature of the high-valent iron-oxo oxidant in Fe(TPA)-catalyzed oxidations. *New J. Chem.* **2013,** *37*, 3411-3415.

(51)   Guo, M., T. Corona, K. Ray W. Nam, Heme and Nonheme High-Valent Iron and Manganese Oxo Cores in Biological and Abiological Oxidation Reactions. *ACS Cent. Sci.* **2019,** *5*, 13-28.

(52)   Wang, D., K. Ray, M. J. Collins, E. R. Farquhar, J. R. Frisch, L. Gómez, T. A. Jackson, M. Kerscher, A. Waleska, P. Comba, M. Costas L. Que, Nonheme oxoiron(IV) complexes of pentadentate N5 ligands: spectroscopy, electrochemistry, and oxidative reactivity. *Chem. Sci.* **2013,** *4*, 282-291.

(53)   Hong, S., Y.-M. Lee, K.-B. Cho, K. Sundaravel, J. Cho, M. J. Kim, W. Shin W. Nam, Ligand Topology Effect on the Reactivity of a Mononuclear Nonheme Iron(IV)-Oxo Complex in Oxygenation Reactions. *J. Am. Chem. Soc.* **2011,** *133*, 11876-11879.

(54)   England, J., J. O. Bigelow, K. M. Van Heuvelen, E. R. Farquhar, M. Martinho, K. K. Meier, J. R. Frisch, E. Münck L. Que, An ultra-stable oxoiron(IV) complex and its blue conjugate base. *Chem. Sci.* **2014,** *5*, 1204-1215.

(55)   Sastri, C. V., J. Lee, K. Oh, Y. J. Lee, J. Lee, T. A. Jackson, K. Ray, H. Hirao, W. Shin, J. A. Halfen, J. Kim, L. Que, S. Shaik W. Nam, Axial ligand tuning of a nonheme iron(IV)–oxo unit for hydrogen atom abstraction. *Proc. Natl. Acad. Sci. USA* **2007,** *104*, 19181-19186.

(56)   Planas, O., M. Clémancey, J.-M. Latour, A. Company M. Costas, Structural modeling of iron halogenases: synthesis and reactivity of halide-iron(IV)-oxo compounds. *Chem. Commun.* **2014,** *50*, 10887-10890.

(57)   Engelmann, X., I. Monte-Pérez K. Ray, Oxidation Reactions with Bioinspired Mononuclear Non-Heme Metal–Oxo Complexes. *Angew. Chem. Int. Ed.* **2016,** *55*, 7632-7649.

(58)   Zhou, Y., X. Shan, R. Mas-Ballesté, M. R. Bukowski, A. Stubna, M. Chakrabarti, L. Slominski, J. A. Halfen, E. Münck L. Que Jr, Contrasting cis and trans Effects on the Reactivity of Nonheme Oxoiron(IV) Complexes. *Angew. Chem. Int. Ed.* **2008,** *47*, 1896-1899.

(59)   Mitra, M., H. Nimir, S. Demeshko, S. S. Bhat, S. O. Malinkin, M. Haukka, J. Lloret-Fillol, G. C. Lisensky, F. Meyer, A. A. Shteinman, W. R. Browne, D. A. Hrovat, M. G. Richmond, M. Costas E. Nordlander, Nonheme Fe(IV) Oxo Complexes of Two New Pentadentate Ligands and Their Hydrogen-Atom and Oxygen-Atom Transfer Reactions. *Inorg. Chem.* **2015,** *54*, 7152-7164.

(60)   Widger, L. R., C. G. Davies, T. Yang, M. A. Siegler, O. Troeppner, G. N. L. Jameson, I. Ivanović-Burmazović D. P. Goldberg, Dramatically Accelerated Selective Oxygen-Atom Transfer by a Nonheme Iron(IV)-Oxo Complex: Tuning of the First and Second Coordination Spheres. *J. Am. Chem. Soc.* **2014,** *136*, 2699-2702.

(61)   Diebold, A. K. S. Hagen, Iron(II) Polyamine Chemistry: Variation of Spin State and Coordination Number in Solid State and Solution with Iron(II) Tris(2-pyridylmethyl)amine Complexes. *Inorg. Chem.* **1998,** *37*, 215-223.

(62)   Britovsek, G. J. P., J. England A. J. P. White, Non-heme Iron(II) Complexes Containing Tripodal Tetradentate Nitrogen Ligands and Their Application in Alkane Oxidation Catalysis. *Inorg. Chem.* **2005,** *44*, 8125-8134.

(63)   Prat, I., A. Company, T. Corona, T. Parella, X. Ribas M. Costas, Assessing the Impact of Electronic and Steric Tuning of the Ligand in the Spin State and Catalytic Oxidation Ability of the Fe^{II}(Pytacn) Family of Complexes. *Inorg. Chem.* **2013,** *52*, 9229-9244.

(64)   Prat, I., A. Company, V. Postils, X. Ribas, L. Que Jr, J. M. Luis M. Costas, The Mechanism of Stereospecific C−H Oxidation by Fe(Pytacn) Complexes: Bioinspired Non-Heme Iron Catalysts Containing cis-Labile Exchangeable Sites. *Chem. Eur. J.* **2013,** *19*, 6724-6738.

(65)   Warren, J. J., T. A. Tronic J. M. Mayer, Thermochemistry of Proton-Coupled Electron Transfer Reagents and its Implications. *Chem. Rev.* **2010,** *110*, 6961-7001.

Chapter VII

General conclusions

Bioinspired complexes have become valuable alternatives to the traditionally used harsh reagents for demanding oxidation reaction, showing the advantage of employing mild and environmentally friendly conditions. In spite of the achievements that have been reached in the field, there are still important issues to address to fully develop the potentiality of such approach. On one side, accomplishment of highly selective C-H bond oxidation represents a longstanding goal, which is limited by the occurrence of overoxidation processes as well as by the presence of multiple C-H bonds with comparable reactivity. On the other side, a deeper understanding of active oxidant properties is desirable, as it is important for the development of efficient systems. In this view, in this thesis we carry out both catalytic and mechanistic studies.

In Chapter III, catalytic hydroxylation of aliphatic C-H bonds has been investigated. Particularly, the effect of using fluorinated alcohol solvents as reaction media on chemo-, enantio- and regioselectivity have been explored, using a series of bioinspired iron and manganese complexes as catalysts. Interestingly, oxidation of alkane substrates highlighted that fluorinated alcohol solvents prevent overoxidation of the first formed alcohol product, by protection of the hydroxyl group attained through the establishment of hydrogen bonds. Consequently, outstanding degrees of chemoselectivity for the first formed product could be achieved. The polarity reversal observed in such transformations, which is responsible for the selectivity outcome, has opened the path to the investigation of substrates bearing polar groups. Indeed, despite the latter are susceptible of oxidation under standard conditions, it was envisioned that in fluorinated alcohol solvents this functionalities could be protected, by establishment of hydrogen bonds, in analogy to what was observed in alkane oxidation reactions, where the first formed alcohol product was preserved. Thus, alcohols, ethers, amides and amines were submitted to the optimized reaction conditions. Remarkably, in line with our expectation, in all the cases oxidation of the polar group was significantly suppressed and in addition excellent degrees of regioselectivity towards the most remote C-H bonds from the functional group were found. Additionally, the selectivity outcome could be a priori predicted, both in terms of chemo- and regioselectivity, so that the developed protocol could be eventually helpfully employed in new synthetic strategies.

In Chapter IV, oxoiron(IV) and oxoiron(V) species bearing the same PyNMe$_3$ ligand were compared. This investigation permitted to directly evaluate the influence of the iron oxidation state on both reactivity and selectivity exhibited by high-valent oxoiron compounds. To this end, synthesis and spectroscopic characterization of $[Fe^{IV}(O)(PyNMe_3)(CH_3CN)]^{2+}$ were carried out. Then, reactivity studies were performed considering both HAT and OAT processes. Comparison of oxoiron(IV) and oxoiron(V) reactivity in OAT processes revealed the oxoiron(V) to be a more electrophilic oxidant, with respect to the oxoiron(IV). Additionally, detailed analysis of their reactivity in HAT processes allowed to figure out important differences among the two species. The oxoiron(V) species reacted

with hydrocarbons four to five order of magnitude faster than the oxoiron(IV) one. This difference was understood on the basis of ground thermodynamics, as the O-H bond formed upon HAT from the substrate to the oxoiron species is ~ 20 kcal·mol^{-1} stronger in the reaction performed with the oxoiron(V) compound. Additionally, while upon HAT long-lived alkyl radicals are generated in the reaction performed by the oxoiron(IV) species, as ascertained by labelling experiments, with the oxoiron(V) compound these radicals are short-lived and rapidly recombine with the hydroxo intermediate, in a rebound step that lead to the final oxidation products. Consequently, only the oxoiron(V) species is capable to afford stereospecific hydroxylation, as in the oxidation performed with the oxoiron(IV) counterpart the diffusion of the alkyl radicals generated upon the first step of the reaction ruled out that possibility. Then, it was highlighted that the oxidation state of the iron center in high-valent oxoiron species affected both their oxidative ability and the rate of the hydroxyl rebound.

In Chapter V, a family of iron(II) complexes bearing electronically tuned ^{R}PyNMe$_3$ (R = OCH$_3$, H, Br, Cl, CO$_2$CH$_3$) ligands were synthetized and characterized. Then, generation of the related oxoiron(IV) species was carried out, with the aim to evaluate the impact of electronic effects on the reactivity of such compounds. Remarkably, with all the oxoiron(IV) compounds the formation of two geometrical isomers, which differ in the relative orientation of the terminal oxo group with respect to the pyridine moiety of the ligand, could be experimentally observed. Reactivity of both isomers was studied in the oxidation of 9,10-dihydroanthracene (HAT) and thioanisole (OAT). Comparison of reaction rates observed for a single isomer, as a function of the different electronic density of the ligand, highlighted the latter to be not a relevant aspect in defining the reactivity of the active oxidant. Indeed, the found changes were minimal in both HAT and OAT transformations. Most notably, comparison of the reaction rates measured for the two isomers bearing the same ^{R}PyNMe$_3$ ligand revealed that the relative position of the oxo ligand and its *cis*-labile site in the oxoiron(IV) species affected its reactivity, and this effect is substantially larger than effects exerted by modifications of the electronic character of the pyridine ligand. Particularly, the isomer having the pyridine moiety in *trans* to the oxo ligand was more reactive in OAT processes, whereas the one having the pyridine moiety in *trans* to an aliphatic amine moiety was more reactive in HAT processes. Therefore, an unprecedented relative reactivity was found for the two isomers, which is dependent by the nature of the studied oxidation.

Annex

Supporting information

Annex 1. Supporting Information Chapter III

Chemoselective aliphatic C-H bond oxidation enabled by polarity reversal

V. Dantignana,[‡] M. Milan,[‡] O. Cussó, A. Company,* M. Bietti,* Miquel Costas*

[‡]both authors contributed equally to this work

Table of contents

1. Experimental Section

1.1. Materials

Reagents and solvents used were of commercially available reagent quality unless stated otherwise and were purchased from Aldrich, SDS, Scharlab and Fluorochem.

1.2. Instrumentation

Oxidation products were identified by comparison of their GC retention times and GC-MS with those of authentic compounds when commercially available, and/or by ^{1}H and ^{13}C-NMR analysis. GC spectra were performed with an Agilent 7820A gas chromatograph equipped with an HP-5 capillary column 30m × 0.32 mm × 0.25 μm and a flame ionization detector. GC-MS analyses were performed on an Agilent 7890A gas chromatograph equipped with an HP-5 capillary column interfaced with an Agilent 5975C mass spectrometer. For electron ionization (EI) the source was set at 70 eV, while a 50/50 NH_3:CH_4 mix was used as the ionization gas for chemical ionization (CI) analyses. NMR spectra were taken on BrukerDPX300 and DPX400 spectrometers using standard conditions. High resolution mass spectra (HRMS) were recorded on a Bruker MicroTOF-Q IITM instrument with an ESI source at Serveis Tècnics of the University of Girona. Samples were introduced into the mass spectrometer ion source by direct infusion through a syringe pump and were externally calibrated using sodium formate. Chromatographic resolution of enantiomers was performed on an Agilent 7820A gas chromatograh using a CYCLOSIL-B column.

2. Synthesis of the complexes

	R$_1$	R$_2$	R$_3$
Fe(pdp)	H	H	H
Mn(pdp)	H	H	H
Fe(mcp)	H	H	H
Mn(mcp)	H	H	H
Fe(^{dMM}pdp)	Me	MeO	Me
Mn(^{dMM}pdp)	Me	MeO	Me
Fe(^{dMM}mcp)	Me	MeO	Me
Mn(^{dMM}mcp)	Me	MeO	Me
Fe(^{Cl}pdp)	H	Cl	H
Mn(^{Cl}mcp)	H	Cl	H
Fe(^{TIPS}pdp)	H	H	Si(iPr)$_3$
Fe(^{TIPS}mcp)	H	H	Si(iPr)$_3$
Mn(^{TIPS}mcp)	H	H	Si(iPr)$_3$
Mn(^{Me2N}pdp)	H	Me$_2$N	H
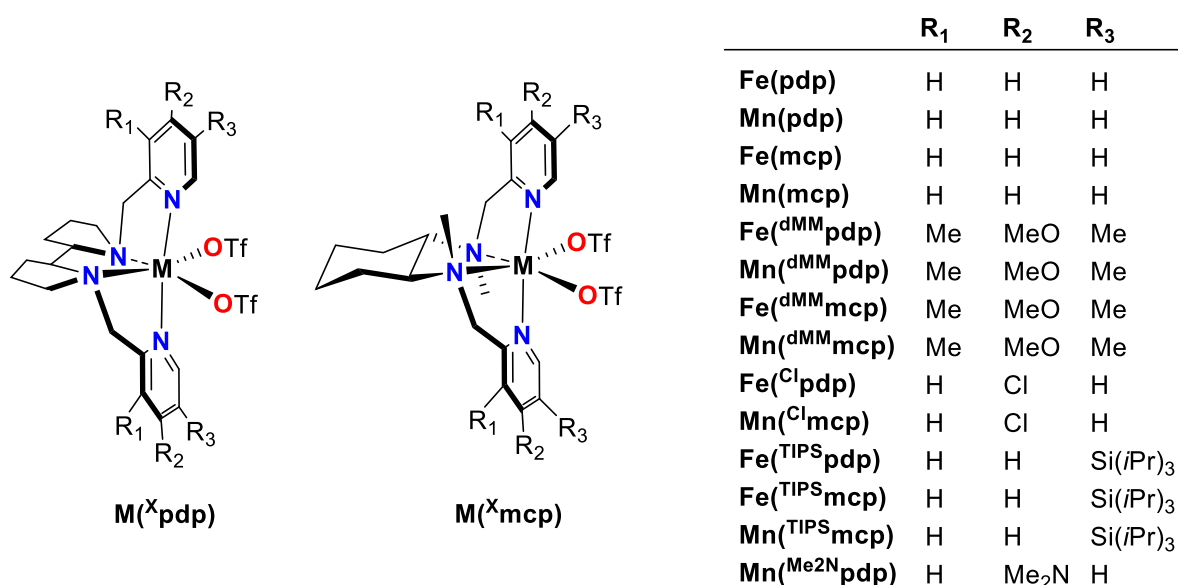
Scheme S1. Schematic representation of the complexes used in this work.

The manganese and iron complexes were prepared and purified according to the reported procedures:

[Fe(CF$_3$SO$_3$)$_2$(pdp)][1] (**Fe(pdp)**)

[Fe(CF$_3$SO$_3$)$_2$(mcp)][2] (**Fe(mcp)**)

[Fe(CF$_3$SO$_3$)$_2$(^{dMM}mcp), [Fe(CF$_3$SO$_3$)$_2$(^{dMM}pdp)], [Fe(CF$_3$SO$_3$)$_2$(^{Cl}pdp)][3] (**Fe(^{dMM}mcp)**, **Fe(^{dMM}pdp)**, **Fe(^{Cl}pdp)**)

[Fe(CF$_3$SO$_3$)$_2$(^{TIPS}mcp)], [Fe(CF$_3$SO$_3$)$_2$(^{TIPS}pdp)][4] (**Fe(^{TIPS}mcp)**, **Fe(^{TIPS}pdp)**)

[Mn(CF$_3$SO$_3$)$_2$(mcp)][5] (**Mn(mcp)**)

[Mn(CF$_3$SO$_3$)$_2$(pdp)][6] (**Mn(pdp)**)

[Mn(CF$_3$SO$_3$)$_2$(^{dMM}pdp)], [Mn(CF$_3$SO$_3$)$_2$(^{dMM}mcp)], [Mn(CF$_3$SO$_3$)$_2$(^{Cl}mcp)][7] (**Mn(^{dMM}pdp)**, **Mn(^{dMM}mcp)**, **Mn(^{Cl}mcp)**)

[Mn(CF$_3$SO$_3$)$_2$(^{TIPS}mcp)][8] (**Mn(^{TIPS}mcp)**)

[Mn(salen)Cl][9]
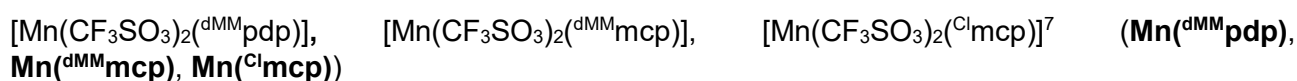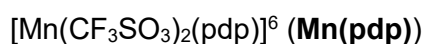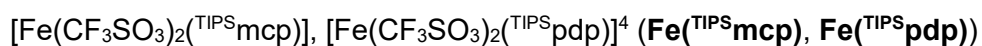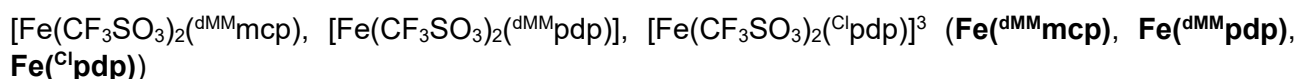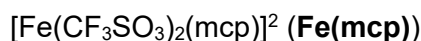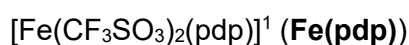
3. Synthesis of the substrates

Substrates **1-15** and **22** were purchased from Aldrich and Fluorochem.

Substrates **16**,[10] **17**, [11] **18**,[11] **20**,[11] **21**[12] and **23**[13] were synthesized following the reported procedures.

Substrate **19** was prepared as described below:
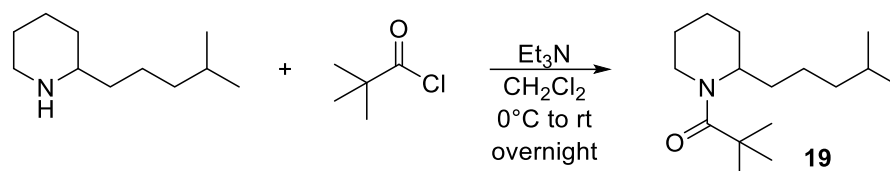
A round-bottom flask capped with a rubber septum and kept under nitrogen was charged with a 0.20 M solution of 2-(4-methylpentyl)piperidine[11] (1.1 equiv) in dichloromethane and cooled to 0 °C. Triethylamine (1.1 equiv) was added to the reaction flask. Pivaloyl chloride (1.0 equiv) was added dropwise and the reaction was stirred overnight at room temperature. At this point, a saturated aqueous Na_2CO_3 solution was added until pH~10-11 and then diluted with dichloromethane. The organic layer was separated from the basic aqueous layer. The aqueous layer was extracted with dichloromethane (2x) and the organic layers were combined. The organic layer was washed with 1N HCl and dried over anhydrous sodium sulfate (Na_2SO_4). The organic layer was evaporated to dryness. The crude amide was purified by flash chromatography over silica gel with hexane:ethyl acetate 2:1 and the product was concentrated to dryness. Product **19** was isolated as a white solid (0.56 g, 88% yield). ^{1}H-NMR (CDCl$_3$, 400 MHz, 300 K) δ, ppm: 4.74 (s, 1H), 4.05 (s, 1H), 3.01 (s, 1H), 1.69 – 1.57 (m, 6H), 1.50 – 1.49 (m, 2H), 1.47 – 1.39 (m, 1H), 1.29 (s, 9H), 1.25 – 1.12 (m, 4H), 0.87 (dd, J = 6.6, 0.8 Hz, 6H). ^{13}C-NMR (CDCl$_3$, 100 MHz, 300 K) δ, ppm: 176.2, 38.9, 38.8, 37.5, 29.7, 28.5, 27.8, 27.2, 26.2, 24.0, 22.6, 22.5, 19.0. HRMS(ESI+) *m/z* calculated for $C_{16}H_{31}NO$ [M+Na]$^+$ 276.2298, found 276.2302.

4. Oxidation reactions

Hydrogen peroxide solutions employed in the oxidation reactions were prepared by diluting commercially available hydrogen peroxide (30% H_2O_2 solution in water, Aldrich) in acetonitrile or fluorinated alcohols to achieve a 0.2 M final concentration. Commercially available glacial acetic acid (99-100%) purchased from Riedel-de-Haën was employed. The purity of the substrates synthetized as described above was in all cases >99%.

4.1 Reaction protocol for catalysis

● Substrate **1** (entries 1-8, Scheme 2b)

A 0.1 M solution (2 mL) of the substrate and the pertinent complex (1.0 mM) was prepared in a vial (10 mL) equipped with a stirring bar using the desired solvent (MeCN, TFE or HFIP). Acetic acid (2.0 equiv.) was added directly to the solution. Then hydrogen peroxide (0.2 equiv.) in the appropriate solvent was added by syringe pump over a period of 30 min. Afterwards, the solution was stirred for further 30 min. At this point, an internal standard was added and the solution was quickly filtered through a silica plug, which was subsequently rinsed with 2 x 1 mL AcOEt. GC analysis of the solution provided product yields relative to the internal standard. Calibration curves were obtained using commercially available pure compounds.

● Substrates **1** (entries 9-14, Scheme 2b), **2-6** (Table 1), **7** (Scheme 3), **8-16** (Scheme 5), **2a** and **3a** (Scheme 5)

A 0.1 M solution (2 mL) of the substrate and the pertinent complex (0.5 mM) was prepared in a vial (10 mL) equipped with a stirring bar using the desired solvent (MeCN, TFE or HFIP) and cooled at 0 ºC in an ice bath. Acetic acid (2.0 equiv.) was added directly to the solution. Then hydrogen peroxide (0.5 equiv.) in the appropriate solvent was added by syringe pump over a period of 30 min. Afterwards, the solution was stirred for further 30 min. At this point, an internal standard was added and the solution was quickly filtered through a silica plug, which was subsequently rinsed with 2 x 1 mL AcOEt. GC analysis of the solution provided product yields relative to the internal standard. Calibration curves were obtained using commercially available pure compounds when available. For **8b**, **9c**, **10b**, **11b**, **11c**, **2c**, **3c** and **3d** the response factor of the corresponding commercially available 1,2-diols was used to calculate the yields. For **12b**,[14] **13c**,[14] **15b**,[15] **16c**[10,14] the response factor of the pure compounds synthetized following the reported procedures were used to calculate the yields. The alcohol **4a_endo** was identified by ^{1}H-NMR in CDCl$_3$ (**4a_endo**: δ (H$_\alpha$) = 4.23 ppm[16]). The axial and equatorial alcohols of **5a**, **5b**, **6a** and **6b** were identified by GC in combination with ^{1}H-NMR. The NMR chemical shift of the alcohol α protons in CDCl$_3$ allowed the distinction of the different isomers, as previously reported (**5b_ax**: δ (H$_\alpha$) = 4.05 ppm;[17] **5b_eq**: δ (H$_\alpha$) = 3.58 ppm;[17] **5a_ax**: δ (H$_\alpha$) = 4.19

ppm;[18] **5a$_{eq}$**: δ (H$_α$) = 3.57 ppm;[18] **6a$_{ax}$**: δ (H$_α$) = 3.76 ppm;[19] **6a$_{eq}$**: δ (H$_α$) = 3.2 ppm;[19] **6b$_{ax}$**: δ (H$_α$) = 4.1 ppm;[19] **6b$_{eq}$**: δ (H$_α$) = 3.58 ppm[19]).

● Intermolecular competition experiment (Scheme 4 and Scheme S2)

A 0.05 M solution (2 mL) of each substrate and the pertinent complex (0.5 mM) was placed in a vial (10 mL) equipped with a stirring bar using the desired solvent (MeCN, TFE or HFIP) and cooled at 0 °C in an ice bath. Acetic acid (2.0 equiv.) was added directly to the solution. Then hydrogen peroxide (0.5 equiv.) in the appropriate solvent was added by syringe pump over a period of 30 min. Afterwards, the solution was stirred for further 30 min. At this point, an internal standard was added and the solution was quickly filtered through a silica plug, which was subsequently rinsed with 2 x 1 mL AcOEt. GC analysis of the solution provided product yields relative to the internal standard. Calibration curves were obtained using commercially available pure compounds.

● Substrates **17**-**21** (Scheme 6 and Scheme 7):
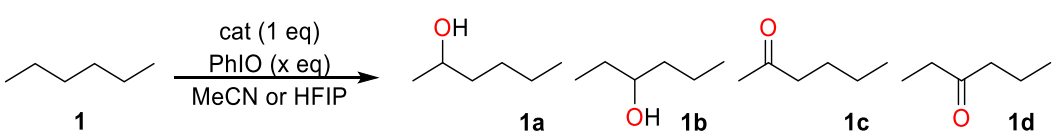
A 25 mL round bottom flask was charged with catalyst (6 μmol, 1.0 mol%), substrate (1.0 equiv.), MeCN or HFIP (3.3 mL) and a magnetic stirring bar. Acetic acid was then added (13 equiv.) and the mixture was cooled at -40 °C in a N$_2$/MeCN bath or at 0 °C in an ice bath under magnetic stirring. Then, hydrogen peroxide solution in MeCN or HFIP (1.0 - 3.5 equiv.) was added by syringe pump over a period of 30 min. At this point, 15 mL of an aqueous NaHCO$_3$ saturated solution were added to the mixture. The resulting solution was extracted with CH$_2$Cl$_2$ (3 x 10 mL). The organic fractions were combined, dried over MgSO$_4$, and the solvent was removed under reduced pressure to afford the oxidized product. The resulting residue was purified by column chromatography over silica gel to obtain the pure product.

● Substrates **22**-**23** (Scheme 8):

A 25 mL round bottom flask was charged with catalyst (6 μmol, 1.0 mol%), substrate (1.0 equiv.), MeCN or HFIP (3.3 mL) and a magnetic stirring bar. Acetic acid was then added (13 equiv.) and the mixture was cooled at 0 °C in an ice bath under magnetic stirring. Then, hydrogen peroxide solution in HFIP or MeCN (1.0 equiv.) was added by syringe pump over a period of 30 min. At this point, the mixture was evaporated to dryness and charged with dichloromethane (15 mL) and cooled to 0 °C. Triethylamine (2.0 equiv) was added to the reaction flask. Pivaloyl chloride (2.0 equiv) was added dropwise and the reaction was stirred for 4 hours at room temperature. At this point, a saturated aqueous Na$_2$CO$_3$ solution was added until pH~10-11 and then diluted with dichloromethane. The organic layer was separated from the basic aqueous layer. The aqueous layer was extracted with dichloromethane (2x) and the organic layers were combined. The organic layer was washed with 1N HCl and dried over anhydrous sodium sulfate (Na$_2$SO$_4$). The organic layer was evaporated to dryness and the crude amide was purified by flash chromatography over silica gel.

4.2. Screening of catalysts for the oxidation of hexane
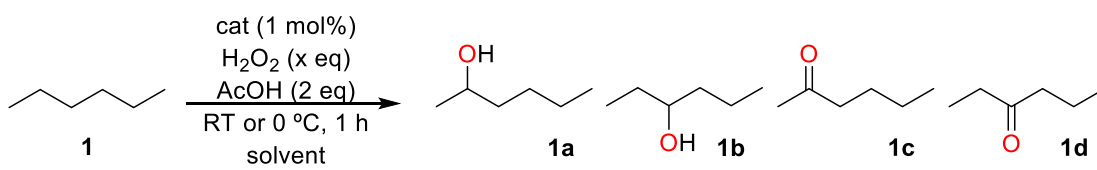
Table S1. Oxidation of hexane (**1**) catalyzed by [Mn(salen)Cl] and [Mn(TCPP)Cl] in MeCN and HFIP.

Catalyst	1a (%)[a]	1b (%)[a]	1c (%)[a]	1d (%)[a]	Yield (%)[a] (% alcohol)[b]	Solvent
[Mn(salen)Cl][c]	-	-	-	-	-	MeCN
	-	-	-	-	-	HFIP
[Mn(TCPP)Cl][d]	3	3	4	4	14(60)	MeCN
	3	3	-	-	6(100)	HFIP

[a]Yields with respect to H_2O_2, determined by GC (FID) against an internal standard. Yields are calculated considering that 2 eq of H_2O_2 are necessary for the formation of the ketone products (**1c** and **1d**). [b]100 x{[**1a**]+[**1b**]/([**1a**]+[**1b**]+[**1c**]+[**1d**])}. [c]21 eq hexane, 84 eq PhIO, 11 eq pyridine N-oxide, 0° C, 4 h.[9] [d]1000 eq hexane, 100 eq PhIO, 2 eq 4-*tert*-butylpyridine, RT, 1h.[20]

Table S2. Oxidation of hexane (**1**) with different catalysts.

Entry	Catalyst	H_2O_2 (eq)	1a (%)[a]	1b (%)[a]	1c (%)[a]	1d (%)[a]	Yield (%)[a] (% alcohol)[b]	Solvent
1	Fe(pdp)	0.2	8	8	24	14	54(46)	MeCN
2		0.2	26	18	8	6	58(86)	TFE
3		0.2	49	33	2	2	86(98)	HFIP
4	Mn(pdp)	0.2	7	5	26	14	52(38)	MeCN
5		0.2	21	14	4	2	41(92)	TFE
6		0.2	39	25	1	1	66(99)	HFIP
7	Fe(TIPSmcp)	0.2	30	19	6	8	63(91)	TFE
8	Mn(TIPSmcp)	0.2	34	20	4	-	58(96)	TFE
9[c]	Fe(TIPSmcp)	0.5	3	2	36	18	59(16)	MeCN
10[c]		0.5	22	14	8	4	48(86)	TFE
11[c]		0.5	40	25	2	2	69(97)	HFIP
12[c]	Mn(TIPSmcp)	0.5	3	3	34	16	56(19)	MeCN
13[c]		0.5	29	18	8	4	59(89)	TFE
14[c]		0.5	34	21	2	2	59(97)	HFIP

[a]Yields with respect to H_2O_2, determined by GC-FID against an internal standard. Yields are calculated considering that 2 eq of H_2O_2 are necessary for the formation of the ketone products (**1c** and **1d**). [b]100x([**1a**]+[**1b**]/([**1a**]+[**1b**]+[**1c**]+[**1d**]). [c]0.5 mol% catalyst was used; oxidations performed at 0ºC.

Table S3. Catalyst screening for the oxidation of hexane (**1**) in TFE.
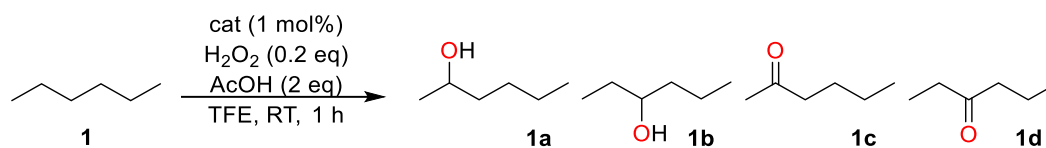
Catalyst	1a (%)[a]	1b (%)[a]	1c (%)[a]	1d (%)[a]	Yield (%)[a] (% alcohol)[b]
Fe(mcp)	18	12	6	4	40(86)
Mn(mcp)	23	14	2	2	41(95)
Fe(dMMpdp)	22	16	4	2	44(93)
Mn(dMMpdp)	23	17	4	2	46(93)
Fe(dMMmcp)	22	17	4	4	47(91)
Mn(dMMmcp)	24	17	4	2	47(93)
Fe(Clpdp)	18	14	8	8	48(80)
Mn(Clmcp)	26	16	6	-	48(93)
Fe(TIPSpdp)	21	14	4	4	43(90)

[a]Yields with respect to H_2O_2, determined by GC (FID) against an internal standard. Yields are calculated considering that 2 eq of H_2O_2 are necessary for the formation of the ketone products (**1c** and **1d**). [b]100 x{[**1a**]+[**1b**]/([**1a**]+[**1b**]+[**1c**]+[**1d**])}.

4.3. Blank experiments for the oxidation of hexane, cyclohexane and cyclohexanol

Table S4. Control experiment for the oxidation of hexane (**1**).
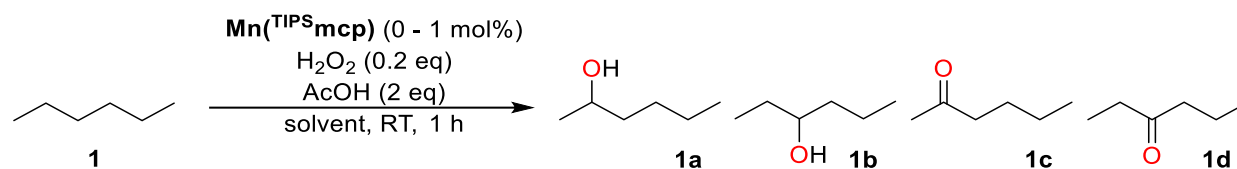
Solvent	Mn(^{TIPS}mcp) (mol%)	1a (%)[a]	1b (%)[a]	1c (%)[a]	1d (%)[a]
MeCN (reference)	1	7	5	14	6
MeCN (**blank**)	0	0	0	0	0
TFE (reference)	1	34	20	4	0
TFE (**blank**)	0	0	0	0	0
HFIP (reference)[b]	1	30	18	2	1
HFIP (**blank**)[b]	0	0	0	0	0

[a]Yields with respect to H_2O_2, determined by GC (FID) against an internal standard. Yields are calculated considering that 2 eq of H_2O_2 are necessary for the formation of **1c** and **1d**. [b]0.5 equiv. of H_2O_2 was used.

Table S5. Control experiment for the oxidation of cyclohexane (**2**).
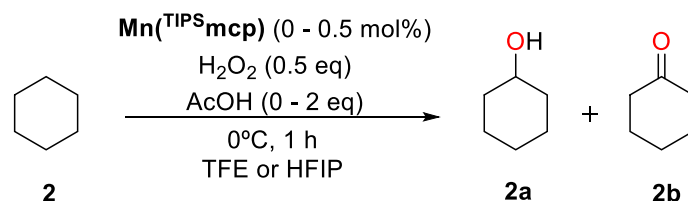
Solvent	Mn(^{TIPS}mcp) (mol%)	AcOH (eq)	2a (%)[a]	2b (%)[a]
TFE (reference)	0.5	2	68	6
TFE (**blank**)	0	2	0	0
TFE (**blank**)	0.5	0	7	2
HFIP (reference)	0.5	2	68	4
HFIP (**blank**)	0	2	0	0
HFIP (**blank**)	0.5	0	39	2

[a]Yields with respect to H_2O_2, determined by GC (FID) against an internal standard. Yields are calculated considering that 2 eq of H_2O_2 are necessary for the formation of **2b**.

Table S6. Control experiment for the oxidation of cyclohexanol (**2a**).
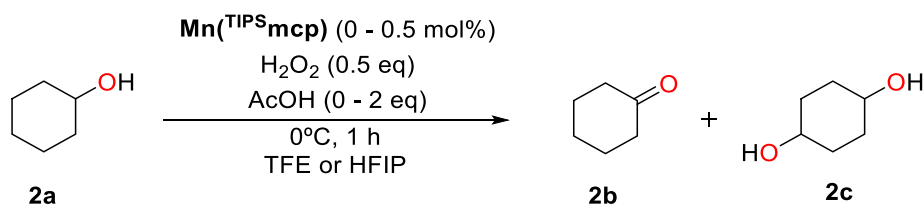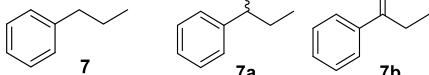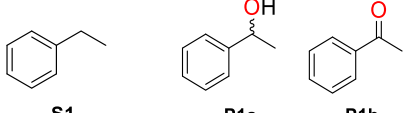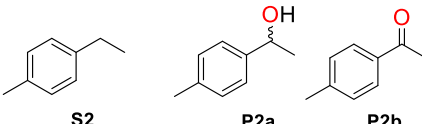
Solvent	Mn(^{TIPS}mcp) (mol%)	AcOH (eq)	2b (%)^a	2c (%)^a
TFE (reference)	0.5	2	53	18
TFE (**blank**)	0	2	3	0
TFE (**blank**)	0.5	0	1	0
HFIP (reference)	0.5	2	36	30
HFIP (**blank**)	0	2	2	0
HFIP (**blank**)	0.5	0	15	6

^{a}With respect to H_2O_2, determined by GC (FID) against an internal standard.

4.4. Screening of catalysts and carboxylic acid for enantioselective hydroxylation

Table S7. Screening of catalysts and/or additives in the enantioselective hydroxylation of benzylic C−H bonds in TFE.
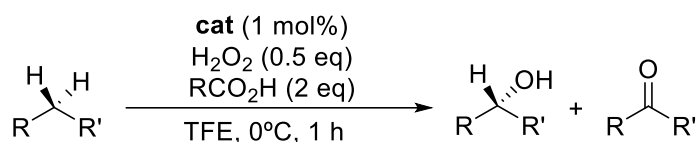
Substrate	Products	Catalyst	RCO$_2$H[a]	Product yields (%)[b]	Hydroxylation selectivity (%)[c]	ee (%)[d]
				7a/7b		
		Mn(pdp)	AcOH	22/2	96	19
		Mn(mcp)	AcOH	18/1	97	12
		Mn(TIPSpdp)	AcOH	17/1	97	9
		Mn(TIPSmcp)	AcOH	12/2	92	8
		Mn(dMMmcp)	AcOH	27/3	95	18
		Mn(dMMpdp)	AcOH	31/5	93	29
		Mn(Me2Npdp)	AcOH	53/15	88	29
		Mn(dMMpdp)	Pva	25/3	94	46
		Mn(Me2Npdp)	Pva	36/11	87	33
		Mn(dMMpdp)	Cha	21/2	95	37
		Mn(Me2Npdp)	Cha	44/7	93	60
		Mn(dMMpdp)	Cpa	25/3	94	34
		Mn(Me2Npdp)	Cpa	7/39	26	10
		Mn(dMMpdp)	2-eha	22/2	96	50
		Mn(Me2Npdp)	2-eha	25/4	93	42
		Mn(dMMpdp)[e]	2-eha	24/2	96	66
		Mn(Me2Npdp)[e]	2-eha	44/7	93	60
				P1a/P1b		
		Mn(dMMpdp)[f]	2-eha	32/4	99	55
		Mn(Me2Npdp)[f]	2-eha	46/11	89	49
				P2a/P2b		
		Mn(dMMpdp)[f]	2-eha	42.5/0.5	99	56
		Mn(Me2Npdp)[f]	2-eha	61/8	94	49

[a]AcOH = acetic acid, Pva = pivalic acid, Cha = cyclohexanecarboxylic acid, Cpa = cyclopropanoic acid, 2-eha = 2-ethylhexanoic acid. [b]Yields with respect to H$_2$O$_2$, determined by GC (FID) against an internal standard. Yields are calculated considering that 2 eq of H$_2$O$_2$ are necessary for the formation of the ketone products. Yields of **7a** and **P2a** calculated with the response factor of **P1a**. Yields of **7b** and **P2b** calculated with the response factor of **P1b**. [c]100x{[**Xa**]/([**Xa**]+[**Xb**])}. [d]ee of the alcohol products determined by GC with a chiral stationary phase. [e]Temperature = -35 °C. [f]**S1** and **S2** were oxidized following the procedure reported in Section 4.1 for substrate **7**.

Table S8. Comparison of the oxidation of propylbenzene (**7**) catalyzed by **Mn(dMMpdp)** and **Mn(Me2Npdp)** in MeCN, TFE and HFIP.
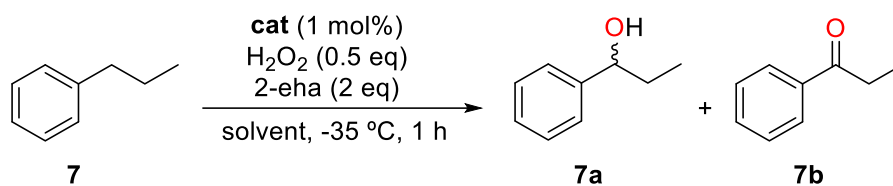
Catalyst	Solvent	Product yields (%)[a] 7a/7b	Hydroxylation selectivity (%)[b]	ee (%)[c]
Mn(dMMpdp)	MeCN	7/26	37	39
	TFE	24/2	96	66
	HFIP	12/0.3	99	46
Mn(Me2Npdp)	MeCN	7/39	26	10
	TFE	44/7	93	60
	HFIP	12/1	96	40

[a]Yields with respect to H_2O_2, determined by GC (FID) against an internal standard. Yields are calculated considering that 2 eq of H_2O_2 are necessary for the formation of the ketone products. Yields of **7a** and **7b** calculated with the response factor of **P1a** and **P1b** (Table S7), respectively. [b]$100 \times \{[7a]/([7a]+[7b])\}$. [c]ee of **7a** determined by GC with a chiral stationary phase.

4.5. Intermolecular competition experiment
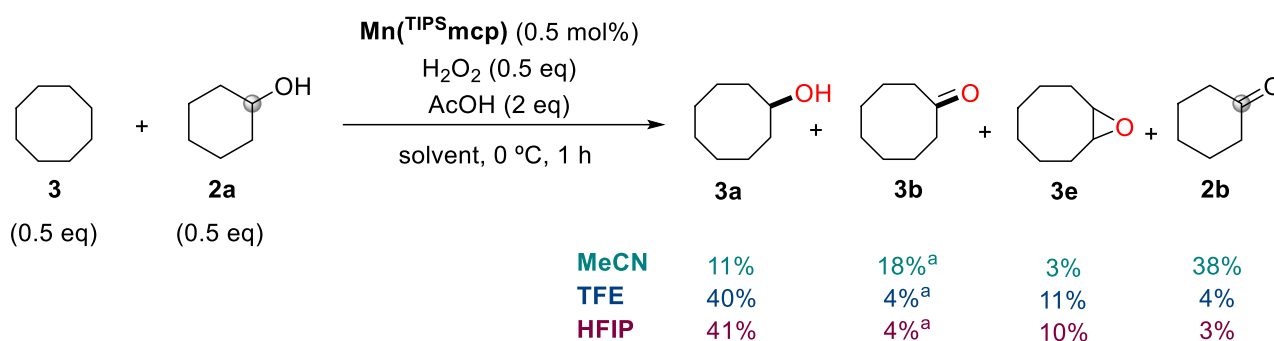
Scheme S2. Intermolecular competition experiment. Yields calculated with respect to H_2O_2, determined by GC (FID) against an internal standard. [a]Yields shown below each of the products are calculated considering that 2 eq of H_2O_2 are necessary for the formation of **3b**.

4.6. Determination of kinetic isotopic effect (KIE)

● Procedure

A 0.05 M solution (2 mL) of each substrate and the pertinent complex (0.5 mM) was prepared in a vial (10 mL) equipped with a stirring bar using the desired solvent (MeCN, TFE or HFIP) and cooled at 0 ºC in an ice bath. Acetic acid (2.0 equiv.) was added directly to the solution. Then hydrogen peroxide (0.5 equiv.) in the appropriate solvent was added by syringe pump over a period of 30 min. Afterwards, the solution was stirred for further 30 min. At this point, an internal standard was added and the solution was quickly filtered through a silica plug, which was subsequently rinsed with 2 x 1 mL AcOEt. GC analysis of the solution provided product yields relative to the internal standard.

MeCN: KIE[a] = 3.8
HFIP: KIE[a] = 3.3

Scheme S3. Determination of KIE. [a]KIE = ([2a]+[2b])/ ([S3a]+[S3b]). [**S3a**] and [**S3b**] calculated with the response factor of **2a** and **2b** respectively.

4.7. Oxidation of alcohols with Mn(^TIPSmcp) in TFE
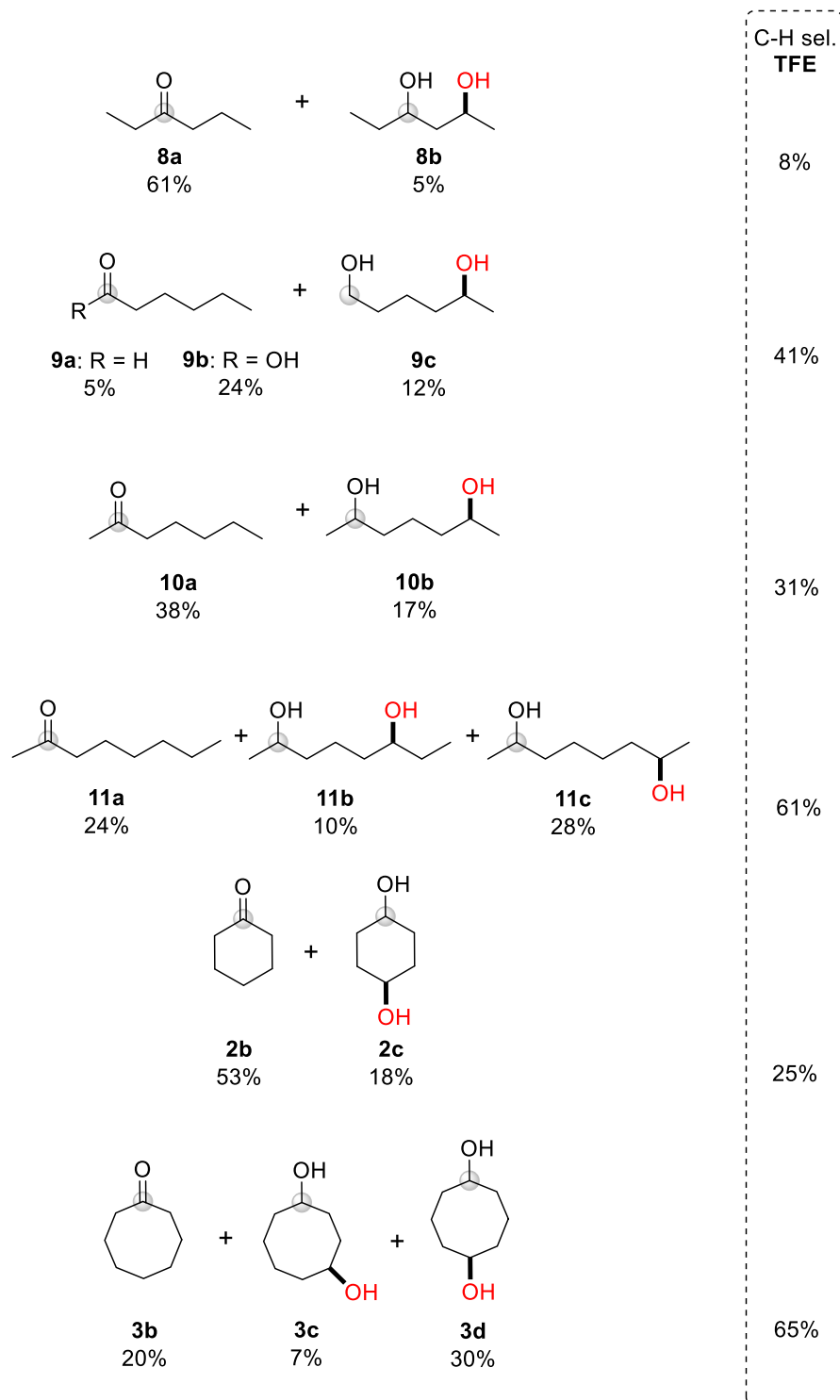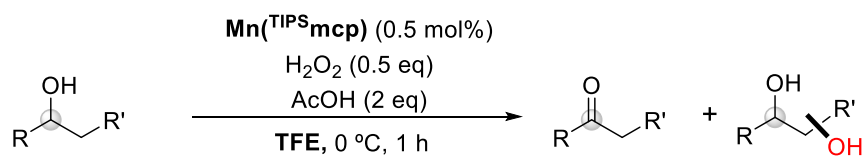
Scheme S4. Catalytic oxidation of alkanols in TFE.

4.8. GC-MS spectra

The diols **8b**, **9c**, **10b**, **11b** and **11c** were identified through their molecular mass peak ascertained by GC-MS in the CI mode. The position of the hydroxyl groups along the chain were defined by analyzing the fragmentation pattern of the mass spectra recorded using the GC-MS in the EI mode.[21]
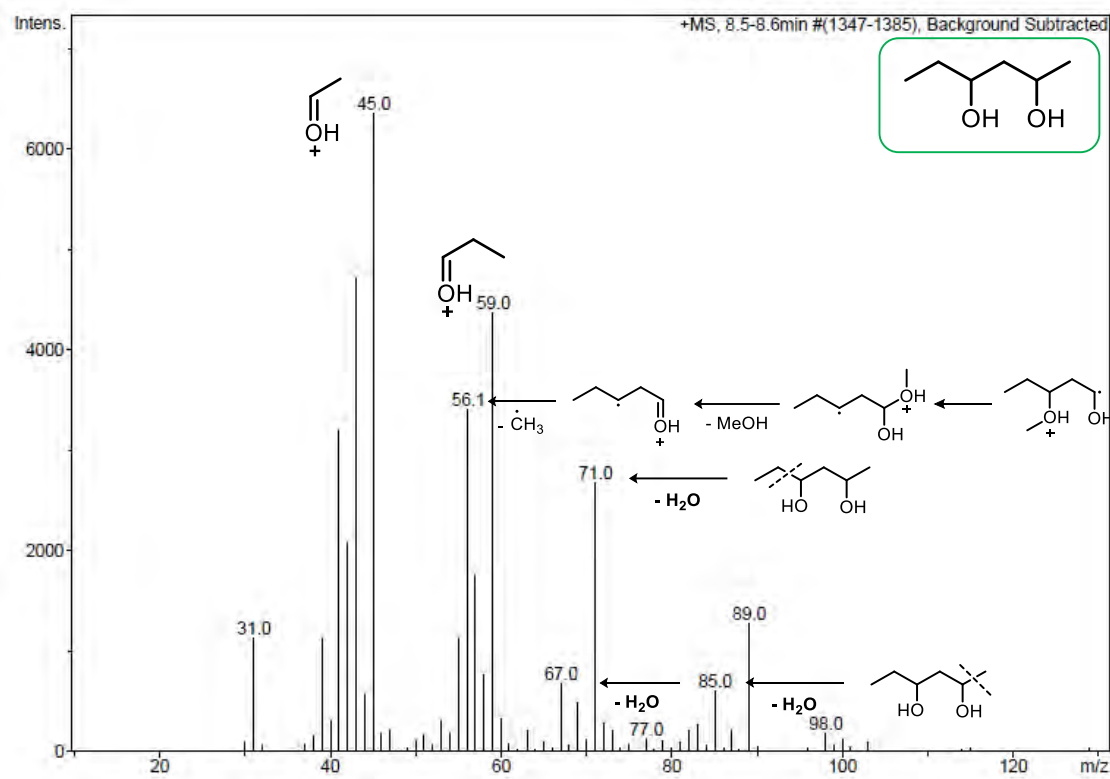
Figure S1. MS (EI) spectra of **8b** (CI: [**8b** + NH$_4$]$^+$ m/z = 136.1)
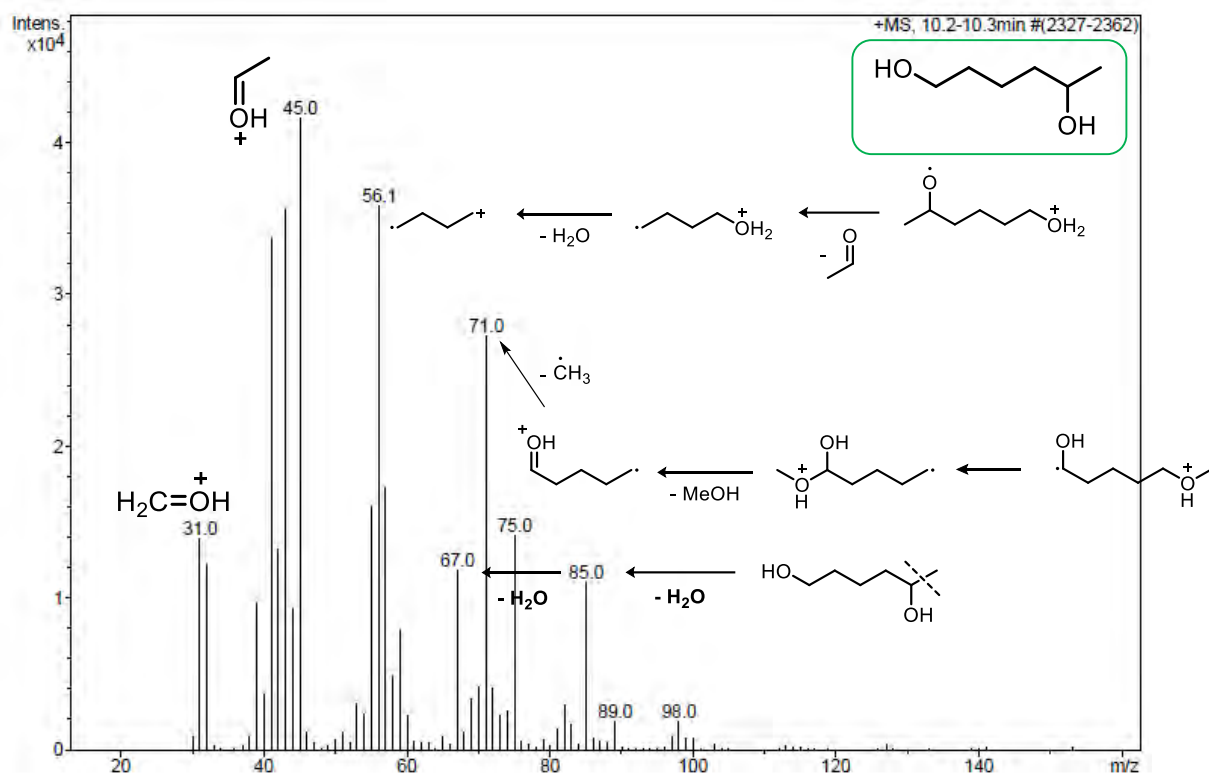
Figure S2. MS (EI) spectra of **9c** (CI: [**9c** + NH₄]⁺ m/z = 134.1)
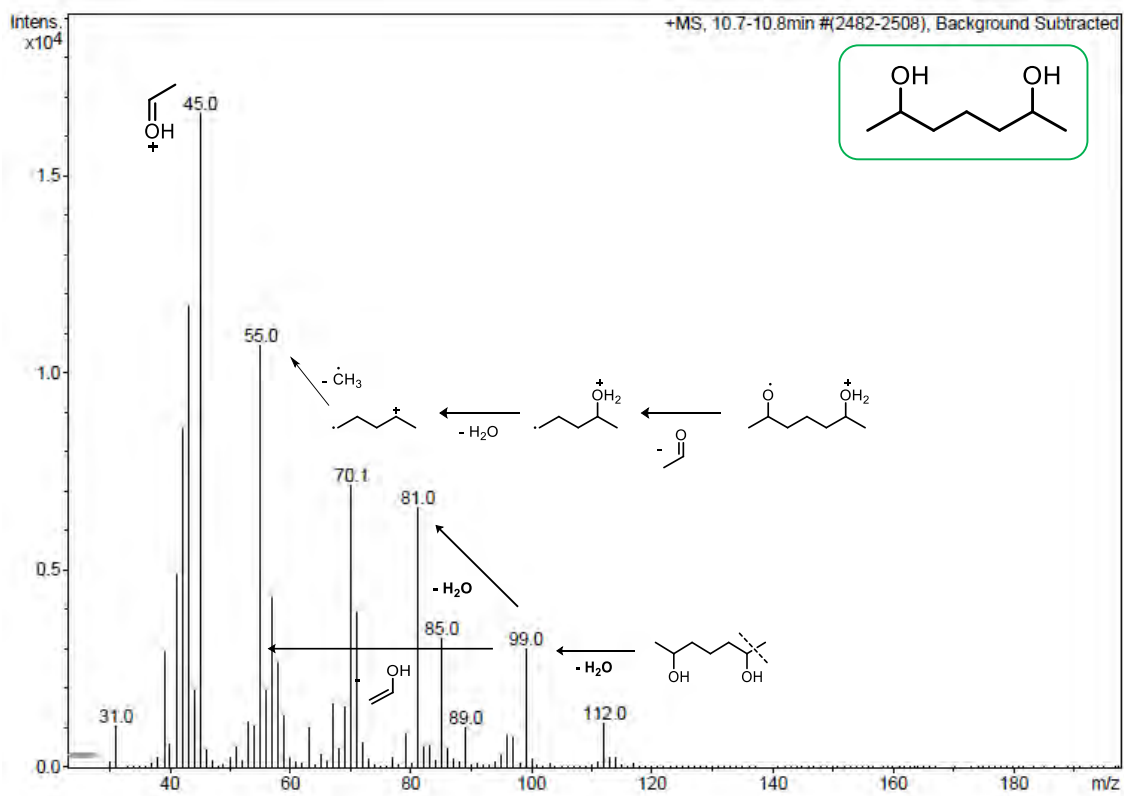
Figure S3. MS (EI) spectra of **10b** (CI: [**10b** + NH₄] ⁺ m/z = 150.1)

Figure S4. MS (EI) spectra of **11b** (CI: [**11b** + NH$_4$] $^+$ m/z = 164.1)

Figure S5. MS (EI) spectra of **11c** (CI: [**11c** + NH$_4$]$^+$ m/z = 164.1)

5. Characterization of the isolated products
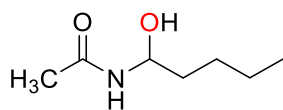
**N-(1-hydroxy)pentylacetamide (17a):** Following the general conditions, the crude mixture was purified by flash chromatography over silica with hexane:ethyl acetate 1:1 and the product was concentrated to dryness. The product was isolated as a white solid (35% yield with **Mn(^dMMpdp)** in MeCN and 16% yield with **Mn(^TIPSmcp)** in HFIP). ^{1}H-NMR (CDCl$_3$, 400 MHz, 300 K) δ, ppm: 6.46 (d, J = 7.8 Hz, 1H), 5.29 (td, J = 8.6, 4.5 Hz, 1H), 4.34 (d, J = 3.5 Hz, 1H), 2.00 (s, 3H), 1.74 – 1.62 (m, 1H), 1.62 – 1.50 (m, 1H), 1.46 – 1.26 (m, 4H), 0.97 – 0.85 (m, 3H). ^{13}C-NMR (CDCl$_3$, 100 MHz, 300 K) δ, ppm: 171.6, 74.3, 34.9, 27.0, 23.3, 22.3, 13.9. HRMS(ESI+) *m/z* calculated for C$_7$H$_{15}$NO$_2$ [M+Na]$^+$ 168.0995, found 168.0991.
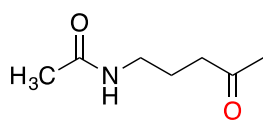
N-(4-oxo)pentylacetamide (17b): Following the general conditions, the crude mixture was purified by flash chromatography over silica with hexane:ethyl acetate 1:1 and the product was concentrated to dryness. The product was isolated as a white solid (51% yield). ^{1}H-NMR (CDCl$_3$, 400 MHz, 300K) δ, ppm: 5.93 (s, 1H), 3.28 – 3.18 (m, 2H), 2.52 (t, J = 6.9 Hz, 2H), 2.16 (s, 3H), 1.97 (d, J = 4.5 Hz, 3H), 1.79 (q, J = 6.9 Hz, 2H). ^{13}C-NMR (CDCl$_3$, 100 MHz, 300 K) δ, ppm: 208.8, 170.3, 41.1, 39.2, 30.0, 23.34, 23.27. HRMS(ESI+) *m/z* calculated for C$_7$H$_{23}$NO$_2$ [M+Na]$^+$ 166.0838, found 166.0843.
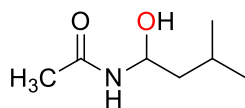
N-1-(1-hydroxy-3-methylbutyl)acetamide (18a): Following the general conditions, the crude mixture was purified by flash chromatography over silica with hexane:ethyl acetate 1:4 and the product was concentrated to dryness. The product was isolated as a white solid (65% yield). ^{1}H-NMR (CDCl$_3$, 400 MHz, 300K) δ, ppm: 6.68 (d, *J* = 8.2 Hz, 1H), 5.38 (td, *J* = 7.7, 5.9 Hz, 1H), 4.64 (s, 1H), 1.97 (s, 3H), 1.81 – 1.66 (m, 1H), 1.57 (dt, *J* = 13.8, 7.1 Hz, 1H), 1.43 – 1.33 (m, 1H), 0.91 (dd, *J* = 6.6, 2.8 Hz, 6H). ^{13}C-NMR (CDCl$_3$, 100 MHz, 300 K) δ, ppm: 171.4, 72.6, 44.1, 29.7, 24.4, 23.3, 22.2. HRMS(ESI+) *m/z* calculated for C$_7$H$_{15}$NO$_2$ [M+Na]$^+$ 168.0995, found 168.0992.
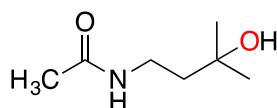
N-(3-hydroxy)pentylacetamide (18b): Following the general conditions, the crude mixture was purified by flash chromatography over silica with hexane:ethyl acetate 1:4 and

the product was concentrated to dryness. The product was isolated as a white solid (62% yield). ^{1}H-NMR (CDCl$_3$, 400 MHz, 300K) δ, ppm: 3.32 – 3.24 (m, 2H), 1.94 (s, 3H), 1.73 – 1.61 (m, 2H), 1.23 (s, 6H). ^{13}C-NMR (CD$_3$OD, 100 MHz, 300 K) δ, ppm: 170.7, 70.5, 41.5, 36.0, 29.5, 23.2. HRMS(ESI+) *m/z* calculated for C$_7$H$_{15}$NO$_2$ [M+Na]$^+$ 168.0995, found 168.0998.
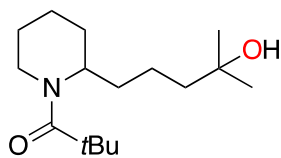
(19b) Following the general conditions, the crude mixture was purified by flash chromatography over silica with hexane:ethyl acetate 3:1 and the product was concentrated to dryness. The product was isolated as a pale yellow oil (46% yield). ^{1}H-NMR (CDCl$_3$, 400 MHz, 300 K) δ, ppm: 4.82 (s, 1H), 4.09 (s, 1H), 3.01 (s, 1H), 1.75 – 1.56 (m, 9H), 1.50 – 1.42 (m, 3H), 1.29 (s, 9H), 1.22 (s, 3H), 1.19 (s, 3H). ^{13}C-NMR (CDCl$_3$, 100 MHz, 300 K) δ, ppm: 176.7, 70.6, 43.3, 38.9, 30.9, 29.9, 29.7, 28.6, 28.5, 26.2, 20.3, 19.1. HRMS(ESI+) *m/z* calculated for C$_{16}$H$_{31}$NO$_2$ [M+Na]$^+$ 292.2247, found 292.2242.
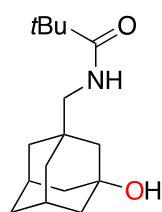
(20c) Following the general conditions, the crude mixture was purified by flash chromatography over silica with ethyl acetate and the product was concentrated to dryness. The product was isolated as a white solid (44% yield). ^{1}H-NMR (CD$_3$OD, 400 MHz, 300 K) δ, ppm: 5.69 (s, 1H), 2.98 (d, J = 5.8 Hz, 2H), 2.23 – 2.14 (m, 2H), 2.08 (s, 1H), 1.67 – 1.55 (m, 4H), 1.50 (d, J = 8.5 Hz, 2H), 1.39 (s, 2H), 1.33 (s, 3H), 1.16 (s, 9H). ^{13}C-NMR (CD$_3$OD, 100 MHz, 300 K) δ, ppm: 178.5, 68.5, 49.7, 47.8, 44.6, 39.0, 38.9, 37.7, 35.4, 30.3, 27.7. HRMS(ESI+) *m/z* calculated for C$_{16}$H$_{27}$NO$_2$ [M+Na]$^+$ 288.1934, found 288.1935.
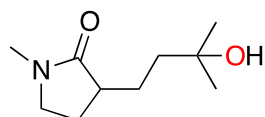
(21a) Following the general conditions, the crude mixture was purified by flash chromatography over silica with ethyl acetate and the product was concentrated to dryness. The product was isolated as a pale yellow oil (49% yield). ^{1}H-NMR (CDCl$_3$, 400 MHz, 300 K) δ, ppm: 3.27 (dd, J = 8.6, 5.4 Hz, 2H), 2.81 (s, 3H), 2.38 (qd, J = 8.7, 4.9 Hz, 1H), 2.21 – 2.12 (m, 1H), 2.05 (d, J = 17.7 Hz, 1H), 1.87 (tt, J = 12.3, 5.2 Hz, 1H), 1.65 (dq, J = 12.7, 8.4 Hz, 1H), 1.58 – 1.37 (m, 3H), 1.20 (s, 3H), 1.19 (s, 3H). ^{13}C-NMR (CDCl$_3$, 100 MHz, 300 K) δ, ppm: 176.8, 70.6, 47.7, 41.7, 40.9, 29.7, 29.4, 29.0, 26.2, 24.9. HRMS(ESI+) m/z calculated for C$_{10}$H$_{19}$NO$_2$ [M+Na]+ 208.1308, found 208.1312.

5.1. ¹H and ¹³C{¹H} NMR spectra of substrates
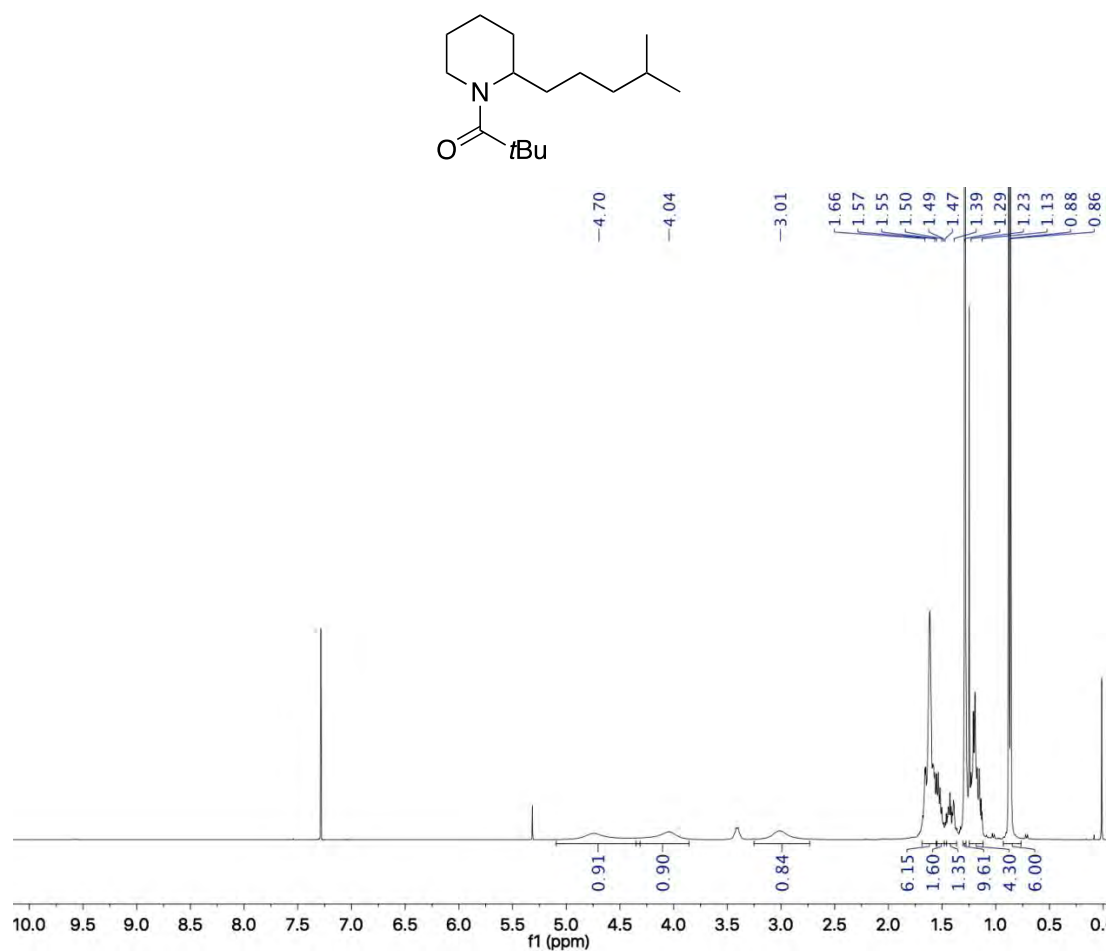
Figure S6. ¹H-NMR of **19** in CDCl₃
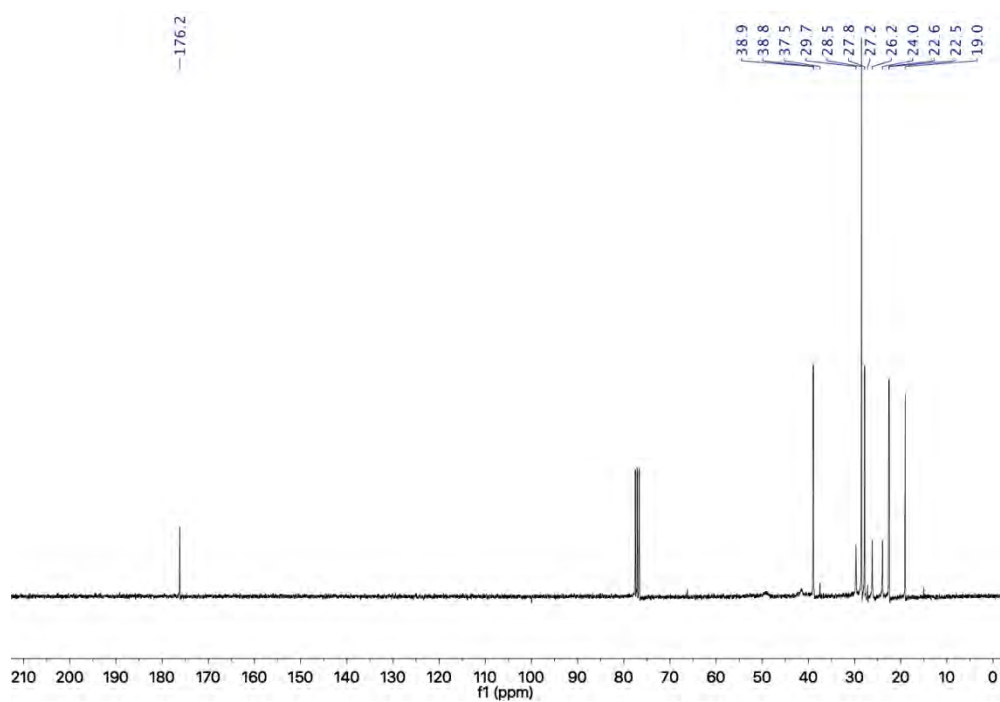
Figure S7. ¹³C{¹H}-NMR of **19** in CDCl₃

5.2 ¹H and ¹³C{¹H} NMR spectra of isolated products
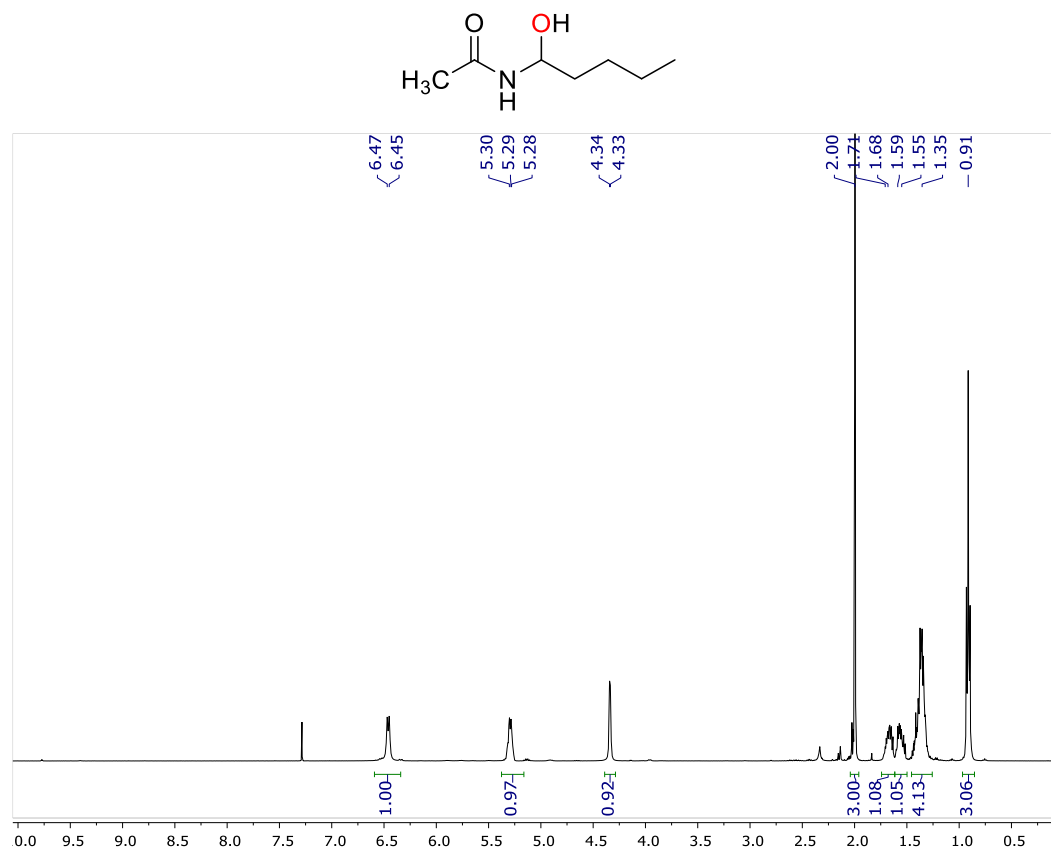
Figure S8. ¹H-NMR of **17a** in CDCl₃
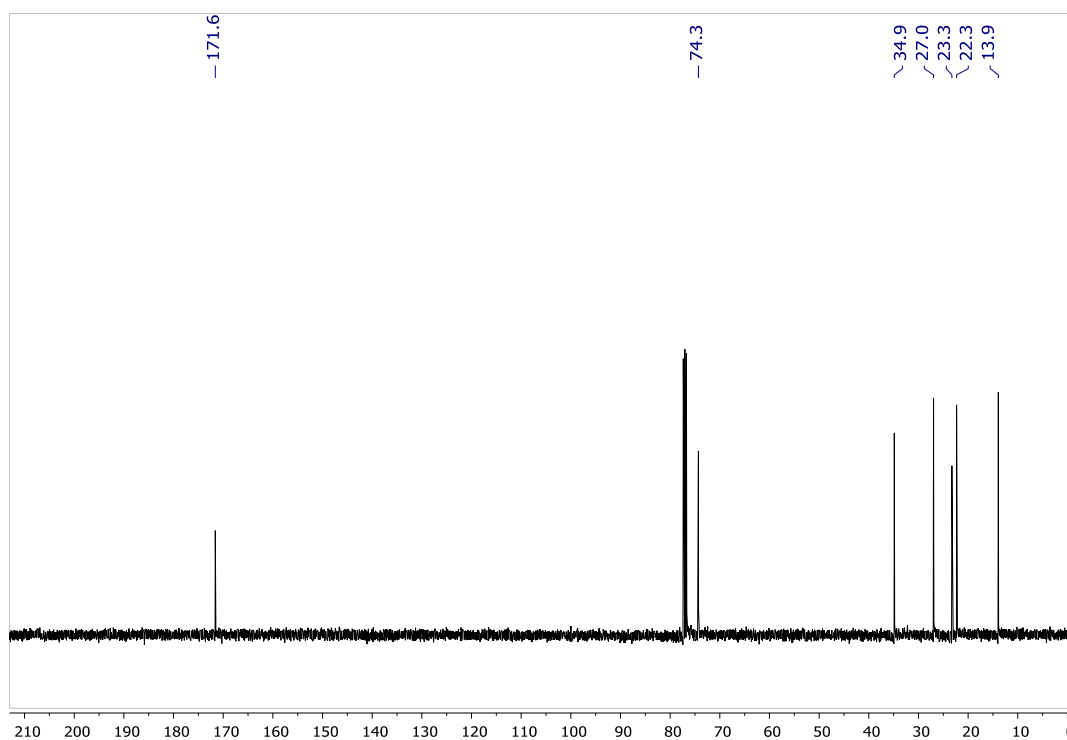
Figure S9. ¹³C{¹H}-NMR of **17a** in CDCl₃
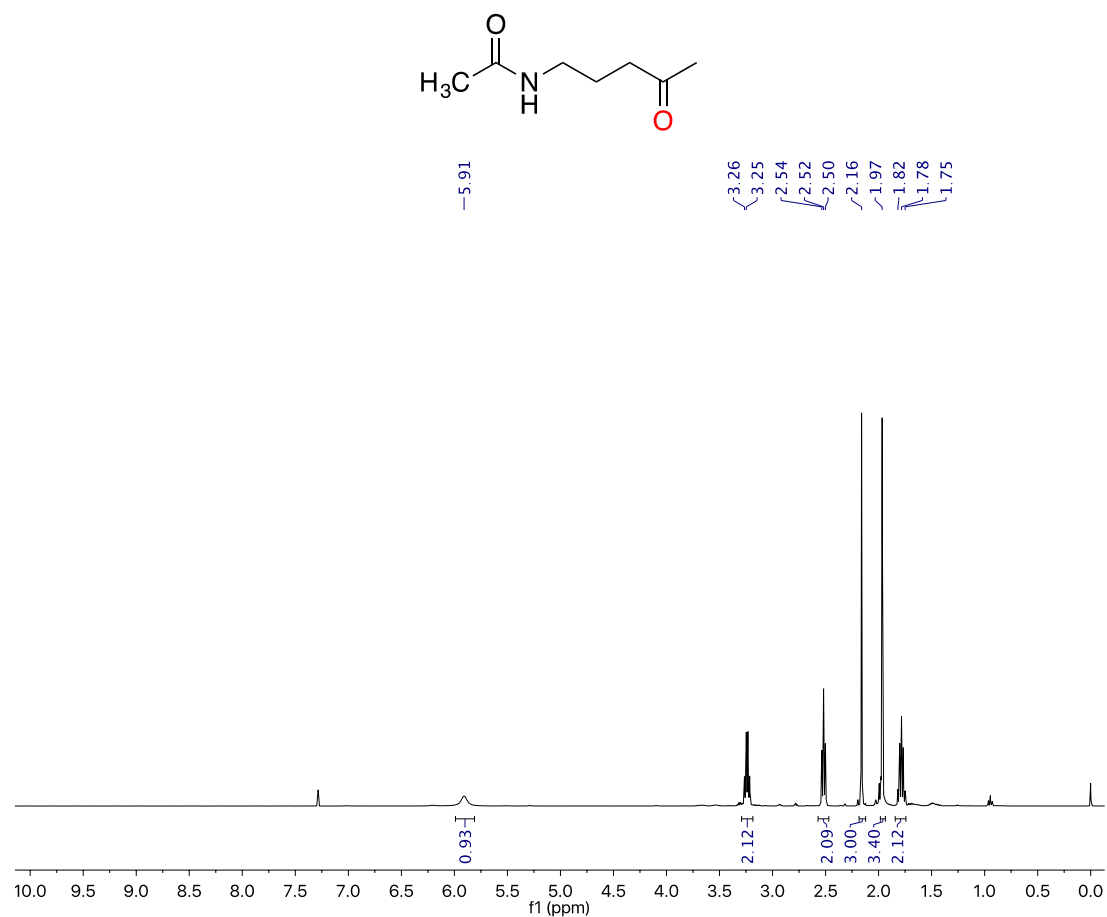
Figure S10. ^{1}H-NMR of **17b** in CDCl$_3$
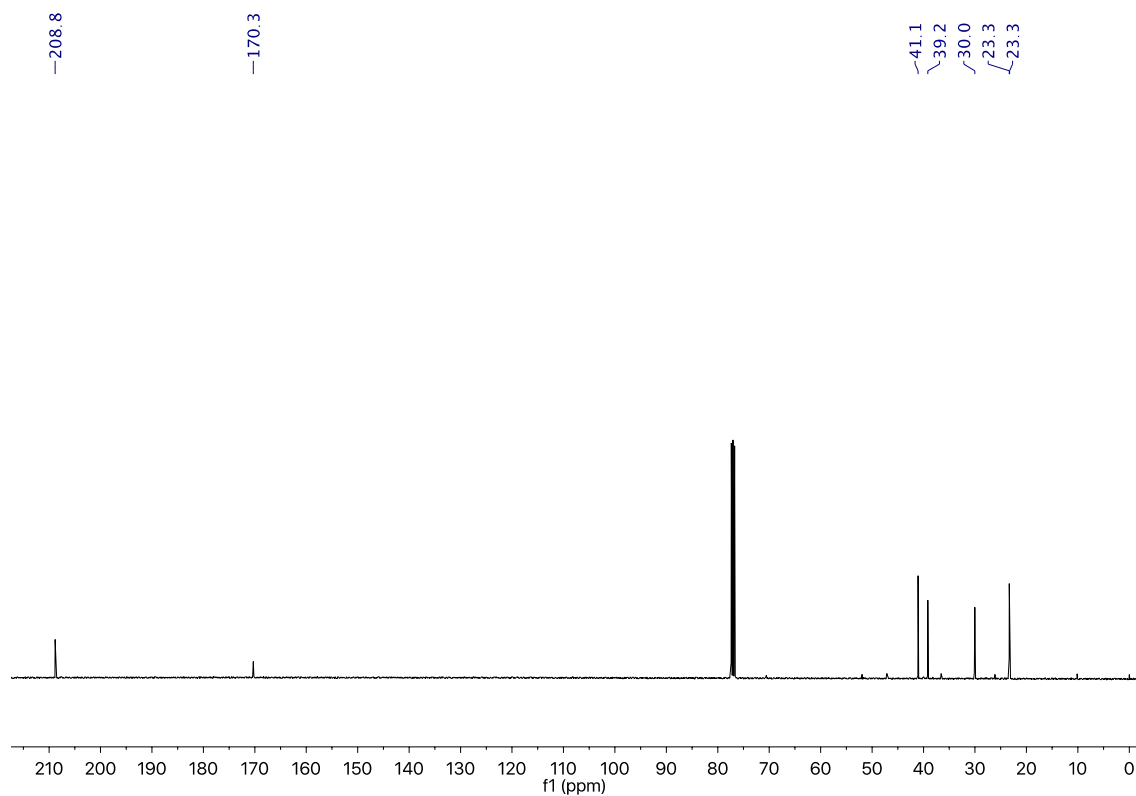
Figure S11. ^{13}C{^{1}H}-NMR of **17b** in CDCl$_3$
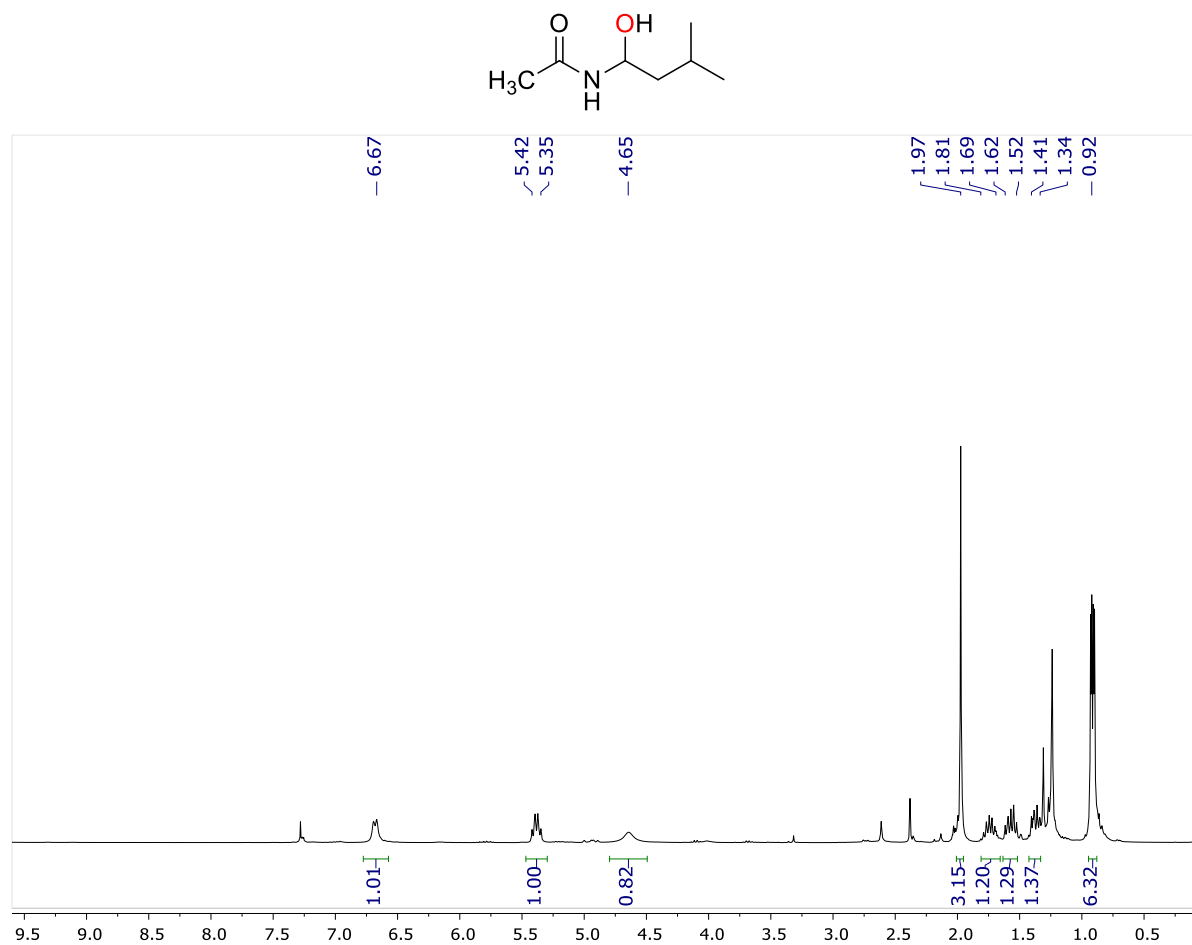
Figure S12. ^{1}H-NMR of **18a** in CDCl[3]
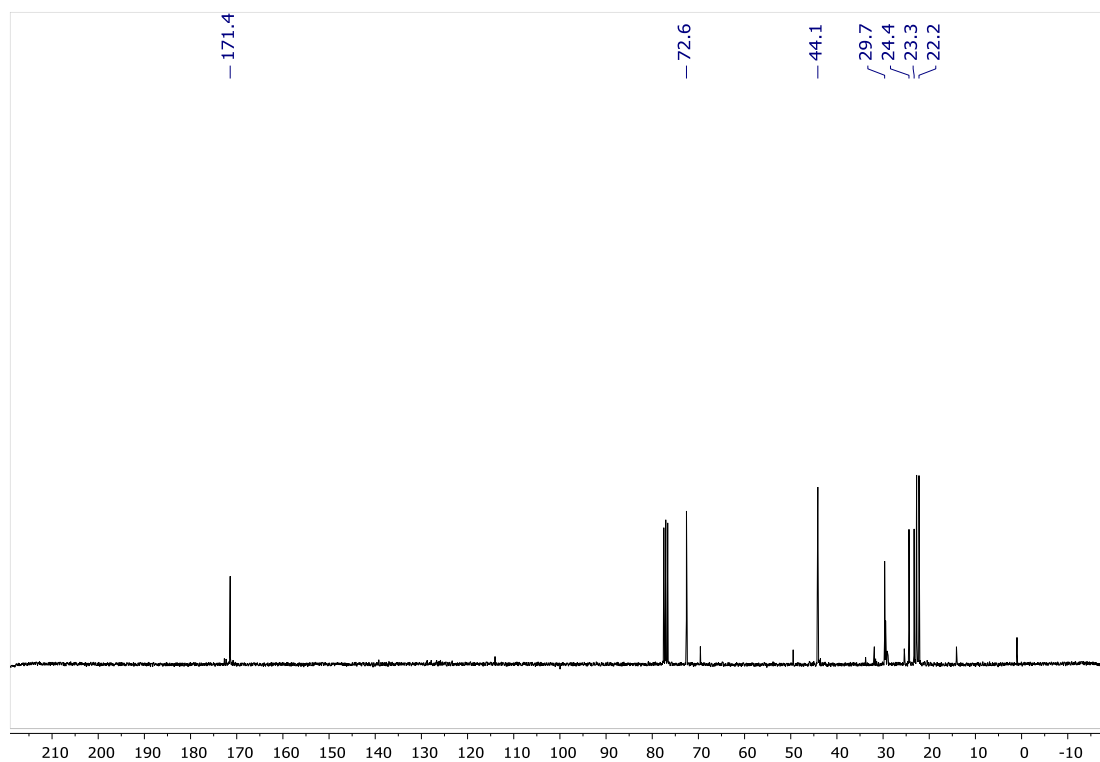
Figure S13. ^{13}C{^{1}H}-NMR of **18a** in CDCl[3]
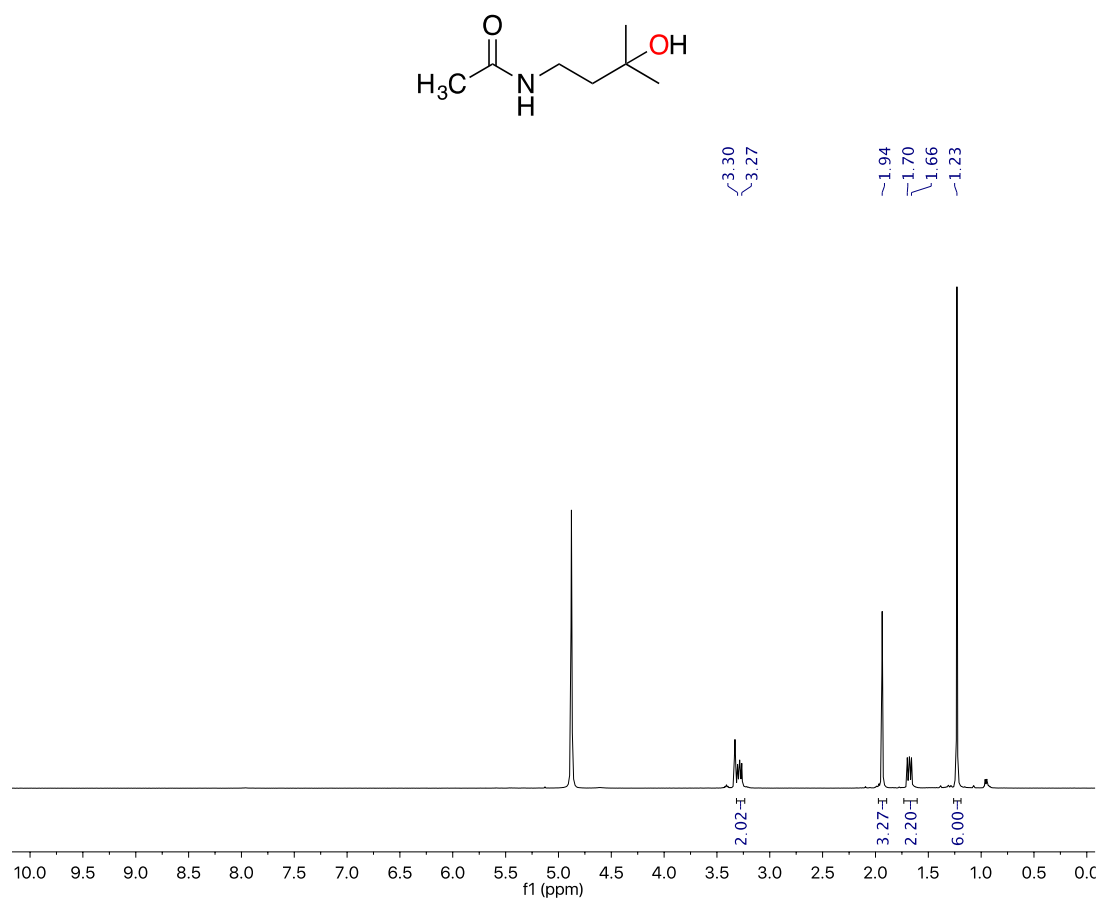
Figure S14. ^{1}H-NMR of **18b** in CDCl$_3$
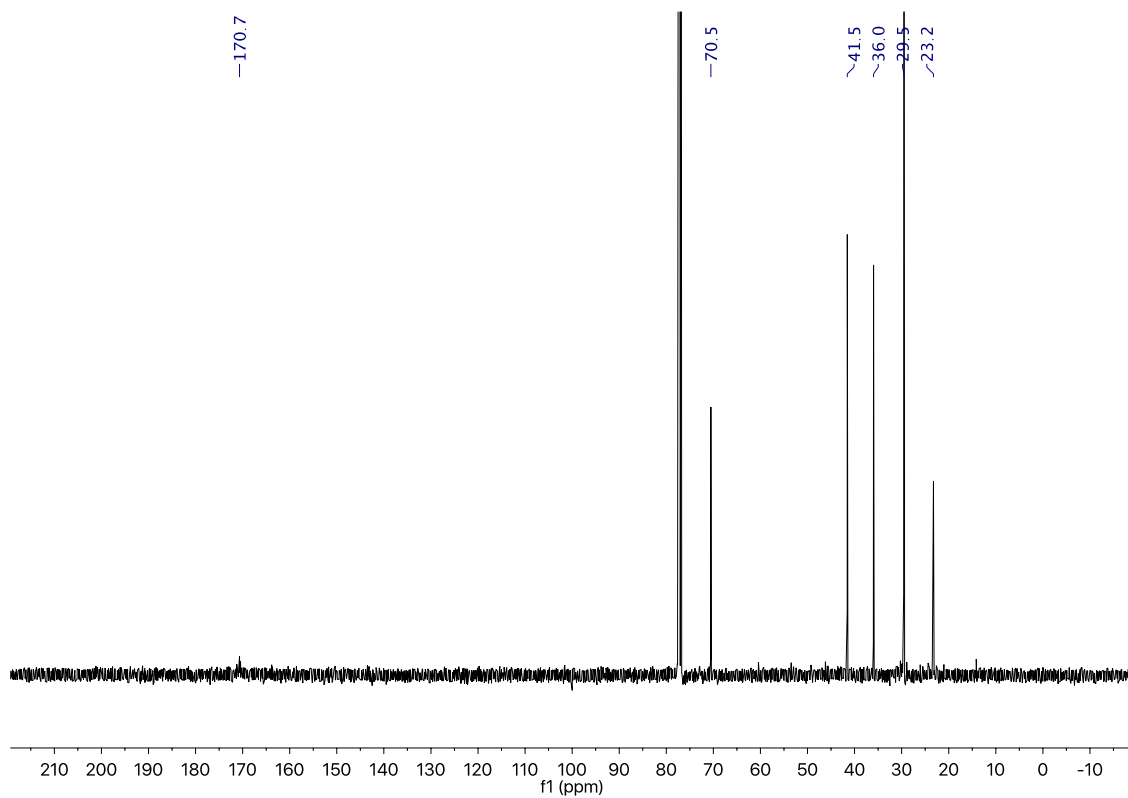
Figure S15. ^{13}C{^{1}H}-NMR of **18b** in CDCl$_3$
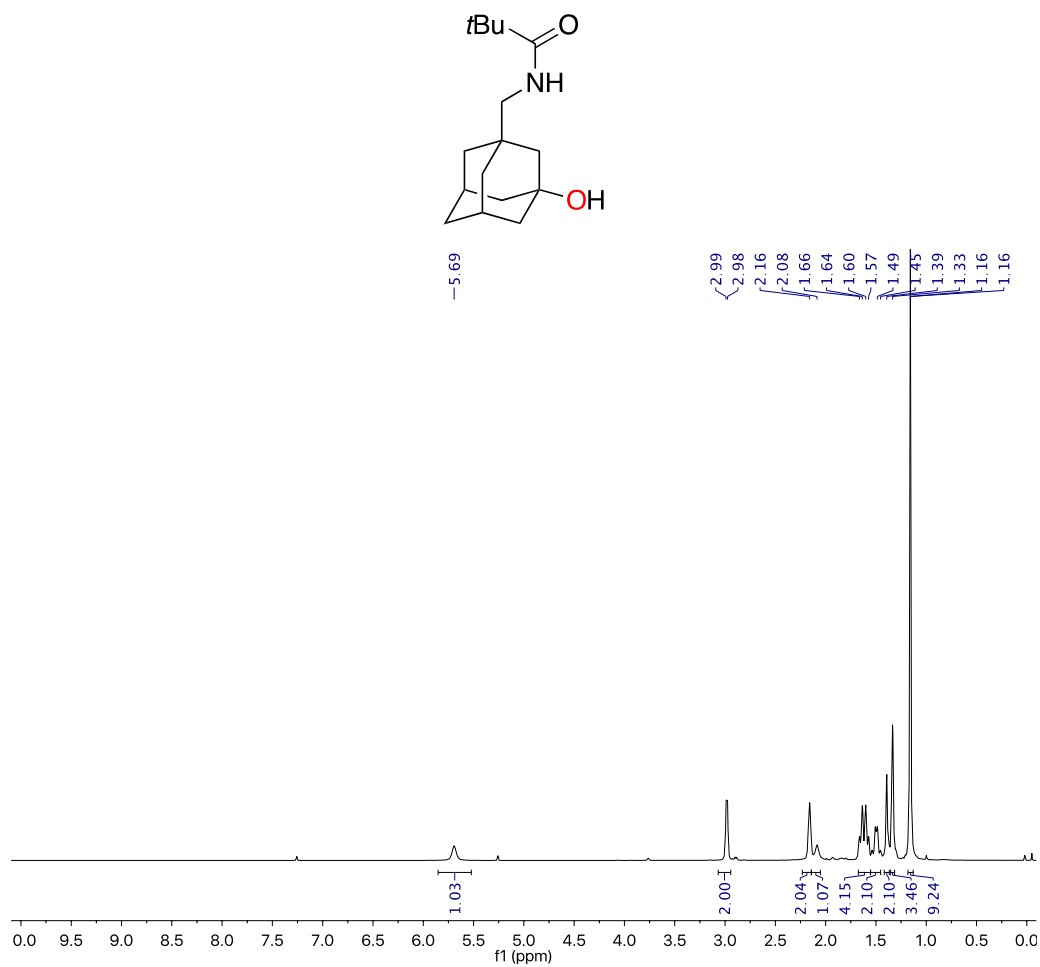
Figure S16. ^{1}H-NMR of **20c** in CDCl$_3$
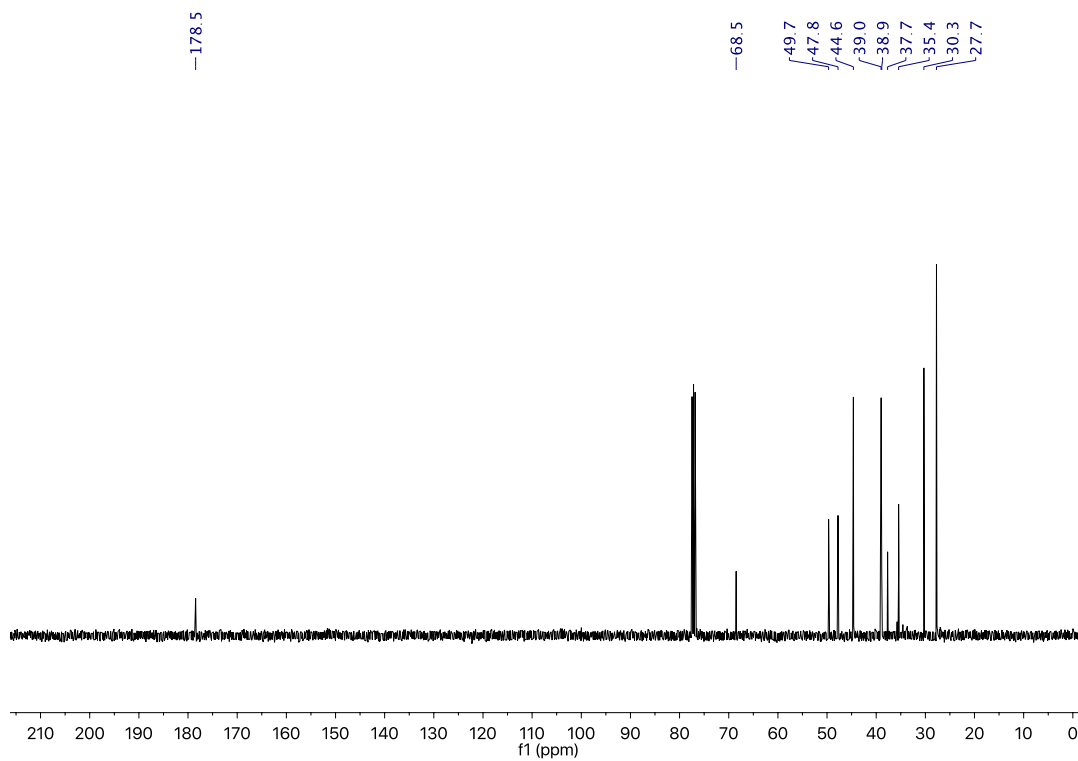
Figure S17. ^{13}C{^{1}H}-NMR of **20c** in CDCl$_3$
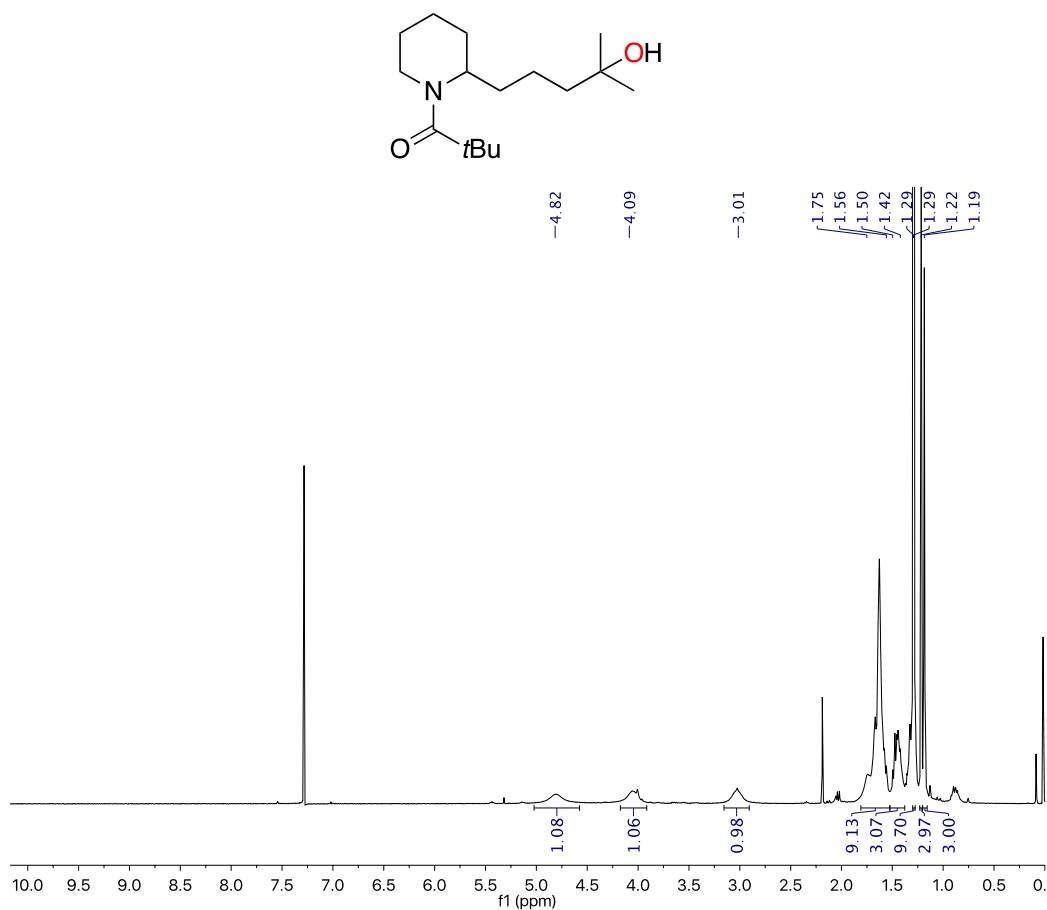
Figure S18. ^{1}H-NMR of **19b** in CDCl[3]
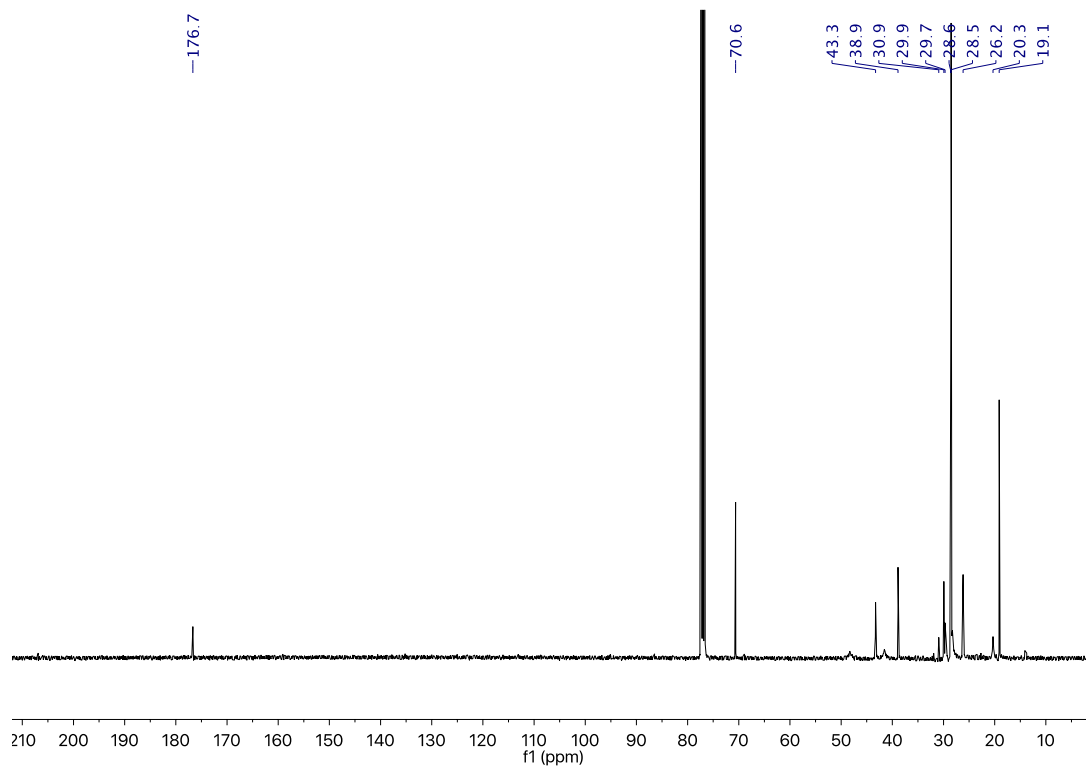
Figure S19. ^{13}C{^{1}H}-NMR of **19b** in CDCl[3]
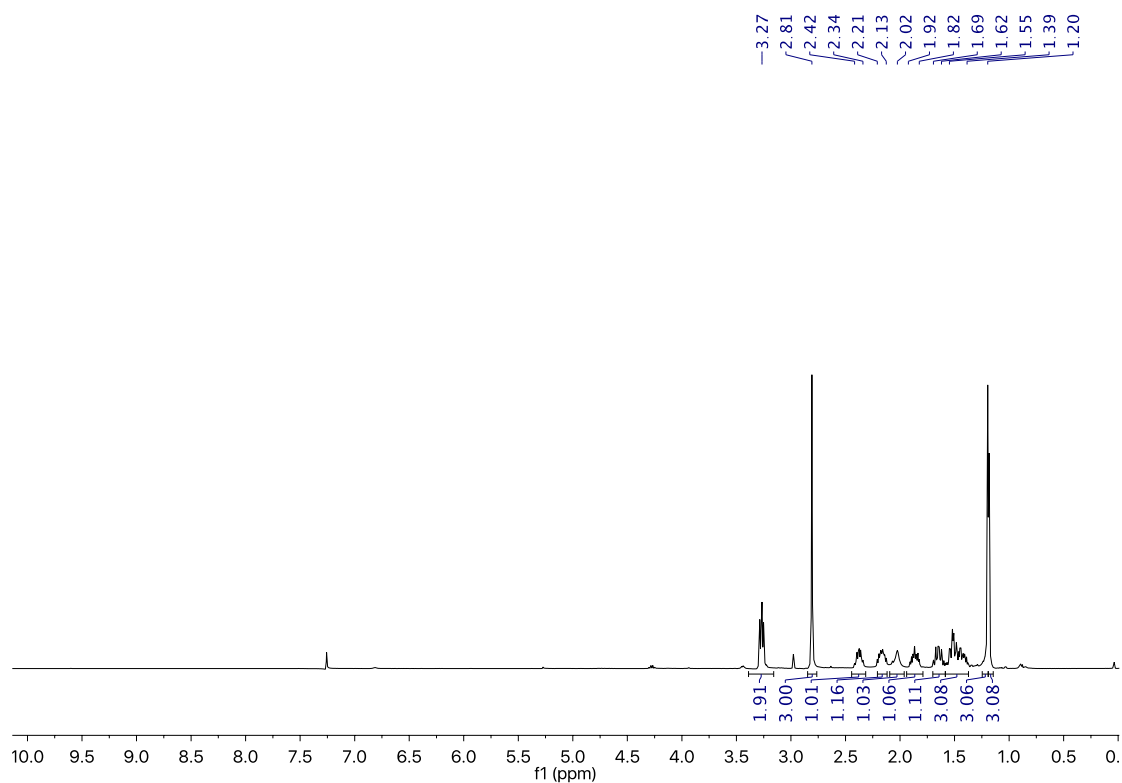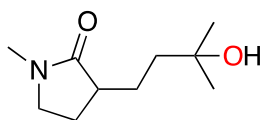
Figure S20. ^{1}H-NMR of **21a** in CDCl$_3$
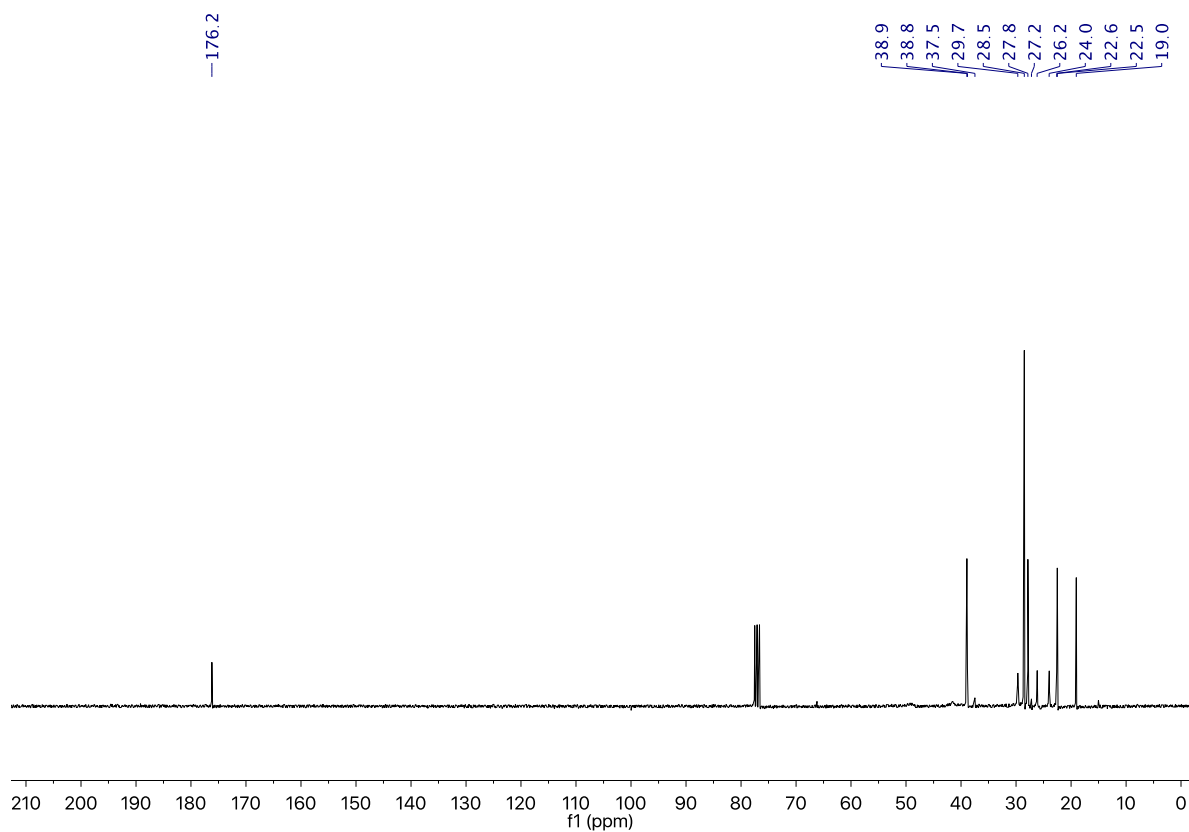
Figure S21. ^{13}C{^{1}H}-NMR of **21a** in CDCl$_3$

5.3 GC spectra of chiral products

The GC spectra of the racemic products were obtained by using the racemic **Mn(dMMpdp)** complex as catalyst in the oxidation of the corresponding substrates (Figures S22, S24 and S26). The representative GC spectra of chiral products shown in Figures S23, S25 and S27 were obtained using chiral **Mn(dMMpdp)** complex as catalysts using 2-ethylhexanoic acid (2-eha) as acid additive in TFE as solvent.
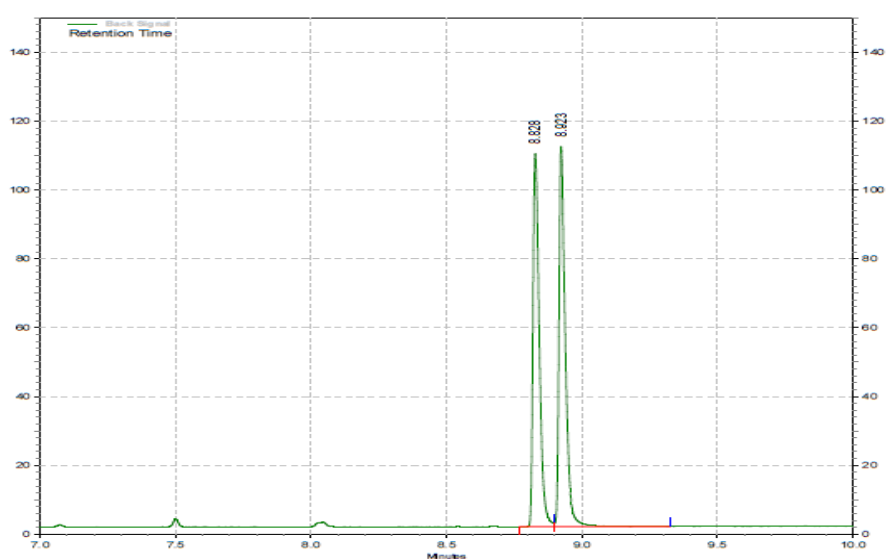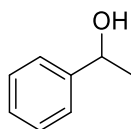
Figure S22. GC spectrum of racemic 1-phenylethanol (**P1a**)
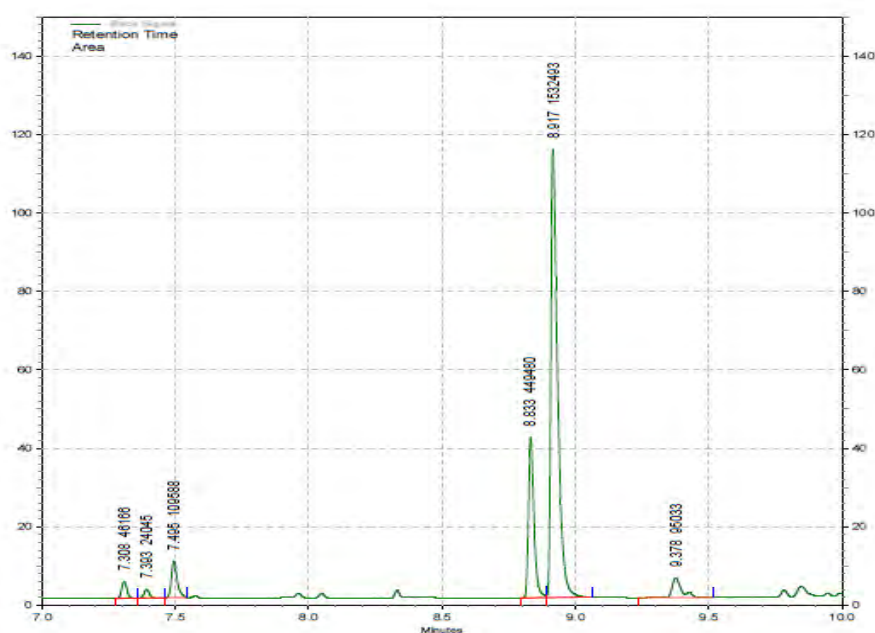
Figure S23. GC spectrum of chiral 1-phenylethanol (**P1a**)
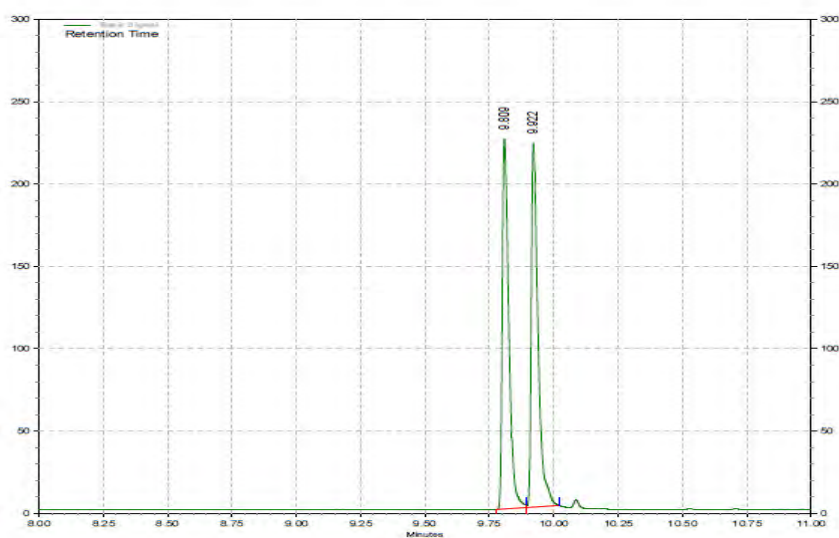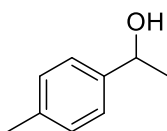
Figure S24. GC spectrum of racemic 4-methyl-1-phenylethanol (**P2a**)
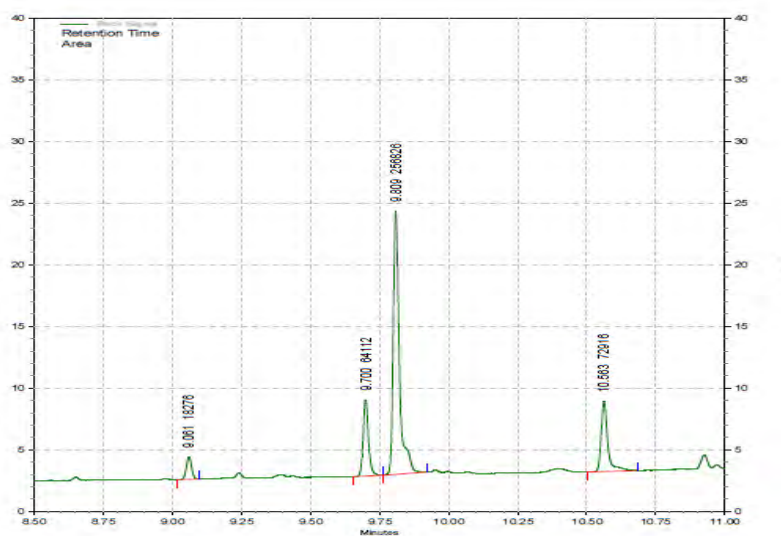
Figure S25. GC spectrum of chiral 4-methyl-1-phenylethanol (**P2a**)
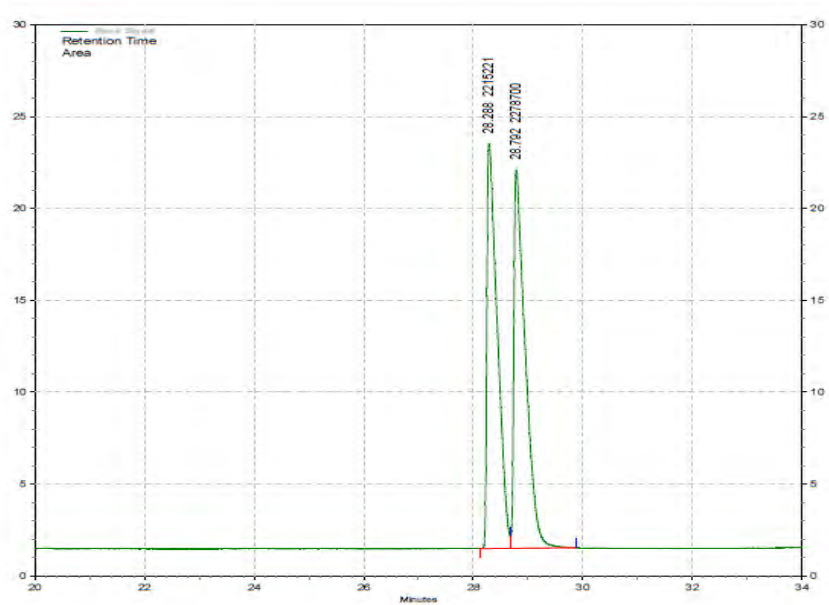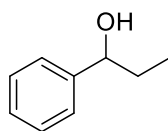
Figure S26. GC spectrum of racemic 1-phenyl-1-propanol (**7a**)
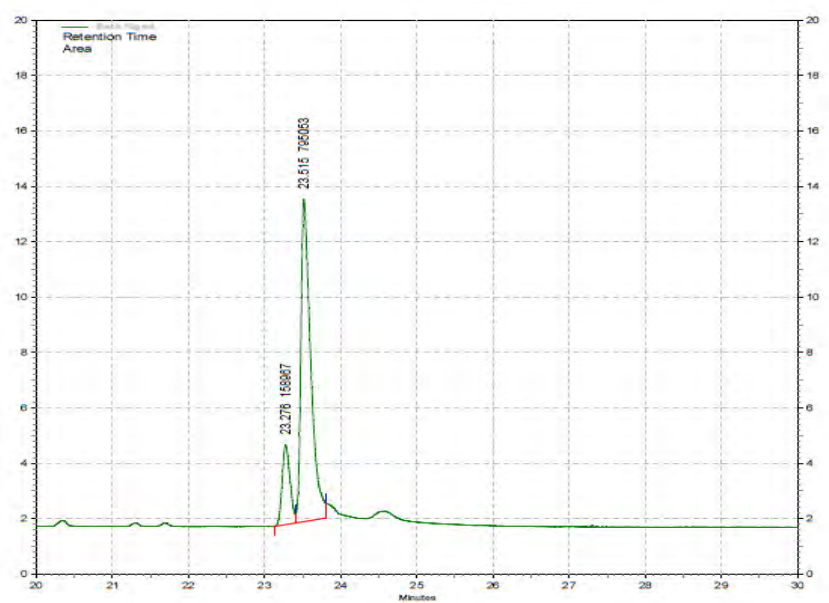
Figure S27. GC spectrum of chiral 1-phenyl-1-propanol (**7a**)

6. References

(1) Chen, M. S.; White, M. C. A Predictably Selective Aliphatic C – H Hydroxylation Reaction. *Science* **2007**, *318*, 783-787.

(2) Costas, M.; Tipton, A. K.; Chen, K.; Jo, D.-H.; Que Jr., L. Modeling Rieske Dioxygenases. The First Example of Iron-Catalyzed Asymmetric *cis*-Dihydroxylation of Olefins. *J. Am. Chem. Soc.* **2001**, *123*, 6722-6723.

(3) Cussó, O.; Garcia-Bosch, I.; Ribas, X.; Lloret-Fillol, J.; Costas, M. Asymmetric Epoxidation with H2O2 by Manipulating the Electronic Properties of Non-heme Iron Catalysts. *J. Am. Chem. Soc.* **2013**, *135*, 14871-14878.

(4) Font, D.; Canta, M.; Milan, M.; Cussó, O.; Ribas, X.; Klein Gebbink, R. J. M.; Costas, M. Readily Accessible Bulky Iron Catalysts exhibiting Site Selectivity in the Oxidation of Steroidal Substrates. *Angew. Chem. Int. Ed.* **2016**, *55*, 5776-5779.

(5) Murphy, A.; Dubois, G.; Stack, T. D. P. Efficient Epoxidation of Electron-Deficient Olefins with a Cationic Manganese Complex. *J. Am. Chem. Soc.* **2003**, *125*, 5250-5251.

(6) Ottenbacher, R. V.; Bryliakov, K. P.; Talsi, E. P. Non-Heme Manganese Complexes Catalyzed Asymmetric Epoxidation of Olefins by Peracetic Acid and Hydrogen Peroxide. *Adv. Synth. Catal.* **2011**, *353*, 885-889.

(7) Cussó, O.; Garcia-Bosch, I.; Font, D.; Ribas, X.; Lloret-Fillol, J.; Costas, M. Highly Stereoselective Epoxidation with H_2O_2 Catalyzed by Electron-Rich Aminopyridine Manganese Catalysts. *Org. Lett.* **2013**, *15*, 6158-6161.

(8) Milan, M.; Bietti, M.; Costas, M. Highly Enantioselective Oxidation of Nonactivated Aliphatic C–H Bonds with Hydrogen Peroxide Catalyzed by Manganese Complexes. *ACS Cent. Sci.* **2017**, *3*, 196-204.

(9) Deng, L.; Jacobsen, E. N. A practical, highly enantioselective synthesis of the taxol side chain via asymmetric catalysis. *The Journal of Organic Chemistry* **1992**, *57*, 4320-4323.

(10) Nishimoto, Y.; Yasuda, M.; Baba, A. Coupling Reaction of Alkyl Chlorides with Silyl Enolates Catalyzed by Indium Trihalide. *Organic Letters* **2007**, *9*, 4931-4934.

(11) Milan, M.; Carboni, G.; Salamone, M.; Costas, M.; Bietti, M. Tuning Selectivity in Aliphatic C–H Bond Oxidation of N-Alkylamides and Phthalimides Catalyzed by Manganese Complexes. *ACS Catalysis* **2017**, *7*, 5903-5911.

(12) Nanjo, T.; de Lucca, E. C.; White, M. C. Remote, Late-Stage Oxidation of Aliphatic C–H Bonds in Amide-Containing Molecules. *Journal of the American Chemical Society* **2017**, *139*, 14586-14591.

(13) Howell, J. M.; Feng, K. B.; Clark, J. R.; Trzepkowski, L. J.; White, M. C. Remote Oxidation of Aliphatic C-H Bonds in Nitrogen-Containing Molecules. *J. Am. Chem. Soc.* **2015**, *137*, 14590-14593.

(14) Ishikawa, H.; Colby, D. A.; Seto, S.; Va, P.; Tam, A.; Kakei, H.; Rayl, T. J.; Hwang, I.; Boger, D. L. Total Synthesis of Vinblastine, Vincristine, Related Natural Products, and Key Structural Analogues. *Journal of the American Chemical Society* **2009**, *131*, 4904-4916.

(15) Kim, H.; Lee, C. Nickel-Catalyzed Reductive Cyclization of Organohalides. *Organic Letters* **2011**, *13*, 2050-2053.

(16) Abraham, R. J.; Mobli, M. *Modelling ^{1}H NMR Spectra of Organic Compounds*; John Wiley & Sons: Wiltshire, 2008.

(17) Kamata, K.; Yonehara, K.; Nakagawa, Y.; Uehara, K.; Mizuno, N. Efficient stereo- and regioselective hydroxylation of alkanes catalysed by a bulky polyoxometalate. *Nat. Chem.* **2010**, *2*, 478-483.

(18) Shiner, V. J.; Ensinger, M. W.; Kriz, G. S.; Halley, K. A. .tau.-Silicon stabilization of carbonium ions in solvolysis. 4. Solvolysis of cis- and trans-3-(trimethylsilyl)cyclohexyl and -3-tert-butylcyclohexyl p-bromobenzenesulfonates. *J. Org. Chem.* **1990**, *55*, 653-661.

(19) Solladié-Cavallo, A.; Ahmed, B.; Schmitt, M.; Garin, F. Heterogeneous hydrogenation of 1-naphtol and 2-naphtol over Ru/Al2O3: a simple ^{1}H NMR method for determination of the diastereoselectivity. *C. R. Chimie* **2005**, *8*, 1975-1980.

(20) Gómez, L.; Bioinspired iron and manganese catalysts for the effective and selective oxidation of alkanes and alkenes. *PhD thesis. University of Girona, 2010*.

(21) Horváth, G.; Kuszmann, J. The mass spectral fragmentation of 1,4-butanediol. *Org. Mass. Spectrom.* **1977**, *12*, 45-50.

Annex 2. Supporting Information Chapter IV

Spectroscopic and reactivity comparisons between nonheme oxoiron(IV) and oxoiron(V) species bearing the same ancillary ligand

V. Dantignana, J. Serrano-Plana, A. Draksharapu, C. Magallón, S. Banerjee, R. Fan, I. Gamba, Y. Guo, L. Que Jr.,* Miquel Costas*, A. Company,*

Table of contents

1. Characterization of d$_4$-PyNMe$_3$, d$_4$-1·CF$_3$SO$_3$ and 1·SbF$_6$
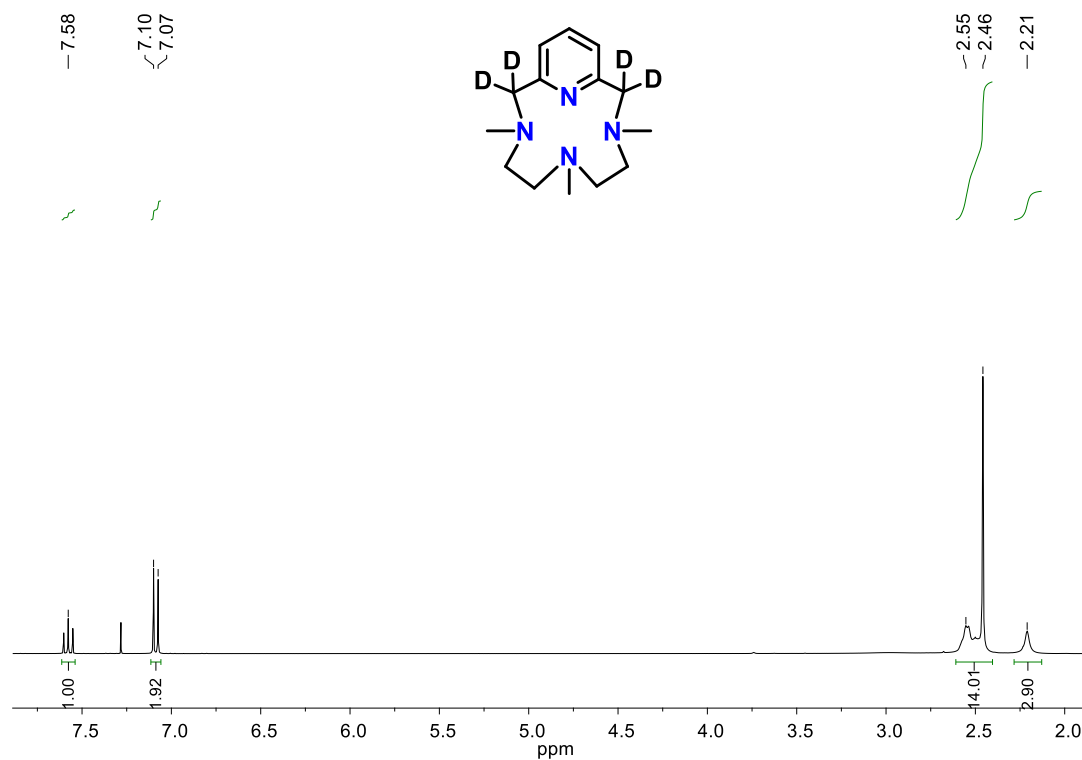
Figure S1. ^{1}H-NMR spectrum of **d$_4$-PyNMe$_3$** in CDCl$_3$ at 298 K (400 MHz).
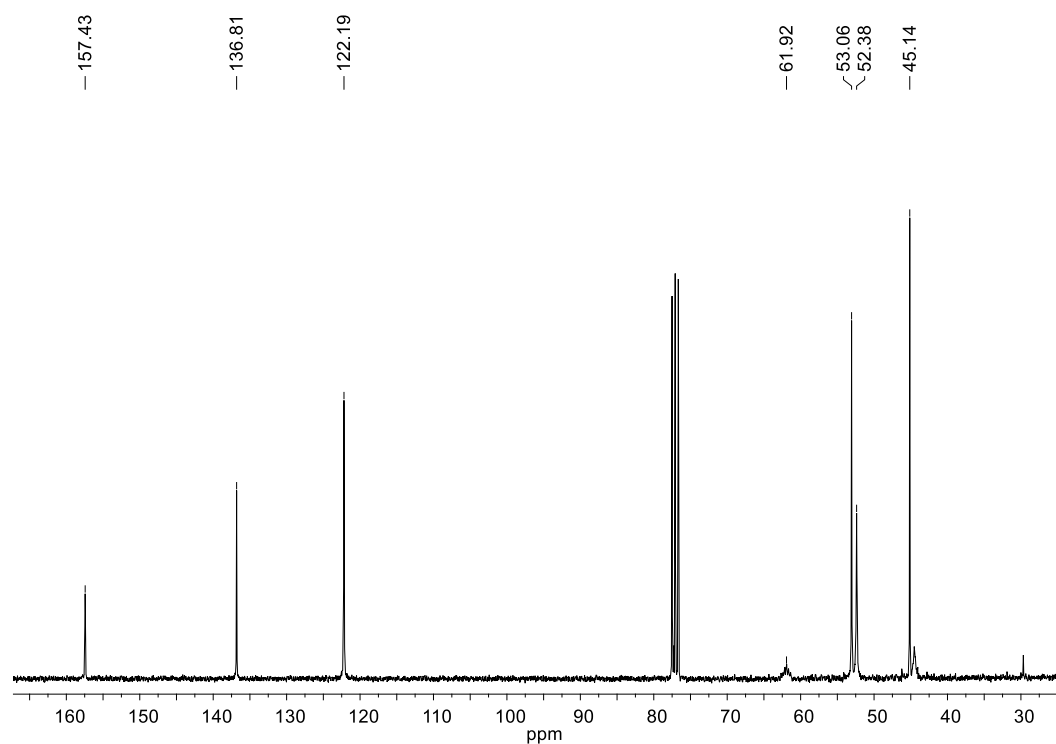
Figure S2. ^{13}C-NMR spectrum of **d$_4$-PyNMe$_3$** in CDCl$_3$ at 298 K (400 MHz).
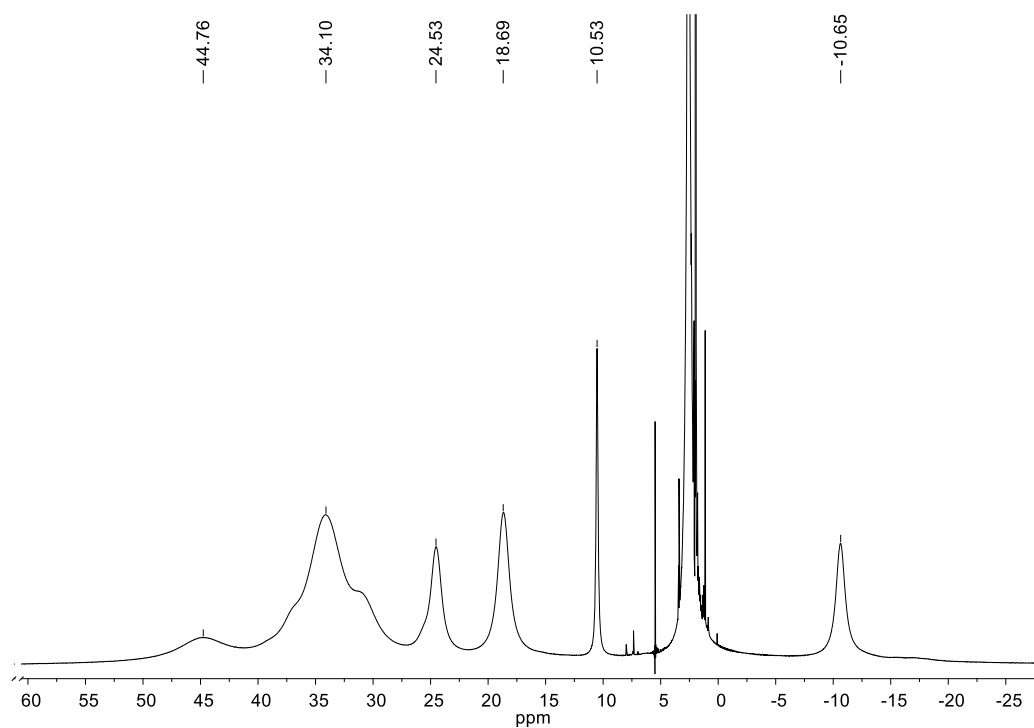
Figure S3. ¹H-NMR spectrum of [Fe^{II}(CF_3SO_3)_2(d_4-PyNMe_3)] (**d_4-1•CF_3SO_3**) in CD_3CN at 243 K (400 MHz).
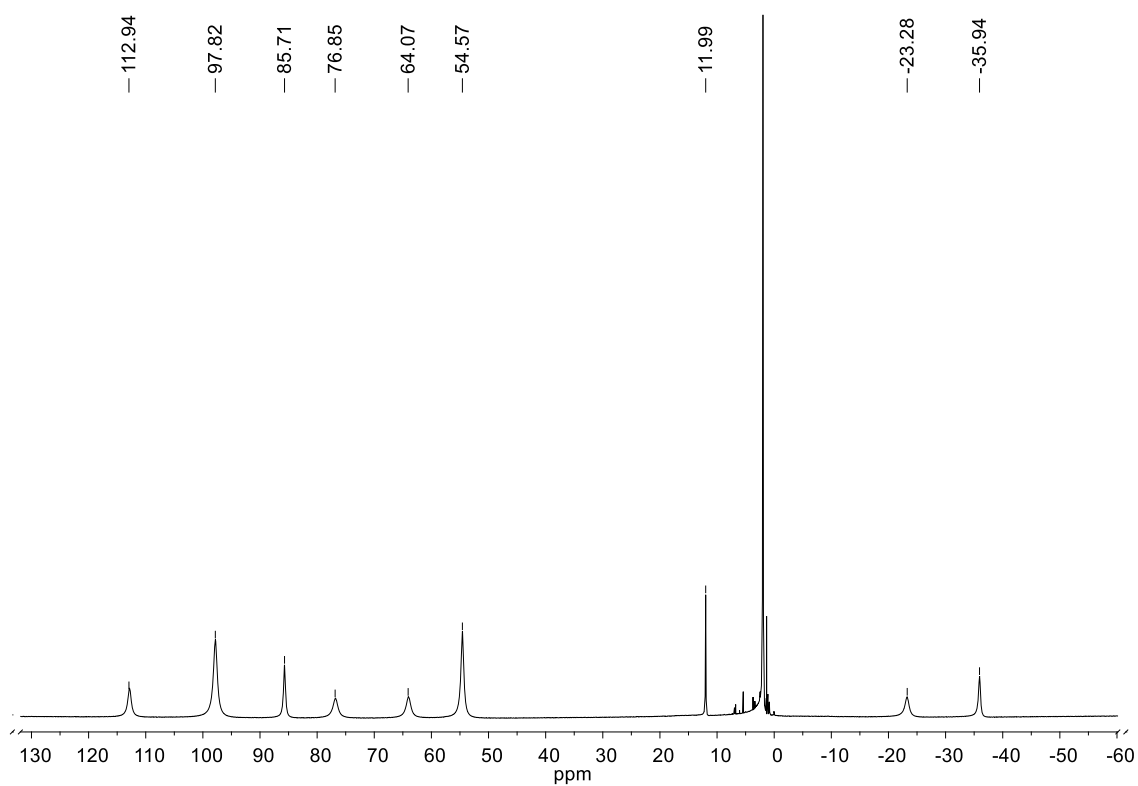
Figure S4. ¹H-NMR spectrum of [Fe^{II}(PyNMe_3)(CH_3CN)_2](SbF_6)_2 (**1•SbF_6**) in CD_3CN at 298 K (400 MHz).

Crystal structure determination for 1•SbF₆

Brown crystals of **C₁₈H₃₀FeN₆F₁₂Sb₂** were grown from slow diffusion of diethyl ether in a CH₂Cl₂/CH₃CN solution of the compound, and used for low temperature (100(2) K) X-ray structure determination. The measurement was carried out on a *BRUKER SMART APEX CCD* diffractometer using graphite-monochromated Mo *K*α radiation (λ = 0.71073 Å) from an X-ray tube. The measurements were made in the range 2.080 to 28.087° for θ. Full-sphere data collection was carried out with ω and φ scans. A total of 42613 reflections were collected of which 6704 [R(int) = 0.0380] were unique. Programs used: data collection, Smart;[1] data reduction, Saint+;[2] absorption correction, SADABS.[3] Structure solution and refinement was done using SHELXTL.[4]

The structure was solved by direct methods and refined by full-matrix least-squares methods on F². The non-hydrogen atoms were refined anisotropically. The H-atoms were placed in geometrically optimized positions and forced to ride on the atom to which they are attached. The data was treated with the TWINROTMAT option of PLATON[5] to find a twin law in which the structure was refined as a two twin component. Twin law: 0 0 -1 0 -1 0 -1 0 0

Figure S5. Thermal ellipsoid plot (50% probability) of [Feᴵᴵ(PyNMe₃)(CH₃CN)₂](SbF₆)₂ (**1•SbF₆**). Hexafluoroantimoniate anions and hydrogen atoms have been omitted for clarity.

Table S1. Crystal data for $[Fe^{II}(PyNMe_3)(CH_3CN)_2](SbF_6)_2$ (**1·SbF$_6$**).

Empirical formula	$C_{18}H_{30}F_{12}FeN_6Sb_2$
Formula weight	857.83
Temperature	100(2) K
Wavelength	0.71073 Å
Crystal system, space group	Monoclinic, P 21/n
Unit cell dimensions	a = 19.573(3) Å α = 90º
	b = 8.2260(11) Å β = 117.913(2)º
	c = 19.595(3) Å γ = 90º
Volume	2787.9(6) Å^3
Z, Calculated density	4, 2.044 Mg/m^3
Absorption coefficient	2.538 mm^{-1}
F(000)	1664
Crystal size	0.28 x 0.28 x 0.28 mm
θ range for data collection	2.080 to 28.087º
Limiting indices	-25<=h<=25, -10<=k<=10, -25<=l<=25
Reflections collected / unique	42613 / 6704 [R(int) = 0.0380]
Completeness to θ = 25.242	99.8 %
Absorption correction	Empirical
Max. and min. transmission	1.0 and 0.802306
Refinement method	Full-matrix least-squares on F^2
Data / restraints / parameters	6704 / 0 / 358
Goodness-of-fit on F^2	1.043
Final R indices [I>2σ(I)]	R1 = 0.0268, wR2 = 0.0711
R indices (all data)	R1 = 0.0280, wR2 = 0.0720
Extinction coefficient	n/a
Largest diff. peak and hole	1.742 and -0.695 e.Å^{-3}

Table S2. Selected bond lengths (Å) and angles (º) for $[Fe^{II}(PyNMe_3)(CH_3CN)_2](SbF_6)_2$ (**1·SbF$_6$**).

Fe(1)-N(1)	1.905(3)	N(5)-Fe(1)-N(3)	91.82(11)
Fe(1)-N(3)	2.049(3)	N(1)-Fe(1)-N(2)	82.62(12)
Fe(1)-N(2)	2.066(3)	N(5)-Fe(1)-N(2)	97.90(11)
Fe(1)-N(4)	2.076(3)	N(6)-Fe(1)-N(2)	95.23(11)
		N(3)-Fe(1)-N(2)	85.55(11)
		N(1)-Fe(1)-N(4)	82.47(12)
N(1)-Fe(1)-N(6)	86.22(11)	N(5)-Fe(1)-N(4)	97.80(12)
N(5)-Fe(1)-N(6)	88.91(12)	N(6)-Fe(1)-N(4)	93.65(11)
N(1)-Fe(1)-N(3)	93.04(11)	N(3)-Fe(1)-N(4)	85.37(11)

2. XAS and Mössbauer analysis for 2a and 2b

2.1 XAS analysis

Table S3. Summary of XAS analysis results for **2a** and **2b**.

Species	K-edge energy (eV)	Pre-edge energy (eV)	Pre-edge area (units)	EXAFS analysis		
				N path	r (Å)	σ^2 (x10^{-3})
2a	7124.8	7114.1	20.9	1 N/O	1.66	1.7
				5 N/O	2.00	7.0
				6 C	2.9	1.7
				3 C	3.04	3.2
2b	7124.4	7114.0	19.6	0.8 N/O	1.65	2.9
				5 N/O	2.00	6.0
				5 C	2.84	3.0
				4 C	2.96	1.7

2.2 Mössbauer analysis
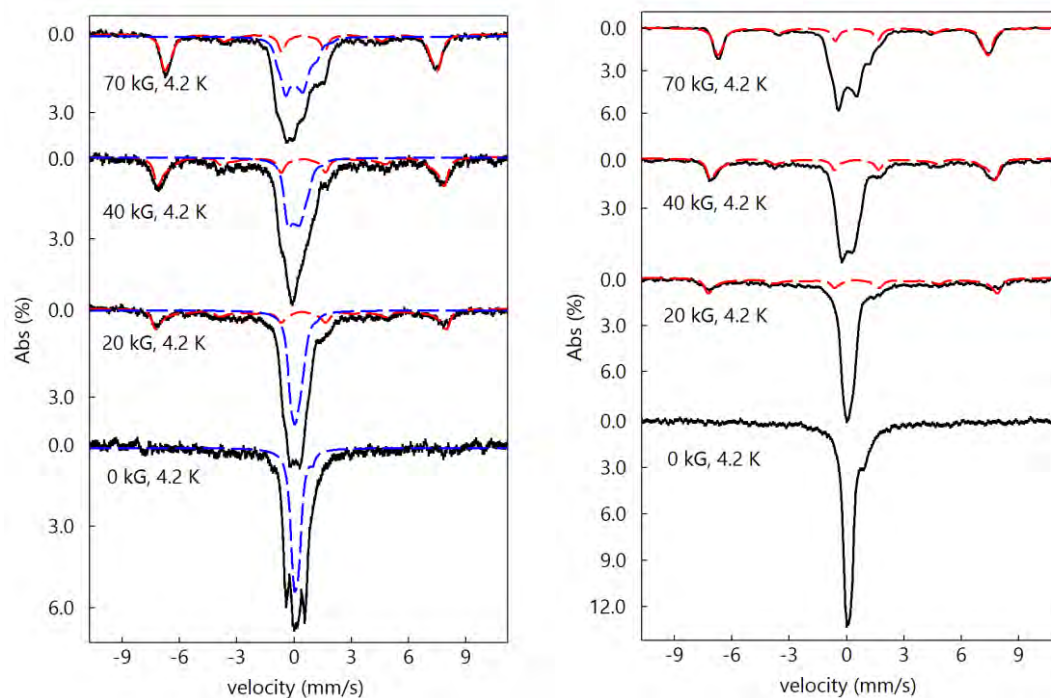
Figure S6. Raw Mössbauer spectra of the samples that mainly contain **2a** (left) or **2b** (right), respectively. Due to the inevasible conversion from species **2a** to species **2b**, the sample on which we collected the spectrum on the left contains almost an equal amount of species **2b**. The dashed red traces in both spectra represent the simulated spectra of an S=5/2 Fe(III) byproduct. The dashed blue traces in the left figure represent the simulated spectra of species **2b**.

- Techniques applied for obtaining "pure" spectra of **2a** and **2b** from the raw spectra

At first, we started from the right figure in Figure S6 as only two species can be discerned in this spectrum. By masking the middle doublets, we can use a typical high-spin ferric parameter set ($A/g_n\beta_n$ = (-21, -21, -21)T, δ = 0.45 mm/s, ΔE_q = -0.90m/s, η = 0.3) to simulate the remaining spectral features at various external fields. By removing the high-spin species with the simulated trace, we can obtain the pure spectrum of **2b** shown in Figure 2.

Secondly, the left figure in Figure S6 contains three species: **2a**, **2b** and high-spin ferric. We removed the high-spin ferric component with the same technique introduced above, and then estimated the percentages of species **2a** and **2b** from zero-field doublets. With simulation parameters of **2b** obtained from above, we can subtract the portion of **2b** from the spectra under various external fields to obtain a "pure" spectrum of **2a** (shown in Figure 2 of main text).

Table S4. Simulation parameters for the two S = 1 species in Figure 2 in the main text.

Site	S = 1 (**2b**)		S = 1 (**2a**)	
Type	Exp	Calc'd	Exp	Calc'd
D	24.5	-	25.0	-
E/D	0.0	-	0.0	-
δ (mm/s)	0.09	0.13	0.07	0.10
ΔE_q (mm/s)	0.24	0.29	0.98	0.86
η	1.0	0.4	0.0	0.1
Ax (kG)	-200	-	-250	-
Ay (kG)	-200	-	-250	-
Az (kG)	N.D.	-	N.D.	-
Percentage over total abs.	60%	-	35%	-

3. NMR characterization of 2b and d₄-2b
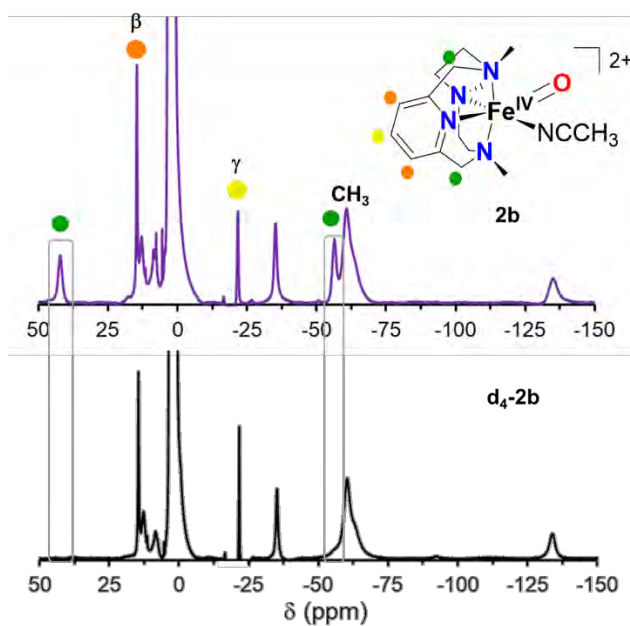
Figure S7. ^{1}H-NMR spectra of **2b** and **d₄-2b** in CD₃CN at -40 ºC. Peak assignments are as follows: benzylic protons at 42 ppm (2H) and -56 ppm (2H); aliphatic CH₂ at 12.9 (2H), 8.5 ppm (2H), -35 ppm (2H) and -133 ppm (2H); CH₃ at -60 ppm (9H); pyridine β at 15 ppm (2H) and pyridine γ at -22 ppm (1H).
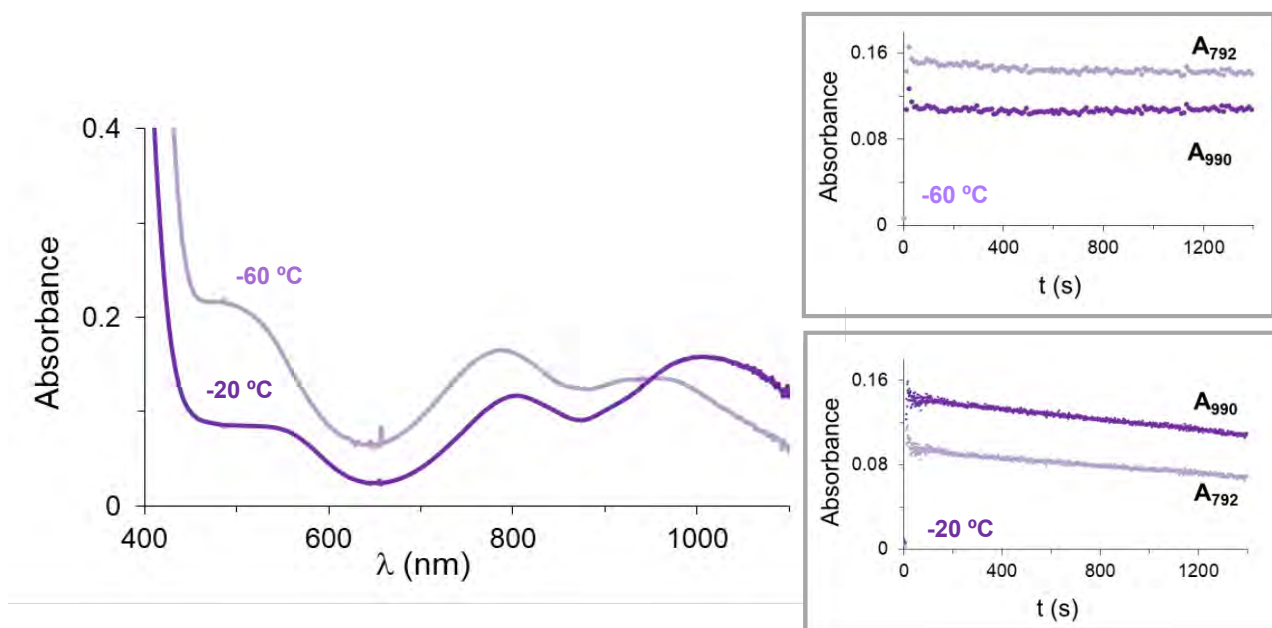
4. Conversion of 2a to 2b and comparison of reactivity

Figure S8. Left: UV-vis absorption spectra of **2** obtained upon reaction of a solution of **1** (1 mM) in CH$_3$CN:CH$_2$Cl$_2$ 1:1 with 1.1 equiv Bu$_4$NIO$_4$ and 0.8 equiv TfOH at -60 ºC (**2a+2b**, light purple line) or -20 ºC (**2b**, dark purple line). Right: kinetic traces at 792 and 990 nm for the reaction at -60 ºC (top) and -20 ºC (bottom).
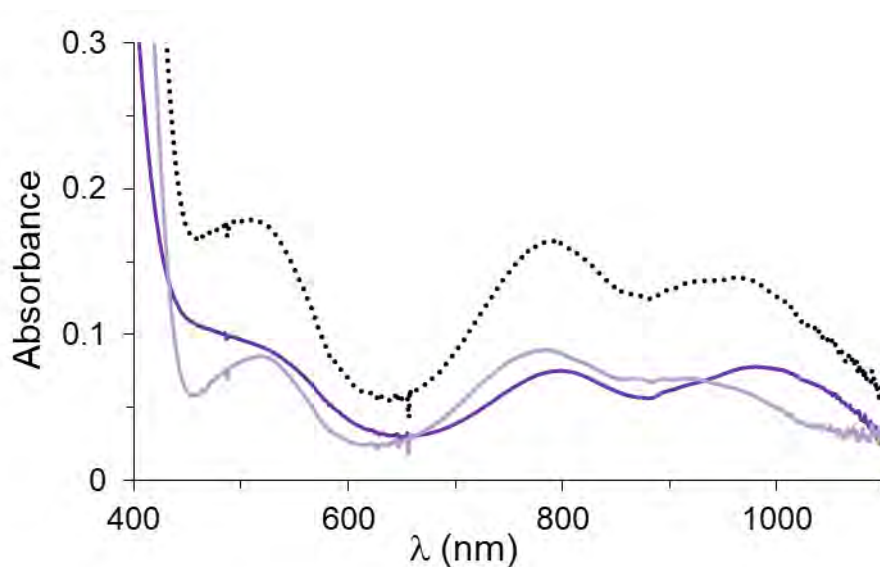
Figure S9. UV-vis absorption spectra of **2a+2b** (dashed black line) generated at -60 ºC upon reaction of a solution of **1** (1 mM) in CH$_3$CN:CH$_2$Cl$_2$ 1:1 with 1.1 equiv Bu$_4$NIO$_4$ and 0.8 equiv TfOH. According to spectroscopic data, this spectrum corresponds to an approximately 1:1 mixture of **2a** and **2b**. The deconvoluted spectrum of **2a** (light purple line) has been obtained by subtracting the contribution of **2b** (dark purple line). The contribution of **2b** corresponds to its UV-vis spectrum at -60 ºC which has been divided by two to get the concentration of **2b** in the mixture.
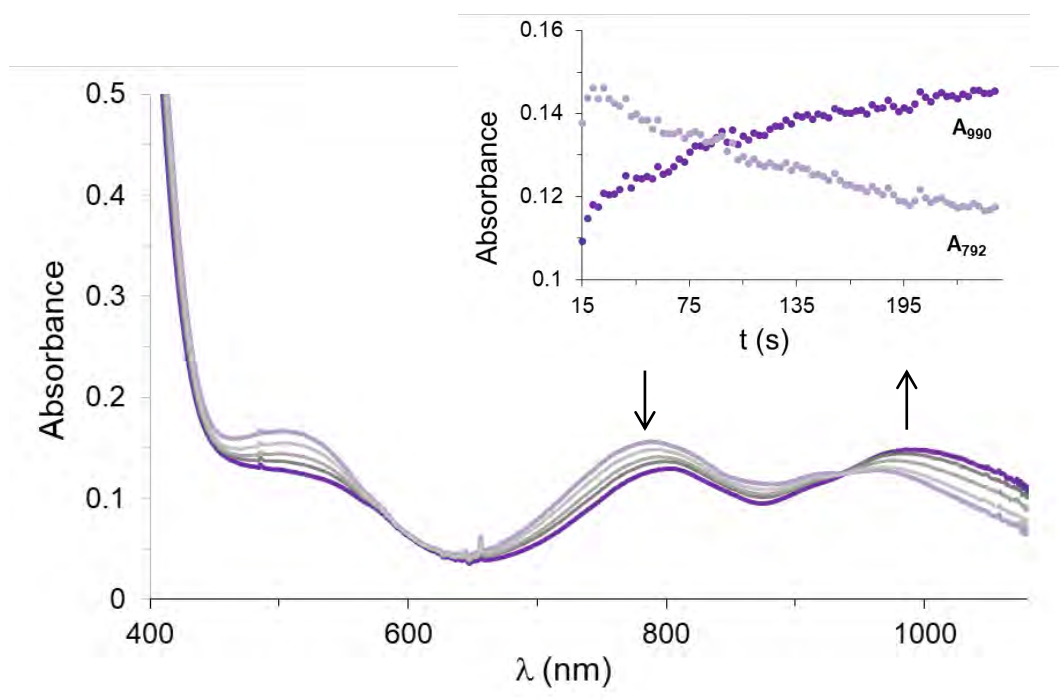
Figure S10. Spectral changes upon reaction of a solution of **1•SbF₆** (1 mM) in CH₃CN with 1.1 equiv Bu₄NIO₄ and 0.8 equiv TfOH at -40 ºC (light purple: initial spectra; dark purple: final spectra). Inset: kinetic traces at 792 and 990 nm.
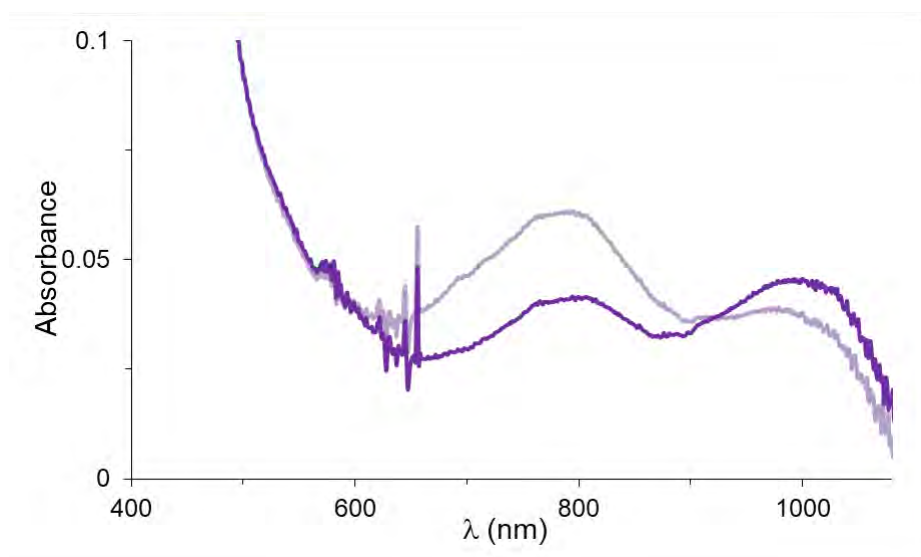

Figure S11. UV-vis absorption spectra of **2** upon reaction of a solution of **1** (1 mM) in CH₃CN with 1.1 equiv 2-*t*BuSO₂-C₆H₄IO at -40 ºC (light purple: initial spectra; dark purple: final spectra).

4.1 Reactivity of 2a and 2b

According to spectroscopic data isomer **2a** is obtained in an approximately equimolar mixture with **2b**. Instead, compound **2b** can be obtained without contamination of **2a** at -40 °C after isomerization. As a consequence, while the decay of **2b** upon reaction with a substrate can be fitted to a single exponential function (f = y_0 + a*e$^{(-b*x)}$), the decay of **2a** has to be fitted to a double exponential function (f = y_0 + a*e$^{(-b*x)}$ + c*e$^{(-d*x)}$), due to the contamination by **2b**. In this case, the experimental k_{obs} value for the reaction of **2b** with substrates can be fixed to finally get the k_{obs} value for the reaction of **2a**. Alternatively, the contribution of **2b** to the decay of the 792 nm band of **2a** can be subtracted and the resulting data can be fitted to a single exponential function that corresponds to the decay of "pure" **2a**.
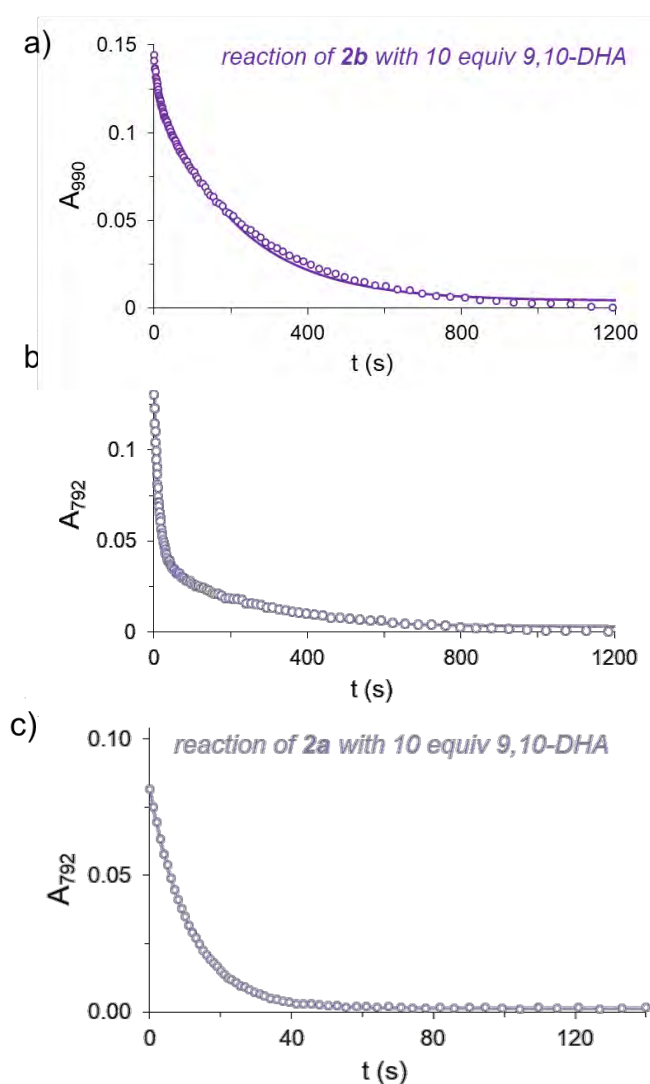
Figure S12. a) Kinetic trace at 990 nm for the reaction of **2b** with 10 equiv 9,10-dihydroanthracene in CH$_3$CN:CH$_2$Cl$_2$ 1:1 at -60 °C (empty circles) and its fitting to a single exponential function (solid line). b) Kinetic trace at 792 nm for the reaction of an approximately 1:1 mixture of **2a**:**2b** with 10 equiv 9,10-dihydroanthracene in CH$_3$CN:CH$_2$Cl$_2$ 1:1 at -60 °C (empty circles) and its fitting to a double exponential function (solid line). c) Kinetic trace at 792 nm for the reaction of **2a** with 10 equiv 9,10-dihydroanthracene in CH$_3$CN:CH$_2$Cl$_2$ 1:1 at -60 °C obtained after subtracting the contribution of **2b** in Figure S12b (empty circles) and its fitting to a single exponential function (solid line).
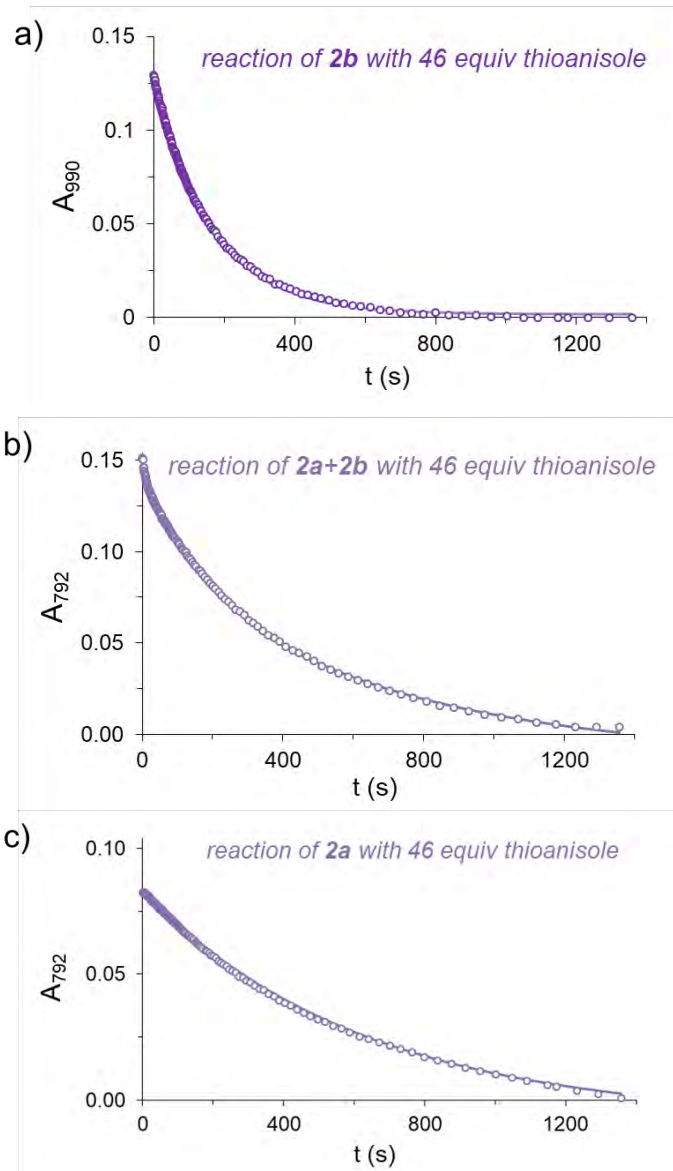
Figure S13. a) Kinetic trace at 990 nm for the reaction of **2b** with 46 equiv thioanisole in CH₃CN:CH₂Cl₂ 1:1 at -60 ⁰C (empty circles) and its fitting to a single exponential function (solid line). b) Kinetic trace at 792 nm for the reaction of an approximately 1:1 mixture of **2a**:**2b** with 46 equiv thioanisole in CH₃CN:CH₂Cl₂ 1:1 at -60 ⁰C (empty circles) and its fitting to a double exponential function (solid line). c) Kinetic trace at 792 nm for the reaction of **2a** with 46 equiv of thioanisole in CH₃CN:CH₂Cl₂ 1:1 at -60 ⁰C obtained after subtracting the contribution of **2b** in Figure S13b (empty circles) and its fitting to a single exponential function (solid line).

5. Reactivity of 2b

5.1 Oxygen atom transfer reactions

Under conditions of excess substrate, the decay of the absorption band of **2b** at 990 nm could be fitted to a single exponential function (Figure S14) indicating a pseudo-first order behavior from which the corresponding k_{obs} values could be extracted. The second order rate constants (k_x) could be calculated affording a value of 0.88 M^{-1}s^{-1} for the reaction with thioanisole. A plot of the logarithm of the reaction rates ratio (k_X/k_H) as a function of the corresponding Hammett parameter (σ_p) gave a good linear correlation with a negative slope (ρ = -1.77), indicating the electrophilic character of **2b** (Figure S15). The Hammett value (ρ) obtained for **2b** is in line with the ones previously reported for the sulfide oxidation carried out by well-defined oxoiron(IV) complexes. For example, Hammett values of -1.4 (at 0 ºC) and -1.5 (at -20 ºC) were described for the oxoiron(IV) complexes bearing pentadentate ligands N4Py and Bn-TPEN, respectively.[6] Similar values were obtained for oxoiron(IV) species with tetradentate ligands such as TPA (ρ = -1.6 at -45 ºC)[6] or Pytacn (ρ= -1.5 at 0 ºC).[7] [TPA = tris(pyridyl-2-methyl)amine; Pytacn = 1,4-dimethyl-7-(2-pyridylmethyl)-1,4,7-triazacyclononane].

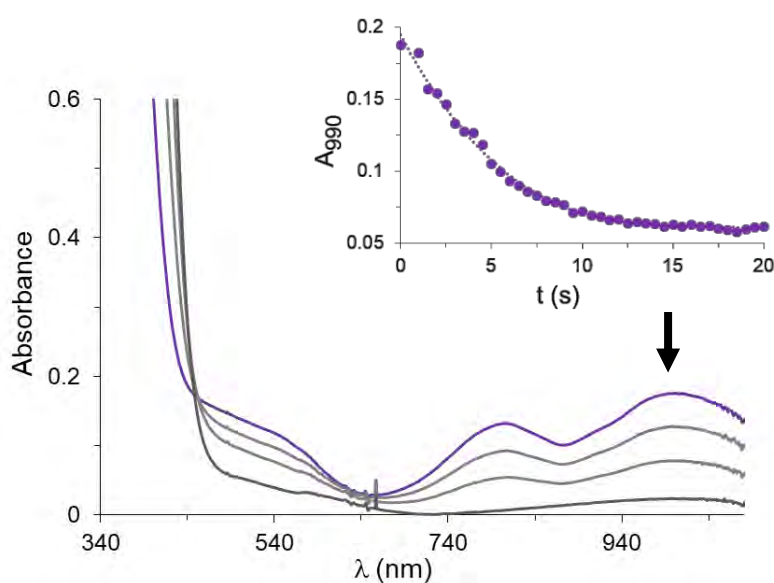**Figure S14.** Decay of **2b** upon reaction with 50 equiv of methyl *p*-tolyl sulfide at -40 ºC in CH$_3$CN. Inset: kinetic trace at 990 nm. [Fe] = 1.0 mM.
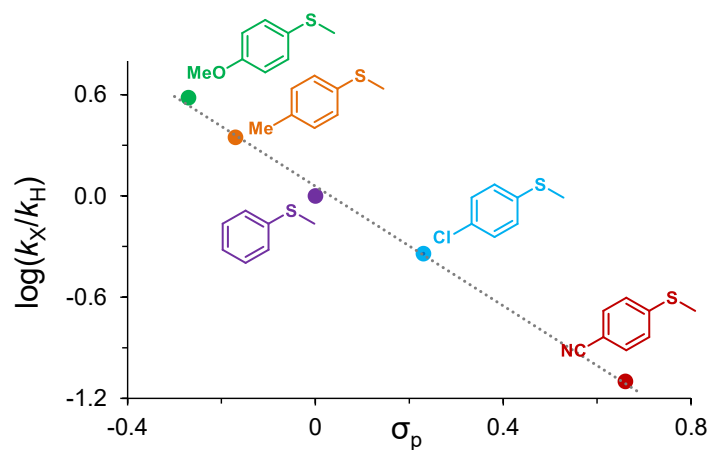
Figure S15. Hammett plot for the reaction of **2b** with *p*-X thioanisoles at -40 ºC in CH₃CN.
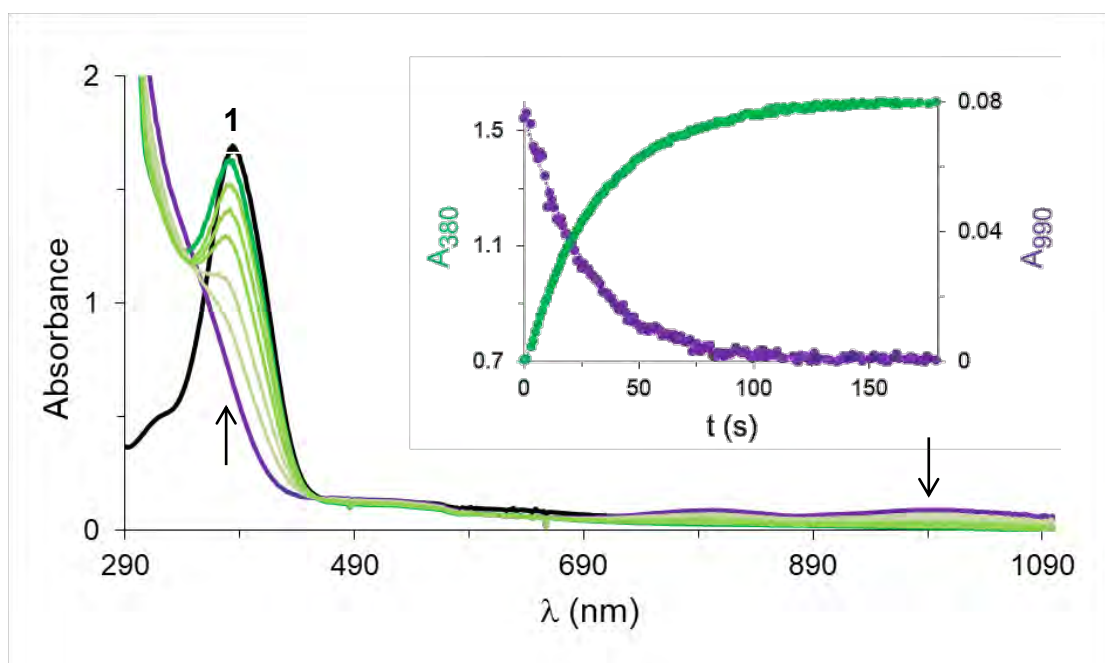

Figure S16. Recovery of **1** (green line) upon reaction of **2b** (dark purple line) with 62 equiv of thioanisole at -40 ºC in CH₃CN. The black line shows the initial spectrum of **1** before **2b** generation. Inset: kinetic traces at 990 nm and 380 nm. [**1**] = 0.5 mM.
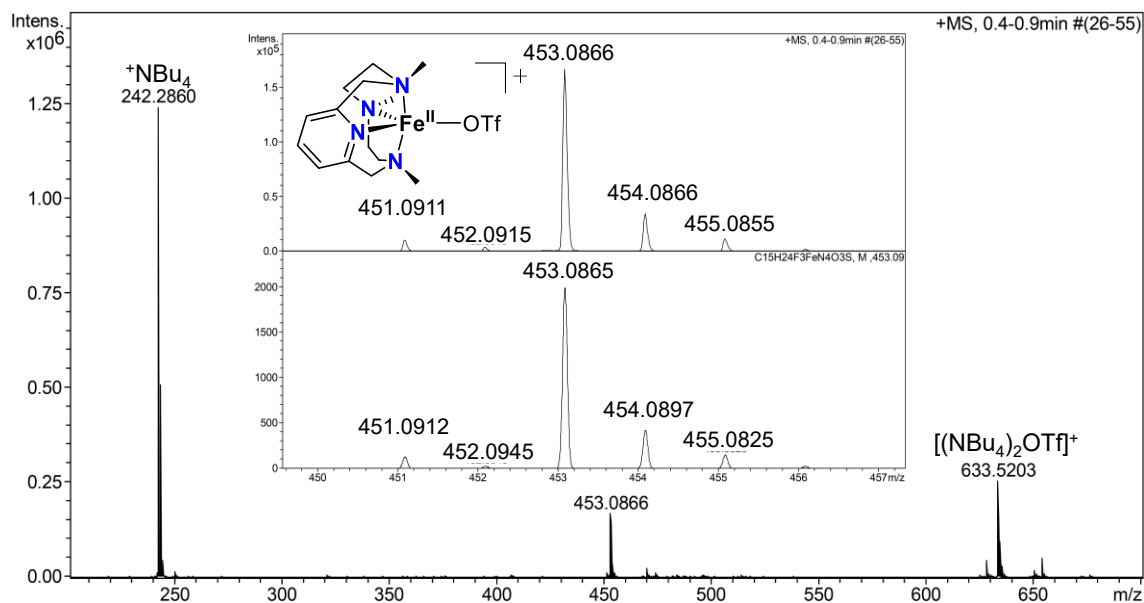
Figure S17. High resolution mass spectrum of the solution obtained after reaction of **2b** with 50 equiv methyl *p*-tolyl sulfide at -40 ºC in CH$_3$CN. The spectrum was recorded at room temperature.

5.2 Hydrogen atom transfer reactions

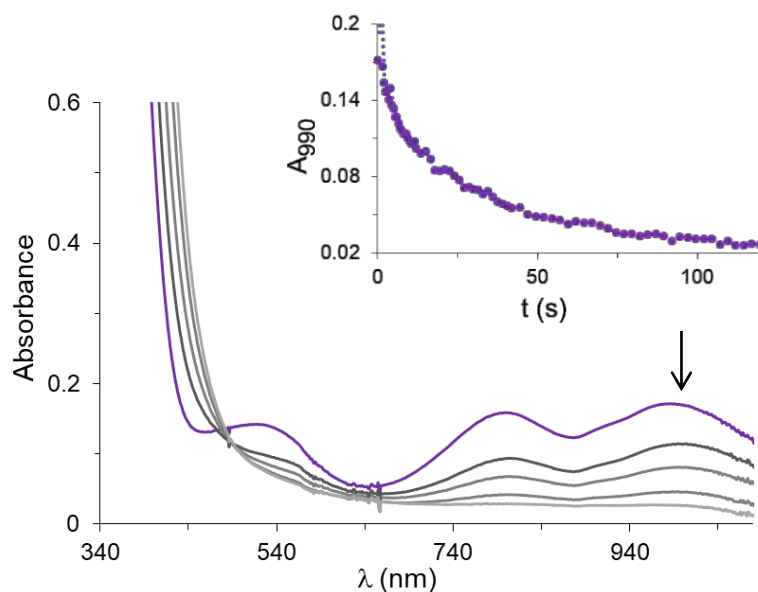**Figure S18.** Decay of **2b** upon reaction with 48 equivalents of 9,10-dihydroanthracene in CH$_3$CN:CH$_2$Cl$_2$ 1:1 at -40 ºC. Inset: kinetic trace at 990 nm. [Fe] = 1.0 mM.
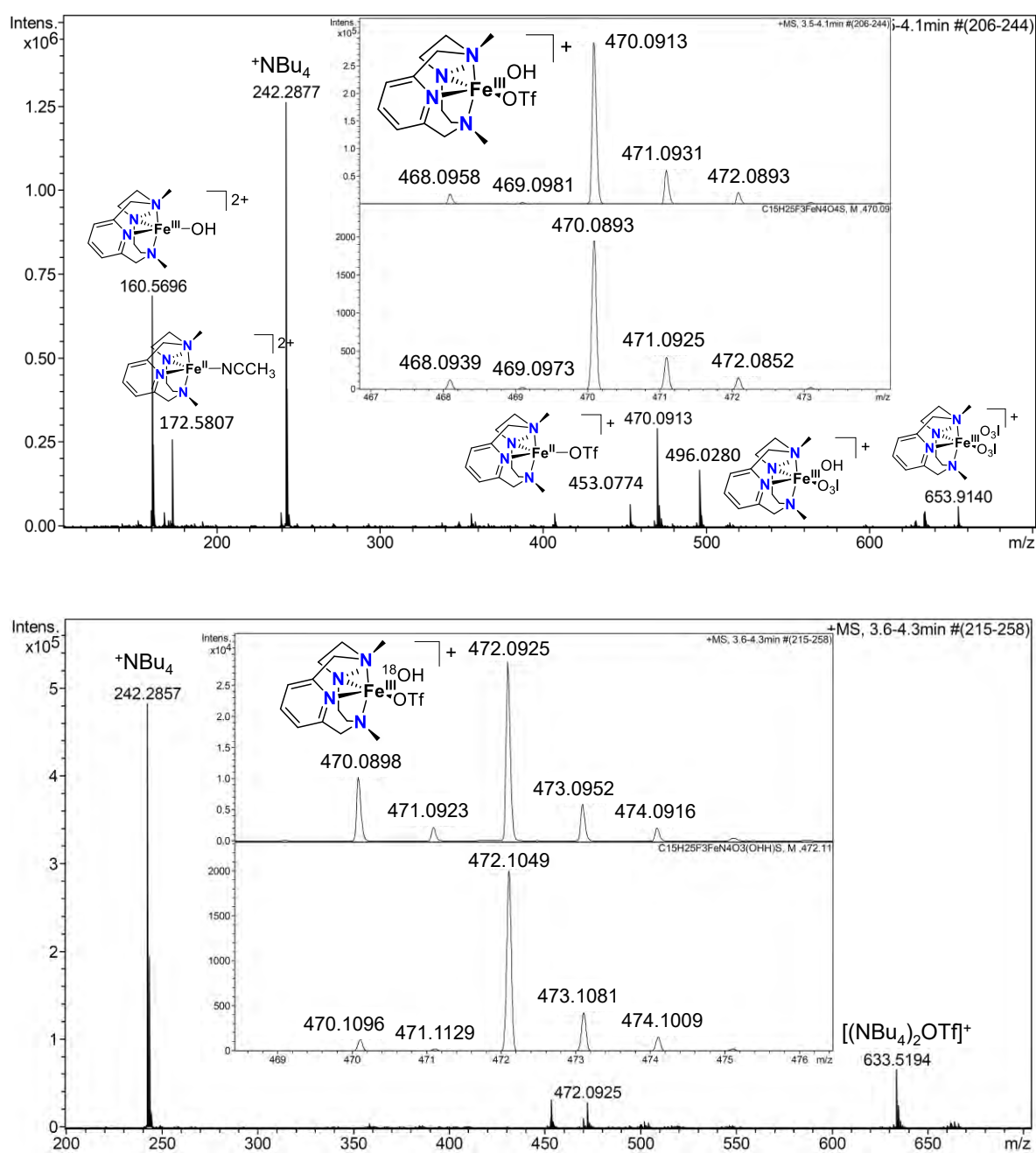
Figure S19. High resolution mass spectrum of the solution obtained after reaction of **2b** with 50 equiv 9,10-dihydroanthracene at -40 ºC in CH_3CN (top). The spectrum was recorded at room temperature. Addition of $H_2^{18}O$ to the solution caused a shift of 2 mass/charge units of the peak corresponding to $[Fe^{III}(OH)(CF_3SO_3)(PyNMe_3)]^+$ (bottom).
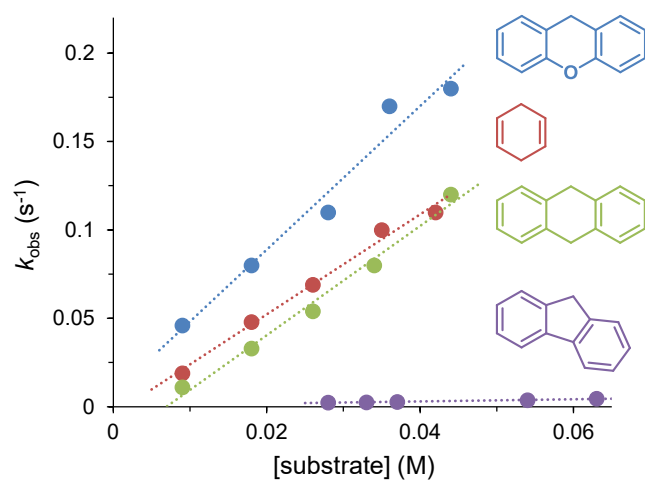
Figure S20. Plot of k_{obs} versus substrate concentration for the reaction of **2b** with different substrates in CH$_3$CN:CH$_2$Cl$_2$ 1:1 at -40 ºC.
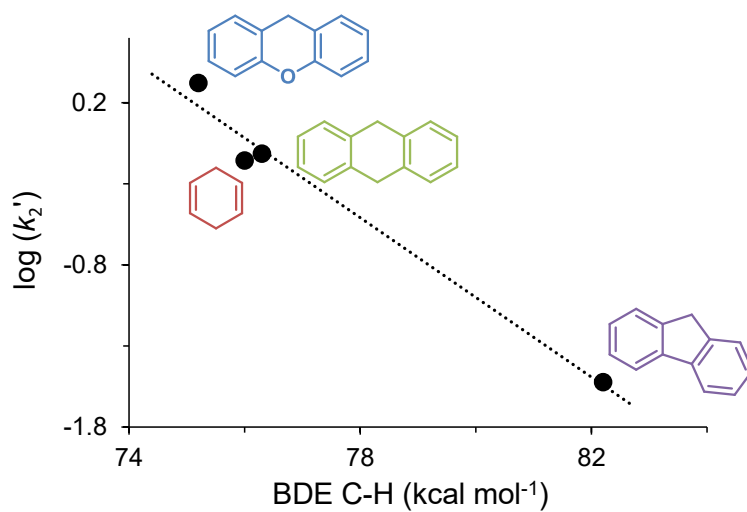
Figure S21. Plot of log(k_2') versus C−H BDEs for the reaction of **2b** with different substrates in CH$_3$CN:CH$_2$Cl$_2$ 1:1 at -40 ºC.
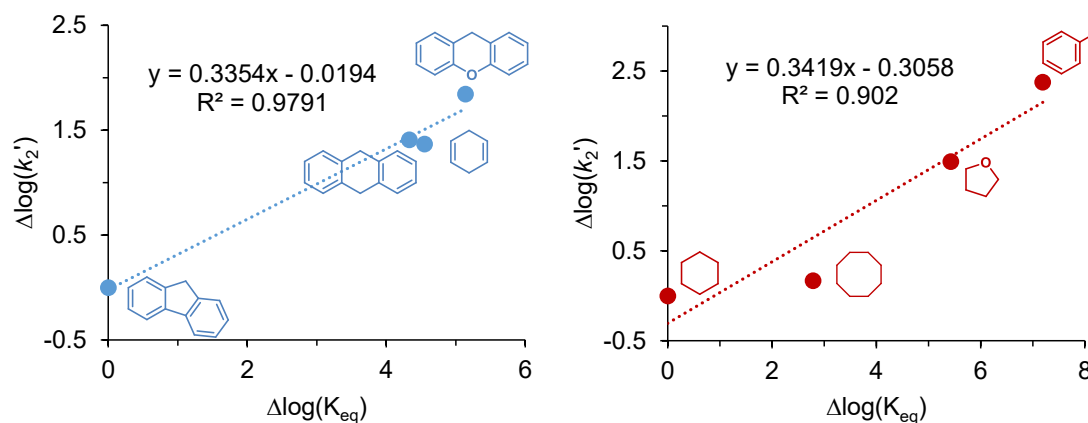
Figure S22. Linear free energy relationship for the reaction of **2b** (left) and **3** (right) with C–H bonds. A unitless slope of 0.34 is obtained in both cases. Log(k_2') corresponds to the logarithm of the normalized second-order rate constant for the reaction of **2b** or **3** with a given substrate. Δlog(K_{eq}) is directly related to the BDE of the C–H bond by considering basic thermodynamics ($\Delta G° = -RT\ln K_{eq}$) and assuming that $\Delta(\Delta G°) = \Delta$BDE. The plotted Δlog(K_{eq}) and Δlog(k_2') values are calculated taking fluorene and cyclohexane as reference for **2b** and **3**, respectively. T = 298 K.

5.3 Kinetic isotope effect
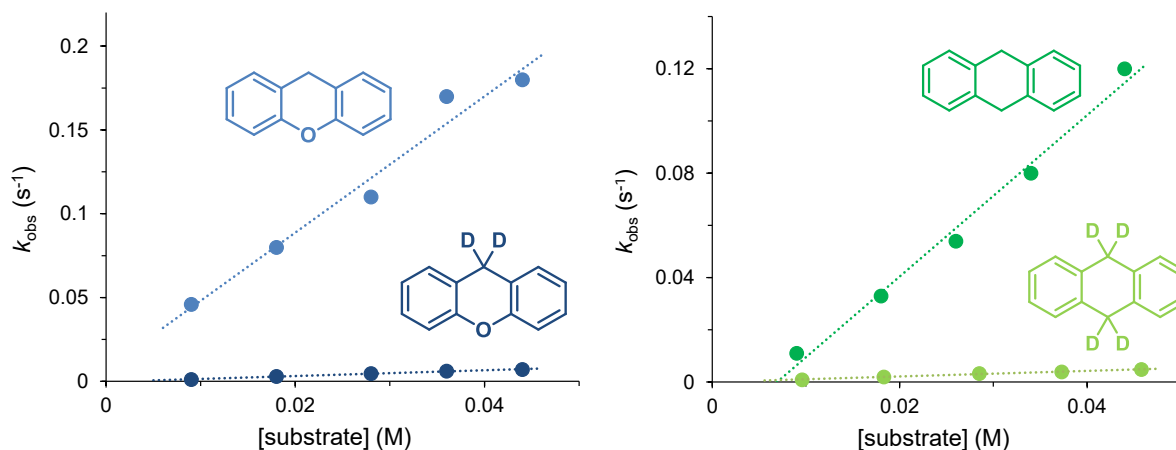
Figure S23. Left: plot of k_{obs} versus substrate concentration for the reaction of **2b** with xanthene and d$_2$-xanthene in CH$_3$CN:CH$_2$Cl$_2$ 1:1 at -40 ºC. Right: plot of k_{obs} versus substrate concentration for the reaction of **2b** with 9,10-dihydroanthracene and d$_4$-9,10-dihydroanthracene in CH$_3$CN:CH$_2$Cl$_2$ 1:1 at -40 ºC.

5.4 Eyring analysis
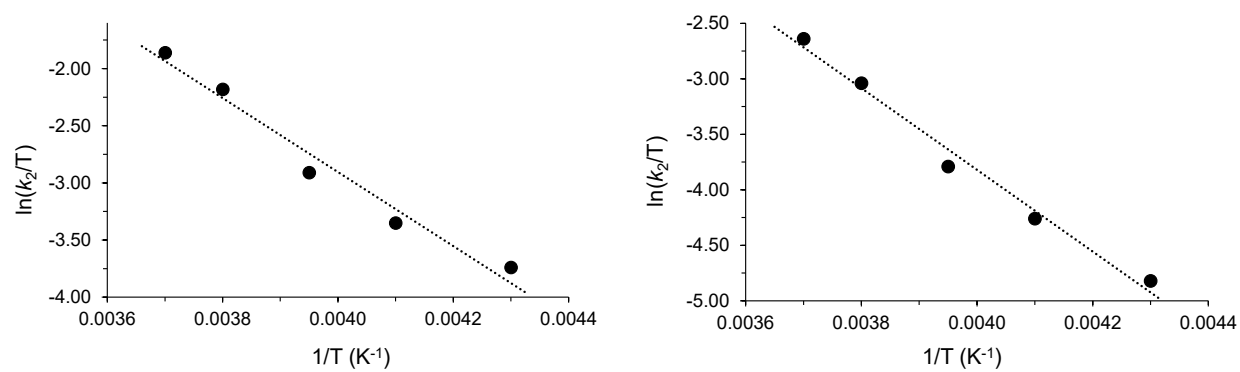
Figure S24. Left: Eyring plot for the reaction of **2b** with xanthene in $CH_3CN:CH_2Cl_2$ 1:1. Right: Eyring plot for the reaction of **2b** with cyclohexadiene in $CH_3CN:CH_2Cl_2$ 1:1.

6. Reaction of 2b and 3 with cyclohexene and cyclohexane
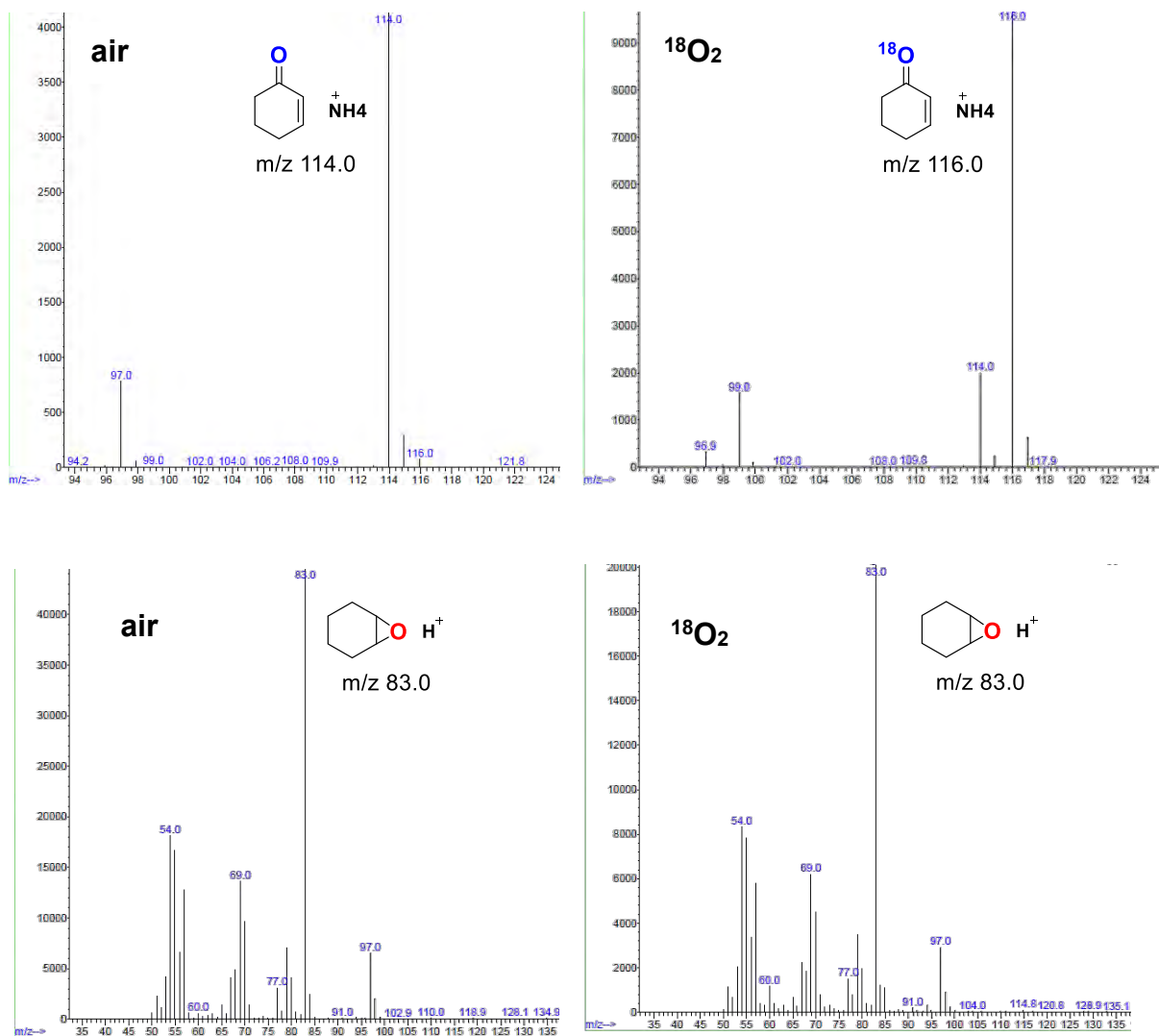
Figure S25. Top: GC-MS spectra (chemical ionization) of the ketone product obtained after reaction of **2b**, in CH₃CN at -40 °C, with 100 equiv cyclohexene under air (left) or $^{18}O_2$ atmosphere (right). Bottom: GC-MS spectra (electron ionization) of the epoxide product obtained after reaction of **3** with 100 equiv cyclohexene under air (left) or $^{18}O_2$ atmosphere (right).

Figure S26. GC-MS spectra (chemical ionization) of cyclohexanol obtained after reaction of **3**, in CH$_3$CN at -40 ºC, with 45 equiv cyclohexane under N$_2$ (left) or ^{18}O$_2$ atmosphere (right).
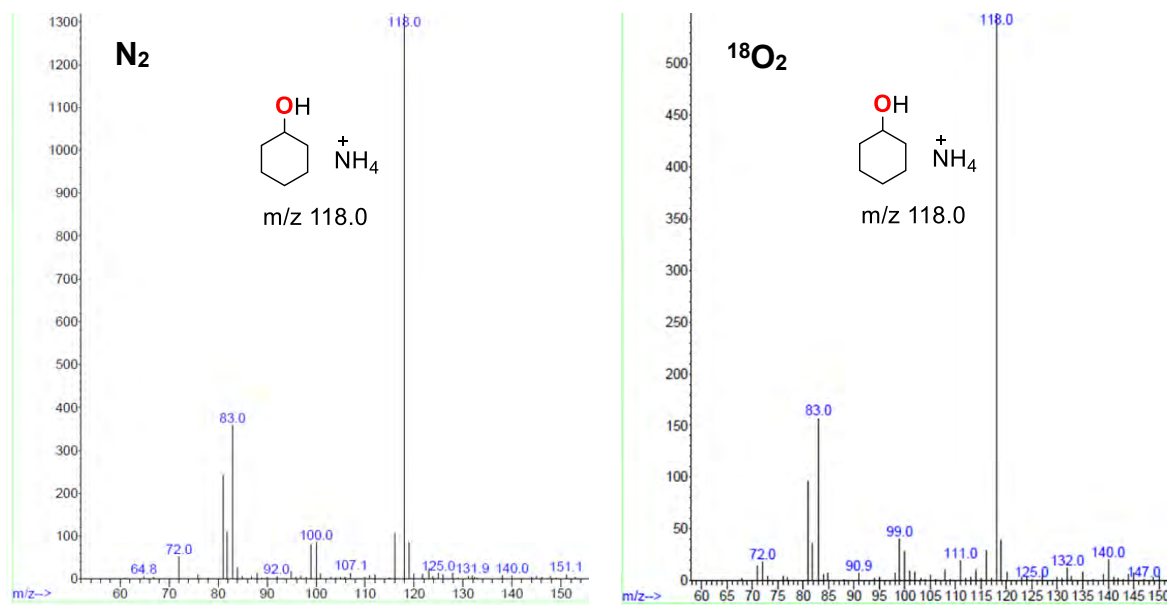
7. DFT calculation of species 2a and 2b

We optimized the structures of complexes **2a** and **2b** in Gaussian 16 (Rev. B01)[8] with fine-tuned B3LYP (labeled as B3LYP* in the following) functionals (Iop(3/76=1000001500) Iop(3/77=0720008000) Iop(3/78=0810010000)), a def2tzvp basis set and a built-in acetonitrile solvation model (scrf=(solvent=acetonitrile)). Then we performed ^{1}H-NMR shift calculations by using the same functional but with a Dunning correlation-consistency basis set cc-pVTZ.

The calculations were carried out by following the protocols described by Bagno and coworkers. [9-12] Geometries were optimized starting from modified XRD structure of **1** by removing counter-ions and adding oxygen.

The calculated ^{1}H-NMR shifts were determined by the following formula:[13,14]

$$\sigma = \sigma_{ref} - (\sigma_{orb} + \sigma_{FC} + \sigma_{PC})$$

where σ_{ref} = 31.02 ppm for TMS was obtained at the same theoretical level as those for the Fe(IV) complexes included in this study. σ_{orb} is the orbital contribution to the proton, which is equivalent to the shielding for diamagnetic systems. The Fermi contact term, σ_{FC}, which originates from the scalar interaction between magnetic field from unpaired electrons and the magnetic momentum of target proton, dominates the paramagnetic component in the ^{1}H-NMR shift arising from the paramagnetic center. The Fermi contact term can be calculated from Fermi's hyperfine interaction parameters as the following:

$$\sigma_{FC} = \frac{2\pi}{\gamma_I} g_{iso} \mu_B A \frac{S(S+1)}{3kT}$$

in which γ_I is the magnetogyric ratio of the nucleus I and g_{iso} is the isotropic g factor of the spin system, μ_B is the Bohr magneton and A is the Fermi hyperfine interaction parameter. The contribution from pseudo-contact term σ_{PC}, can be approximated by the theory developed by Hrobárik et al.[15] Usually it is small and can be ignored compared with σ_{FC}. In this work we estimate the ^{1}H-NMR shift only by the orbital term and Fermi-contact term. All calculations were done at 208 K, the same temperature at which the ^{1}H-NMR measurements were performed in this work.
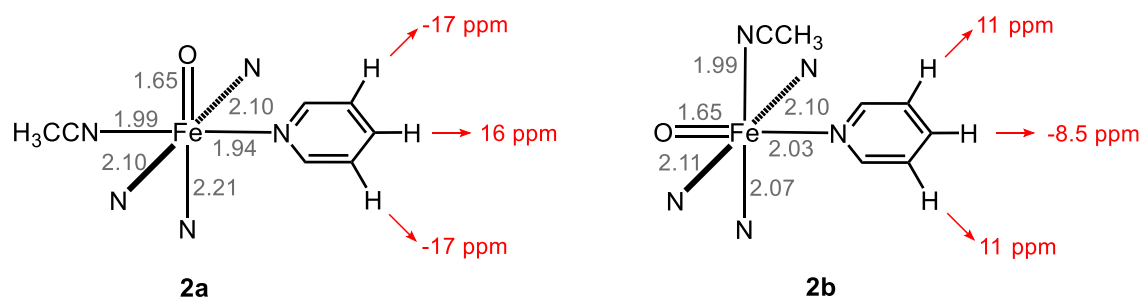

Figure S27. Important bond lengths (gray, in Angström) in DFT-optimized geometry structure of **2a** (left) and **2b** (right); calculated ^{1}H-NMR chemical shifts of β,γ-H's (red).
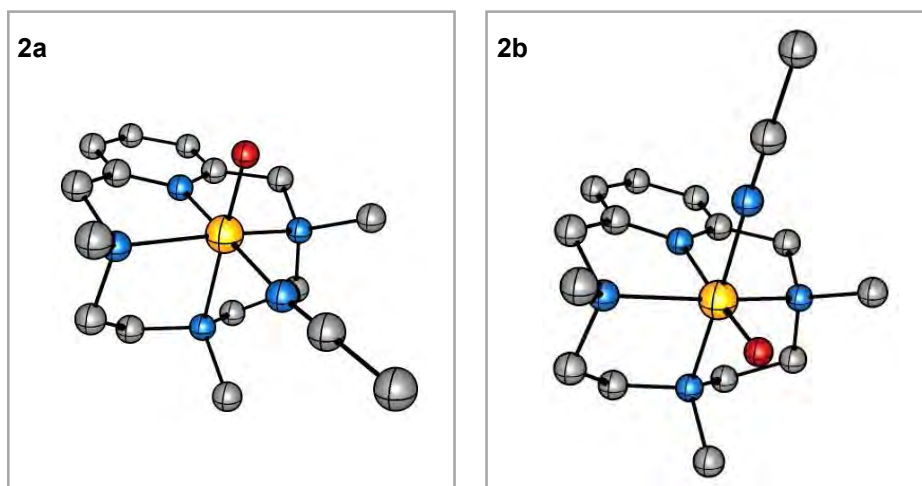
Figure S28. DFT calculated structure of **2a** (left) and **2b** (right).

7.1 Geometry coordinates for 2a and 2b

2a			
Fe	0.380569	0.000005	-0.44734
N	0.130219	-2.07027	-0.20333
N	0.537948	0.000159	1.754284
N	0.129978	2.070268	-0.20342
C	-3.62012	-1.22541	-0.29979
H	-4.15004	-2.1886	-0.29925
C	-2.21584	-1.19074	-0.37885
C	-1.30305	-2.37827	-0.6309
H	-1.29148	-2.55959	-1.72673
H	-1.66363	-3.30667	-0.14064
C	1.065125	-2.91988	-1.03699
H	0.819525	-3.99556	-0.90625
H	2.106037	-2.7389	-0.71285
H	0.954531	-2.63276	-2.0993
C	0.3196	-2.41401	1.27663
H	1.399756	-2.59622	1.433802
H	-0.21108	-3.36127	1.510683
C	-0.1728	-1.26679	2.179086
H	-1.26566	-1.11605	2.087849
H	0.039826	-1.50388	3.244564
C	1.923416	0.000433	2.369724
H	1.830599	0.000525	3.47728
H	2.488756	0.894134	2.05241
H	2.488984	-0.89319	2.052589
C	-0.17327	1.266846	2.17905
H	0.039207	1.504037	3.244537

H	-1.26607	1.115728	2.087728
C	0.318816	2.414194	1.276587
H	-0.21238	3.36121	1.510437
H	1.39884	2.596919	1.434043
C	1.065041	2.91992	-1.03685
H	0.954742	2.632785	-2.09918
H	2.105881	2.739009	-0.71244
H	0.819341	3.995595	-0.90619
C	-4.32127	-0.00019	-0.23798
C	-3.6202	1.225089	-0.30009
H	-4.1502	2.188239	-0.2998
C	-1.30318	2.378007	-0.63149
H	-1.66394	3.306604	-0.14174
H	-1.2913	2.558804	-1.72741
N	2.367398	0.000056	-0.51885
C	3.519056	0.000013	-0.72123
C	4.966724	-2.3E-05	-0.96406
H	5.41785	0.905996	-0.51006
H	5.156034	-9.9E-05	-2.05713
H	5.417811	-0.90603	-0.50999
O	0.321902	0.000036	-2.09401
N	-1.55341	-0.0001	-0.36016
C	-2.21595	1.190515	-0.37916
H	-5.41948	-0.00023	-0.16584

2b

Fe	-0.41036	-0.67272	0.037453
N	-0.3208	-0.43185	-2.05276
N	-2.10347	0.510415	-0.04832
N	-0.35795	-0.18725	2.08564
C	2.068365	2.516349	-1.35986
H	2.40676	2.876465	-2.34215
C	1.259644	1.368988	-1.25937
C	0.896407	0.426544	-2.39984
H	1.7561	-0.26062	-2.55038
H	0.727956	0.96004	-3.35852
C	-0.23505	-1.7325	-2.82298
H	-0.22773	-1.52746	-3.91504
H	-1.10805	-2.35788	-2.56133
H	0.692148	-2.26389	-2.54045
C	-1.60354	0.294842	-2.45724
H	-2.38049	-0.47619	-2.61711
H	-1.4539	0.820274	-3.42381
C	-2.02947	1.278099	-1.35607
H	-1.3037	2.105979	-1.242
H	-3.01643	1.728466	-1.59477

C	-3.40546	-0.27524	-0.01828
H	-4.25362	0.439674	-0.07209
H	-3.47006	-0.86845	0.909104
H	-3.44752	-0.97506	-0.86949
C	-2.05817	1.421017	1.165767
H	-3.05109	1.890071	1.332458
H	-1.3324	2.234117	0.973399
C	-1.65209	0.571317	2.379553
H	-1.5255	1.203353	3.283621
H	-2.42911	-0.18203	2.609099
C	-0.2794	-1.38809	3.004125
H	0.653562	-1.94416	2.798719
H	-1.14645	-2.04397	2.805562
H	-0.2883	-1.05615	4.064425
C	2.438862	3.17923	-0.16715
C	2.040073	2.667726	1.089028
H	2.354907	3.147661	2.026798
C	0.848922	0.714768	2.351297
H	0.658711	1.359631	3.234461
H	1.7078	0.056717	2.60204
N	0.825435	0.930934	-0.04664
C	1.234464	1.513641	1.112395
N	1.271369	-1.728	0.113699
C	2.233029	-2.39155	0.159264
C	3.437412	-3.23039	0.207547
H	3.999787	-3.01483	1.138945
H	3.142637	-4.29948	0.191843
H	4.077956	-3.00946	-0.67061
O	-1.31255	-2.0509	0.112365
H	3.059597	4.086811	-0.21587

8. References

(1)   Bruker Advanced X-ray Solutions. SMART: Version 5.631, 1997-2002.

(2)   Bruker Advanced X-ray Solutions. SAINT +, Version 6.36A, 2001.

(3)   G. M. Sheldrick, Empirical Absorption Correction Program, Universität Göttingen, 1996.

(4)   M. Sheldrick, Program for Crystal Structure Refinement, Universität Göttingen, 1997. Bruker Advanced X-ray Solutions. SHELXTL Version 1996.1914, 2000-2003. SHELXL-2013 (Sheldrick, 2013).

(5)   Spek, A. L. (2005). PLATON, A Multipurpose Crystallographic Tool, Utrecht University, Utrecht, THe Netherlands.

(6)   Park, M. J.; Lee, J.; Suh, Y.; Kim, J.; Nam, W. Reactivities of Mononuclear Non-Heme Iron Intermediates Including Evidence that Iron(III)−Hydroperoxo Species Is a Sluggish Oxidant. *J. Am. Chem. Soc.* **2006**, *128*, 2630-2634.

(7)   Company, A.; Prat, I.; Frisch, J. R.; Mas-Ballesté, D. R.; Güell, M.; Juhász, G.; Ribas, X.; Münck, D. E.; Luis, J. M.; Que, L.; Costas, M. Modeling the cis-Oxo-Labile Binding Site Motif of Non-Heme Iron Oxygenases: Water Exchange and Oxidation Reactivity of a Non-Heme Iron(IV)-Oxo Compound Bearing a Tripodal Tetradentate Ligand. *Chem. Eur. J.* **2011**, *17*, 1622-1634.

(8)   M. J. Frisch, G. W. T., H. B. Schlegel, G. E. Scuseria, M. A. Robb, J. R. Cheeseman, G. Scalmani, V. Barone, G. A. Petersson, H. Nakatsuji, X. Li, M. Caricato, A. V. Marenich, J. Bloino, B. G. Janesko, R. Gomperts, B. Mennucci, H. P. Hratchian, J. V. Ortiz, A. F. Izmaylov, J. L. Sonnenberg, D. Williams-Young, F. Ding, F. Lipparini, F. Egidi, J. Goings, B. Peng, A. Petrone, T. Henderson, D. Ranasinghe, V. G. Zakrzewski, J. Gao, N. Rega, G. Zheng, W. Liang, M. Hada, M. Ehara, K. Toyota, R. Fukuda, J. Hasegawa, M. Ishida, T. Nakajima, Y. Honda, O. Kitao, H. Nakai, T. Vreven, K. Throssell, J. A. Montgomery, Jr., J. E. Peralta, F. Ogliaro, M. J. Bearpark, J. J. Heyd, E. N. Brothers, K. N. Kudin, V. N. Staroverov, T. A. Keith, R. Kobayashi, J. Normand, K. Raghavachari, A. P. Rendell, J. C. Burant, S. S. Iyengar, J. Tomasi, M. Cossi, J. M. Millam, M. Klene, C. Adamo, R. Cammi, J. W. Ochterski, R. L. Martin, K. Morokuma, O. Farkas, J. B. Foresman, and D. J. Fox; Gaussian, Inc., Wallingford CT: 2016.

(9)   Borgogno, A.; Rastrelli, F.; Bagno, A. Characterization of Paramagnetic Reactive Intermediates: Predicting the NMR Spectra of Iron(IV)–Oxo Complexes by DFT. *Chem. Eur. J.* **2015**, *21*, 12960-12970.

(10)   Borgogno, A.; Rastrelli, F.; Bagno, A. Predicting the spin state of paramagnetic iron complexes by DFT calculation of proton NMR spectra. *Dalton Trans.* **2014**, *43*, 9486-9496.

(11)   Rastrelli, F.; Bagno, A. Predicting the 1H and 13C NMR spectra of paramagnetic Ru(III) complexes by DFT. *Magn. Reson. Chem.* **2010**, *48*, S132-S141.

(12)   Rastrelli, F.; Bagno, A. Predicting the NMR Spectra of Paramagnetic Molecules by DFT: Application to Organic Free Radicals and Transition-Metal Complexes. *Chem. Eur. J* **2009**, *15*, 7990-8004.

(13)   Bertini, I.; Luchinat, C.; Parigi, G. *Solution NMR of Paramagnetic Molecules: Applications to Metallobiomolecules and Models*; 1st ed.; Elsevier, 2001; Vol. 2.

(14)   Bertini, I.; Luchinat, C.; Parigi, G. *Reson. Spectrosc.* **2002**, *40*, 249-273.

(15)   Hrobárik, P.; Reviakine, R.; Arbuznikov, A. V.; Malkina, O. L.; Malkin, V. G.; Köhler, F. H.; Kaupp, M. *J. Chem. Phys.* **2007**, *126*, 024107.

Annex 3. Supporting Information Chapter V

Ligand effects on the reactivity of oxoiron(IV) species supported by electronically tuned azamacrocycles

V. Dantignana, J. Serrano-Plana, Á. Martínez Camarena, E. García-España, Miquel Costas*, A. Company,*

Table of contents

V. Dantignana, J. Serrano-Plana, Á. Martínez Camarena, E. García-España, A. Company,

M. Costas. "Ligand effects on the reactivity of oxoiron(IV) species supported by electronically tuned

azamacrocycles". (2020). Manuscript in preparation.